Drug repurposing:

Fast-tracking Antifungal Drug Discovery for Cryptococcal Meningitis

Megan Truong

The ithree institute

University of Technology Sydney

July 2019

A thesis submitted in fulfilment of the requirements
for the degree of Doctor of Philosophy

Certificate of Original Authorship

I, Megan Truong, declare that this thesis is submitted in fulfilment of the requirements for the award of Doctor of Philosophy, in the Faculty of Science at the University of Technology Sydney.

This thesis is wholly my own work unless otherwise reference or acknowledged. In addition, I certify that all information sources and literature used are indicated in the thesis.

This document has not been submitted for qualifications at any other academic institution.

This research is supported by the Australian Government Research Training Program.

Production Note:
Signature removed prior to publication.

Megan Truong, July 15th 2019

Acknowledgements

My primary supervisor always said that a PhD is a journey. And what a journey indeed it was! It has been one long, heck of a ride and there are so many people who have given me their unconditional support, for whom I am so thankful for. In no particular order,

To my primary supervisor, Ian Charles – Thank you Ian for being my supervisor and mentor over the past few years. It's been a pleasure learning from you and I'm so thankful for the sincere care you show for my mental health and PhD progress despite all the challenges we've had, and the effort you put in to call in from afar even just to check in. I hope you know I appreciate all that.

To my number one rock, Leigh Monahan – Thank you so much Leigh for being my co-supervisor, my mentor and my friend. You have been such an amazing support and driver for this me and this project, and I cannot imagine how I would have gotten as far as I have without you. With all the challenges we've had, you've always been the calm person I needed to see it through. I hope that trait rubs off a bit on me as well as your writing skills! Thank you also for being patient and accommodative of me whenever I needed help (especially for my final seminar). I'm so lucky and grateful to have had you as my go-to person.

To Dee Carter, the Carter Lab and G08 friends – Thank you Dee for supervising me and being on-board this project. Navigating through this PhD has been a lot more challenging than either of us would have ever imagined, so thank you very much for your patience, your guidance, your time and all your efforts in supporting me and this project. You are an amazing editer and I hope to be able write as well as you one day. Special thanks to Yuwen and Kenya for your friendship. I wouldn't be who and where I am today, if it were not for your unconditional support at all my highs and lows. Doing a PhD was much more tolerable with you both! Thank you also to the autoclave/morning tea ladies and workshop guys for your support and all that you have done for me and the lab over the years. Your help is always much appreciated!

To Steve Djordjevic – You have done more for me than you give yourself credit for. Thank you for standing in in Ian's absence and for that time you listened to everything I had to say even though I was sick. I appreciate your sincere care, the shits and giggles and all the wine talks. Thank you!

To my collaborators at UNSW – thank you so much Prof Marc Wilkins and Dr Ignatius Pang for being a part of my transcriptome project. Your contributions and support mean so much to me and I could not have completed this without your help. Special thanks to Igy for all your help with the bioinformatics components. Thank you for being so patient with me, and your willingness to teach and guide me through many processes. I am also grateful to you for sharing so much of your time in helping me read drafts (especially at time when you were most busy), and your unconditional moral support (they always pick me up when I am down).

To my friends at Duke – Joe & the Heitmania Lab, thank you for welcoming me to your lab so warmly and helping me so readily when I needed help. Thank you to Prof John Perfect and Prof Andy Alspaugh for also being so welcoming of this little Aussie. You and your lab members freely shared your time with me and I hope you know I appreciate that so much. If you ever fly down to Sydney, please feel free to reach out as I would love to catch up! Special thanks also to Di Dong for being an amazing roommate during my time at Duke. My time at Duke was one of my highlights during my PhD. I met so many people, travelled around a bit and learnt so much (personally & academically).

To my family – Special thanks to my mum and dad, for being ever so patient, accommodative and understanding of my long hour days and overnight stays. Thank you for making sure I'm well fed and that I get home safely every single day. Thank you to my older brother for supporting the family. Thank you my little brother for checking in on me, being patient with me on my bad days, having shits and giggles with me, and especially for bringing Leon into our family. Thank you Leon and Mikky for always making me smile.

To my mentor and friend Dr John Pitt – thank you so much for your friendship, guidance and support over the past few years. Thank you for all the opportunities you have given me and always reminding me that it is completely ok, and rather better, to have a challenging PhD experience.

To my immediate PhD family – Thank you so much for your friendship and support over the years. I'm grateful to have been surrounded by such an amazing, intelligent, funny, hard-working, caring and supportive group of people. It's been such a pleasure knowing you all over the past few years and I'm excited to see what's in stall for each of us. Special thanks to Iain, Marz, Ethan and Ronnie for always being supportive, especially on my bad days. Special thanks to Michael, Isa and Iain, particularly in the lead up to my thesis submission. Without your help in formatting, spot-checking, moral support on many levels and keeping me in one piece, I could not imagine how I could have submitted this thesis.

To my non-PhD friends who still stuck around – thank you for being understanding and supportive despite me being largely MIA. Special thanks to Helen Pang and Tina Nguyen for your unconditional support on so many levels. Your support and friendship mean the world to me. I look forward to catching up with you all and spending some long overdue quality time.

Thank you to Prof John Perfect for providing strains that I tested in my first data chapter. Thank you to Assistant Prof Lukasz Kozubowski for providing the GFP strain LK128 that I used in my third data chapter. Thank you to Dr Connie Nichols for providing a list of fluorescent strains for my work. Many, many thanks also to Dr Louise Cole for your guidance at the start of my microscopy venture and helping me navigate through technical discussions and meetings. Many, many thanks also to Dr Christian Evenhuis for all your help with my microscopy work. Thank you for being so patient with me, for being involved in this work and a great teacher! Thank you also to Dr Mike Johnson for your technical support in the microscopy work. I am so lucky and grateful to have done microscopy with you all and would love to learn more from you!

Abbreviations

Abbreviation	Chemicals and Media
DMSO	Dimethyl sulfoxide
MOPS	4-Morpholinepropanesulfonic acid
RPMI-1640	Roswell Park Memorial Institute media
SDA	Sabouraud dextrose agar
YNB	Yeast nitrogen base
YPD	Yeast peptone dextrose

Abbreviation	Antifungal susceptibility
5-FC	5-flucytosine
AMB	Amphotericin B
FLB	Flubendazole
FLC	Fluconazole
MEB	Mebendazole
MIC	Minimum inhibitory concentration
MFC	Minimum fungicidal concentration

Abbreviation	Units
cells/mL	Cells per millilitre
°C	Degrees Celsius
h or hr	Hours
µg/mL	Micrograms per millilitre
mg/mL	Milligrams per millilitre
µm	Micrometre
µM	Micromolar
min	Minutes
OD	Optical density
pH	Potential hydrogen
rpm	Revolutions per minute
sec	Seconds

Abbreviation	Others
WT	Wild-type
FDR	False discovery rate
GFP	Green fluorescent protein
logFC	log fold-change
ROI	Regions of interest

Table of Contents

Table of Figures

Table of Tables

Abstract

Cryptococcal meningitis is the most common form of meningitis in HIV-infected persons. It is a life-threatening fungal infection of the brain that disproportionately affects the poorest and most resource-limited regions of the world. Current antifungal therapies used to treat cryptococcal meningitis are critically limited, toxic, expensive and have issues with drug resistance, highlighting an urgent need for more effective and affordable drugs. However, developing a new drug can cost over $2 billion and take over a decade to succeed, causing many development pipelines to dry up. To address this issue, this thesis uses drug repurposing as an alternative approach to accelerate antifungal drug discovery efforts to treat cryptococcal meningitis. This involves investigating existing drugs, approved for other purposes, for candidates with antifungal activities that can be developed into new antifungal drugs.

An untested library of drugs was screened for compounds that inhibited the growth of *Cryptococcus deuterogattii.* This approach successfully identified multiple candidates that are not currently approved to treat fungal infections. The most potent candidate was flubendazole, a drug used to treat intestinal worms in veterinary and clinical settings. A diverse list of *Cryptococcus* species were highly susceptible to low concentrations of flubendazole and this effect was fungicidal. This is important for efficient clearing of fungal burden, and may subsequently help improve clinical outcomes, prevent clinical relapse and deter the development of drug resistance. Flubendazole was also equally effective against fluconazole-resistant *Cryptococcus* strains, and was highly specific to *Cryptococcus* species and did not inhibit other clinically-important, human fungal pathogens.

To understand the antifungal mechanism of action of flubendazole, a combination of RNA-Seq and microscopy approaches were used. Gene expression data and image analyses demonstrated that tubulin was inhibited and cell morphology was compromised in *Cryptococcus* cells treated with flubendazole. This provides evidence to support the involvement of tubulin as a probable target of flubendazole in its antifungal mechanism of action. The RNA-Seq data generated also represents a resource for future studies to comparatively investigate genes of interest for drug discovery, such as transcription factors and kinases.

This thesis encompasses a body of work that exemplifies the benefits of combining drug screening and repurposing efforts in an attempt to address the unmet medical needs of cryptococcal meningitis. The discovery of flubendazole as a potential antifungal agent and preliminary characterisation of its

antifungal action provides a platform that may inform and aid future developmental work including medicinal chemistry studies.

Chapter 1: Introduction

Invasive fungal infections are a major global problem, both in terms of their burden on human health and their associated economic impact. Surveillance studies indicate that fungal infections significantly increase patient mortality and hospital costs [1-3]. Brain infections such as meningitis caused by fungi require more extensive disease management and are more costly than those caused by bacteria [4]. The economic cost of managing systemic fungal infections in 1998 in the United States alone was previously estimated to be US$2.6 billion, with hospitalisation-associated costs accounting for over 50% of the total cost [5]. The Infectious Diseases Society of America has since revised this estimate to more than US$7.2 billion in 2017, highlighting the economic health burden in a developed society [6].

Cryptococcal meningitis is a major cause of morbidity and mortality and a recurrent global health burden [1, 7, 8]. Despite this, cryptococcal meningitis was named one of 'the most poorly funded neglected diseases' by the 2017 G-FINDER survey annual report, receiving less than 0.5% of global funding for research and development (R&D) in 2016 [9]. Treatment options are limited and not suitable or readily accessible in developing countries where they are needed most, and drug resistance is an increasing problem. The treatment and management of cryptococcal meningitis varies depending on the treatment regimen but is nonetheless expensive [10]. In 2017, approximately US$260 million was spent on cryptococcal infections in the United States [11]. There is an important need to address the lack of antifungal drug treatments available to treat cryptococcal meningitis, and to find new agents that are safe (non-toxic) and effective. This thesis will focus on cryptococcal meningitis, and the identification of novel potential treatment options to combat this deadly and neglected disease.

1.1 *Cryptococcus* and cryptococcal meningitis – a silent killer and neglected disease

Cryptococcal meningitis is a fungal infection of the central nervous system (CNS), which affects a substantial number of people globally. Caused by a small, yeast-like, environmental fungus called *Cryptococcus*, cryptococcal meningitis is the most common form of meningitis in resource-limited areas where HIV is highly prevalent [12, 13]. The advent of the antiretroviral therapy (ART) to treat HIV had a tremendous health impact, significantly reducing the morbidity and mortality of HIV/AIDS [14, 15], including HIV-associated cryptococcal meningitis [16-18]. While the incidence and mortality of cryptococcal meningitis was reduced as a result of ART, ART does not treat cryptococcal meningitis and if acquired, the disease remains very difficult to resolve [19, 20].

An updated surveillance study by Rajasingham *et al*. (2017) evaluated the global burden of HIV-associated cryptococcal meningitis and revealed disease burden caused by *Cryptococcus* was indeed still prevalent and worldwide [21]. Unfortunately, an unacceptably high percentage of deaths due to cryptococcal meningitis still occur in sub-Saharan Africa (75%) per year, as shown in Figure 1.1 [8, 21].

Furthermore, HIV drug resistance is predicted to have substantial consequences including 890,000 AIDS deaths, 450,000 new infections and US$6.5 billion spent on ART programs in sub-Saharan Africa between 2016-2030 [22]. This highlights the importance of continued efforts to find therapeutic solutions for cryptococcal meningitis, that are improved and more effective than current standard clinical practices, which were last updated in 2010 [23].

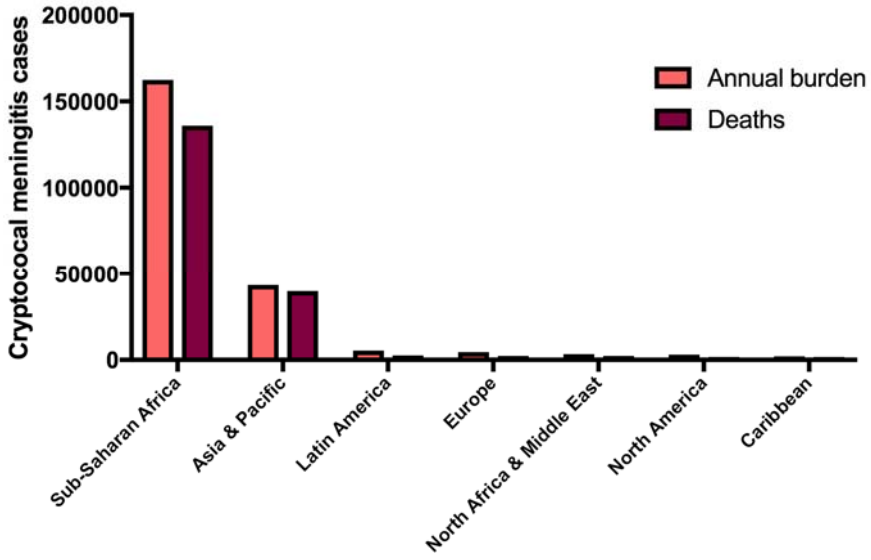

Figure 1.1. Global burden of cryptococcal meningitis. Adapted from Rajasingham *et al*. 2017 [21] using GraphPad Prism 7.

Cryptococcal disease begins with the inhalation of desiccated yeasts or basidiospores, which are the infectious propagules. These are found ubiquitously in the environment, including soil, trees and pigeon droppings (Figure 1.2) [24-26]. These infectious propagules deposit into the alveoli of the lung, the primary site of infection, and if not cleared by lung alveolar macrophages they can proliferate [27]. A pulmonary infection can manifest as cryptococcal pneumonia and/or lung cryptococcomas [28, 29]. However, dissemination of the infection to the CNS often occurs, leading to brain cryptococcomas or to cryptococcal meningitis, which is the infection and inflammation of the meninges [28-30]. This can progress into cryptococcal meningoencephalitis, a more critical stage where additional inflammation of the cerebral brain occurs [28, 29]. Clinical symptoms of cryptococcal infection are non-specific, with patients often experiencing headaches, fever, neck pain, vomiting and neurological derangements [12, 30, 31]. Cryptococcal disease can also affect animals [32-34]. Pigeons are recognised as carriers of *Cryptococcus*, as cryptococci can survive at avian body temperatures (42 °C), although generally they do not exhibit cryptococcal disease [35, 36]. This is reportedly due the ability of avian macrophages to suppress the growth of internalised *Cryptococcus* cells [35].

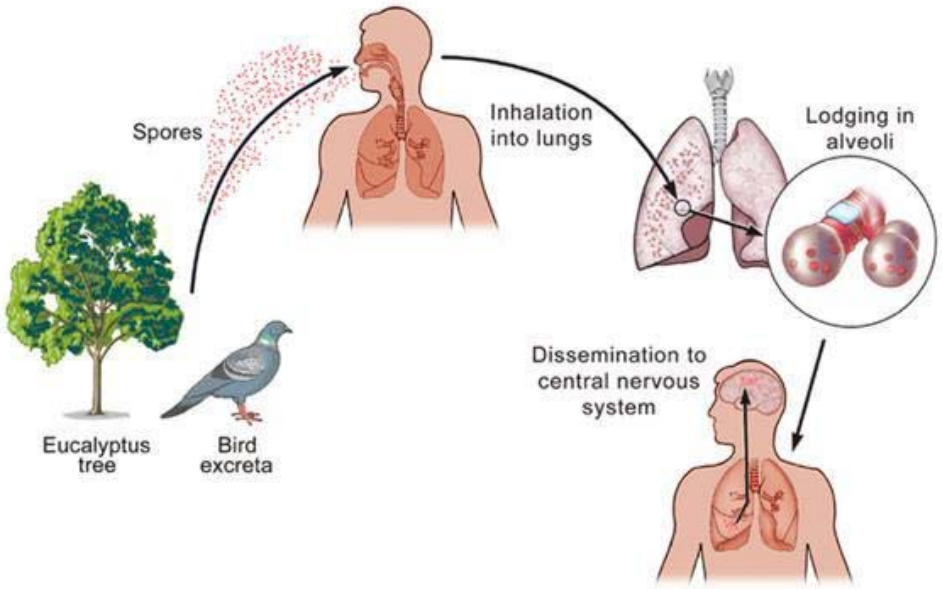

Figure 1.2. Mode of infection by *Cryptococcus*. *Cryptococcus* exists ubiquitously in the environment, often associated with Eucalyptus trees and bird excreta. Infection occurs through the inhalation of infectious propagules in the form of desiccated yeasts or spores, which lodge into the alveoli of the lungs, the primary site of infection. Infection can then disseminate to other body organs, most notably the brain. Figure adapted from Hull and Heitman (2002) [37].

1.2 *Cryptococcus neoformans* and *Cryptococcus deuterogattii* – the major causative agents

The taxonomy of *Cryptococcus*, which encompasses a species complex, has been extensively revised in recent years. The two main pathogenic and distinct species known to cause cryptococcal disease were previously known as *Cryptococcus neoformans* and *Cryptococcus gattii*. *C. neoformans* was divided into two varieties (*C. neoformans* variety *grubii* and *C. neoformans* variety *neoformans*) and further sub-classified into four genotypes VNI–VNIV, while *C. gattii* was sub-classified into four genotypes VGI-VGIV (see reviews [38, 39]). In 2015, Hagen *et al*. proposed changes to cryptococcal taxonomy based on phylogenetic analyses and mass spectrometry and described seven phylogenetically distinct species [40]. *C. neoformans* variety *grubii* and *C. neoformans* variety *neoformans* were proposed as two different species within the *C. neoformans* species complex, namely *C. neoformans* and *C. deneoformans,* respectively, while *C. gattii* was described as a species complex encompassing five discrete species: *C. gattii* (VGI), *C. deuterogattii* (VGII), *C. bacillisporus* (VGIII), *C. decagattii* (VGIV/VGIIIc), and *C. tetragattii* (VGIV) [40]. As the new nomenclature is still in the state of transition, in this chapter members of the *C. gattii* species complex will be referred to as *C. gattii* unless referencing primary literature where the new names have been employed, in which case the new species names will be used.

Cryptococcus neoformans is regarded as the major causative agent of cryptococcal disease. Distributed ubiquitously in the environment worldwide, *C. neoformans* is an opportunistic pathogen often affecting immunocompromised subpopulations, including HIV positive and solid organ transplant recipients [41-46]. Unlike *C. neoformans*, the ecological niche of *C. gattii* was thought to be restricted to tropical and subtropical climates [47-50]. This includes Australia where *C. gattii* is of particular significance as there has been a high incidence in the Australian indigenous community [47, 48, 51]. After 1999, however, *C. gattii* began to receive significant attention as an emerging fungal pathogen following a major outbreak affecting immunocompetent humans and animals in Vancouver Island, British Columbia, Canada [32, 52, 53]. The emergence and spread of cryptococcal infections outside of its usual ecological niche suggested *C. gattii* could adapt to climates that are more temperate, raising concerns it could potentially cause other outbreaks [52, 54, 55]. In the ensuing years, epidemiological and surveillance studies indicated that the outbreak had spread to other regions including Northern Europe [56], the Pacific Northwest region of America [33, 54, 57, 58], as well as other American States [30]. Almost twenty years since the major outbreak, *C. gattii* is increasingly recognised as a primary pathogen of cryptococcal disease.

Cryptococcus gattii (VGI and VGII) predominantly affect immunocompetent individuals, for reasons that remain not completely understood, with a propensity to cause respiratory symptoms and fatal lung infections [45, 58, 59]. Mortality and the cost of drug treatment is reportedly higher in patients with cryptococcal meningitis not associated with HIV, suggesting a greater need for effective antifungal drugs to treat both immunocompromised and uncompromised patient populations [11, 41, 42]. Also concerning are reports that show clinical development of cryptococcal disease up to two years after travel to regions where cryptococcal infections are present [58, 60, 61], suggesting the possibility of latency in some infections.

Cryptococcal disease caused by different pathogenic strains of *Cryptococcus* have similar clinical manifestations, and to date there are no clear clinical characteristics that distinguish disease caused by one species over another. Identification to the species level is not a routine practice in clinical laboratories, which is not critical in terms of treatment as prescribed treatments are often identical between species; however, this may mean the infecting species may be underdiagnosed and its prevalence underestimated.

1.3 Treatment of cryptococcal meningitis – the need for new therapeutic alternatives

The three staple antifungal agents used to treat cryptococcal meningitis are amphotericin B, 5-flucytosine and fluconazole [23]. Patients diagnosed with cryptococcal meningitis undergo a three-phase therapy program with these drugs, designed to mitigate fungal burden rapidly, to suppress residual fungal cells and to minimise the risk of relapse. In an ideal situation where all drugs are available, patients are treated initially with a combined therapy of amphotericin B and 5-flucytosine, administered daily for two weeks (induction phase), followed by fluconazole alone for eight weeks (consolidation phase), and fluconazole again at a lower dose for an additional two weeks (suppression/maintenance phase) [23]. A patient's treatment regimen may slightly vary in the formulation of amphotericin B, the drug combination or the drug dosage depending on different factors including the availability and/or accessibility of a specific drug, whether the infection is associated with HIV, or whether a patient is a transplant recipient.

Amphotericin B is a polyene antifungal agent that targets ergosterol, a vital cell membrane sterol component unique to fungi (Figure 1.3). The binding of amphotericin B to ergosterol induces the formation of porin channels that compromise cell membrane integrity and increase permeabilisation [62-64]. 5-Flucytosine is a fluoropyrimidine [65]. The drug itself has no antifungal toxicity, however its metabolism by fungal cells produces toxic metabolites that inhibit DNA and RNA synthesis (Figure 1.4) [65].

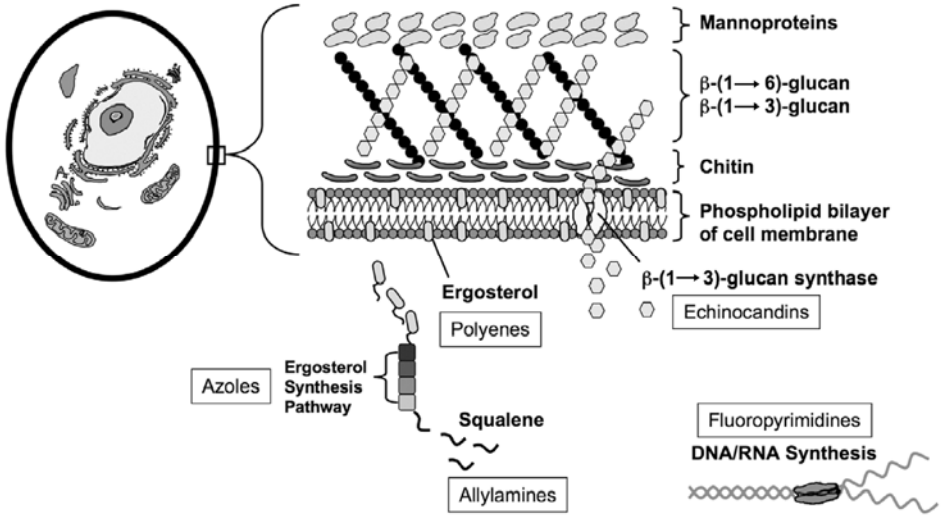

Figure 1.3. Antifungal drug classes and their respective targets. Polyenes target cell membrane component ergosterol.

Azoles and allylamines are groups of ergosterol biosynthesis inhibitors that target different steps of the biosynthesis pathway of ergosterol. Echinocandins target the synthesis of the cell wall component β-1,3-D-glucan. Fluoropyrimidines inhibit the synthesis of fungal DNA/RNA. Figure modified from Ashley *et al*. (2006) [66].

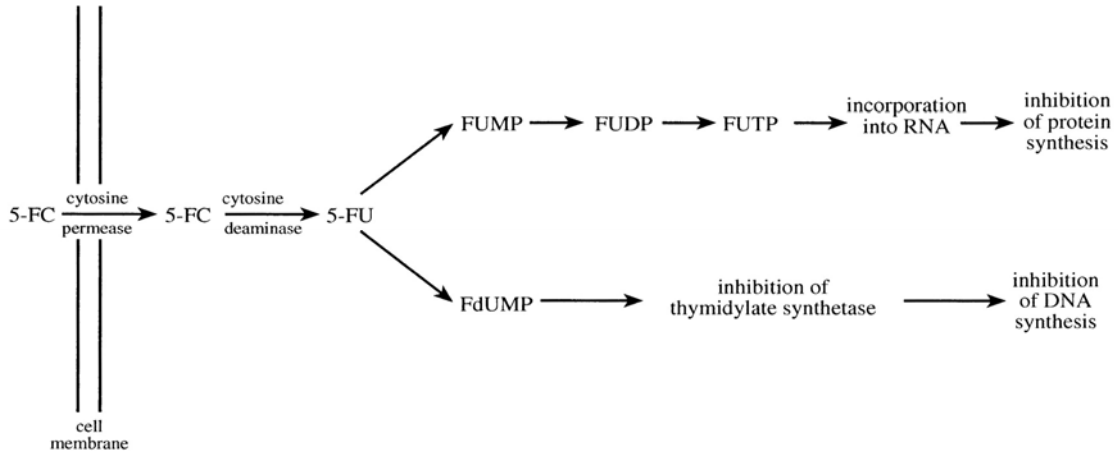

Figure 1.4. Mechanism of action of 5-flucytosine.In fungal cells, 5-flucytosine (5-FC) is converted into 5-fluorouracil (5-FU) which is further metabolised into different products that inhibit protein or DNA synthesis. Abbreviations: 5-flucytosine (5-FC); 5-fluorouridine monophosphate (FUMP); 5-fluorouridine diphosphate (FUDP); 5-fluorouridine triphosphate (FUTP); 5-fluorodeoxyuridine monophosphate (FdUMP). Figure sourced from Vermes *et al.* (2000) [67].

Amphotericin B and 5-flucytosine together form the most effective combination for optimal (short and long-term) patient survival for cryptococcal meningitis [10, 68, 69]. However, the application of these drugs is not without complications. Anaemia, hypokalaemia, nephrotoxicity, hepatotoxicity and bone marrow suppression are among the most common toxicities experienced by patients [65, 68, 70-72]. Treatment of adverse events can also be costly, reported to account for over 68% of the total cost of amphotericin B depending on the formulation [73].

In addition to toxicity, the use of amphotericin B and 5-flucytosine is limited by costs, scarce licensing access and poor availability in many parts of the world [74]. Although amphotericin B is widely available, it is unavailable in many African nations [74], due to lack of registered licensing [74, 75]. Pricing varies demographically, as daily prices for 50 mg of amphotericin B have been as high as US$171.47 in Canada, US$85.44 in Finland and US$81.66 Germany, while in African countries amphotericin B is marketed for less than US$12 [74, 75].

5-flucytosine is often not registered or licensed and therefore not available in many countries across the globe [74]. This includes many African countries, where it is needed most, a situation that has remained unchanged for over twenty years [74-76]. Where 5-flucytosine is available, prices can soar as high as US$278 daily in Australia for intravenous therapy and US$1409 daily in the United States for oral doses [74]. The high cost of 5-flucytosine has been associated with market failure, characterised by a lack of supply and demand and lack of competition between supply chains, and the

inherently expensive nature of the manufacturing process [10, 65, 75]. Efforts to simplify the manufacturing of 5-flucytosine could reduce production costs and potentially increase the availability of 5-flucytosine to poorer nations like Africa [77]. Despite the efficacy of 5-flucytosine and its recommendation by health authorities, this antifungal agent remains expensive and largely inaccessible.

Where amphotericin B and 5-flucytosine are not available, fluconazole is recommend by the Infectious Diseases Society of America [23]. Fluconazole belongs to the azole class of antifungals, which inhibit the biosynthesis of ergosterol (Figure 1.3). Fluconazole is globally licensed and accessible, orally available and a cheaper alternative to amphotericin B and flucytosine [69, 74]. However, as it is a fungistatic drug (one that inhibits fungal growth but does not directly kill fungal cells), it does not effectively clear fungal burden and is associated with high mortality and treatment failure, poor clinical outcomes, sequelae, and clinical relapse with increased fluconazole resistance [78-80]. Therefore, an urgent need exists for alternative treatments that are more effective, accessible and available in resource-limited regions.

Even with current best treatment by antifungal drugs, the mortality rates for cryptococcal meningitis remain unacceptably high [69]. The average one year mortality rate using amphotericin B and 5-flucytosine combined for induction was estimated at 35%, less than fluconazole monotherapy at 60%, but still undesirable [69]. In addition to poor survival rates, patients that overcome cryptococcal infection are often left with medical disabilities or impairments and are at risk of clinical relapse [79-81]. These concerns highlight the crucial need for new or alternative antifungals that are effective with minimal adverse effects. An ideal anti-cryptococcal drug would be characterised by: (i) fungicidal activity alone or in combination with other agent(s); (ii) the ability to penetrate the blood-brain barrier to reach the central nervous system; (iii) good oral absorption properties to reduce costs in areas with limited resources; and (iv) effectiveness against *Cryptococcus* cells even when they reside inside macrophages [82].

1.4 Antifungal drug resistance

One of the major concerns with the use of antimicrobial agents is the development of drug resistance. Clinical laboratories measure drug resistance using minimal inhibitory concentration (MIC) assays, which indicate the lowest concentration at which a drug inhibits the growth of a microorganism, usually by 50% (MIC_{50}) or 90% (MIC_{90}) relative to untreated cells [83]. Resistance refers to the ability of a microorganism to survive and continue to cause clinical disease despite the administration of a drug at the normal therapeutic dose. According to the clinical guidelines for the management of cryptococcal disease outlined by the Infectious Diseases Society of America, an isolate with an MIC greater than or equal to 16 μg/mL for fluconazole or 32 μg/mL for flucytosine may be considered resistant [23]. Resistance to treatment can be attributed to different factors including acquired resistance where previous exposure to antifungal drugs can place selective pressure to develop adaptive mechanisms [84], and may vary with fungal species and strains [85].

Multiple surveillance studies monitoring drug resistance in *Cryptococcus* have reported varied results. MIC profiling of widely used antifungal drugs including amphotericin B, fluconazole and 5-flucytosine found that most MIC values were within the range of susceptibility, suggesting there is no significant evidence of antifungal drug resistance in *Cryptococcus* spp. [86-89]. A recent study evaluated a set of clinical isolates of *C. deuterogattii* from Brazil between 1999 and 2015 and found that all tested antifungal drugs, including amphotericin C, fluconazole and 5-flucytosine, were effective and had MICs within the accepted ranges of susceptibility [86]. A more extensive study conducted by Pfaller *et al.* (2015) surveyed the antifungal susceptibility of 496 clinical isolates of major human fungal pathogens in the Asia and Western Pacific region between 2010 and 2012 [89]. The authors found no detectable azole resistance among *C. neoformans* isolates, and overall concluded that antifungal resistance is not often observed in invasive fungal infections in the Asia and Western Pacific region [89]. In a Zimbabwe study, the majority of clinical isolates were also found susceptible and responsive to antifungal drugs [90]. Fortunately, resistance to amphotericin B is rarely observed, with clinical isolates consistently susceptible across different studies [91-93]. These studies suggest that antifungal resistance in *Cryptococcus* spp. does not currently threaten the use or comprise the efficacy of available antifungal drugs.

In contrast to these studies, incidents of resistant clinical isolates and reports of higher MIC profiles in *Cryptococcus* spp. continue to be documented worldwide. Increased resistance to fluconazole in *C. neoformans* has been reported in Taiwan and Cambodia, including a 12-year study in Southern Taiwan [94-96]. This finding was reiterated in a recent study surveying the presence of antifungal resistance in clinical isolates retrieved from HIV-positive patients with cryptococcal meningitis in Uganda (2010-2014) [91]. The study reported fluconazole MIC values had increased compared to previous studies in

1998-1999, with 31% of clinical *C. neoformans* isolates identified with MIC values greater than or equal to 16 µg/mL for fluconazole [91]. An analysis of 29 studies between 1988-2017, found the average prevalence of fluconazole resistance in clinical isolates was 12.1%, and was often occurring in relapse isolates compared to incident isolates (24.1% vs 10.6%) [97].

Mechanisms of azole resistance has been reported by several investigators [98, 99]. One phenomenon that is of notable interest is heteroresistance. Heteroresistance refers to the capacity for a susceptible strain to harbour a resistance sub-population. The molecular basis for heteroresistance is unclear, however there is evidence to suggest it can be mediated by drug-induced aneuploidy that reverts in the absence of antifungal selection pressure [100-103]. In *Cryptococcus*, aneuploidy frequently increases the copy number of genes associated with azole resistance, for example *ERG11* and *AFR1* [84, 102]. This form of genomic plasticity is thought to be one explanation for how *Cryptococcus* adapts to higher concentrations of antifungal agents, resulting in decreased drug susceptibility [84]. Further, the reversible nature of heteroresistance may account for differences observed between clinical and concomitant *in vitro* drug susceptibilities, and independent surveillance efforts monitoring antifungal drug susceptibility [102, 104].

While the extent of resistance to widely used antifungal drugs is inconclusive, the emergence and persistence of clinical isolates with fluconazole resistance stands as an important global health threat in both immunocompromised and immunocompetent populations. As fluconazole is frequently and widely used, this warrants continued global surveillance studies to monitor the prevalence of resistance. At the same time, this highlights the need for new solutions to treat cryptococcal infections, as there are limited therapeutic options that are effective.

1.5 Economic and regulatory challenges in drug development

The pursuit of new antifungal drugs continues to be an immense challenge that is constrained by scientific, regulatory and financial barriers. From a scientific perspective, it is difficult to find druggable targets unique to fungi that provide exploitable selective toxicity, as fungi share various structures and multiple metabolic pathways in common with mammalian cells [105-108]. Furthermore, to treat cryptococcal meningitis, drugs must be able to penetrate the blood-brain barrier, which is a formidable barrier for most drugs to transverse [109]. Drugs targeting the CNS have one of the highest attrition rates through the drug development pipeline compared to other therapeutic areas undergoing development [110, 111]. These challenges compound the ongoing problems associated with traditional drug development, which will be discussed below.

The journey of a drug candidate from bench to market is incredibly challenging, undergoing lengthy and costly processes with high risk of failure. Multiple studies have analysed the cost of an approved agent, with the latest estimate totalling a total capitalised cost of up to US$3 billion per approved agent covering pharmaceutical R&D costs [112-117]. The high cost associated with developing a new drug is largely characterised by the expensive and high-risk nature of clinical trial phases (Phases I-III) that assess drug candidates for safety and efficacy. Phase I involves testing for safety in a small cohort of healthy human subjects, Phase II involves testing for efficacy and proof-of-concept with a larger group of people with the condition to be treated and Phase III is a more extensive study of Phase II, with a much larger number of participants [118]. The likelihood of a drug successfully obtaining FDA approval from phase I and thus making it to market, is 9.6%, averaging $25 million per drug in that phase alone [115, 119]. The successful transition from one clinical phase to another varies due to their respective demands and expectations that differ in scale. Surveillance analyses have indicated the percentage probability of success (completion) in clinical phases have decreased in the last twenty years, with phase II consistently being the most challenging and difficult to surpass [110-112, 115]. In addition to high attrition rates, average time to complete a clinical trial phase has increased 1.5-fold, a substantial difference considering 45-50% of total development costs are attributed to time costs [112, 115]. This suggests that the level of complexity, rigor and scale of clinical trials have increased and may be a contributing factor to the lack of FDA approvals over the last two decades [112, 115, 120, 121].

Aside from regulatory and financial barriers, the progression from drug discovery to successful marketing is a lengthy process. For a new drug, this can be an estimated 10 – 17 year process from discovery to successfully obtaining FDA approval [122, 123]. This process took even longer for the latest class of antifungal agents, the Echinocandins (30 years) [124]. While successfully bringing a drug to market as efficiently as possible is important for patients, it is also important for stakeholders as the period of exclusivity granted by regulatory agencies are limited. The defined period of market exclusivity is the most important sales opportunity for an approved drug to make returns on investments [125]. It varies between different regulatory agencies and is dependent on the granted status of a drug (e.g. a new chemical entity or orphan drug) [126, 127]. For example, the FDA grants five years of market exclusivity for new chemical entity designations, while the European Medicines Agency offers up to 11 years of exclusivity [126]. As the nature of drug development is typically time-consuming, successfully approved and marketed drugs are often left with a limited time frame to make sales sufficient for investment returns, before the period of market exclusivity expires. This has been a deterring factor for drug discovery and development efforts in the anti-infective space for microbial and eukaryotic pathogens. As a result of lack of cost recovery, many pharmaceutical companies

including Novartis and Sanofi have withdrawn their financial investments and exited antimicrobial R&D programs, shifting focus to chronic conditions where opportunities for investment returns are better [128, 129]. Novartis is the latest pharma giant to have closed its doors on antimicrobial research, following AstraZeneca, Sanofi and Allergan [129, 130]. This leaves only Merck & Co, GlaxoSmithKline, Roche and Pfizer with active antimicrobial programs [131], and is most concerning as efforts into antimicrobial research are diminishing in an era where these are needed more than ever.

To support academic and pharmaceutical research in the antimicrobial sector, the American and European regulatory bodies have made efforts to improve financial risks and incentives. The Generating Antibiotic Incentives Now (GAIN) act was implemented in 2012 to offer an economic incentive by providing an additional five years of exclusivity rights to enable investment returns to manufacturing companies with a 'qualified infectious disease product' (QIDP) [132-134]. QIDPs, defined as "an antibacterial or antifungal drug for human use intended to treat serious or life-threatening infections" caused by "qualifying pathogens", which includes *Cryptococcus* spp., are also eligible for Fast Track designation and priority review by the FDA under the GAIN act, which helps expedite and accelerate the regulatory approval process [133-135]. The limited population pathway for antibacterial and antifungal drugs (LPAD) allows eligible drug candidates to undergo a streamlined development program with simpler clinical trials that encourage the output of drugs with a limited market [136]. Last year, the FDA approved the highest number of drugs in over two decades [121]. Only a select few of these approved agents, however, were antimicrobial agents and none were for fungal diseases [121].

New antifungal agents, target molecules and therapeutic approaches are currently under investigation with the aim of developing new antifungal treatments and strategies but these are at very early stages of development [137]. Potential vaccines and adjunctive therapies investigated for *Cryptococcus* spp., have reached as far as preclinical or early clinical phases of development, but no progress has since been reported or updated [138-145]. To date, no successful vaccines for cryptococcal meningitis have been developed.

1.6 Repurposing: a powerful approach for drug development

The lack of new antifungal agents and the shortage of successfully marketed new drugs has emphasised the need for more effective and efficient drug development strategies. This has led researchers to consider alternative strategies to inhibit *Cryptococcus* spp. One approach is to use drug combinations that act synergistically against *Cryptococcus* cells [106, 146-150]. While this is a growing area of research, no promising combination therapies have progressed to clinical trials. Another increasingly popular strategy, which offers competitive and attractive benefits to traditional drug discovery methods, is the high-throughput screening of small-molecule, compound or FDA-approved drug collections with the aim of identifying candidates with potential to be repurposed. Drug repurposing, or repositioning, is an attractive and promising approach for antimicrobial discovery programmes, in both academia, pharma and private start-up companies [151]. Drug repurposing is the process by which an existing drug is shown to have a novel, undescribed activity that enables it to be 'repurposed' and used in a different clinical context to that of its original indication [152]. These include drugs with or without FDA approval, and compounds that were unsuccessful in clinical trial phases [153]. Compared to *de novo* drug development, repurposing drugs offers increased rewards such as reduced time to market, improved cost and lower risk (e.g. target validity), and this has therefore has been highlighted as the most effective current strategy in drug development [122]. Furthermore, drug repurposing enables optimal use of current drug reservoirs to address the seemingly limitless need to develop alternative therapeutics to meet unmet medical needs. Depending on the mechanism of action, promising drug candidates may also provide a framework to initiate lead drug discovery programs or medicinal chemistry programs, thereby opening new areas of research and R&D.

Drug approval (e.g. in the U.S. by the Food and Drug Administration [FDA] or in Europe by the European Medicines Evaluation Agency [EMEA]) is essential for a product to be marketed, as approval indicates that a product has undergone rigorous development where sufficient clinical evidence for drug safety and efficacy exists to support use in humans [154]. Repurposing drugs that have already been approved by agencies like the FDA has the advantage that drug profiles (including drug safety, pharmacokinetic and pharmacodynamic data, and mechanism of action), have been established. This profile may assist in uncovering the mechanism of action of drugs being used in a new application [155]. The availability of existing data has the advantage that it may also allow drug candidates to bypass preclinical and early clinical phases of development, thereby advancing them through the drug development pipeline with a greater probability of successfully obtaining FDA approval [151]. This is highly desirable as it can facilitate faster translational research by reducing developmental timelines

and costs, and this may improve the probability of success through clinical trial studies with lower risk. To this effect, repurposing can substantially reduce development costs, saving drug developers about 40% of the total cost per approved drug [112, 115, 156]. It also offers a higher rate of success than developing a drug from scratch (estimated at ~30% vs 10%), with the cost to establish a new indication for an existing drug has been estimated to approximately US$300 million [123, 157].

1.7 Drug repurposing for cryptococcal meningitis

Repurposing existing drugs for neglected and poorly funded diseases such as cryptococcal meningitis is a smart strategy to develop new therapeutic alternatives. The process of drug repurposing begins with a known drug (approved for a primary indication with a known molecular target) that has identified efficacy in a new indication for the same or new molecular targets [158]. The efficacy of an existing drug in a new indication might be produced by the drug alone or synergistically in combination with another drug [159]. Several studies have conducted high-throughput screens of large libraries of drugs, compounds and small molecules in search for agents that inhibit *Cryptococcus* (Table 1.1). In these studies, antifungal activity against *C. neoformans* was identified in at least one candidate not primarily indicated for antifungal use. To date, *C. neoformans* has been the main target pathogen tested, with only one reported screen against *C. gattii*. Presumably, this is because *C. neoformans* has been historically recognised as the main causative agent of cryptococcal disease. However, the emergence of *C. gattii* as a primary fungal pathogen highlights the importance of including it to minimise missed opportunities due to species-specificity [106].

Table 1.1. Drug screening studies and repurposing ventures for *Cryptococcus* spp.

Study	**Library**	**Fungal pathogen used in screen**	**Significant findings**
Spitzer *et al.* (2011) [106]	Prestwick Library (n=1,120)	*C. gattii,* *C. neoformans,* *C. albicans,* *S. cerevisiae*	• Compounds found to potentiate fluconazole activity have species or genus specificity between different pathogenic and model yeast strains.
Butts *et al.* (2013) [82]	Prestwick Library (n=1,120)	*C. neoformans*	• 31 compounds with fungicidal activity, about half of which are novel. • Amiodarone and thioridazine interferes with intracellular *C. neoformans.*
Dehdashti *et al*. (2013) [160]	Library of Pharmaceutically Active Compounds (n=1,280)	*C. neoformans*	• Niclosamide, malonoben, 6-bromoindirubin-3'-oxime, and 5-[(4-ethylphenyl) methylene]-2-thioxo 4-thiazolidinone have fungicidal activity.
Rabjohns *et al*. (2013) [161]	Library of Pharmaceutically Active Compounds (n=1,280)	*C. neoformans*	• Compound 10058-F4 has fungicidal activity under nutrient-deprived conditions.
Brown *et al.* (2014) [162]	439 small molecules	*C. neoformans*	• *Candida* biofilm inhibitor compound S8 induced cell cycle arrest in *C. neoformans* at G2/M phase. • Identification of a number of synergistic pairs with fluconazole or geldanamycin.
Samantaray *et al.* (2016) [163]	Prestwick Chemical Library (n=1,200)	*C. neoformans*	• 19 compounds reduced *C. neoformans* growth in macrophages. • Fendiline hydrochloride promoted intracellular killing of *C. neoformans* by enhancing the maturation rate of phagosomes.
Joffe *et al.* (2017) [164]	National Institutes of Health clinical collection (n=727)	*C. neoformans*	• Mebendazole has fungicidal activity against intracellular *C. neoformans* and cryptococcal biofilms. Antifungal activity was also extended to *C. deuterogattii*. • Antifungal activity of mebendazole may involve protein scramblase and nucleolar protein NOP16.

Beyond the simple aspect of discovering a potential new indication for a known drug, drug screening efforts have led to insightful lessons and discoveries that have progressed the drug development pipeline within the last decade. A combinatorial screening approach testing the Prestwick library of 1,120 off-patent drugs for synergistic agents that enhance the activity of fluconazole demonstrated hit specificities on a species and genus level between *C. neoformans*, *C. gattii*, *C. albicans* and *S. cerevisiae* [106]. This suggests that when searching for agents with broad-spectrum antifungal activity, opportunities may be missed or limited by screening drugs against only one fungal species. This therefore highlights the benefits of screening more than one species, especially where there is more than one causative agent for a medical condition.

There have been instances where a hit candidate from a drug screen has advanced into clinical trial phases for cryptococcal meningitis. This has been the case for oestrogen receptor antagonist tamoxifen whose antifungal mechanism of action was suggested to be based on interfering with calcium homeostasis [82, 146]. Tamoxifen is currently undergoing phase 2 clinical trials assessing efficacy and safety in combination with amphotericin B and fluconazole in patients with cryptococcal meningitis [https://clinicaltrials.gov/ct2/show/NCT03112031]. At the forefront of drug repurposing for cryptococcal meningitis is antidepressant agent sertraline [165, 166]. Sertraline has recently completed a phase III clinical trial, assessing whether it can be used as an adjunctive agent to standard cryptococcal meningitis therapy to improve the survival of patients with HIV-associated cryptococcal meningitis over an 18-week period [http://clinicaltrials.gov/show/NCT01802385] [167]. The results from this clinical study are yet to be published.

Overall, these studies demonstrate the potential of high-throughput screening of drug libraries and drug repurposing as valuable strategies for discovering new anti-cryptococcal agents that either possess antifungal activity alone, or are able to enhance the effect of existing antifungal agents in combination. As Nobel laureate Sir James Black stated, “the most fruitful basis of the discovery of a new drug is to start with an old drug” [168].

1.8 Systems biology as a way of understanding how drugs perturb fungal cells

Systems biology involves the high-throughput, comprehensive quantification and characterisation of molecular entities including genes, proteins and RNA [169]. This effectively allows for global analyses of molecular networks and offers insight to how dynamic networks change in response to stimuli. In the development of new medicines, understanding the global effects of a pharmacological agent in a holistic context, as opposed to its target alone, can help identify potential off-target effects that may impede progression and success of a drug to market [170].

The perturbing effects of a drug can be investigated using multi-omic technologies, including genomic, proteomic and transcriptomic platforms. Each systems biology technology offers different outputs to address different investigational needs and comes with its own benefits and shortcomings. Genomics is informative of the structure, function, and potential for expression of all genes and variations within a genomic sequence [171]. However, it does not show whether the expression of genes is increased or decreased, or show post-transcriptional and post-translational modification events that affect protein function. Proteomics allows the study of all proteins that are expressed, however it requires very specialised facilities and is limited in its ability to accurately detect proteins expressed in low abundance [172]. Transcriptomics is the systematic study of an organism's or cell's total mRNA, otherwise known as the transcriptome. mRNA serves as the biological template that encodes the amino acid sequences for protein synthesis. Whole transcriptome shotgun sequencing, more commonly referred to as RNA-Seq, is a next-generation sequencing technology that allows for high-throughput sequencing of mRNA with high resolution and low background noise [173]. The process of sequencing a transcriptome produces raw reads, which are processed and assembled into transcripts. The abundance of transcripts can be measured and reflects the active or inactive expression of genes, from which protein function can be implied. RNA-Seq enables effective profiling of the transcriptome and subsequent qualitative and quantitative analysis of changes in biochemical pathways or patterns of biological significance in the holistic context of an entire cell or organism, which could otherwise be missed in targeted studies [174]. This has been a particularly useful tool in understanding biological and adaptive responses of *Cryptococcus* to stimuli such as acetic acid [175] and hydrogen peroxide [176], or insults such as fluconazole treatment [177] and synergistic antifungal combinations [178]. Transcriptomics can therefore be used to elucidate mechanisms of the likely therapeutic outcomes following exposure to a candidate drug.

1.9 The scope of this research

The repertoire of antifungal agents that are safe and effective is scarce and largely unavailable in poor countries where there is the highest incidence of cryptococcal infections. To this end, there has been an ongoing demand for new antifungal drugs that are safe, efficacious, and ideally possess good orally bioavailability. This research primarily aims to provide evidence to support alternative therapeutic solutions with potential to be repurposed for the treatment of cryptococcal meningitis. The aims of this thesis are to:

1. To employ a drug repurposing strategy to identify novel approved therapeutic agents with activity against *Cryptococcus*.

2. To characterise potentially promising agents discovered in aim 1 for 1) their influence on the cell transcriptome in attempt to elucidate potential mechanisms of action; 2) their effect on cellular morphology; and 3) their influence on global cell regulators.

Chapter 2: Repurposing drugs to fast-track therapeutic agents for the treatment of cryptococcosis

2.1 Declaration

I declare that the following publication included in this thesis in lieu of a chapter meets the following criteria:

- The majority of the content in the following publication included in this chapter has been planned, executed and prepared for publication by me. For detailed contribution, please refer to statement below.
- The work presented here has been peer reviewed and accepted for publication.
- The initial draft of the work has been written by me and any subsequent changes in response to co-authors and editors reviews were performed by me.

Publication title: Repurposing drugs to fast-track therapeutic agents for the treatment of cryptococcosis

Authors: Megan Truong, Leigh G. Monahan, Dee A. Carter, Ian G. Charles

Author's contributions: Megan performed all experiments, wrote the paper and edited all drafts of the paper. Leigh, Dee and Ian all read and provided comments on the drafts.

Journal name: PeerJ

Volume/page numbers: Volume 53, pages 2-9

Status: Published May 2018

DOI: 10.7717/peerj.4761

I declare that the publication above meets the requirements to be included in the thesis.

Candidate's name: Megan Truong

Candidate's signature: Production Note: Signature removed prior to publication.

Date: 02/04/19

2.2 Abstract

Many infectious diseases disproportionately affect people in the developing world. Cryptococcal meningitis is one of the most common mycoses in HIV-AIDS patients, with the highest burden of disease in sub-Saharan Africa. Current best treatment regimens still result in unacceptably high mortality rates, and more effective antifungal agents are needed urgently. Drug development is hampered by the difficulty of developing effective antifungal agents that are not also toxic to human cells, and by a reluctance among pharmaceutical companies to invest in drugs that cannot guarantee a high financial return. Drug repurposing, where existing drugs are screened for alternative activities, is becoming an attractive approach in antimicrobial discovery programs, and various compound libraries are now commercially available. As these drugs have already undergone extensive optimization and passed regulatory hurdles this can fast-track their progress to market for new uses. In this study, the Screen-Well Enzo library of 640 compounds was screened for candidates that phenotypically inhibited the growth of *Cryptococcus deuterogattii*. The anthelminthic agent flubendazole, and L-type calcium channel blockers nifedipine, nisoldipine and felodipine, appeared particularly promising and were tested in additional strains and species. Flubendazole was very active against all pathogenic *Cryptococcus* species, with minimum inhibitory concentrations of 0.039 – 0.156 μg/mL, and was equally effective against isolates that were resistant to fluconazole. While nifedipine, nisoldipine and felodipine all inhibited *Cryptococcus*, nisoldipine was also effective against *Candida, Saccharomyces and Aspergillus*. This study validates repurposing as a rapid approach for finding new agents to treat neglected infectious diseases.

2.3 Introduction

Cryptococcal meningitis is a devastating fungal disease that disproportionately affects the poorest, most resource-limited, underdeveloped regions of the world, where the health burden is extremely high. Those who are most at risk are patients who are immunocompromised, including HIV/AIDS populations and patients receiving rigorous immunosuppressive treatments such as chemotherapy. Mortality rates are unacceptably high and vary significantly with demography, with estimates as low as 9% among patients in developed countries compared to 70% in sub-Saharan Africa [8], where cryptococcal meningitis clinically presents in up to 40% of HIV/AIDS patients [21, 179]. This high mortality is largely attributable to lack of access and difficulty in administering the most effective standard treatment, amphotericin B combined with flucytosine [23, 74], which is expensive and requires medical infrastructure for therapeutic monitoring due to adverse effects including nephrotoxicity, hepatotoxicity, and bone marrow suppression [65, 70, 74]. Fluconazole is commonly used in place of amphotericin B and flucytosine, however as it is a fungistatic drug it does not effectively clear fungal burden and is associated with clinical relapse, greater mortality and poorer clinical outcomes, as well as the risk of inducing drug resistance [79, 91, 180]. Overall, there is an urgent need for new antifungal treatments that are more effective, economical, accessible and available to regions where they are needed most. Drug repurposing, or repositioning, is becoming an increasingly popular avenue in drug discovery. This is the establishment of a new indication for a drug entity that has been previously approved for another purpose by authoritative bodies such as the US Food and Drug Administration (FDA). For pharmaceutical industries and drug developers, repurposing offers attractive benefits as previously established pharmacokinetic and pharmacodynamics profiles provide the potential to fast-track drugs through the development pipeline, avoiding substantial costs associated with expensive clinical trials [181]. The antidepressant sertraline is a leading example of a non-antifungal drug in the process of being repurposed for cryptococcal meningitis. First discovered through a drug screen in 2010, sertraline has potent fungicidal activity against *Cryptococcus* and is synergistic in combination with fluconazole [150, 165]. *In vivo*, sertraline alone or in combination with fluconazole reduced fungal burden in infected mice [165]. Most importantly, sertraline achieved more efficient clearance of fungal burden in HIV-infected patients in Uganda, with no relapse during the clinical study [166].

Cryptococcus encompasses a range of phylogenetically discrete genotypes and species that can cause cryptococcal meningitis. *Cryptococcus neoformans* is an opportunistic pathogen commonly infecting groups with compromised immune systems. *C. neoformans* is the most well-studied cryptococcal species and has been the main target of drug discovery efforts to identify new anti-cryptococcal

agents. However, *Cryptococcus deuterogattii* (formerly known as *Cryptococcus gattii* genotype VGII) has recently emerged as a primary pathogen, responsible for recent outbreaks affecting otherwise immunocompetent individuals [40, 57]. In this study, we phenotypically screened the Enzo library consisting of 640 FDA-approved agents against *C. deuterogattii* to identify compounds with novel anti-cryptococcal activity. We report multiple compounds that inhibited the growth of *C. deuterogattii* and that were subsequently screened against various pathogenic fungal species to determine the spectrum of activity. Flubendazole was the most potent compound and was found to specifically target *Cryptococcus* species. Nifedipine, nisoldipine and felodipine demonstrated antifungal activity toward *Cryptococcus* species and to varying degrees toward other yeast and mould pathogens. Our findings highlight the value of repurposing strategies to rapidly screen drug libraries that can reveal new classes of antifungal agents for further development.

2.4 Methods

2.4.1 Strains

Fungal strains used in this study are listed in Table 2.1 and 2.2. Strains were maintained as glycerol stocks stored at -80 °C. Strains were grown on sabouraud dextrose agar (SDA) for 48 h at 30 °C before use.

2.4.2 Enzo drug library and drug stocks

The Screen-Well FDA-approved drug library was purchased from Enzo Life Sciences (Farmingdale, New York; catalogue no. BML-2841). The 640 compounds in this library were provided at 2 mg/mL in dimethyl sulfoxide (DMSO). Flubendazole (FLB), mebendazole (MEB), benomyl (BEN), nisoldipine (NIS), nifedipine (NIF), felodipine (FEL), niguldipine (NIG), amphotericin B (AMB), itraconazole (ITZ), voriconazole (VRZ) and 5-flucytosine (5FC) were obtained from Sigma-Aldrich (St. Louis, Missouri). Fluconazole (FLC) was obtained from Sapphire Bioscience (Australia). Stock solutions of amphotericin B, itraconazole and voriconazole were prepared at 1.6 mg/ml in water; 5-flucytosine was made at 6.4 mg/ml in water; fluconazole was made at 12.8 mg/ml in water and all remaining drugs were dissolved in DMSO at 2 mg/mL. All compounds were stored at -80 °C.

2.4.3 Primary drug screening

We evaluated all 640 FDA-approved compounds in the Enzo library for efficacy against *C. deuterogattii* strain R265. In the primary screen, each compound was tested once at 10 µg/mL and once at 40 µg/mL using 96-well flat-bottom microtitre plates. Amphotericin B was included as a standard antifungal control. Untreated cells and broth-only controls were also included. Cell suspensions of *C. deuterogattii* strain R265 were prepared following the reference methods of the Clinical and Laboratory Standards Institute (CLSI) for broth dilution antifungal susceptibility testing of yeasts [182]. Briefly, an isolated colony of *C. deuterogattii* strain R265 from a 2-day old plate was inoculated into 1 mL of Yeast Nitrogen Broth (YNB; Sigma Aldrich, pH 7). A working cell suspension was prepared at 1 x 10^6 – 5 x 10^6 cells/mL by cell counting using a haemocytometer, and was diluted 1:100. Final cell concentrations were 0.5 x 10^3 – 2.5 x 10^3 cells/mL with a final volume of 200 µL per well. Plates were incubated at 37 °C (humidified) without agitation for 72 h. Initial 'hit' candidates were defined as compounds that visibly inhibited the growth of *C. deuterogattii.*

To identify compounds with the greatest potential for repurposing as novel antifungal agents, compounds that complied with the following were excluded from further assessment: i) compounds that were active only at concentrations greater than 10 µg/mL; ii) compounds that were known antineoplastic agents or had otherwise unwanted adverse profiles; and iii) currently established

antifungal agents or non-antifungal agents with antifungal activity that had already been described and assessed at the time of testing.

2.4.4 Broth microdilution test

The *in vitro* antifungal activities of 'hit' compounds were re-evaluated using the stocks supplied in the library as well as from independently sourced stocks, and testing was extended to additional pathogenic fungal species (Table 2.1 and 2.2). Drug compounds were serially diluted 2-fold in YNB medium (final concentrations: 0.078125 - 40 µg/mL). Amphotericin B was included as an antifungal control for reference. Niguldipine, a member of the same class of 1, 4 – dihydropyridines (CCB) that had been identified as a non-'hit' compound in the screen was included as a negative control for the CCB series. Fungal cell suspensions were prepared following the CLSI standard method for broth dilution antifungal susceptibility testing of yeasts [182] or filamentous fungi [183]. Plates were incubated without agitation at 35 °C or 37 °C (humidified) for 48 h for non-*Cryptococcus* species or 72 h for *Cryptococcus* species. The MIC was determined as the lowest drug concentration at which a compound visibly inhibited growth (100% for FLB, MEB, BEN, NIF, NISO, FELO, NIG, AMB and 5FC; 80% for FLC, ITZ and VRZ). To obtain the MFC, 30 µL from each dilution well at the MIC concentration and higher was spread onto SDA plates. The MFC was defined as the lowest drug concentration that yielded three or fewer colonies after 72 h incubation [184]. All microdilution assays were tested in technical duplicates with at least two biological replicates unless otherwise specified.

2.4.5 Checkerboard microdilution assay

Checkerboard assays determine the interaction between two drugs based on the fractional inhibitory concentration index (FICI) value. Interactions can be synergistic (FICI ≤ 0.5), additive/indifferent (0.5 < FICI ≤ 4) or antagonistic (FICI > 4) [147]. Briefly, drug A (flubendazole, mebendazole or benomyl) was serially diluted from 0.31 – 0.0024 µg/mL and aliquoted in a 96-well flat-bottom plate and combined with drug B that was serially diluted and aliquoted in the following concentration ranges: amphotericin B (2 – 0.016 µg/mL); fluconazole (32 – 0.25 µg/mL); itraconazole (2 – 0.016 µg/mL); voriconazole (2 – 0.016 µg/mL); 5-flucytosine (32 – 0.25 µg/mL).

FICI values were calculated as:

$$FICI = \frac{MIC\ drug\ A\ in\ combination}{MIC\ drug\ A\ alone} + \frac{MIC\ drug\ B\ in\ combination}{MIC\ drug\ B\ alone}$$

All drug combinations were tested against *C. deuterogattii* strain R265 and *C. neoformans* strain H99 as per CLSI guidelines. All plates were incubated at 37 °C and inhibition was read visually at 72 h.

2.4.6 Time-kill assay

C. neoformans strain H99 was grown overnight to exponential phase in YNB media, shaking at 37 °C 180 rpm. Cells were adjusted to 1 x 10^6 cells/mL using a haemocytometer and sub-cultured in fresh YNB media. Three hours post sub-culturing, two 50 mL aliquots were taken. One culture was not treated, while the other was treated with 0.06 μg/mL flubendazole (1.5 x MIC). Cultures were returned to the shaking incubator and monitored for cell growth at 2, 3, 4, 5, 6, 9 and 24 h post-treatment. At each time point, each culture was sampled in technical duplicates, serially diluted in milli-Q water and spread onto SDA plates. All plates were incubated at 37 °C and observed at 48 h and 72 h for viability counts.

2.5 Results

2.5.1 Primary drug screening identifies non-antifungal compounds with anti-cryptococcal activity

The preliminary screening of the Enzo library revealed a diverse variety of compounds that inhibited the growth of *C. deuterogattii* strain R265 (Figure 2.1; Supplementary Figure S1, Supplementary Table S1). A significant proportion (15%) of 'hits' from this initial screen were antineoplastic drugs. This antifungal affect may be attributed to the cytotoxic nature of these compounds since cryptococcal and humans cells are eukaryotic and may share cellular structures and processes that result in non-selective toxicity. For this reason, this group of drugs were not pursued as potential antifungal candidates. Using the selection criteria described in the methods section, 16 of the remaining compounds identified in the primary screen were short-listed for further evaluation by minimum inhibitory concentration (MIC) assays against *C. deuterogattii*. Antifungal activity was confirmed for ten compounds using drug stocks sourced from the library. The most potent compounds (MICs < 5 µg/mL) were aripiprazole, nisoldipine, oxatomide, flubendazole, nifedipine and anethole-trithione. Lack of commercial availability restricted further evaluation to flubendazole, an anthelmintic drug (Figure 2.2), and nisoldipine and nifedipine, which are antihypertensive calcium channel blockers (CCBs, Figure 2.3). Felodipine and niguldipine, which are CCBs structurally related to nifedipine and nisoldipine, were also included in the assay.

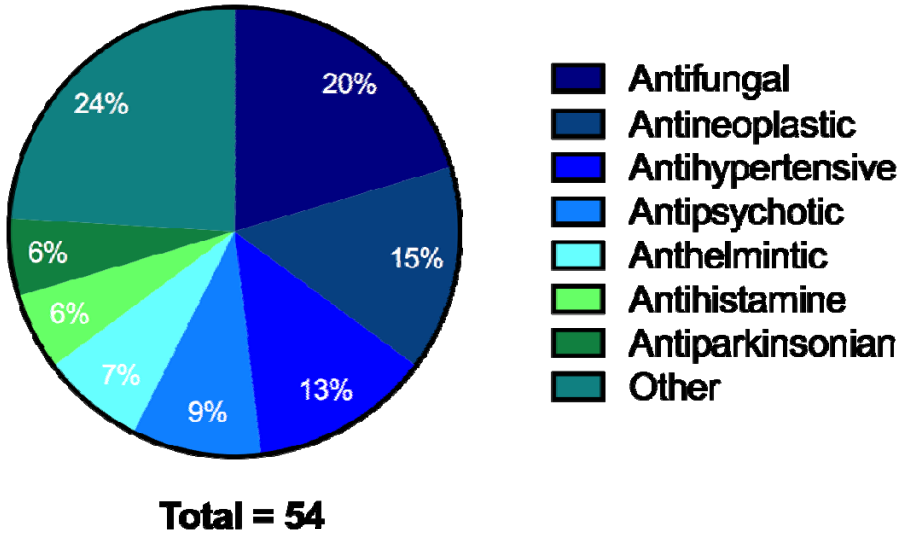

Figure 2.1. Pie chart of drug compound classes that inhibited the growth of *C. deuterogattii* strain R255 at 10 µg/mL.A total of 54 compounds inhibited the growth of *C. deuterogattii* strain R265 at 10 µg/mL. Classes of drugs included: antifungal (20%); antineoplastic (15%); antihypertensive (13%); antipsychotic (9%); anthelmintic (7%); antihistamine (6%); antiparkinsonian (6%); other (24%).

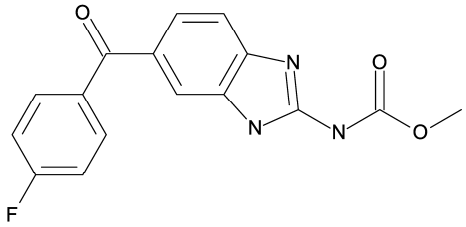

Figure 2.2. Chemical structure of flubendazole.Flubendazole was drawn with BIOVIA Draw 2017 R2 (Version 17.2; Dassault Systèmes, San Diego, CA, USA).

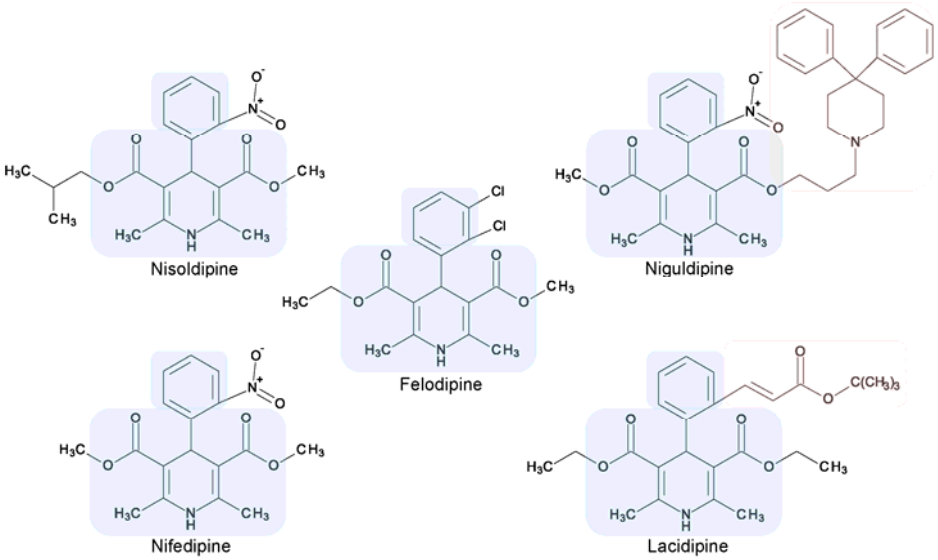

Figure 2.3. Chemical structures of 1,4-dihydropyridine calcium channel blockers: nisoldipine, nifedipine, felodipine, niguldipine and lacidipine.The core structure shared by members of the 1,4-dihydropyridine class is shaded in blue. Large side groups are shaded in pink. Chemical structures were drawn with BIOVIA Draw 2017 R2 (Version 17.2; Dassault Syste`mes, San Diego, CA, USA).

2.5.2 *In vitro* spectrum of antifungal activity of calcium channel blockers and flubendazole

To investigate the spectrum of antifungal activity, MICs were determined for nisoldipine, nifedipine, felodipine, niguldipine and flubendazole against nine additional strains from four fungal species (Table 2.1). MIC assays using independently sourced drug stocks confirmed the MICs established for *C. deuterogattii* strain R265 and demonstrated a diverse range of antifungal activities against other fungal strains and species (Table 2.1). Flubendazole was the most potent compound against *Cryptococcus* species with MICs as low as 0.078 µg/mL, but was ineffective even at the highest tested concentration (40 µg/mL) against other fungal species. The series of CCBs presented an interesting array of activities across the fungal species. Nifedipine demonstrated consistent antifungal activity

against the *Cryptococcus* species (5 – 10 μg/mL) and inhibited *Candida glabrata*, an emerging fungal pathogen, with an MIC of 20 μg/mL. In contrast, nisoldipine had higher and more variable MICs against different *Cryptococcus* species (5 – 40 μg/mL) and was the only drug that had activity against all nine fungal species. Niguldipine was not effective at the highest tested concentration against the fungal strains in this assay, while felodipine demonstrated activity against the *Cryptococcus* species with MICs between those of nifedipine and nisoldipine, but was only active against *Cryptococcus* species.

Table 2.1. Minimum inhibitory concentrations of flubendazole and a series of calcium channel blockers against *Cryptococcus, Saccharomyces, Candida* and *Aspergillus species*.

Genus	Species	Strain	MIC (μg/mL)[a]				
			FLB	NIF	NIG	FELO	NISO
Cryptococcus	*deuterogattii*	R265	0.078	10	>40	10 - 20	5 - 20
	gattii	WM179	0.078	5	>40	10	10 - 40
	tetragattii	M391	0.078	10	>40	≥20	40
	neoformans	H99	0.078	10	>40	10	20 - 40
Saccharomyces	*cerevisiae*	S288c	>40	≥40	>40	>40	10
Candida	*parapsilosis*	ATCC22019	>40	>40	>40	>40	20
	albicans	M23	>40	>40	>40	>40	40
	glabrata	M27	>40	20	>40	>40	10
	glabrata	M63	>40	20	>40	>40	10
Aspergillus	*fumigatus*	ATCC204305	>40	>40	>40	>40	10 - 20

[a] MICs obtained from four biological replicates each with technical duplicates. MIC ranges are given for compounds with variable results. MICs greater than 40 mg/mL (shaded in grey) indicate where an MIC was not obtained at the highest testing concentration. Flubendazole (FLB), nifedipine (NIF), niguldipine (NIG), felodipine (FELO), nisoldipine (NISO)Antifungal activities of Flubendazole.

To test whether flubendazole is broadly active across *Cryptococcus* species, we extended the study to encompass all members of the *C. gattii* species complex, as well as the major molecular genotypes of

C. neoformans (Table 2.2; Supplementary Table S2), including veterinary, clinical and environmental isolates from various geographic locations. Flubendazole inhibited all isolates of both *Cryptococcus* species at consistently low concentrations (MIC 0.039 – 0.156 µg/mL). Furthermore, for isolates where fluconazole MIC data were available, flubendazole was found to be equally effective regardless of fluconazole susceptibility (Table 2.2; Supplementary Table S2).

Table 2.2. Minimum inhibitory and minimum fungicidal concentrations of flubendazole against *Cryptococcus* species from varied sources.

Species (molecular genotype)	**Strain**	**Source**	**Geographic origin**[a]	**MIC (µg/mL)**		**MFC (µg/mL)**
				FLC[b]	**FLB**[c]	**FLB**[c]
C. gattii (VGI)	ENV316	Environmental	Australia		0.078	0.156
	PNG14	Clinical	Papua New Guinea		0.078	0.078
	2005/215	Clinical	France		0.078	0.078
	V15/571_103	Veterinary	Australia		0.078	0.078
	97/170	Clinical	France	64	0.078	0.078
	R265	Clinical	Canada	4	0.078	0.078
C. deuterogattii (VGII)	CBS1930	Veterinary	Aruba		0.078	0.078
	ICB184	Environmental	Brazil		0.039	0.039
	14.1431	Veterinary	Australia	32	0.039	0.078
	LA499	Clinical	Columbia	32	0.039	0.039
	V5	Veterinary	Australia	8	0.039	0.078
	03-201073	Clinical	Australia	16	0.078	0.078
C. bacillisporus (VGIII)	VBP62270	Veterinary	Australia		0.078	0.078
	97/427	Clinical	Mexico		0.156	0.313
	WM161	Environmental	USA		0.156	0.156
	B13C	Clinical	Asia		0.078	0.156
C. tetragattii (VGIV)	MMRL3013	Clinical	Africa		0.039 - 0.156	0.039 - 0.156
	M250	Clinical	Malawi		0.156	0.156

	WM779	Veterinary	South Africa		0.078	0.078
	MMRL2650	Clinical	India		0.039	0.078
C. neoformans (VNI)	1043.ENR.STOR	Clinical	Africa		0.078	0.156
	1020.CLIN1	Clinical	Africa		0.039	0.078
	H99	Clinical	USA	4	0.039	0.039
	WM625	Clinical	Australia	8	0.02	0.039
	WM385	Clinical	Thailand	4	0.039	0.039
C. neoformans (VNII)	1023.ENR	Clinical	Africa		0.039	0.078
	1045.ENR.STOR	Clinical	Africa		0.078	0.156
C. neoformans	1050.ENR.CLIN	Clinical	Africa		0.078	0.156
C. neoformans (VNBII)	1033.ENR	Clinical	Africa		0.039	0.078
	1052.ENR.STOR	Clinical	Africa		0.039	0.078
	1049.THER1.STOR	Clinical	Africa		0.039	0.039

[a] USA, United States of America; FLU, fluconazole. [b] FLC (fluconazole) MIC data obtained from Chong et al. (2010) and Lai et al. (2016). [c] FLB (flubendazole) MICs and MFCs are shown as modes from four biological replicates, each with technical duplicates. A concentration range is given where variable results were obtained.

To explore the inhibitory effect of flubendazole on *Cryptococcus* cells, cell viability was assessed using a time-kill assay and determining the minimum fungicidal concentration (MFC) in a microwell format. Analysis by time-kill curve over 24 h demonstrated that *Cryptococcus* cells exposed to flubendazole had slowly declining growth for up to 9 h post-treatment prior to loss of viability (Figure 2.4; Supplementary Table S3). Microbroth dilution assays generated MFC values that were similar to the respective MIC values (MFC 0.039 – 0.156 µg/mL; Table 2.2).

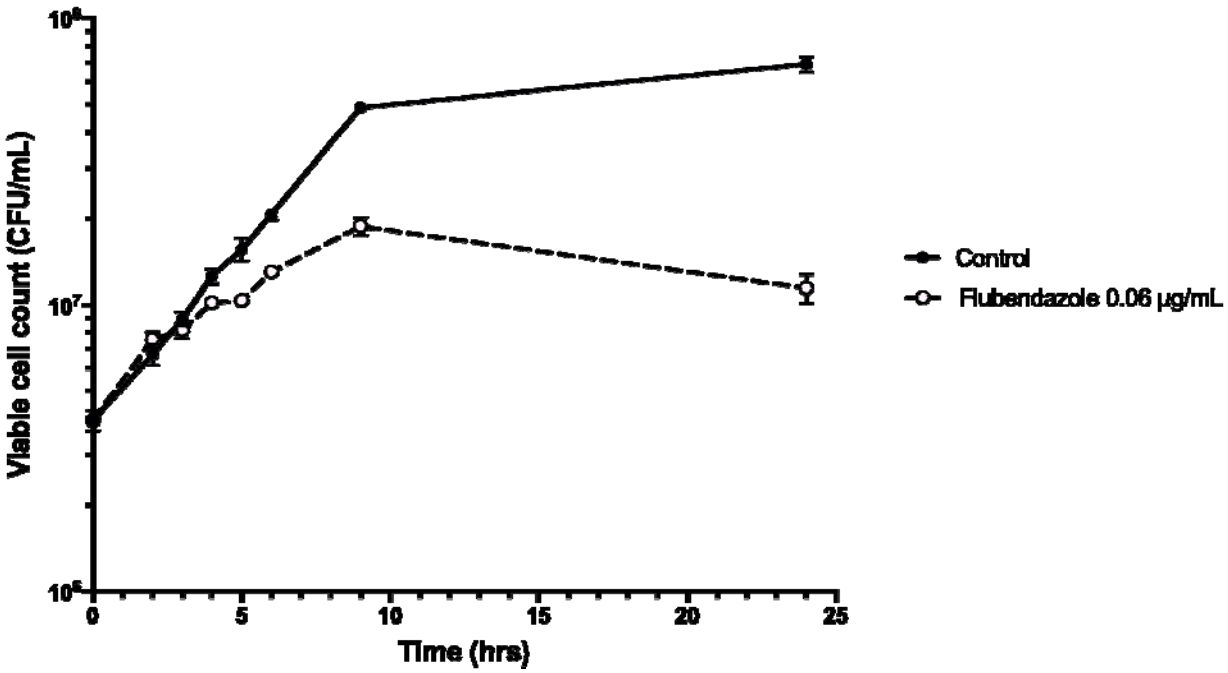

Figure 2.4. Time-kill assay of *C. neoformans* strain H99 treated with flubendazole.*C. neoformans* cells in logarithmic growth phase were treated with 0.06 mg/mL flubendazole and incubated at 37°C with shaking. The growth of treated cells tracked the untreated control cells for 3–4 h post-treatment and began to slow thereafter. Viability declined markedly by 9 h and did not recover by 24 h. Growth curve was generated using Prism 7 (Version 7.0b; GraphPad Software, La Jolla, CA, USA).

To explore interactions with current, commonly used antifungals, flubendazole and the other benzimidazole agents mebendazole and benomyl was tested in combination with amphotericin B,

fluconazole, itraconazole, voriconazole and 5-flucytosine against *C. deuterogattii* and *C. neoformans* in a checkerboard assay. All combinations produced additive/indifferent results and no synergistic or antagonistic interactions we seen (Table 2.3; Supplementary Table S4-5).

Table 2.3. Fractional inhibitory concentration index values of flubendazole, mebendazole and benomyl in combination with various antifungals against *C. neoformans* H99 and *C. deuterogattii* R265.

Cryptococcus **species**	**Benzimidazole**	**Fractional Inhibitory Concentration Index** [a]				
		AMB	**FLC**	**ITZ**	**VRZ**	**5FC**
C. neoformans H99	Flubendazole	(0.75 - 2)	(1.5 - 2)	(1.5 - 3)	(1 - 1.25)	2
	Mebendazole	(1 - 2)	1.5	(1 - 2.5)	(1 - 1.125)	(1.5 - 2)
	Benomyl	(0.75 - 1.5)	(1.25 - 1.5)	(1.25 - 1.5)	(0.75 - 1.125)	(1.25 - 1.5)
C. deuterogattii R265	Flubendazole	(1.5 - 3)	(2 - 3)	(1.5 - 2.5)	(1 - 1.5)	(1 – 1.5)
	Mebendazole	(1.5 - 2.5)	(1.5 - 2.5)	(1 - 2.5)	(0.75 - 1.5)	1.5
	Benomyl	(1 - 2.25)	(1.25 - 1.5)	(1.25 - 1.5)	(0.625 - 1)	(1 - 1.25)

[a] AMB, amphotericin B; FLC, fluconazole; ITZ, itraconazole; VRZ, voriconazole; 5FC, 5-flucytosine. Data shown were produced from two independent replicates

2.6 Discussion

Despite the major health problems caused by cryptococcal infections, there is a lack of new antifungal drugs. Promising, albeit limited, research has demonstrated the potential for repurposing drugs and the implications of this approach for treating cryptococcal infections have been highlighted [82, 106, 160, 161, 163, 164, 166]. Most studies have screened the Prestwick Chemical Library (n=1,120), the Library of Pharmaceutically Active Compounds (n=1,280) and the National Institutes of Health clinical collection (n=727). Within the last decade, these drug screening studies have led to the discovery of multiple non-antifungal compounds with antifungal activities, which were often novel and fungicidal [82, 106, 160, 161, 163, 164]. Some have demonstrated the ability to target intracellular *C. neoformans* in macrophages and cryptococcal biofilms and to act synergistically with the widely-used drug fluconazole [82, 106, 160, 161, 163, 164]. However, these studies have focused on *C. neoformans* with only one reporting on *C. deuterogattii* strain R265 [106]. There can be significant differences in target specificity among closely related genera and species of pathogenic yeasts [85, 106]. Thus, while *C. neoformans* and *C. deuterogattii* are sibling species, drugs may work differently between them. Here we report the first screening of a 640-compound FDA-approved library against *C. deuterogattii* strain R265*,* with subsequent testing of additional pathogenic cryptococci (encompassing an extensive list of *C. neoformans* species and the entire *C. gattii* species complex) and other fungi.

2.6.1 Repurposing calcium channel blockers as antifungal agents

Calcium channel blockers, widely used in the treatment of hypertension, are broadly divided into dihydropyridines and non-dihydropyridines classes [185]. Our screen identified nifedipine, felodipine and nisoldipine (Table 2.1 and Figure 2.3) as having antifungal activity against *Cryptococcus*. These are all 1, 4–dihydropyridines and therefore present as intriguing leads for a potential new class of antifungal drugs.

Members of the 1, 4–dihydropyridine CCB group share a core phenyl group attached to a 1, 4–dihydropyridine that has two ester side groups (Figure 2.3). Variations in side groups may account for the diverse antifungal activities observed, as compounds with the bulkier side groups (lacidipine and niguldipine) were ineffective against *C. deuterogattii*. Nifedipine, felodipine, nisoldipine and niguldipine target L-type calcium channels – one of 5 types of voltage-gated calcium channels (VGCCs) designated L-, N-, P/Q-, R- and T-type [185]. In the model yeast *Saccharomyces cerevisiae*, Cch1 and Mid1 are homologs of the mammalian VGCCs, and L-type CCBs are known to inhibit fungal growth via a Cch1-Mid1 protein channel complex located in the plasma membrane [186, 187]. Cch1 acts as the calcium channel and has homologs in almost all fungi, while Mid1 is a regulatory subunit that interacts

with Cch1 to mediate calcium influx [188]. Hence, it appears likely that the antifungal effects of CCBs involve the Cch1-Mid1 calcium channel.

Our findings support a growing body of evidence suggesting a crucial role of calcium regulation and calcium channels in determining the growth and survival of yeasts under stressful conditions [189-191]. In *C. neoformans*, Cch1 facilitates calcium entry with Mid1 when there is a depletion of intracellular calcium [189]. In the presence of the calcium chelator BAPTA, the growth of *Δcch1* mutants is markedly diminished at elevated temperature (25 – 38.5°C), a key virulence factor that is critical for human infection [190]. Cch1 and Mid1 also appear linked to the regulation of intracellular redox under cell stress, as *S. cerevisiae Δcch1* and *Δmid1* (single- and double-knockout) mutants are sensitive to cold stress (10°C) and iron toxicity due to a compromised ability to cope with oxidative stress [191]. Cell growth can be re-established following supplementation with either 10 mM calcium or reduced glutathione (an antioxidant), indicating that a functional Cch1-Mid1 complex is essential for stress tolerance [191].

As well as possessing antifungal properties, CCBs have also been shown to act synergistically with fluconazole against fluconazole-resistant and -susceptible strains of *C. albicans* [192]. Interestingly, CCBs alone or in combination with fluconazole do not significantly alter the gene expression level of *CCH1* and *MID1* [192] suggesting that either the cell is not sensing a disruption to calcium homeostasis, or CCBs act on targets other than calcium channels. Recently, a screen of the Prestwick Chemical Library® of FDA-approved small molecules identified fendiline hydrochloride, a non-dihydropyridine CCB, as having unique activity to potentiate phagosomal killing of intracellular *C. neoformans* in host macrophages [163]. Although it has a very different structure to the antifungal CCBs identified here, fendiline is an L-type CCB, suggesting this class of CCBs may be the most promising for antifungal drug development. Furthermore, the antifungal activity of L-type CCBs in combination with standard antifungals have been characterized in *C. albicans* and *Aspergillus* [192, 193]. As hypertensive agents, L-type CCBs are currently administered in long term use with relatively minimal side effects [194]. Of clinical relevance, some CCBs including nifedipine and nisoldipine can traverse the blood-brain barrier and may therefore be able to treat cryptococcal meningitis [195]. We therefore suggest L-type CCBs are promising leads for repurposing and redevelopment as potential new antifungal agents.

2.6.2 Repurposing flubendazole as an anti-cryptococcal agent

Flubendazole is an anthelmintic drug belonging to a family of benzimidazole carbamates. First introduced in 1980, it is currently used to treat parasitic gastrointestinal worm infections in humans and animals [196]. Flubendazole acts by binding to and inhibiting the polymerisation of tubulin, a cytoskeletal protein that polymerises to form microtubules [196-198]. Microtubules play major roles in various cell processes including division, motility, adhesion and intracellular transport [197]. Benzimidazoles have been found to act selectively against fungal tubulin and not mammalian tubulin, possibly due to differences in their β-tubulin sequence [198].

Benzimidazoles were originally developed as agricultural fungicides prior to their use as anthelmintic drugs, [199]. While the antifungal activities of benzimidazoles and their potential to be developed as anti-cryptococcal agents have been known for over two decades (Patent US5434163) [200-202], no further development as antifungal agents has occurred since 1998 [202]. Our study indicated that flubendazole is fungicidal at extremely low concentrations against *C. neoformans* and *C. deuterogattii* (Table 2.2). Our findings show that flubendazole equally inhibits pathogenic and environmental isolates of *Cryptococcus*, as well as strains that are resistant to fluconazole. This indicates that flubendazole may be an effective treatment against genetically and physiologically diverse *Cryptococcus* species and strains. As resistance to fluconazole is frequently induced during prolonged treatment and has been associated with clinical failure in *Cryptococcus*-infected patients [79, 91, 180], flubendazole may have promise as a second-line therapy when fluconazole fails, particularly in resource-poor regions where there are often no suitable alternatives.

Flubendazole interferes with normal cell growth as early as 3 hours post-treatment and continues to render treated *Cryptococcus* cells unviable (Figure 2.4), and in a microwell format with 72 h incubation the MFC values were either the same or one increment higher than the respective MIC values (Table 2.2). This indicates that flubendazole is a fungicidal drug, and with the correct clinical administration, it could effectively clear fungal burden. As high fungal burden is a strong determinant for mortality and overall poor clinical outcomes, and currently amphotericin B is the only fungicidal agent that is effective against cryptococcosis, this reinforces the potential utility of flubendazole as an anti-cryptococcal agent [180]. It is noted however, that unlike amphotericin B, flubendazole does not act synergistically with other standard antifungal agents, consistent with previously published data (Table 2.3) [164].

The current findings support a recent screening of 727 compounds in the National Institute of Health Clinical Collection [164]. Flubendazole and three related anti-helminthic benzimidazoles (mebendazole, albendazole and triclabendazole; sharing the benzimidazole scaffold) were among 17 compounds active against *C. neoformans* [164]. However, that study focused on mebendazole on the basis that the drug is able to penetrate the blood-brain barrier. Low MIC and MFC values were reported, and efficacy against biofilms and against cryptococcal cells internalized in macrophages were shown, along with additive activity when combined with amphotericin B [164]. Flubendazole may mirror the antifungal capabilities observed for mebendazole as they share structural similarities, and there is evidence that like mebendazole, flubendazole can traverse the blood-brain barrier [203] making these compounds favourable candidates for the treatment of cryptococcal meningitis. However, as flubendazole is formulated to treat gastrointestinal worms, it is not yet known whether it would be able to reach therapeutic concentrations in the brain required to elicit an antifungal effect.

The precise mechanism underlying the antifungal activity of flubendazole is unclear, however it is thought that it targets β-tubulin in *C. neoformans* [198]. The kill-curve demonstrated initial growth after treatment followed by declining viability and death at 9 hours, which is consistent with a mode of action that works by interfering with cell growth and division. In *Echinococcus granulosus*, a tapeworm parasite, flubendazole has been found to disrupt a wide spectrum of cellular homeostatic mechanisms, including energy metabolism and calcium homeostasis. In the latter it appears to increase cytosolic calcium from extracellular and intracellular stores [204], demonstrating an interesting overlap with the CCBs outlined above.

Overall, flubendazole (and more generally the benzimidazole scaffold) may be a promising starting point for the treatment of cryptococcal disease. This view is further encouraged by a lack of evidence of serious adverse side effects in patients undergoing anti-helminthic treatment and in mice experimentally treated with flubendazole [203, 205-207]. In preliminary cryptococcal meninigitis studies, flubendazole demonstrated fungicidal activity in a hollow fiber infection model and efficacy *in vivo*, reducing fungal burden in both a rabbit and mice model [208]. However, whether flubendazole can accumulate in the brain to concentrations that are clinically achievable and able to elicit an antifungal effect, and whether this can be sustained in the absence of adverse reactions, remains unknown and requires more extensive *in vivo* testing.

2.7 Conclusion and Perspectives

This study, and others like it, demonstrate the utility of drug repurposing to discover novel agents for the treatment of neglected diseases like cryptococcosis. L-type CCBs and anti-helminthic benzimidazoles have emerged in different drug screens and appear particularly promising as both are registered for use in other applications, are well tolerated and appear able to traverse the blood-brain barrier. Phenotypic screening approaches have repeatedly demonstrated utility, ensuring that identified drug candidates possess the desired phenotype of inhibiting growth of the pathogen prior to further mechanistic investigations. In addition to serendipitously finding a molecules or compounds that can be used directly in the clinic, repurposing strategies may identify related classes of compounds with activity and thus provide a scaffold for subsequent medicinal chemistry to initiate lead drug discovery programs.

Currently, it costs billions of dollars for a drug to successfully obtain FDA-approval and reach market. To help alleviate this financial risk and provide an incentive, there are moves by regulatory agencies in the United States and Europe to encourage academic and pharmaceutical research to bring new antimicrobials to market. For example, the GAIN Act (Generating Antibiotic Incentives Now) grants companies manufacturing a “qualified infectious disease product” an additional period of market exclusivity, with or without a patent, to ensure a better return on their investment. This applies to the repurposing of existing drugs with new indications, and should encourage pharmaceutical companies to develop some of these newly identified agents as therapeutics for fungal diseases, which are urgently required in global health.

Chapter 3: Profiling the transcriptional response of *C. neoformans* to flubendazole using RNA-Seq

3.1 Introduction

Flubendazole belongs to a family of benzimidazoles, which are anthelmintic agents commercially used to treat gastrointestinal worm infections in humans and animals. Benzimidazoles and their derivatives are known to be biologically active that target tubulin, with a diverse spectrum of applications including antimicrobial, anticancer and anti-inflammatory [196, 209-215]. The antifungal activity of flubendazole against *Cryptococcus*, identified in the previous chapter, is of particular interest as the number of effective drug options for antifungal therapy is critically limited. The antifungal properties of benzimidazole compounds have briefly been explored against *C. neoformans* previously, however flubendazole was not included in these studies and very little work has since been published [200]. Work from the previous chapter found the antifungal activity of flubendazole was quite specific to *Cryptococcus* spp. and there is evidence to support further studies into its antifungal activity [164, 208].

Tubulin is a cytoskeletal protein and the fundamental unit of microtubules. Comprised of α- and β-tubulin subunit monomers, tubulin polymerises to form hollow, cylindrical structures called microtubules (Figure 3.1) [197]. Microtubules are important cellular structures with functionally diverse roles in cell division, cellular infrastructure, intracellular transport and motility [197, 216, 217]. In *Saccharomyces cerevisiae*, tubulin subunits are encoded by four separate genes designated *TUB1-4*. *TUB1* and *TUB3* both encode α-tubulin monomers and *TUB2* encodes β-tubulin [218, 219]. While *TUB1* and *TUB3*, and their protein products, are highly homologous, only *TUB1* is essential for survival in *S. cerevisiae* suggesting that it may play a more critical role [219, 220]. *TUB2* encoding β-tubulin is also essential for function and survival [218]. Comparative analyses between *S. cerevisiae* and animal brain α- and β-tubulin revealed high amino acid sequence identity (71-74%) [218, 219]. In *C. neoformans*, β-tubulin is encoded by *TUB1* (CNAG_01840) and *TUB2* (CNAG_04948), with the former reportedly the main target of benzimidazole agents [198]. Similar to *S. cerevisiae, C. neoformans* strain H99 and human β-tubulin are also highly homologous (90% identity) [208]. A gene name has not been assigned for α-tubulin in *C. neoformans*, although CNAG_03787 is orthologous to α-tubulin-encoding *TUB1/TUB3* genes in *S. cerevisiae*. *TUB4* encodes the gamma tubulin protein, and while it does not form part of the microtubule structure, it is an essential component of the gamma-tubulin complex that is important for microtubule nucleation [221]. Microtubule nucleation is the initiation process that enables the polymerisation of tubulin into microtubule structures. This process is facilitated by the gamma-tubulin complex comprised of Tub4, Spc98 and Spc97, which forms a ring-like structure that serves as a platform on which tubulin heterodimers bind and grow [221, 222].

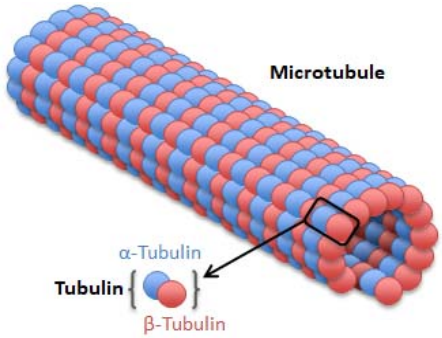

Figure 3.1. Schematic diagram of tubulin and microtubule composition.Microtubules are hollow cylindrical structures made up of tubulin heterodimers that consist of α- and β-tubulin subunit monomers. α- and β-tubulin are represented by blue and red circles, respectively.

The mechanism of action (MOA) underlying the antifungal activity of flubendazole is yet to be defined. Evidence from a number of human cancer cell line studies investigating the anti-cancer activity of flubendazole suggests the inhibition of microtubule activity may be involved [196, 210, 211, 223]. In agreement, a genetic study investigating the interaction between benzimidazoles and tubulin found that a single-point mutation in *C. neoformans TUB1* (encoding β-tubulin) lead to resistance in *C. neoformans* to albendazole (benzimidazole) [198]. More recently, however, a screening of the benzimidazole drug mebendazole against a library of *C. gattii* deletion strains suggested other targets (involved in membrane permeability, lipid metabolism and ribosomal biogenesis) may participate in mediating susceptibility [164]. While these studies provide some evidence and leads for further investigation, they are target-specific and do not reflect the dynamic biological response of *C. neoformans* to flubendazole.

Systems biology approaches, including transcriptomics and proteomics analyses, have been used to understand the biology of *Cryptococcus* challenged with various clinical and stress-inducing conditions [176, 224-226]. To date, few studies have employed these technologies to understand the biological response of *Cryptococcus* to antifungal agents [177, 178, 226]. Florio *et al*. 2011 investigated the adaptive response of *C. neoformans* to fluconazole and found increased expression of multiple genes involved in the ergosterol pathway, including *ERG11*, which was consistent with the known mechanism of action of fluconazole [177]. Pang *et al*. (2017) analysed the response of *S. cerevisiae* to the synergistic effect of amphotericin B and lactoferrin and found disturbances in metal ion homeostasis and a dysregulated stress response [178]. However, while these studies demonstrate the value of transcriptomic studies in providing a holistic insight on cellular responses they focused on a single time-point and could not portray dynamic changes. By sampling and analysing more than one time-point, cell dynamics can be captured across a time-course that covers how the cell responds,

adapts and is ultimately inhibited or killed by an antifungal agent. This approach has been used for *Cryptococcus* treatments, including a five-point time-course on hydrogen peroxide treatment, a three-point time-course with gamma radiation exposure, and another three-point time-course with fluconazole treatment [176, 225, 226]. Consistent across all studies, the number of differentially expressed genes, functional biological processes and translated proteins varied over time. The time-course design enabled the studies to observe unique protein networks and patterns of differential gene and protein expression over time; a global and dynamic response that may not have been achievable otherwise [176, 225, 226].

To investigate possible antifungal mechanism(s) of flubendazole against *C. neoformans*, the current chapter shows data from a systems-wide global approach to analyse changes in biological pathways and processes that are perturbed when *C. neoformans* cells are treated with flubendazole. As the mechanism of flubendazole is often associated with the inhibition of tubulin and the functioning of microtubules, this study hypothesises tubulin genes will be differentially expressed in the presence of flubendazole. In addition, as tubulin is functionally important for cell division, the dysregulation of tubulin (and subsequently the microtubules it forms), is anticipated to have down-stream or secondary affects within the cell, particularly on cell division genes.

3.2 Methods

3.2.1 Strains, culture and drugs

C. neoformans strain H99 was used for whole transcriptome shotgun sequencing (RNA-Seq) analyses. Cells were maintained in glycerol stocks stored at -80 °C and grown on sabouraud dextroase agar (SDA) for 48 h at 30 °C before use. Broth cultures were made using Yeast Nitrogen Base (YNB, pH 7; Sigma-Aldrich, St. Louis, MO, USA) and cultured at 37 °C in a shaking incubator at 180 rpm. Flubendazole (Sigma-Aldrich, St. Louis, MO, USA) was prepared to a stock solution of 2 mg/mL in dimethyl sulfoxide (DMSO).

3.2.2 Time-kill curve assay and experimental design

This protocol was performed similarly to that of Pang *et al*. (2017) with modifications [178]. *C. neoformans* strain H99 was subcultured onto SDA at 30 °C for 48 h. Overnight cultures were prepared in YNB and incubated with shaking at 37 °C, 180 rpm. After ~17 h, overnight cultures were subcultured into fresh YNB and adjusted to 5 x 10^6 cells/mL using a haemocytometer (total volume of 500 mL in a 1 L conical flask). Cultures were grown to exponential phase with shaking at 37 °C, 180 rpm, for 3 h prior to treatment. After 3 h, 200 mL of culture was aliquoted into 2 separate 500 mL Schott bottles and one culture was treated with flubendazole at 1 x MIC (0.04 µg/mL, Sigma-Aldrich). Cultures were incubated with shaking at 37 °C, 180 rpm. At 6, 8 and 12 h post-treatment, 7 mL of each culture was aliquoted into 15 mL Falcon tubes in triplicate. Each sample was centrifuged at 4 °C, 4000 rpm for 1 minute and snap-frozen in liquid nitrogen prior to freeze-drying overnight. All samples were stored at -80 °C until ready for RNA extraction.

Cell viability assays were also performed at each time point by collecting 500 µL culture aliquots (in duplicate) and mixing each aliquot with 4.5 mL of Milli-Q water. Serial dilutions of up to 10^{-5} were performed and 100 µL of each dilution was plated onto SDA and incubated at 37 °C for 72 h for viability count. Plates with 30 – 300 colonies were selected for counting. Three biological replicates of this experiment were performed on separate days and with fresh starter cultures.

3.2.3 RNA extraction and sequencing

Total RNA was isolated from approximately 200 µL of freeze-dried cells, using the Qiagen RNeasy Mini Kit (Qiagen, Hilden, Germany) with modifications [178]. In a sterile cryogenic tube, cells were disrupted by beating with 0.5 mm glass beads in a homogeniser at 5 000 rpm for a total of 2 min and cooled on ice after every 1 min of beating (Bertin Instruments, Minilys). Following this, 700 µL of lysis buffer was added to each tube, which was gently mixed and kept on ice. Tubes were then centrifuged in a desktop centrifuge at 4 °C for 3 minutes at 14 000 rpm to separate the sample from debris and

glass beads. The supernatant was transferred to a new Eppendorf tube and mixed with an equal volume of 70% ethanol. A 700 µL aliquot was then transferred to a Qiagen RNA spin-through column, which was centrifuged for 30 seconds at 14 000 rpm. The flow-through was discarded and the column was washed once with 700 µL RW1 buffer (Qiagen) and twice with 500 µL RPE buffer (Qiagen). Each wash was done by centrifugation for 30 seconds at 14 000 rpm, and flow-through discarded. The column was then transferred into a new 2 mL collection tube and spun dry for 2 minutes at 14 000 rpm. The tube containing eluate was then discarded and replaced with a new 1.5 mL Eppendorf tube. RNA was eluted by centrifugation with 50 µL of RNase-free water. A 3 – 5 µL aliquot was taken to assess RNA quantity and purity using a NanoDrop 1000 (version 3.6.0, Thermo Scientific, Waltham, MA, USA).

Total RNA was sent to the Ramaciotti Centre for Genomics (University of NSW, Sydney, Australia) for Illumina RNA sequencing, as per the submission guidelines of the sequencing centre. All samples were rescreened at the Ramaciotti Centre for quantity, purity and integrity using a Nanodrop and an Agilent B2200 TapeStation. TruSeq Stranded mRNA-seq sample preparation was completed for 18 samples. High output RNA-sequencing was performed using an Illumina NextSeq 500 to generate 75 bp paired-end reads.

3.2.4 RNA-Seq data processing

The data processing and analysis described in sections 3.2.4 and 3.2.5 were completed with the assistance of Dr. Ignatius Pang at the Ramaciotti Centre of Genomics (University of NSW, Sydney, Australia). Sequencing reads for all samples were assessed for quality using FastQC (version 0.10.1; www.bioinformatics.babraham.ac.uk/projects/fastqc). The *C. neoformans* var. *grubii* H99 CNA3 and mitochondrial reference genomes and genome annotations (Assembly 2, version 29/07/2013) from the Broad institute of Harvard and MIT (http://www.broadinstitute.org/) were used to map the reads. Read mapping was performed using HISAT2 (version 2.0.4) [227] with following settings: “hisat2 -p 6 --rna-strandness RF --known-splicesite-infile splicesites.txt -x $INDEX_DIR -1 ${job_name}_R1.fastq.gz -2 ${job_name}_R2.fastq.gz -S ${job_name}.sam”. The number of unique reads were calculated using the featureCount function of Subread (version 1.4.6) [228] and the *C. neoformans* var. grubii H99 CNA3 gene annotation GTF file. The following featureCounts settings were used: “featureCounts -s 2 -T 12 -p -a $GTF_FILE -t CDS -g gene_id -o ${job_name}_featurecounts.txt ${job_name}.sorted.bam”.

3.2.5 Analysis of Differential Gene Expression

Differential expression was analysed in *C. neoformans* cells following flubendazole treatment versus no treatment at 6 h, 8 h, and 12 h (determined from the growth curve assays performed above), with three biological replicates for each sample, totalling 18 samples. Genes with low raw read counts were removed and only genes with at least one read for at least nine samples were kept for analysis.

Biological variability between biological replicates were accounted for using edgeR [229, 230]. The edgeR tool calculates a trended dispersion for each individual gene. The average dispersion across all genes and samples determines the common dispersion, of which the square root calculates the biological coefficient of variation (BCV). The BCV indicates the degree of variability in expression values between biological replicates. Variability in sample replicates can also be assessed by multiple dimension scaling (MDS). Multiple dimension scaling is a graphical representation of distances between samples from which a level of similarly in read counts and reproducibility can be assessed. Samples that are similar to each other cluster closer together, while those that are not similar are positioned further apart. R software (version 3.4.4) and the edgeR library (version 3.20.9) were used to analyse the differential expression of genes [231]. The gene expression profiles for the 18 samples were normalised with respect to the library size and tag-wise biological coefficient of variation using edgeR.

Once gene expression profiles were normalised, the RUVSeq tool (version 1.10.0) was used to remove unwanted variation in the data [232]. Unwanted variations refer to variations or changes within the data that are caused by technical factors. Since these are not of biological significance or relevance, the removal of unwanted variations (RUV) between samples acts as a normalisation strategy to improve the quality of the RNA-Seq data prior to analysis [232]. To do this, the RUVs function and four unwanted factors (k=4) were used. The number of unwanted factors maximised the number of significantly differentially expressed genes for comparing flubendazole to control at 12 h, which was the comparison where the change in the transcriptome was found to be highest in this study. Statistically significant, differentially expressed genes were identified using edgeR and the Benjamini-Hochberg adjustment method [231]. The change in gene expression between two types of treatments was represented as a log fold-change (base 2). Genes with false discovery rate (FDR), also known as an adjusted p-value, of 0.05 or less were statistically significant.

Relative log expression (RLE) plots are graphical representation of data characterised by box-and-whiskers plots that compares the distribution of unwanted variations across multiple samples. It therefore is a useful tool to visualise both the degree of unwanted variation present among the samples of a RNA-Seq experiment and an assessment of the performance of RUV in improving the quality of data [233]. For every gene in one sample, the difference in expression levels with respect to the median expression of the corresponding gene across all samples was calculated to estimate the amount of unwanted variation. This was procedure was repeated for every sample to obtain the distribution of unwanted variations for all samples. All samples with a median value at zero and an interquartile range within -0.2 and 0.2 characterise a dataset of good quality with negligible effect from unwanted variations [234].

3.2.6 Gene Ontology Enrichment analysis

Gene Ontology (GO) enrichments were visualised as annotation networks using Cytoscape (version 3.6.0), and comprised genes that were significantly enriched from a hypergeometric distribution test and had been assigned to a functional annotation or GO term. On these networks, enriched genes sharing GO term annotations group together as nodes represented by circles [235], with the size of a node reflecting enrichment significance such that larger node size indicate smaller p-values. Nodes with similar gene annotations are connected by lines, known as edges. Nodes with similar GO terms form a cluster, where all nodes share the same colour. Within a cluster of nodes, the most significant (leading) term has the greatest percentage of significantly differentially expressed genes out of all genes annotated with the term. The leading term bolded to represent the whole cluster. Herein, genes described with significant differential expression refer to genes with a statistically significant increase or decrease in gene expression (adjusted p-value < 0.05), unless otherwise stated.

3.3 Results

3.3.1 Establishing conditions to sample flubendazole-treated *Cryptococcus neoformans*

To establish optimal sampling conditions for RNA-Seq, a kill-curve for *C. neoformans* strain H99 was constructed, monitoring the viability of cells treated with or without flubendazole over time (1 x MIC). Cells treated with flubendazole were affected by 3 h post-treatment and cell viability was irreversibly inhibited over the course of 48 hours (Figure 3.2). Cell viability was compromised post-treatment, with the viable cell count decreasing by 15% at 6 h, 22% at 8 h, and 44% at 12 h, relative to the untreated control at the same time points.

It was considered important to identify conditions in which flubendazole treatment had caused sufficient impact on cell viability so that relevant changes in gene expression could be detected, whilst avoiding the domination of general apoptotic pathways in the observed results. This minimises the presence of confounding effects of metabolic pathways unrelated to the specific antifungal mode of action of flubendazole (e.g. activation of gene expression of general apoptotic pathways) and allows for biologically important changes in expression to be identified. This consideration has been highlighted in a previous transcriptome study in *Cryptococcus* that harvested and analysed treated cells at 20% inhibition relative to control [178]. Thus, analysing cells at 6, 8, and 12 h may provide insights into the early, mid and late response of *Cryptococcus* to flubendazole before induction of an apoptotic response.

Establishing conditions to sample flubendazole-treated cells for RNA-Seq was a challenging and laborious process. This was largely due to variability in results in the absolute number of viable cells in any one culture at a specific time point, obtained via back-plating method, and required a series of trial-and-error attempts. Establishing sampling conditions based on a viable cell count at ~ 20% inhibition was considered important to avoid overriding apoptotic responses that may produce confounding effects when analysing the RNA-Seq data [178], however as the cells continued to grow following treatment before declining this point was often difficult to reproduce (Figure 3.2). Once the sampling conditions were established, RNA was extracted from *Cryptococcus* cells and assessed for quantity and quality. All samples were then sent to the Ramaciotti Centre for Genomics for Illumina sequencing.

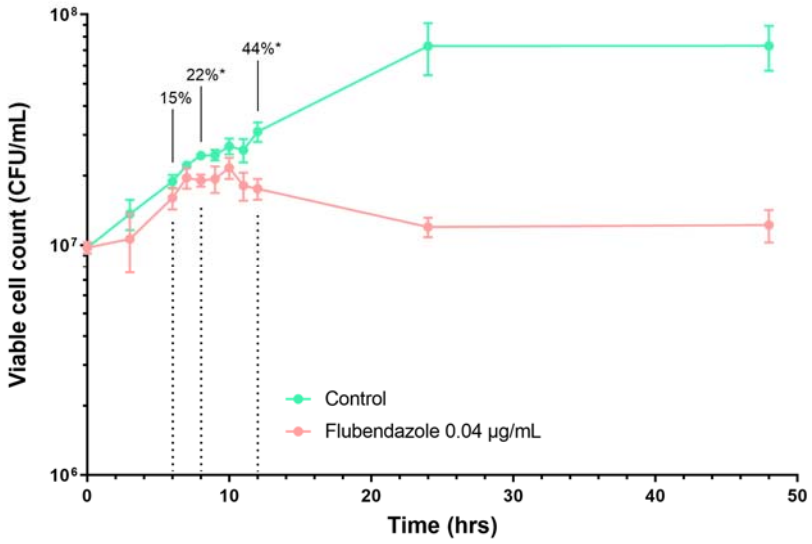

Figure 3.2. The effect of flubendazole on the growth of *C. neoformans* strain H99 over 48 h.Flubendazole treatment (0.04 µg/mL) irreversibly disrupts normal cell growth around 3 h post-treatment. At 6, 8 and 12 h post-treatment, cells were inhibited by 15% (p-value = 0.2483), 22% (p-value = 0.0175) and 44% (p-value = 0.00189), respectively. These time-points were selected for RNA-Seq analysis as they represented a time-course series where the response to drug treatment was at the early-mid stage and was not anticipated to be overwhelmed by cellular apoptosis. The green and red lines indicate untreated and treated cultures, respectively. Each time-point represents the average of three independent biological replicates with technical duplicates. Error bars represent the standard error of the mean. Asterisks indicate where p-values were < 0.05.

3.3.2 Data analysis rationale to identify significantly differentially expressed genes

In a previous study, Chong *et al*. (2012) analysed the global cellular response of *C. gattii* to fluconazole using a three time-point series [226]. The time-course design employed in their study enabled the analysis of changes in differential expression of proteins in fluconazole-treated cells, which led to the identification of potential proteins and pathways that could be targeted to improve the antifungal activity of fluconazole [226]. To understand the antifungal mechanism of flubendazole on *C. neoformans*, the current study adopted a transcriptomic approach using a similar experimental design, with the aim of assessing changes due to disruption of homeostasis and the dynamics of the cellular stress response. To enable this, the expression data acquired from RNA-Seq was analysed in two ways as shown in Figure 3.3. To observe changes in the transcriptome at each sampled time point, differential expression data from flubendazole treatment groups were compared to respective controls groups at each time point (Figure 3.3; Flubendazole vs Control). To view the global changes in gene transcript expression over the time-course period, treatment groups alone were compared between time points (Figure 3.3; Flubendazole-only).

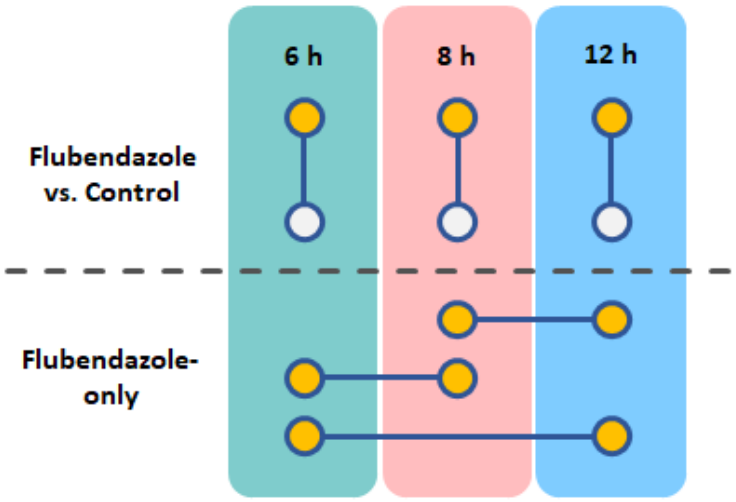

Figure 3.3. Schematic diagram of time-course analysis.The transcriptome of *C. neoformans* was analysed at 6, 8 and 12 h post-treatment with flubendazole. Test groups were analysed between treatment (flubendazole) versus control groups at each individual time point (upper panel), and treatment–only groups between time points (lower panel). Treatment (flubendazole) and controls groups are represented by orange and white circles, respectively.

3.3.3 Analysis of RNA-Seq data

3.3.3.1. Data quality control and removal of unwanted variation

Initial analysis of the RNA-Seq data using the software FastQC produced Phred scores which reflect the probability of error for a given nucleotide or base call. All samples had an average Phred score of 30 or greater, indicating good quality Illumina data (>99.9% base call accuracy). There were on average 26 million reads per sample with a median coverage of approximately 205x. Biological variability between biological replicates was investigated using edgeR and the results are shown in Figures 3.4 and 3.5. Figure 3.4 shows the trended dispersion for each individual gene. The common (average) dispersion of the RNA-Seq data across all genes and samples was 0.019. The square root of this value calculates the average biological coefficient of variation (BCV) of 0.14. This indicates that the expression value of a gene varies by 14% between biological replicates. This outcome indicates low variability between biological replicates and is consistent with a published yeast transcriptome study (BCV = 0.0987) [178].

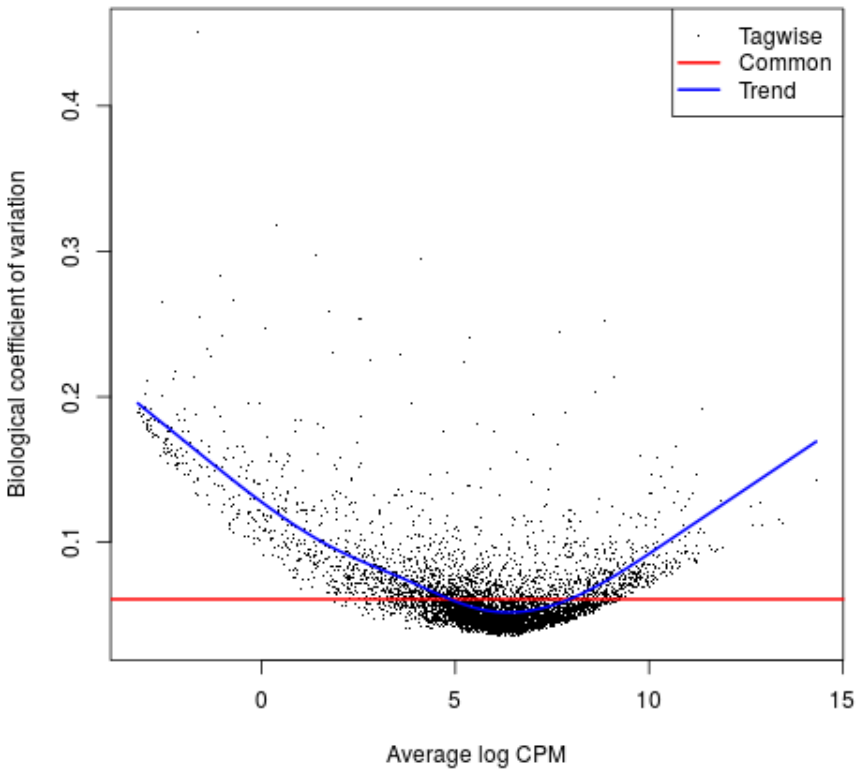

Figure 3.4. Plot of biological coefficient of variation versus average expression of RNA-Seq data.The plot shows the biological coefficient of variation (y-axis) and the average $\log_2$ counts per million (CPM; x-axis) for RNA-Seq samples. Each data point represents the tag-wise dispersion for each gene. The common dispersion of all genes (0.019), and the trended dispersion are indicated by the red and blue lines respectively. The average biological coefficient of variation of the RNA-Seq data is 0.14.

The removal of unwanted variation (RUV) made significant improvements to the quality of the RNA-Seq data prior to analysis (Figure 3.5A-D). Prior to RUV, relative log expression (RLE) plots revealed heterogeneity across all samples, characterised by dissimilar medians and variable interquartile ranges (Figure 3.5A). RUV resulted in consistent medians that were close to zero and interquartile ranges that were within -0.2 and 0.2 for almost all samples (Figure 3.5B). These plots suggest the presence of batch effects that may skew the interpretation of the RNA-Seq data, and these were effectively removed after applying RUV. Similar results were observed in MDS plots before and after the application of RUV. MDS plots originally showed poor clustering or grouping of biological replicates from the same experimental condition, with significant overlap between biological replicates from different experimental conditions (Figure 3.5C). This may be due to the presence of batch effects or unwanted variation. However, after the reduction of batch effects with RUV, clustering of biological replicates from the same experimental condition were significantly improved and occupied more distinct regions from other groups (Figure 3.5D).

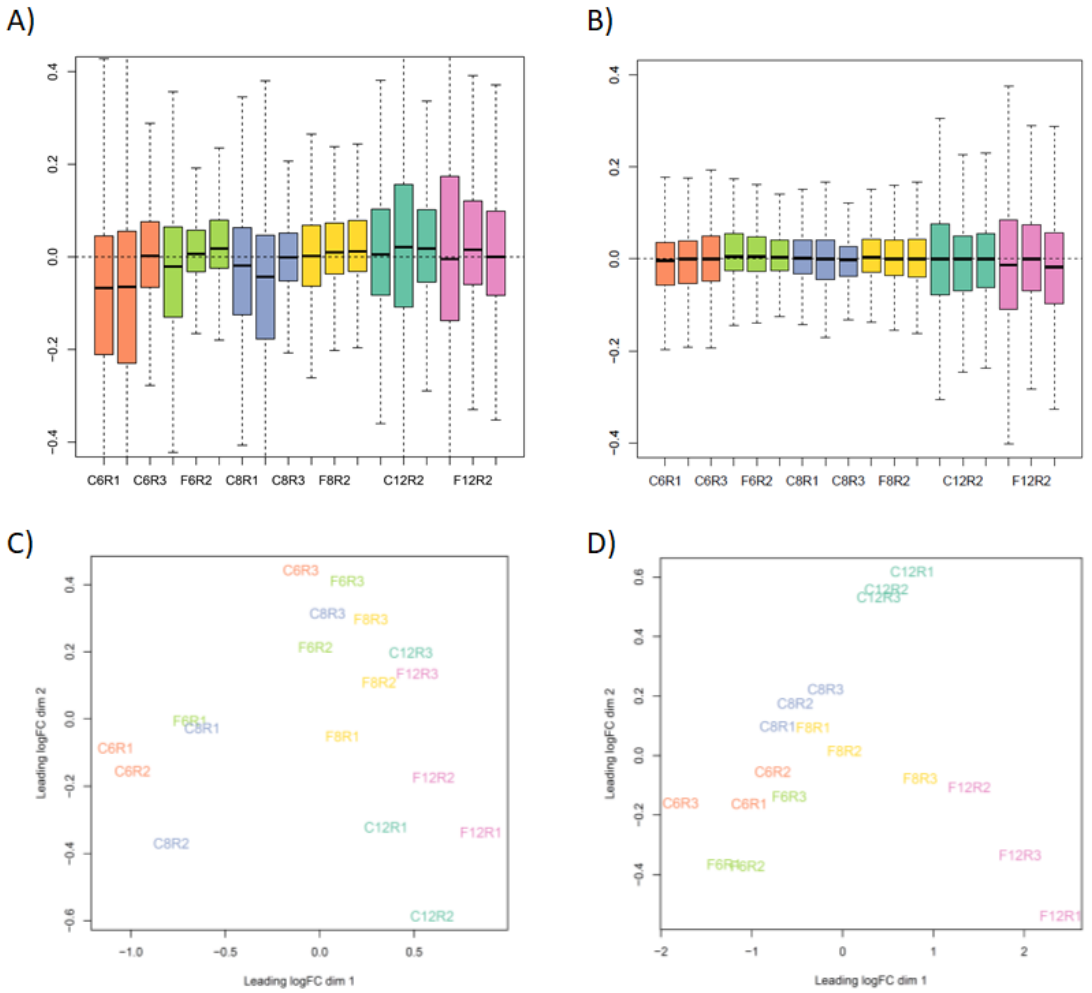

Figure 3.5. Removal of unwanted variation improves consistency of Relative Log Expression (RLE) plots and clustering via multiple dimensional scaling (MDS).

(A-B) RLE plots before (A) and after (B) removal of unwanted variation. The plots show the distribution of the estimated unwanted variation across all genes (y-axis) in each of the 18 samples (x-axis). From left to right, biological replicates of each sample were arranged as control and treatment samples at 6 h, followed by those at 8h and 12 h. All samples were labelled such that the experimental conditions would be identified. The first letter identifies a control (C) or flubendazole-treated (F) sample. The number that follows indicates the time-point (hour) the sample was taken (6, 8 or 12). The ending letter and number represents the biological replicate (R1, R2, and R3). For visualisation purposes, biological replicates from the same experimental treatment or control group have been coloured the same. Initially, variability in median values and interquartile ranges was evident in samples. After applying RUV, variability among samples was improved. (C-D) MDS plots before (C) and after (D) removal of unwanted variation. Before RUV, MDS demonstrated poor clustering of biological replicates of the same experimental treatment and there were areas of significant overlap among biological replicates from different experimental treatments. Post-RUV, biological replicates of the same experimental treatment were grouped closer together and occupied more distinct regions. The colouring and labelling of samples are consistent with those used for the RLE plots.

3.3.3.2. Identification of differentially expressed genes in response to flubendazole treatment

Gene expression analysis using R software and the edgeR library found genes were significantly differentially expressed (adjusted p-value < 0.05) over a time-course series of 6, 8 and 12 h post-treatment with flubendazole in comparison to control groups. At 6 h post-treatment, 12 genes showed significant differential expression compared to controls (Table 3.1), with nine increased and three decreased in expression. At 8 h post-treatment, the expression of 57 genes was significantly increased, while the expression of 41 genes was significantly decreased. The greatest number of significantly differentially expressed genes was at 12 h post-treatment, with 1163 genes with increased transcripts and 1151 genes with decreased transcripts relative to controls. The results show a clear progression in the transcriptomic response to flubendazole over time, as could be expected. However, consistent with the growth curve (Figure 3.2) this effect took some time to develop, and at earlier time points the treated cells showed transcriptomic profiles very similar to controls. Therefore, further analysis focussed predominantly on flubendazole versus control at 12 h. When flubendazole-only treatments between different time points were compared, the greatest number of differentially expressed genes occurred between 6 and 12 h (n = 1776) and 8 and 12 h (n = 1431). The substantially greater number of genes differentially expressed in the last time-point suggests the greatest amount of change may be observed in the last time point.

Table 3.1. Number of differentially expressed genes across different test groups (adjusted p-value < 0.05).

	Number of differentially expressed genes (number of hypothetical genes)		
	Increased	**Decreased**	**Total**
FLBvsCTRL[1] at individual time points			
FLBvsCTRL. 6h	9 (5)	3 (0)	12 (5)
FLBvsCTRL. 8h	57 (22)	41 (20)	98 (42)
FLBvsCTRL. 12h	1163 (390)	1151 (491)	2314 (881)
FLB-only between time points			
FLB. 6h - FLB. 8h (FLB.6-8h)	26 (14)	33 (14)	59 (28)
FLB. 12h - FLB. 8h (FLB.12-8h)	721 (268)	710 (278)	1431 (546)
FLB. 12h - FLB. 6h (FLB.12-6h)	793 (323)	983 (385)	1776 (708)

[1] FLB, flubendazole; CTRL, control.

Interestingly, hypothetical or uncharacterised genes comprised a substantial proportion of the differentially expressed genes. Thirty-eight percent of the total number of genes differentially expressed in at 12 h comparing flubendazole treated and untreated cells (FLBvsCTRL.12h) were identified as hypothetical or uncharacterised. Of the list of differentially expressed genes, many of the genes with the greatest log fold-change (greater than ± 1) were also hypothetical (Table 3.2). To explore these hypothetical genes, the top 10 genes with the greatest increase or decrease in log fold-change at 12 h were tested for the presence of conserved domains using the National Center for Biotechnology Information (NCBI) protein BLAST function. A total of eight genes were identified with conserved domains, half of which were specific hits (Table 3.3). The greatest increase in differential expression was for hypothetical gene CNAG_02300 (log FC 1.78). A BLAST search of its protein sequence found a domain with conserved homology to a Kelch motif, which is largely involved with the cytoskeletal element actin, and affects cellular growth and morphology [236-241]. The greatest decrease in differential expression was for hypothetical gene CNAG_01656 (log FC -0.89). A BLAST search of its protein sequence found a domain with conserved homology to ESCO1/2 acetyl-transferase, which is involved in chromosome segregation and microtubule stability [242-246].

Table 3.2. List of genes with greater than one log fold-change in differential expression in response to flubendazole at 12 h (FLBvsCTRL.12h).

Gene ID	logFC[1]	FDR[2]	Broad gene description
Increased expression			
CNAG_03107	4.427297	0.029561	hypothetical protein
CNAG_06854	4.239344	0.000624	hypothetical protein
CNAG_01368	2.811095	3.05E-06	hypothetical protein
CNAG_00813	2.55758	0.015835	hypothetical protein
CNAG_09000	2.216988	0.002963	NADH dehydrogenase subunit 1
CNAG_02300	1.780102	2.31E-19	hypothetical protein
CNAG_02544	1.753308	1.40E-09	DNA repair protein Swi5/Sae3
CNAG_04245	1.677958	8.54E-13	chitinase
CNAG_04183	1.60493	7.04E-13	hypothetical protein
CNAG_01995	1.513288	5.32E-06	hypothetical protein
CNAG_06205	1.439793	3.83E-23	hypothetical protein
CNAG_03516	1.369735	9.04E-17	hypothetical protein
CNAG_04459	1.349898	1.06E-05	hypothetical protein
CNAG_07711	1.348842	0.002522	hypothetical protein
CNAG_05660	1.295456	3.91E-18	hypothetical protein
CNAG_04687	1.216957	1.14E-11	stearoyl-CoA desaturase (delta-9 desaturase)
CNAG_02031	1.172913	0.039253	hypothetical protein
CNAG_02984	1.162191	0.019745	sarcosine oxidase
CNAG_02850	1.145798	2.44E-11	glucan endo-1,3-alpha-glucosidase agn1
CNAG_00295	1.126987	0.018471	hypothetical protein
CNAG_02701	1.119983	0.002236	hypothetical protein
CNAG_06853	1.116613	1.91E-13	hypothetical protein
CNAG_05278	1.10479	0.000159	hypothetical protein
CNAG_07888	1.103707	3.52E-11	hypothetical protein
CNAG_00799	1.0825	1.13E-13	cellulase
CNAG_00854	1.081965	4.69E-10	C-8 sterol isomerase
Decreased expression			
CNAG_06745	-1.02573	2.00E-22	histone H3
CNAG_06298	-1.06789	0.000632	hypothetical protein
CNAG_02864	-1.85344	9.16E-12	hypothetical protein
CNAG_07306	-3.24017	0.01464	hypothetical protein
CNAG_07592	-3.28397	0.005319	hypothetical protein

[1] logFC: log fold-change. [2] FDR: false discovery rate (adjusted p-value < 0.05).

Table 3.3. Predicted conserved domain hits within 10 hypothetical genes with the greatest increase or decrease log fold-change at 12 h (FLBvsCTRL.12h)

Gene ID	logFC	Name	Accession	Description	Interval	E-value
CNAG_02300 *	1.780102	Kelch_5	pfam13854	Kelch motif	29-71	1.77E-03
CNAG_04183	1.60493	PRK14949	PRK14949	DNA polymerase III subunits gamma and tau; Provisional	651-952	7.94E-03
CNAG_06205 *	1.439793	DPBB_1	pfam03330	Lytic transglycolase	441-470	1.71E-05
CNAG_03516	1.369735	PHA03247	PHA03247	large tegument protein UL36; Provisional	401-667	2.17E-05
CNAG_01656 *	-0.8930734	Acetyltransf_13	pfam13880	ESCO1/2 acetyl-transferase	372-437	1.35E-17
CNAG_06296	-0.8625772	HSP9_HSP12	pfam04119	Heat shock protein 9/12	48-98	5.92E-03
CNAG_03363	-0.7303225	PRELI	pfam04707	PRELI-like family	21-197	2.35E-23
CNAG_03044 *	-0.7187131	HDc	cd00077	Metal dependent phosphohydrolases with conserved 'HD' motif	28-142	4.64E-04

All genes had an adjusted-p-value < 0.05. Genes with a specific hit are indicated with an asterisk. Genes without an asterisk returned a non-specific hit.

3.3.3.3. Further analysis of differential gene expression at 6 and 8 h post-treatment (FLBvsCTRL)

Very few genes were significantly differentially expressed comparing flubendazole treated and untreated cells at 6 h (FLBvsCTRL.6h; n = 12; Appendix Table S6.1.1). A ClueGO network analysis for this comparison found no significant GO terms, and the small number of genes may account for this observation. Differentially expressed genes of potential interest included CNAG_02300 (log FC 0.76), CNAG_00149 (log FC 0.53) and CNAG_01464 (log FC -0.91), which encode a hypothetical protein, NADPH dehydrogenase (ubiquinone) 1 alpha sub-complex 4 and nitric oxide dioxygenase respectively. A similar observation was found comparing flubendazole treated and untreated cells at 8 h (FLBvsCTRL.8h). Similar with the first time-point (6 h), a limited number of genes were significantly differentially expressed (n = 98, Appendix Table S6.1.2) which was not sufficient to generate significant GO terms. The greatest increase in transcript level was observed for CNAG_04245 (log FC 1.30) that encodes chitinase. Consistent with the previous time-point, hypothetical protein-encoding gene CNAG_02300 (log FC 1.14) had increased gene expression relative to untreated cells. The transcript levels for this gene was greater than that of the previous time-point suggesting an accumulative gene expression across time-points. In addition, a number of genes in the ergosterol biosynthesis pathway had increased gene expression. These included CNAG_00854 (log FC 0.58), CNAG_02830 (log FC 0.44), CNAG_0.2918 (log FC 0.39), which are homologous to *S. cerevisiae ERG2*, *ERG4* and *ERG10* respectively. Other differentially expressed genes of potential interest included CNAG_01023 (log FC 0.55), CNAG_07756 (log FC 0.50), CNAG_03453 (log FC 0.30) and CNAG_02566 (log FC 0.23). These are cell cycle-related genes homologous to cohesion subunit *SCC1*, APC/C activator *CDC20*, kinesin-like protein *KIP1* and transcription factor *FKH2* in *S. cerevisiae* respectively.

3.3.3.4. Gene Ontology enrichments of differentially expressed genes at 12 h post-treatment

The greatest number of significantly differentially expressed genes was observed at 12 h post-treatment comparing flubendazole-treated and control samples (Table 3.1). At this time point, the major functional groups with significantly decreased gene expression included mismatch repair, DNA conformation change, sister chromatid segregation, DNA replication, DNA metabolic process and organelle organisation. This suggests that the global impact of flubendazole includes DNA-related processes, and may reflect damage or stress-response effects. Major functional groups with significantly increased gene expression included nucleotide metabolic process, dicarboxylic acid metabolic process, organonitrogen compound biosynthetic process, and cellular detoxification (Figure 3.6). Other significantly differentially expressed genes were found functionally associated with the metabolic processing of organonitrogen compounds, organic acid and glutamine family amino acids

(Figure 3.6). Key findings of genes associated with some of these biological processes and their roles are depicted in Figure 3.7 and discussed in the following sections.

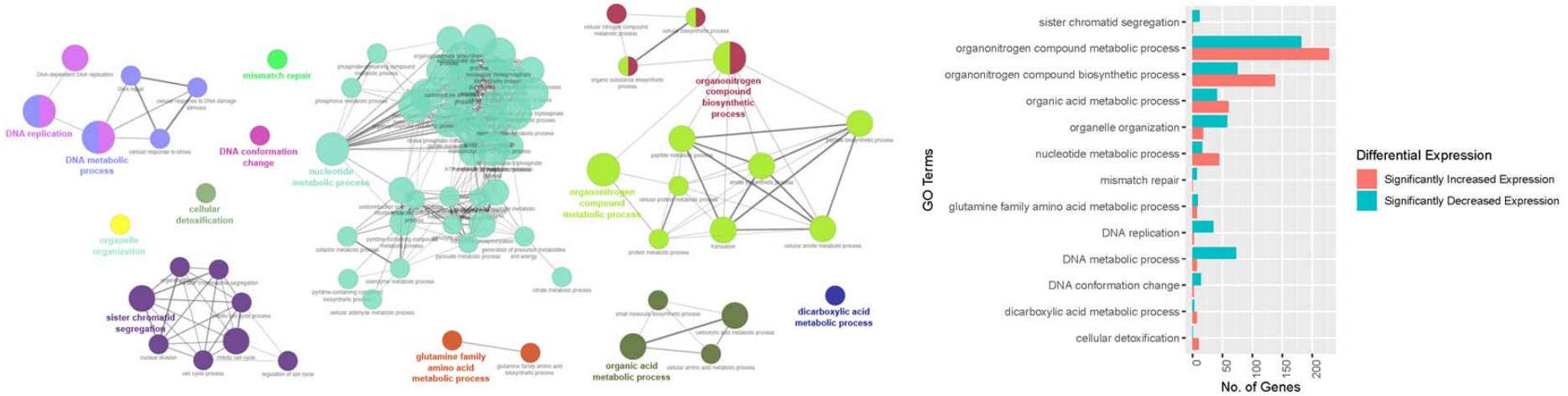

Figure 3.6. Gene Ontology (GO) network of enriched genes at 12 h post-treatment, comparing flubendazole-treated and control cells.GO terms are represented as circular nodes. Similar GO terms are coloured the same and a representative leading term for the functional group is bolded. Red and blue bars on the histogram show the number of differentially expressed genes (within leading GO terms) with significantly increased or decreased expression, respectively. Leading functional groups (bolded) included sister chromatid segregation, organonitrogen compound metabolic process, organonitrogen compound biosynthetic process, organic acid metabolic process, organelle organisation, nucleotide metabolic process, mismatch repair, glutamine family amino acid metabolic process, DNA replication, DNA metabolic process, DNA conformation change, dicarboxylic acid metabolic process and cellular detoxification.

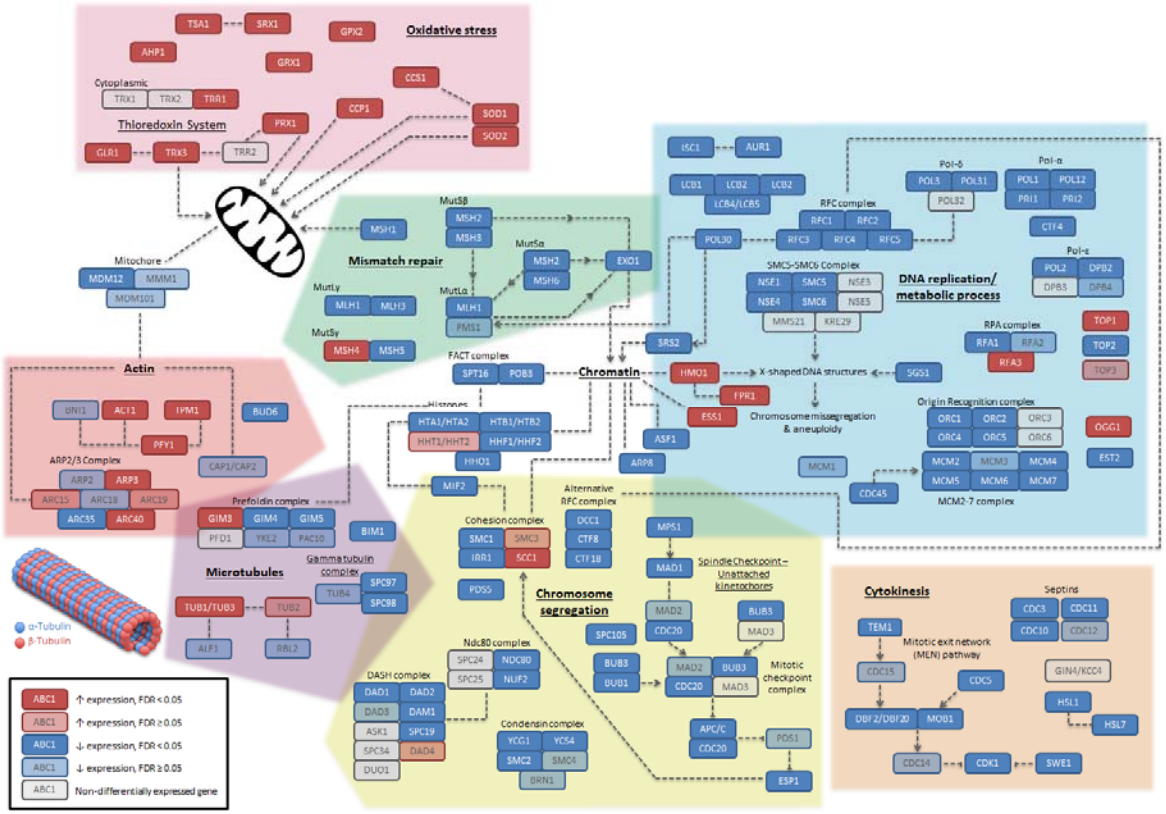

Figure 3.7. Schematic diagram of the expression of genes differentially expressed at 12 h comparing flubendazole treated and untreated cells (FLBvsCTRL).Genes are *Saccharomyces cerevisiae* orthologs represented as rectangular objects. Dark red or dark blue rectangular objects indicate genes with significantly increased or decreased expression (FDR < 0.05), respectively. Light red or light blue rectangular objects indicate genes that were not significantly differentially expressed (FDR > 0.05). Light grey rectangular objects indicate genes that were not differentially expressed in this dataset. Dash lines indicate some evidence of interaction based from published literature, with arrowheads indicating the direction of interaction where available. The expression data used to model this figure are listed in Appendix Table S6.1.5.

3.3.3.4.1. Expression of cytoskeletal genes alpha-tubulin and actin are significantly increased after flubendazole treatment

Figure 3.8 shows a schematic diagram of the expression of tubulin genes, actin and associated genes in response to flubendazole. The *TUB1/TUB3* genes encoding α-tubulin had significantly increased expression in response to flubendazole treatment at 12 h (CNAG_03787; Tubulin alpha-1 chain; Tubulin alpha-3 chain, log FC 0.39). The β-tubulin gene *TUB2* was also induced, although this was not statistically significant relative to the control (CNAG_01840; Tubulin beta chain, log FC 0.10). In contrast, the expression of *SPC97* (log FC -0.31) and *SPC98* (log FC -0.37), which encode two of three components of the gamma tubulin complex, was significantly decreased. Other cytoskeletal genes with decreased expression (albeit not statistically significant) included *TUB4*, and *ALF1* and *RBL1,* which encode tubulin-folding proteins. Decreased transcription of these genes may result in a lack of microtubule formation, which would likely lead to microtubule network dysfunction and disruption of microtubule-dependent biological processes such as chromosome segregation. Actin, encoded by *ACT1*, is another cytoskeletal element. *ACT1* and actin-binding proteins that promote actin nucleation and stability (*PFY1*, *TPM1* and subunits of the ARP2/3 complex) has significantly increased transcript levels in response to flubendazole.

3.3.3.4.2. Flubendazole influences the expression of genes related to cell cycle and cell division

Beyond the context of tubulin and microtubules, there is little literature that explores the peripheral and broader effects of flubendazole on other biological processes. In *C. neoformans*, genes involved in chromosome segregation, DNA replication and metabolism, mismatch repair and cytokinesis were differentially expressed, with significantly decreased transcript levels in the presence of flubendazole (Figure 3.9). These results indicate that cell cycle and cell division processes were perturbed and down regulated in the presence of flubendazole. The nature of this consequence however, being a primary or secondary effect of flubendazole remains unknown.

The spindle assembly checkpoint (SAC) is a mechanism by which mitotic progression is delayed to prevent the erroneous segregation of chromosomes when kinetochores are incorrectly attached to mitotic spindles [247, 248]. The expression of multiple genes in this pathway was significantly decreased, which suggests mitotic cell division and cell cycle progression may be disrupted with flubendazole treatment. Consistent with this idea, genes encoding protein complexes that affect chromosomes during cell division also had decreased expression. These included the cohesion complex, the alternative replication factor C complex, the Ndc80 complex and the condensin complex.

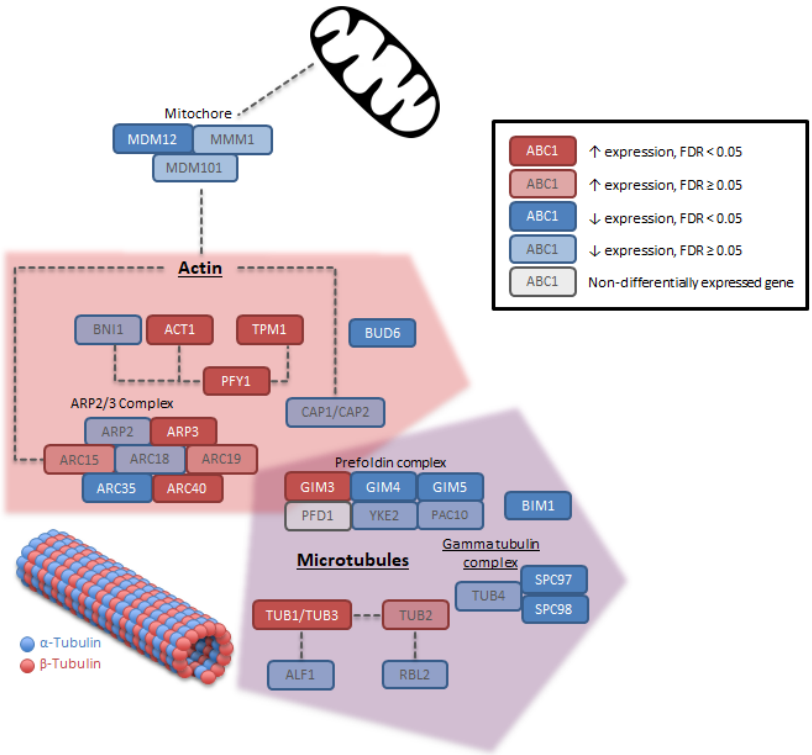

Figure 3.8. Schematic diagram of the expression of genes associated with tubulin and actin at 12 h (FLBvsCTRL).Genes are *Saccharomyces cerevisiae* orthologs represented as rectangular objects. Dark red or dark blue rectangular objects indicate genes with significantly increased or decreased expression (FDR < 0.05), respectively. Light red or light blue rectangular objects indicate genes that were not significantly differentially expressed (FDR > 0.05). Light grey rectangular objects indicate genes that were not differentially expressed in this dataset. Dash lines indicate some evidence of interaction based from published literature, with arrowheads indicating the direction of interaction where available. The expression data used to model this figure are listed in Appendix Table S6.1.5.

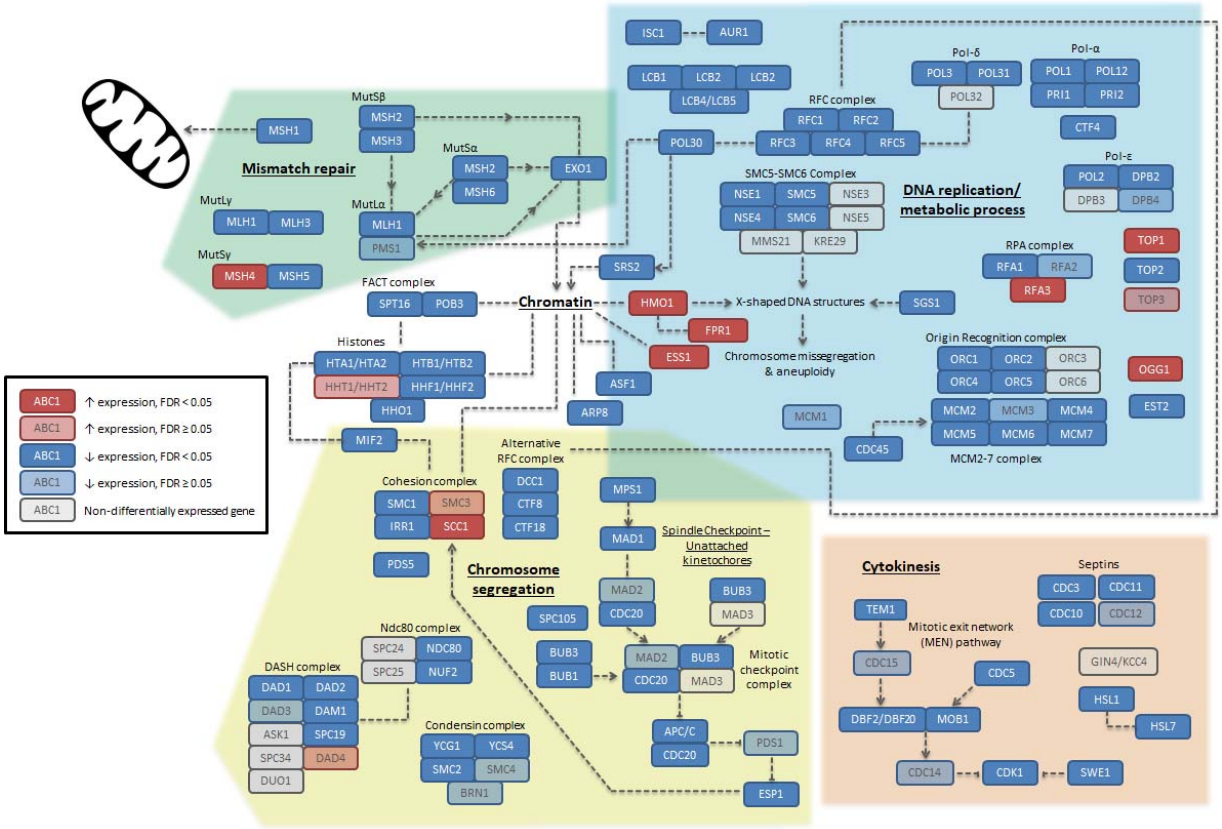

Figure 3.9. Schematic diagram of the expression of genes associated with cell division processes: chromosome segregation (yellow), DNA replication/metabolism (blue), mismatch repair (green), and cytokinesis (orange) at 12 h (FLBvsCTRL).Genes are *Saccharomyces cerevisiae* orthologs represented as rectangular objects. Dark red or dark blue rectangular objects indicate genes with significantly increased or decreased expression (FDR < 0.05), respectively. Light red or light blue rectangular objects indicate genes that were not significantly differentially expressed (FDR > 0.05). Light grey rectangular objects indicate genes that were not differentially expressed in this dataset. Dash lines indicate some evidence of interaction based from published literature, with arrowheads indicating the direction of interaction where available. The expression data and references used to model this figure are listed in Appendix Table S6.1.5.

The replication and metabolic processing of DNA are complex processes involving complex multi-protein machineries, many of which had significantly decreased transcript levels in response to flubendazole (Figure 3.9). This was evident for core histone genes and genes that encode the histone chaperone FACT (facilitators chromatin transcription) complex. These genes are associated with the assembly, disassembly and remodelling of chromatin and therefore have functional roles in the structural packaging of DNA [249]. These included the origin recognition complex and Mcm2-7 complex that together form part of the pre-replicative complex that is involved in the initiation of DNA replication; DNA polymerases Pol-α, Pol-ε and Pol-δ which synthesise DNA; the replication factor-C complex, which facilitates the functioning of the proliferating cell nuclear antigen (PCNA) Pol30, to enable the processivity of replicative DNA polymerases; and the replication protein-A complex, which

his important for genome stability. Other differentially expressed genes involved with DNA replication and metabolism include genes encoding the Smc5-Smc6 complex, which repairs X-shaped intermediate DNA structures [250]; DNA glycosylase *OGG1* and telomerase subunit *EST2* which have roles in telomere maintanence [251]; and DNA topoisomerases *TOP1*, *TOP2* and *TOP3.* DNA topoisomerases are important genes that maintain genome integrity by resolving the topology of DNA when structures such as DNA supercoils, catenanes and hemicatenanes occur [252].

Consistent with previously mentioned genes involved in DNA repair and maintaining genome integrity, the expression of mismatch repair genes were also significantly decreased in response to flubendazole. The mismatch repair system is a compensatory mechanism that corrects genomic errors incurred during DNA replication and recombination [253-255], dysregulation of which could lead to aberrant DNA mutations and abnormal phenotypes [254]. In yeasts, the mismatch repair genes correct errors in packaged DNA and maintain DNA stability [256]. The MutS homologs (MSH1-6) recognize mismatched DNA and initiate a mismatch repair response by recruiting MutL homologs (MLHs) to excise and correct the mismatch [255]. Flubendazole treatment resulted in a significant decrease in expression of genes that encode proteins in complexes that repair DNA mismatches (Figure 3.9). These include MSH1, MLH1, the MutSβ complex (MSH2 and MSH3), the MutSα complex (MSH2 and MSH6), and MutLγ complex (MLH1 and MSH3). Similarly, the expression of *EXO1*, an exonuclease required for proper functioning of mismatch repair [256-258], was decreased with flubendazole treatment.

Mitotic exit and cytokinesis are late stage mitotic events that result in the separation of a pair of mother-daughter budding cells. This occurs via the mitotic exit network (MEN) pathway, which begins with the activation of Tem1, and sequential activation of Cdc15 and Dbf2/Dbf20-Mob1 that enables the Cdc14-dependent inactivation of cell cycle cyclin-dependent kinase Cdk1 [259-261]. In *C. neoformans*, the prolonged exposure to flubendazole led to the decreased expression of these genes suggesting a down-regulation of the MEN signalling pathway and subsequent preclusion of cytokinesis. Septin proteins are essential for cytokinesis and in agreement with the decreased expression of MEN pathway genes, the transcript levels of septin genes and associated genes (*CDC3*, *CDC10*, *CDC11*, *HSL1* and *HSL1*; Figure 3.9; Appendix Table S6.1.5) were decreased following flubendazole treatment [262].

3.3.3.4.3. Flubendazole triggers stress-responsive genes in *C. neoformans*

Oxidative stress occurs when reaction oxygen species (ROS) accumulate above homeostatic levels and exceed the antioxidant capacity of a cell. Antioxidant enzymes exist to counter high levels of ROS, and include superoxide dismutases, catalase, glutathione peroxidases, thioredoxins, peroxiredoxin and glutathione transferases. In this study, prolonged treatment with flubendazole significantly induced the expression of stress-responsive genes at 12 h (Figure 3.10). These included *SOD1*, *SOD2*, *TSA1*, *AHP1*, *CCS1*, *PRX1*, *GPX2*, *TRR1*, *GLR1*, *TRX3* and *SRX1*. Increased transcripts of these genes at 12 h suggests prolonged exposure to flubendazole causes *Cryptococcus* cells stress.

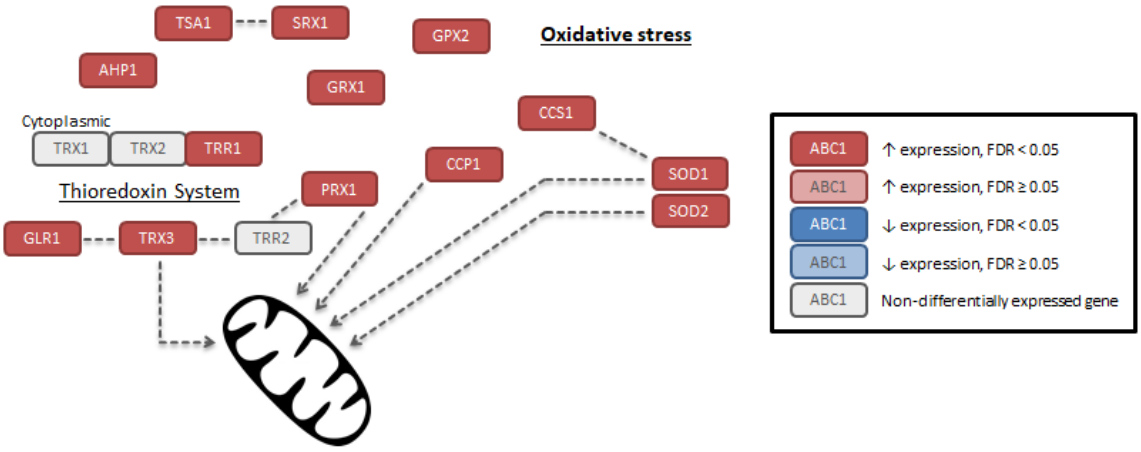

Figure 3.10. Schematic diagram of the expression of oxidative stress genes at 12 h (FLBvsCTRL).Genes are *Saccharomyces cerevisiae* orthologs represented as rectangular objects. Dark red or dark blue rectangular objects indicate genes with significantly increased or decreased expression (FDR < 0.05), respectively. Light red or light blue rectangular objects indicate genes that were not significantly differentially expressed (FDR > 0.05). Light grey rectangular objects indicate genes that were not differentially expressed in this dataset. Dash lines indicate some evidence of interaction based from published literature, with arrowheads indicating the direction of interaction where available. The expression data and references used to model this figure are listed in Appendix Table S6.1.5.

3.3.3.4.4. Antifungal efflux pumps and transporters are not differentially expressed with flubendazole treatment

Efflux pumps are mechanisms of adapting to drug treatment. They are a major contributor to antimicrobial resistance, and continue to be a challenge for antimicrobial drugs to overcome. Genes encoding some major azole efflux pumps in *C. neoformans* include ABC transporters *AFR1*, *AFR2, PDR11* and *MDR1* [263, 264]. The expression of these genes are known to increase in the presence of fluconazole [263]. While flubendazole and fluconazole are different drugs, belonging to different classes of drugs and possess different targets, it was interesting that this dataset reveals that most efflux pump genes were not significantly differential expressed even at the latest time point (Appendix Table S6.1.3). These results suggest that flubendazole has an antifungal mechanism of action unique to that of azoles, which target the ergosterol pathway.

3.3.3.5. Time-course study over 12 h treatment

To understand the transcriptional response of *Cryptococcus* to flubendazole in more detail, the progression of gene expression changes over time in flubendazole treated cells was analysed.

3.3.3.5.1. A comparison of flubendazole-treated cells at 6 and 8 h (FLB.8vs6)

The fewest number of significantly differentially expressed genes was observed comparing time-points 6 and 8 h (n = 59, Table 3.1). A ClueGO network analysis found no significant GO terms for this comparison, and the small number of genes may account for this. Despite this, a select few genes of potential interest were identified in this group (Appendix Table S6.1.4). Increased gene expression was observed for CNAG_07756 (log FC 0.38), CNAG_03453 (log FC 0.34), CNAG_03212 (log FC 0.23) and CNAG_05130 (log FC 0.29), which encode proteins orthologous to *CDC20*, kinesin-like protein *KIP1*, S-phase transcription factor *HCM1* and multidrug transporter *QDR3* in *S. cerevisiae* respectively (Appendix Table S6.1.1). In contrast, decreased gene expression was observed for CNAG_04351 (log FC -0.26) and CNAG_03215 (log FC -0.46), which encode proteins orthologous to NADPH oxidoreductase OYE2/OYE3 and multidrug transporter ADR1/QDR1/QDR2 in *S. cerevisiae* (Appendix Table S6.1.1). In addition, transcript levels were also significantly decreased for cytochrome p450 *ERG110*-encoding gene CNAG_05842 (log FC -0.38, Appendix Table S6.1.1), which has a role in the metabolism of toxic compounds including drugs and is homologous to *S. cerevisiae ERG11*.

3.3.3.5.2. A comparison of flubendazole-treated cells at 6 and 12 h (FLB.12vs6)

The greatest number of differentially expressed genes were observed by comparing treated cells between the time-points 6 and 12 h, and between 8 and 12 h (Table 3.1). Between 6 and 12 h post-treatment, enriched functional groups included cellular component assembly, carbohydrate metabolic process, carboxylic acid metabolic process, porphyrin-containing compound metabolic process, cofactor metabolic process and generation of precursor metabolites and energy (Figure 3.11A).

Multiple genes involved in glycolysis/gluconeogenesis, the pentose phosphate pathway, the tricarboxylic acid (TCA) cycle and glycoxylate cycle had significantly increased expression (Table 3.4). Up-regulation of these metabolic genes may suggest an increased demand for energy production in the presence of flubendazole. Presumably, the production of energy may then be geared towards other internal mechanisms to cope with the accumulated stress inflicted by flubendazole. In contrast, genes involved in the proline biosynthesis pathway (*PRO1, PRO2, PRO3*) had significantly decreased expression (Table 3.4). This may have potential significance in the stress response of Cryptococcus to flubendazole.

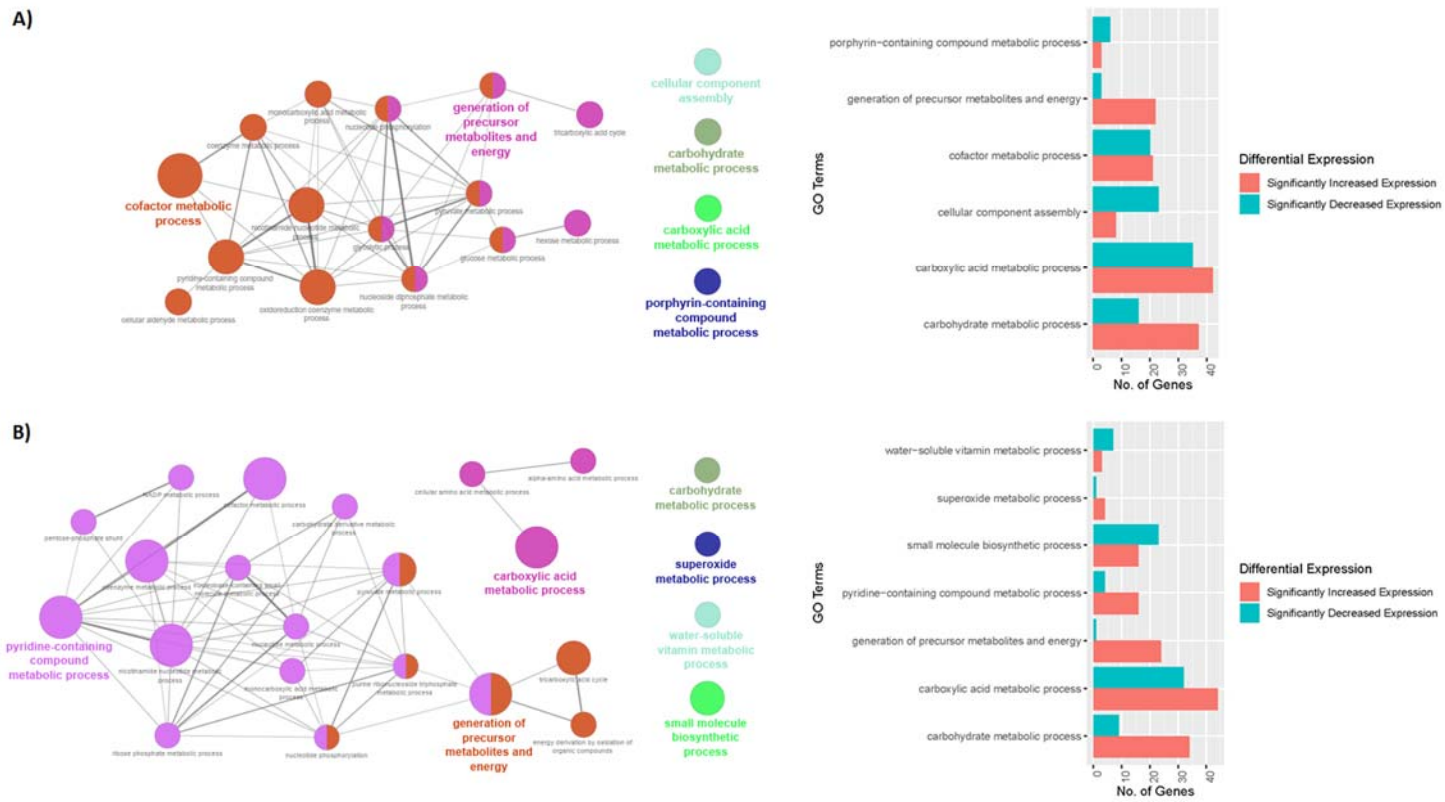

Figure 3.11. Gene ontology (GO) analysis comparing flubendazole-treated cells at over time.GO terms are represented as circular nodes. Similar GO terms are coloured the same and a representative leading term for the functional group is bolded. Red and blue bars on the histogram show the number of differentially expressed genes (within leading GO terms) with significantly increased or decreased expression, respectively. (A) ClueGO network comparing flubendazole-treated cells between 6 and 12 h. Leading functional groups (bolded) included cellular component assembly, carbohydrate metabolic process, carboxylic acid metabolic, porphyrin-containing compound metabolic process, cofactor metabolic process and generation of precursor metabolites and energy. (B) ClueGO network comparing flubendazole-treated cells between 8 and 12 h. Leading functional groups (bolded) include pyrimidine-containing compound metabolic process, generation of precursor metabolites and energy, carboxylic acid metabolic process, carbohydrate metabolic process, superoxide metabolic process, water-soluble vitamin metabolic process and small molecule biosynthetic process.

Table 3.4. List of metabolic pathways affected at FLB.12vs6h.

Gene ID	logFC[1]	FDR[2]	Broad gene name	Sc[3] ortholog	Sc ortholog descriptions
Glycolysis/gluconeogenesis					
CNAG_04523	1.98341616	9.17E-12	glyceraldehyde-3-phosphate		
CNAG_04217	1.31402615	0.001434721	phosphoenolpyruvate	PCK1	Phosphoenolpyruvate carboxykinase
CNAG_05907	1.11761023	1.11E-11	pyruvate carboxylase	PYC1; PYC2	Pyruvate carboxylase 1; Pyruvate
CNAG_06770	0.49590357	0.014360354	fructose-bisphosphate aldolase 1	FBA1	Fructose-bisphosphate aldolase
CNAG_00057	0.50497296	0.002568005	fructose-1,6-bisphosphatase I	FBP1	Fructose-1,6-bisphosphatase
CNAG_01820	0.4899635	0.000339764	pyruvate kinase	CDC19; PYK2	Pyruvate kinase 1; Pyruvate kinase 2
CNAG_06699	0.54628428	0.001573689	glyceraldehyde-3-phosphate	TDH1	Glyceraldehyde-3-phosphate
CNAG_03916	0.59551151	0.000112539	glucose-6-phosphate isomerase	PGI1	Glucose-6-phosphate isomerase
CNAG_03358	0.42481719	0.002568005	phosphoglycerate kinase	PGK1	Phosphoglycerate kinase
CNAG_07660	0.55101607	1.19E-05	pyruvate dehydrogenase (acetyl-	PDA1	Pyruvate dehydrogenase E1 component
CNAG_02035	0.55088125	0.000294605	triose-phosphate isomerase	TPI1	Triosephosphate isomerase
CNAG_03769	0.39155323	0.005404439	hexokinase	EMI2; GLK1	Putative glucokinase-2; Glucokinase-1
Tricarboxylic acid cycle and Glycoxylate cycle					
CNAG_03375	0.596191	5.77E-08	succinyl-CoA synthetase alpha	LSC1	Succinyl-CoA ligase [ADP-forming]
CNAG_00747	0.85300278	9.17E-12	succinyl-CoA synthetase beta	LSC2	Succinyl-CoA ligase [ADP-forming]
CNAG_03226	0.82253171	8.68E-06	succinate dehydrogenase	SDH2	Succinate dehydrogenase [ubiquinone]
CNAG_01137	0.8221159	0.004359205	aconitate hydratase, mitochondrial	ACO1; ACO2	Aconitate hydratase, mitochondrial
CNAG_07908	0.23852132	0.033225552	aconitate hydratase, mitochondrial	ACO1; ACO2	Aconitate hydratase, mitochondrial
CNAG_05653	0.74207873	6.60E-06	malate synthase A	DAL7; MLS1	Malate synthase 2, glyoxysomal; Malate
CNAG_01657	0.33108226	0.005905592	fumarate hydratase, mitochondrial	FUM1	Fumarate hydratase, mitochondrial
CNAG_03674	0.31371445	0.009999086	oxoglutarate dehydrogenase	KGD1	2-oxoglutarate dehydrogenase,
CNAG_07851	0.47249059	0.000493436	isocitrate dehydrogenase, NAD-	IDH1	Isocitrate dehydrogenase [NAD] subunit
CNAG_03225	0.50856725	0.000221723	malate dehydrogenase, NAD-	MDH1	Malate dehydrogenase, mitochondrial
CNAG_03920	0.74122112	1.72E-09	isocitrate dehydrogenase, NADP-	IDP1	Isocitrate dehydrogenase [NADP],

CNAG_05653	0.50819859	0.00479733	malate synthase A	DAL7; MLS1	Malate synthase 2, glyoxysomal; Malate
Pentose phosphate pathway					
CNAG_01984	0.588094923	0.001159296	transaldolase	TAL1	Transaldolase
CNAG_03245	0.296160644	0.029596519	glucose-6-phosphate	ZWF1	Glucose-6-phosphate 1-dehydrogenase
CNAG_07561	0.53117321	0.002867607	6-phosphogluconate	GND1; GND2	6-phosphogluconate dehydrogenase,
CNAG_00684	-	6.81E-06	ribulose-phosphate 3-epimerase	RPE1	Ribulose-phosphate 3-epimerase
Proline biosynthesis					
CNAG_05386	-0.2881819	0.002521994	glutamate 5-kinase	PRO1	Glutamate 5-kinase
CNAG_04990	-0.442841	7.89E-06	glutamate-5-semialdehyde	PRO2	Gamma-glutamyl phosphate reductase
CNAG_05899	-0.4738039	6.70E-05	pyrroline-5-carboxylate reductase	PRO3	Pyrroline-5-carboxylate reductase
CNAG_03542	-0.2597139	0.017922853	arginase	CAR1	Arginase
Heme biosynthesis and heme-related genes					
CNAG_00345	-0.2665688	0.005824485	porphobilinogen synthase	HEM2	Delta-aminolevulinic acid dehydratase
CNAG_02460	-0.2628937	0.01302673	coproporphyrinogen III oxidase	HEM13	Oxygen-dependent coproporphyrinogen-
CNAG_05809	-0.2790079	0.013282969	ferrochelatase	HEM15	Ferrochelatase, mitochondrial precursor
CNAG_03187	-0.294366	0.015232554	protoporphyrinogen oxidase	HEM14	Protoporphyrinogen oxidase
CNAG_06063	-0.3479572	0.038525146	cytochrome c oxidase assembly	COX15	Cytochrome c oxidase assembly protein
CNAG_03523	-0.2766122	0.049865922	solute carrier family 25, member	YDL119C	Solute carrier family 25 member 38
CNAG_06799	0.38244532	3.74E-06	uroporphyrinogen decarboxylase	HEM12	Uroporphyrinogen decarboxylase
CNAG_05852	0.48846207	1.91E-05	heme oxygenase 2		
CNAG_03939	0.38520475	0.006950214	5-aminolevulinic acid synthase	HEM1	5-aminolevulinate synthase,
Cellular component assembly					
CNAG_00318	-0.2714857	0.009979577	arp2/3 complex 16 kda subunit	ARC15	Actin-related protein 2/3 complex
CNAG_02094	-0.4159045	1.48E-05	arp2/3 complex 34 kda subunit	ARC35	Actin-related protein 2/3 complex
CNAG_04765	-0.3908976	2.17E-05	arp2/3 complex 21 kda subunit	ARC18	Actin-related protein 2/3 complex
CNAG_05246	-0.342871	0.000455225	hypothetical protein	AIM7	Protein AIM7

CNAG_03900	-0.3182539	0.003042787	capping protein (actin filament)	CAP2	F-actin-capping protein subunit beta
CNAG_01110	-0.2599159	0.026352538	co-chaperone	RBL2	Tubulin-specific chaperone A
CNAG_05927	-0.297567	0.005259219	ATP synthase mitochondrial F1	ATP11	Protein ATP11, mitochondrial precursor
CNAG_01818	-0.4245406	0.000504696	ATP synthase mitochondrial F1	ATP12	Protein ATP12, mitochondrial precursor
CNAG_04288	-0.4337426	0.001005516	Fe-S protein assembly co-	JAC1	J-type co-chaperone JAC1, mitochondrial
CNAG_05011	-0.2802166	0.031273765	iron donor protein CyaY	YFH1	Frataxin homolog, mitochondrial
CNAG_05626	-0.2538686	0.035134469	hypothetical protein	SCO1	Protein SCO1, mitochondrial precursor
CNAG_02792	-0.3627235	0.000199328	mitochondrial chaperone BCS1	BCS1	Mitochondrial chaperone BCS1

[1] logFC: log fold-change

[2] FDR: false discovery rate (adjusted p-value < 0.05)

[3] Sc: *Saccharomyces cerevisiae*

Comparing flubendazole-treated cells at 6 and 12 h, a number of actin-associated genes were differentially expressed. The expression of actin (*ACT1*) and the actin-nucleating formin gene *BNI1* were significantly increased, while the expression of actin-associated genes that inhibit actin polymerisation or nucleation (*CAP2* and *AIM7*) were significantly decreased. In contrast, ARP2/3 complex genes *ARC15*, *ARC18* and *ARC35*, which are involved in actin nucleation, had significantly decreased expression levels. These data may suggest that the actin dynamics, in the form of actin nucleation and debranching of actin filaments, are disturbed in the presence of flubendazole.

Genes encoding mitochondrial components also had decreased expression levels in flubendazole treated cells compared between 6 and 12 h (FLB.12vs6; Table 3.4). These include *BCS1*, *ATP11* and *ATP12* involved in the assembly of complex III and F1F0 ATP synthase; *SCO1*, a copper-binding protein involved in the assembly of cytochrome c oxidase; and *JAC1* and *YFH1,* which are involved in iron metabolism and the biogenesis or assembly of iron-sulfur (Fe-S) clusters in mitochondria. The significantly decreased expression of these genes suggests dampened mitochondrial functions in the presence of flubendazole. In addition to decreased expression of iron metabolism genes, genes involved in the biosynthesis of heme were significantly decreased in the presence of flubendazole. These included *COX15*, *HEM2*, *HEM25*, *HEM13*, *HEM14* and *HEM15* (Table 3.4). Heme is an iron-binding porphyrin compound and in yeast, influences the ability of pyruvate to induce mitochondrial respiration in response to structural changes to chromatin [265, 266]. These findings may suggest reduced iron metabolism and mitochondrial function.

3.3.3.5.3. A comparison of flubendazole-treated cells at 8 and 12 h (FLB.12vs8)

Gene ontology network analysis comparing flubendazole-treated cells at 8 and 12 h generated similar and unique functional groups to that of flubendazole-treated cells at 6 and 12 h (Figure 3.11). Leading GO terms within the FLB.12vs8 dataset included carbohydrate metabolic process, superoxide metabolic process, small molecule biosynthetic process, water-soluble vitamin metabolic process, organic acid metabolic process and pyrimidine-containing compounds metabolic process (Figure 3.11B). Consistent with the FLB.12vs6 dataset, expression of genes involved in glycolysis/gluconeogenesis, the TCA cycle and pentose phosphate pathway remained significantly increased. This suggests a sustained up-regulation in metabolic pathways to increase energy production in flubendazole-treated cells, which may be geared towards other internal mechanisms to cope with the damage and accumulated stress inflicted by flubendazole. Similarly, the expression of proline biosynthesis genes *PRO1-3* were also significantly decreased in this dataset. Unique to this dataset was the decreased expression of genes related to vitamin metabolic process, such as *BUD16* (log FC -0.23), *FMN1* (log FC -0.22) and *RIB1* (log FC -0.17) which encode vitamin biosynthesis enzymes.

Superoxides are a form of oxygen-containing free radicals that can be toxic to cells alone or in combination with metal ions. Oxidative stress-responsive genes *TRR1*, *CCS1*, *SOD2*, and *SOD1* were enriched at FLB.12-8h and had significantly increased levels of expression. These findings suggest prolonged exposure to flubendazole eventually accumulates oxidative stress in *Cryptococcus* cells, prompting an antioxidant stress response for detoxification. Consistent with this, a significant increase in transcription of cell detoxification genes was observed in flubendazole-treated cells versus control at 12 h.

3.4 Discussion

This chapter used RNA-Seq technology to analyse dynamic, transcriptional changes in *C. neoformans* that may elucidate biological proteins or pathways that are relevant to the antifungal action of flubendazole. Previous studies in parasites and a cancer cell line suggest that the mode of action of flubendazole involves an inhibition of tubulin and its polymerisation into microtubules [196, 267]. The data obtained in this chapter are consistent with flubendazole inhibiting tubulin, but also provide important new insights into the global response of *C. neoformans* to the drug. Furthermore, the results and expression data available from this study may also provide a starting point for understanding the nature of the highly specific antifungal action of flubendazole against *Cryptococcus* which remains unknown.

3.4.1 Flubendazole alters expression of tubulin genes: implications for microtubule-related biological processes

Microtubules, comprised of α- and β-tubulin heterodimers, are hollow structures involved in a variety of important cellular functions including nuclear migration and the movement of genetic material during cell division, and the intracellular transport and organisation of organelles and vesicles [216, 217]. In this study, the expression of both α- and β-tubulin-encoding genes *TUB1/TUB3* and *TUB2* respectively, was increased after 12 h of flubendazole treatment relative to controls. Only the expression of *TUB1/TUB3*, however, was statistically significant. This is consistent with a study by O'Neill *et al*. (2016) who observed an increased gene expression of tubulin genes in the nematode *Brugia malayi* treated with flubendazole [212]. The authors of this study similarly observed that the increased expression of α- and β-tubulin genes in response to flubendazole were not consistent between both genes and differed between time points [212].

Studies have indicated that the ratio between α- and β-tubulin is important for cell viability [268, 269]. An imbalance of tubulin subunits, where β-tubulin is in excess of α-tubulin, is toxic and lethal, due to consequential loss of chromosome [268, 269]. However, for reasons unknown, toxicity only occurs when there is excess β-tubulin and toxicity is not observed in *S. cerevisiae* overexpressing α-tubulin alone or in conjunction with β-tubulin, which display intact microtubules [268]. Instead, the presence of excess α-tubulin suppresses and delays the loss of viability caused by excess β-tubulin [268]. Furthermore, α-tubulin protein levels accumulate to greater quantities and at a faster rate in comparison to β-tubulin [268], suggesting the overproduction of α-tubulin acts as a counteractive mechanism to prevent toxic levels of β-tubulin [269]. This may explain the increased expression profile of tubulin genes observed in this study. If β-tubulin in *C. neoformans* is inhibited by flubendazole similarly to how it is inhibited in parasites, *Cryptococcus* cells may be responding by inducing the

expression of α-tubulin to prevent an overabundance of β-tubulin. In contrast to increased expression of tubulin subunit genes, the expression of gamma-tubulin complex genes was significantly decreased (Appendix Table S6.1.5). As the gamma-tubulin complex has a primary role in the nucleation of microtubules, which facilitates and enables the polymerisation of tubulin, this reduced number transcription may suggest nucleation is impaired. This is consistent with the idea that microtubule polymerisation is disturbed in the presence of flubendazole.

Consistent with the concept of disrupted tubulin dynamics was the differential expression of CNAG_02300. CNAG_02300 was one of the most highly expressed genes (log FC 1.78) and encodes a hypothetical protein that contains a conserved domain homologous to a Kelch motif. The Kelch motif is an evolutionary conserved 44-56 amino acid sequence motif that occurs in up to seven repeats to form a β-propeller tertiary structure [236]. Functionally diverse, the Kelch motif is largely involved with the cytoskeletal element actin, and affects cellular growth and morphology [236-241]. This expression of CNAG_02300 was significantly increased across the time course analysis, which is consistent with the increased expression of *ACT1*, suggesting actin activity may be induced in the presence of flubendazole.

Since microtubules are made up of tubulin heterodimers and have functional roles in chromosome segregation, it is understandable that genes that encode proteins involved in chromosome segregation may be affected as a consequence of flubendazole treatment. RNA-Seq revealed a number of genes involved in chromosome segregation were affected by flubendazole in addition to tubulin genes. These included the alternative RFC complex, cohesion and condensin complexes, which are involved in chromosome segregation and architectural organization of chromosomes [270-274]; the DASH complex, which enables the structural anchorage of microtubules to kinetochores and spindle function [275, 276]; and the Ndc80 complex which associates with DASH to facilitate kinetochore-microtubule interaction and their attachment [276, 277]. These results are consistent with results reported by Best *et al*. (2013) when characterising the chemogenomic profiles of different microtubule-perturbing agents in *S. cerevisiae*, including benomyl and nocodazole [278]. In the study, the authors identified GO enrichments that indicated genes involved in spindle checkpoint, chromosome segregation, prefoldin complex and kinetochore were affected in the presence of benzimidazoles agents nocodazole and benomyl [278, 279]. This report is interesting as earlier studies in this thesis found flubendazole did not inhibit the growth of *S. cerevisiae* at the highest tested concentration (see Chapter 2) and yet genes involved in mitosis and cell division were disturbed in *S. cerevisiae* similarly, to how flubendazole disturb *C. neoformans* in the current study. One possible explanation for this is the differences in drug concentration.

In the current study the expression of genes for septins and bud neck proteins, which are involved in cytokinesis, were also significantly decreased which suggests that cells may not be undergoing cytokinesis in the presence of flubendazole. Interestingly, multiple genes involved in the SAC were significantly decreased with flubendazole treatment, suggesting the signalling pathway for cell arrest (due to spindle damage or unattached sister chromatids/kinetochores to mitotic spindles) may be impaired. Faithful chromosome segregation is important for viability and when impeded or disrupted, can lead to abnormal phenotypes. This includes increased susceptibility to microtubule-destabilizing agents such as thiabendazole and benomyl [271, 280-282], multinucleated cells [280, 283] and loss of viability at high temperatures [277].

Consistent with the above observations was the significant differential expression of CNAG_01656. The expression of CNAG_01656 was one of the most significantly reduced (log FC -0.89) and encodes for a hypothetical protein that has a conserved domain homologous to ESCO1 and ESCO2 acetyl-transferase. Acetyl-transferases are a family of catalytic enzymes that participate in post-translational modification of various proteins, including tubulin, by transferring an acetyl group to a substrate. Human *ESCO1* and *ESCO2* acetylate cohesion protein Smc3 to promote the cohesion of sister chromatids and therefore take part in regulating the separation of sister chromatids [242, 243]. Simultaneous inactivation of both *ESCO1* and *ESCO2* impairs chromosome segregation and is lethal [244]. More recently, new evidence has led to the proposal of Esco1 and Esco2 with distinct functions pertaining to mitotic cohesion [242, 245]. In mouse oocyte, Esco1 influences microtubule stability by binding to and acetylating α-tubulin [246]. In the absence of Esco1, acetylated α-tubulin levels are significantly reduced while a significant increase in aberrant spindles, misaligned chromosomes, defective kinetochore-microtubule attachments and impaired microtubule stability has been observed [246]. In this time-course analysis, the decreased expression of CNAG_01656 was only observed at 12 h post-treatment with flubendazole. The conserved domain found in CNAG_01656 that is common with *ESCO1/ESCO2* suggests CNAG_01656 may have a similar role to Esco1 in acetylation and or the regulation of microtubule stability. Interestingly, flubendazole has also been shown to influence the acetylation of microtubules, in addition to affecting dynamic microtubules [213]. In HeLa cells, Chauhan *et al*. (2015) revealed flubendazole increases acetylated α-tubulin levels and that this was responsible for the ability of flubendazole to induce potent autophagic effects in HeLa cells [213].

On the basis of the transcriptional data obtained from this study alone, a reason that may account for the specific antifungal activity of flubendazole against *Cryptococcus* spp. cannot be suggested. However, it can be speculated that differences in tubulin homology between human fungal pathogens may have role [284]. *Cryptococcus* spp. are classified as basidiomyctes and therefore are phylogenetically distinct organisms from *Candida* spp. and *Aspergillus* spp., which are ascomycetes. Accordingly, the tubulin amino acid sequences of *Cryptococcus* has been shown to be topologically distinct [284] and is therefore a plausible cause for the differences in the antifungal susceptibilities observed in Chapter 2.

3.4.2 Genes involved in DNA replication and metabolism are affected in the presence of flubendazole

The expression of numerous genes involved in DNA replication, DNA metabolic processing and mismatch repair were significantly decreased in the presence of flubendazole. These included the origin recognition complex, Mcm2-7 complex, DNA polymerases (δ, α and ε), the RFC and RPA complexes, which collectively suggest flubendazole results in a down-regulation of DNA synthesis and metabolism. Due to structural similarities shared between benzimidazoles and purines, benzimidazole-derived or based agents have been suggested to competitively bind and interfere with DNA, which could inhibit DNA replication [285-287], and inhibit human and bacterial topoisomerase [285, 286]. Alternatively, the significantly reduced expressions of these functional protein machineries may reflect stalling of the replication fork, which may induce genomic alterations in DNA sequences and replication stress if they are not resolved [288].

Consistent with the above observations, the expression of genes encoding core histone, chromatin remodelling and FACT complexes, and the SMC5-SMC6 complex were significantly decreased. The FACT complex is a heterodimer complex consisting of *SPT16* and *POB3.* It serves as a histone chaperone interacting with nucleosomes to facilitate chromatin remodelling [289, 290]. Both *SPT16* and *POB3* had significantly decreased expression in the presence of flubendazole, which may impede DNA replication processes [291]. Yeast mutants deficient in FACT have been shown to be highly susceptible to genotoxic agents such as hydroxyurea and methyl methanesulfonate (MMS), are defective in cell cycle progression, and exhibit genome instability [292].

The SMC5-SMC6 complex is a multi-protein complex that functions to remove recombination intermediates or X-shaped recombination structures (sister chromatid junctions, SCJs) that occur between sister chromatids. Absent or defective SMC5-SMC6 activity has been observed to lead to defective rDNA replication and the accumulation of SCJs and recombination intermediates [250, 293]. In addition, chromosome mis-segregation and aneuploidy have been observed in MMS-treated smc5-

smc6 mutants, indicating an important role of SMC5-SMC6 for faithful chromosome segregation and deterring aneuploidy [250]. Increased SCJ formations have also been documented in the absence of SGS1 helicase. In *S. cerevisiae*, *SGS1* is involved in the decatenation of DNA [294]. Therefore the significant decrease in *SGS1* expression suggests the ability to disentangle chromosome structures is impeded in *Cryptococcus*. In support of this, the expression of the gene encoding DNA bender *HMO1* was significantly induced in this study. *HMO1* has been implicated in promoting SCJ formation and facilitating the formation of catenations or hemicatenations [295].

α-OGG1, the mammalian (human) isoform of yeast *OGG1*, has a crucial role in maintaining the integrity of mitochondrial DNA under oxidative stress [296]. In *S. cerevisiae*, this has been associated with the removal of oxidized guanines (purines), where accumulated levels led to the lengthening of telomeres [251]. Telomeres serve a crucial role in maintaining genome integrity by 'capping', i.e. protecting, chromosome ends. The functional activity of telomeres is effected by their length, which can be extended or shortened by genes including *OGG1* and *EST2* [251]. In this dataset, the expression of *OGG1* was significantly increased while telomere-shortening gene *EST2* expression was decreased with flubendazole treatment, suggesting disruption of telomere elongation activity.

DNA mismatch repair (MMR) genes are important corrective mechanisms that rectify errors that arise during DNA replication and recombination, to maintain genome integrity. The abundance of transcripts encoding for MMR genes were notably decreased in response to flubendazole, including *MSH1*, *MSH2-MSH6* (MutSα complex), *MSH2-MSH3* (MutSβ), *MLH1-PMS1* (MutLα), *POL30*, and *MLH1-MLH3* (MutLγ) [297]. Mismatched DNA is recognised by the MutSα and MutSβ complexes, which in addition to Pol30, activate MutLα [298, 299]. Exonuclease EXO1 is also instrumental in MMR and was similarly repressed with flubendazole treatment. Interacting with MutSα, MutSβ and MutLα complexes, mutants with defective or absent Exo1 exhibit defective MMR activity [298]. Therefore, the reduced expression of MMR genes and *EXO1* suggest MMR activity may be reduced or impaired in the presence of flubendazole. It is unclear, however, whether this would be an effect of flubendazole treatment (e.g. an interference of signalling pathways that disable MMR function to correct genetic errors), or due to the disruption of key processes. Such processes may be important for mitotic progression resulting from exposure to flubendazole (e.g. the disruption of chromatin dynamics or the lack of need for MMR activity due to the down-regulation of DNA replication and DNA metabolism genes). Taken together, these results suggest that mechanisms important for maintaining genomic integrity are disturbed in the presence of flubendazole.

3.4.3 Flubendazole induces oxidative stress-responsive genes

After 12 h of flubendazole treatment, a significant increased expression of genes responsive to oxidative stress was observed. These included *SOD1, SOD2, TSA1, AHP1, CCS1, PRX1, GPX2, TRR1, GLR1, TRX3* and *SRX1*. Increased transcript levels of some of these (*TSA1*, *GPX2*, *TRR1*) were reported by Ko *et al*. (2009) when examining gene expression in *C. neoformans* in response to hydrogen peroxide [300]. Superoxide dismutases *SOD1* and *SOD2* predominantly operate in the cytosol and mitochondria, respectively, and detoxify sources of oxidative stress including hydrogen peroxide–induced reactive oxygen species (ROS) [301]. *SOD1* has been implicated in the regulation of over 120 genes in response to hydrogen peroxide, with a large proportion of these relating to replication and oxidative stress [301]. *SOD2* is considered to be a virulence factor as it facilitates the growth of *Cryptococcus* at physiological temperatures [302, 303]. Thioredoxin reductase *TRR1* is an important component of the thioredoxin system that functions to protect against redox stress. Its induced expression alongside other redox stress-responsive genes including *TSA1*, *TRX3* and *GLR1*, implicates active ROS detoxification processes in *Cryptococcus* cells in response to flubendazole. Consistent with this result, the expression of a number of genes involved in the biosynthesis of sphingolipids were significantly reduced (*ISC1*, *AUR1*, *LCB1*, *LCB2*, *LCB3*, and *LCB4/LCB5*). Sphingolipids have a functional role in modulating ROS levels, and their absence can lead to the accumulation of aberrant levels of ROS, to mitochondrial apoptosis and the loss of cell viability [304-306].

The differential expression of genes involved in redox detoxification provides evidence for increased redox stress and increased levels of reactive oxygen species (ROS) in the presence of flubendazole. This is consistent with significantly increased activity of detoxification enzyme glutathione S-transferase in *Haemonchus contortus* (a parasitic nematode) during flubendazole treatment [307], and increased ROS production during flubendazole treatment in a breast cancer cell line [308]. Increased ROS production by microtubule-perturbing agents, including flubendazole, has been associated with ROS-mediated autophagy and apoptosis [211, 213, 308, 309], and therefore may be associated with the fungicidal effect of flubendazole on *C. neoformans*. In support of this, genes within the proline biosynthesis pathway had significantly decreased expression with flubendazole treatment, suggesting a down regulation of the pathway and proline production. Proline has a significant role in modulating oxidative stress by detoxifying reactive oxygen species and therefore a lack of proline production may contribute to increased ROS levels and oxidative stress [310, 311]. The presence of flubendazole-induced oxidative stress may have significantly consequences and may account for the down regulation of the MMR system. In a human cell line, non-cytotoxic levels of hydrogen peroxide impairs the level of activity of MMR, suggesting the DNA repair pathway is sensitive to oxidative stress [312]. Notably, this increased expression of stress-responsive genes was only observed at the last time point.

This may suggest the targeting of tubulin and microtubule has ramifications that are not acutely apparent as in this study, and rather reflects a delayed response as a consequence of accumulated cellular stressed and eventual cell death.

3.4.4 Dynamic analysis of the trancriptomic response to flubendazole: limitations and challenges

To investigate the effects of flubendazole on *C. neoformans*, transcriptional profiling was performed on cells over a three-point time course to observe for dynamic changes over time. A substantial proportion of differentially expressed genes in this dataset were identified as encoding hypothetical proteins. While this may not be surprising as the *Cryptococcus* genome remains poorly annotated to date, it is a reminder that much about the organism is not well understood. In contrast to other transcriptional studies however, an unexpectedly small number of genes were significantly differentially expressed comparing treatment and control samples as well as treatment samples between time points. This was particularly the case for the first two time points (6 and 8 h). This may be due to the proximity between the first two time points, being less than one full cell division cycle as the doubling time of *Cryptococcus* is about 132 minutes [313, 314]. The greatest number of significantly differentially expressed genes was observed between treated and untreated cells (FLBvsCTRL) at 12 h ($n = 2314$; p-value < 0.05). A high number of significantly differentially expressed genes were also found comparing treated cells (FLB-only) at 6 and 12 h, and 8 and 12 h. These results suggest flubendazole causes minimal transcriptional changes in *C. neoformans* for at least 8 h, despite the rapid decline in viability shortly after this point. Despite having observed minimal transcriptional changes in the first 2 time points, the results found in this study is supported by transcriptional results obtained by Spagnuolo *et al*. (2010). The authors investigating the anticancer mechanism of action of flubendazole found genes functionally associated with chromosomal segregation and cytoskeletal were down regulated in leukemia cells after a 4 h exposure to flubendazole [196].

3.5 Conclusions

This study provides transcriptional evidence suggesting that microtubules are involved in the mechanism of action of flubendazole against *C. neoformans*. This is consistent with available literature suggesting microtubules, the benzimidazole target in parasites, are also targeted in *C. neoformans*. In 1997, Cruz *et al*. identified and reported the β-tubulin gene *TUB1* as the specific target in albendazole-treated *C. neoformans* [198]. In this study, *C. neoformans* β-tubulin gene *TUB1* was not significantly differentially expressed (CNAG_01840; log FC 0.10; adj. p-value = 0.436124) and instead observed a significant increase in α-tubulin transcripts following flubendazole treatment.

The comprehensive nature of data generated by RNA-Seq, revealed a variety of biological processes were affected in response to flubendazole treatment. DNA-related processes such as sister chromatid segregation and DNA replication were significantly decreased, while energy production and cell detoxification mechanisms were significantly increased. The time-course approach for this study revealed limited homeostatic disturbances to the biology of *C. neoformans* occur on a transcriptional level, when treated with flubendazole. It is not until the final time-point, at 12 h, where substantial biological changes are observed, suggesting there is a period of delay before the onset of the drug working and *C. neoformans* being affected. It is noted that the cells analysed in this study were not from a synchronised culture, which may affect the observed transcript levels of genes.

Figure 3.12 depicts a proposed model of the biological response of *C. neoformans* treated with flubendazole. Consistent with other studies, flubendazole causes microtubules to destabilise, resulting in an increased expression of tubulin genes to compensate. As microtubules are important in cell cycle progression, the presence of unstable or dysfunctional microtubules consequentially disrupts chromosome segregation, DNA synthesis and replication as well as mismatch repair mechanisms. This may cause levels of oxidative stress to accumulate within the cell, leading to the increased expression of oxidative stress-responsive genes for cellular detoxification. Increased genes within the tricyclic acid (TCA) cycle and gluconeogenesis suggests there is a demand for increased energy production to facilitate mechanisms to cope with flubendazole treatment.

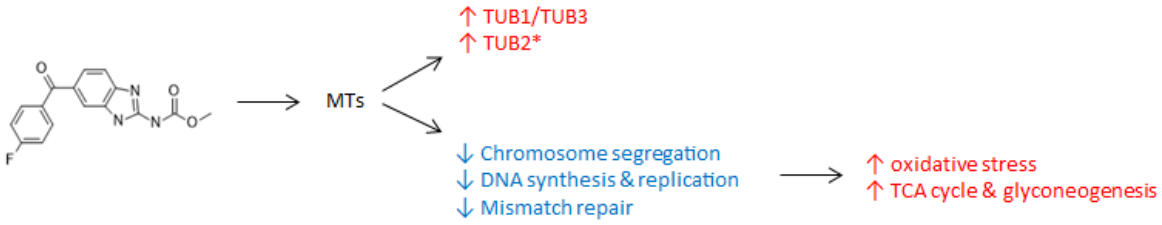

Figure 3.12. *C. neoformans* response to flubendazole treatment.Flubendazole targets microtubules (MTs) causing them to destabilise. This induces the expression of tubulin genes TUB1/TUB3 and TUB2. As a result of perturbed microtubules, chromosome segregation, DNA synthesis and replication and mismatch repair processes are consequently impaired. This causes the accrual of cellular stress and the increased expression of oxidative stress genes, the tricarboxylic acid (TCA) cycle and gluconeogenesis. Red and blue indicate increased and decreased gene expression, respectively. Asterisk indicates that gene expression was increased but this was not statistically significant (adjusted p-value > 0.05).

Chapter 4: Further investigation into the flubendazole mode of action: the physiological response of *Cryptococcus* cells

4.1 Introduction

Previous work in this thesis identified the antifungal activity of flubendazole against *Cryptococcus* spp., and an analysis of the transcriptome found two key pieces of evidence that may help elucidate its mechanism of action: first, the differential expression of tubulin, and second, the down-regulation of genes involved in cell-cycle and cell division-related processes including the replication, repair and metabolism of DNA. This suggests flubendazole may be interfering with the cell-cycle progression of *C. neoformans*. Therefore, it is plausible that following exposure of cells to the drug, there will be changes in morphology that can be microscopically visualised. In addition, the transcriptomics data provided a wealth of differentially expressed genes that might be exploited for both understanding and enhancing flubendazole as an antifungal agent. Both transcription factors and kinases are cellular regulatory components that have been used in screens for the discovery of a variety of indications [315-318]. As they have the capacity to activate or repress signalling pathways that are critical for cellular survival in response to drug exposure, transcription factors and kinases may represent good targets for new antifungal agents.

The development and advancement of microscopy has made it possible to visualise and probe biology on a microscopic level. The use of microscopy expanded when cells and sub-cellular components could be genetically tagged with fluorescent proteins that could be visualised, tracked and imaged [319]. This created the field of fluorescent microscopy. Fluorescent proteins are ~25kD proteins that excite and fluoresce (blue, cyan, green, yellow, orange, red or far red) when subjected to wavelengths of light within a specific range [319]. A widely used fluorescent protein is the green fluorescent protein (GFP) acquired from the *Aequorea victoria* jellyfish, which fluoresces green when exposed to light. In *Cryptococcus*, fluorescent microscopy has been used to study the microtubule cytoskeleton and dynamics of cell division in response to drug exposure [101, 280, 320, 321]. Under normal growth conditions (e.g. not exposed to any drug treatment), microtubules in *C. neoformans* strains expressing GFP-tagged tubulin are arranged as defined, straight, string-like structures within the cell [321]. The structure and cellular dynamics of microtubules become disrupted and absent in the presence of microtubule inhibitors including methyl benzimidazole-2-yl carbamate, nocodazole, thiabendazole, vincristine and benomyl [280, 320, 321]. Other reported morphological alterations observed in *Cryptococcus* include abnormal cell morphology and multinucleate cells, which indicate disrupted mitosis [280, 320]. Fluorescent microscopy has been previously undertaken on *Cryptococcus* treated with mebendazole, an analogous benzimidazole agent to flubendazole [164]. The authors reported abnormal cell wall and chitin morphologies, however microtubules were not investigated. Therefore, the morphological response of *Cryptococcus* to flubendazole remains unknown.

Transcription factors and kinases are important regulators that fundamentally modulate a plethora of signalling cascades and pathways in response to a stimulus. Transcription factors are proteins that act as biological switches to activate or repress the transcription of genes whose protein products participate in a particular cellular process or pathway [315]. They have a DNA-binding domain that recognises and binds to specific DNA sequences. This can be used to categorize classes of transcription factors, and the location of the domain heavily influences whether a transcription factor functions as an activator, a repressor or both [315, 322]. Kinases are protein enzymes that are responsible for phosphorylation, a biochemical process that involves adding a phosphate group to a protein substrate [323]. Phosphorylation alters the function of a protein and activates the signal transduction of various biological pathways including cell cycle progression, metabolism and apoptosis [323]. Hence kinases are crucial enzymes in post-translational modification, cell signalling and signalling transduction [323]. The proper functioning of transcription factors and kinases is critically important and their dysregulation can be detrimental, giving rise to disease [323-326]. Due to the capacity of transcription factors and kinases to affect a diversity of biological pathways, there is an increasing interest in investigating them as therapeutic targets in drug discovery programs [327-331]. This is reflected in an increasing number of approved kinase-inhibiting drugs and therapies since 2004, with many others either in preclinical or clinical development [318, 328]. While kinases are recognised and validated druggable targets, transcription factors are still emerging as targets for drug discovery [331].

To date, the development of inhibitors of these regulatory factors has largely benefitted the anti-cancer area and their application as anti-infective targets, particularly in the context of fungal disease, is not extensively studied. Extensive research efforts in recent years has facilitated an improved capability to study fungal transcriptomes and kinomes. Recent studies have constructed libraries of transcription factor and kinase overexpression mutants in *S. cerevisiae,* and knockout mutants in *C. neoformans*, generating a wealth of comprehensive data [322, 332, 333]. Jung *et al*. (2015) and Lee *et al*. (2016) comprehensively studied a collection of transcription factor and kinases in *C. neoformans,* respectively, genetically and phenotypically characterising an extensive list of 155 putative transcription factors and 183 putative kinases (http://tf.cryptococcus.org) [322, 333]. This encompassed a broad range of data including pathogenicity, phylogenetic relationships between *C. neoformans* and other eukaryotic orthologues, antifungal susceptibility and tolerance to a diversity of cell stresses [322, 333]. These studies provide resources that enable fungal transcriptomes and kinomes to be better studied and data that can be compared in subsequent studies [322, 332, 333]. These systematic gene knockout libraries are highly valuable in the context that they enable reproducible analyses of comprehensive sets of gene knockout strains by different laboratories. This enables the characterisation of *Cryptococcus* genes which are not as extensively characterised

compared to *S. cerevisiae*. In particular, *Cryptococcus* transcription factors and kinases are poorly characaterised and are of high research interests due to their role in regulating virulence. Therefore, these knockout libraries may aid in the identification of potential druggable signalling and regulatory targets.

To date, few studies have demonstrated the functional significance of transcription factors and kinases in facilitating fungal infection, pathogenesis, virulence, and stress response, including antifungal susceptibility [334-340]. In *Candida albicans*, Flowers et al. (2012) studied mechanisms of azole resistance pertaining to the increased expression of *ERG11*, which encodes lanosterol demethylase in the ergosterol biosynthesis pathway. The study found that mutations within the transcription factor *UPC2* gene, an upstream regulator of the ergosterol biosynthesis pathway, was often observed with an increased expression of the *ERG11* gene. Increased transcript levels of *ERG11* was associated with decreased susceptibility to fluconazole [339]. A following study on the *UPC2* gene by Gallo-Ebert et al. (2014) found that the growth of *C. albicans* can be inhibited by compounds that block *UPC2* expression [341]. These compounds were found to reduce the expression of *UPC2* as well as *ERG11* in fluconazole-treated cells [341]. Since Upc2 acts upstream of the ergosterol biosynthesis pathway, the development of these compounds may be able to circumvent mechanisms of drug resistance encountered by azole drugs. In a different study, a discovery of a unique mechanism of resistance in *Aspergillus fumigatus* was reported when a mutation in a transcription factor subunit HapE, caused by an amino acid substitution, led to azole resistance [340]. Furthermore, the transcription factor Mbs1 has been investigated for its role in *C. neoformans* following a 90 minute exposure to 5-flucytosine and its potential as an antifungal target [342]. The expression of *MBS1* was induced following exposure to 5-flucytosine and the deletion of the gene lead to increased susceptibility to the drug [342]. The deletion was also shown to modulate the susceptibilities to other antifungal drugs including decreased susceptibility to amphotericin B but an increased susceptibility to fluconazole [342].

Kinases have also been explored in antifungal drug discovery due to their diverse roles in cellular regulation and signalling. For example, the kinases Pkc1 and Pkh2 are involved in multiple cellular processes including the activation of downstream kinases (e.g. Pkc1) which are responsible for cell wall integrity. In *S. cerevisiae*, the inhibition of Pkh1/2 led to the disruption of cell wall integrity, suggesting these kinases may be viable targets for antifungal drug development [343]. Similar results were obtained in *C. albicans*, demonstrating that the inhibition of the *Pkc1* kinase inhibited fungal growth and increased the drug susceptibility to an echinocandin analogue [344]. These studies exemplify how regulatory proteins can have a significant influence in antifungal drug susceptibility.

Therefore, investigating the most highly differentially expressed transcription factors and kinases in the presence of flubendazole may elucidate important regulatory elements that that may be targeted for antifungal drug development [323].

The work presented in this chapter aims to build on the transcriptomic data findings from the previous chapter by analysing the response of transcription factors and kinases to flubendazole. Based on previous work and available literature, it was hypothesised that flubendazole would affect the gross morphology of *Cryptococcus* cells, as well as the morphology of microtubule structures within the cells. In addition, gene ontology analyses in Chapter 3 suggests that genes in involved in DNA replication processes and cellular division are affected by flubendazole treatment. Specifically, the expression of transcription factors and kinases are of interest in drug development due to their regulatory role in multiple pathways and their potential to affect multiple and down-stream targets. Therefore, investigating transcription factors and kinases that are differentially expressed in response to flubendazole treatment may lead to the identification of novel antifungal targets and/or further elucidate the mechanism of action of flubendazole on a regulatory level in *C. neoformans*.

To address these hypotheses, this chapter aimed to 1) use fluorescent microscopy to visualise morphological changes that occur in a *C. neoformans* strain expressing GFP-tagged β-tubulin in response to flubendazole; and 2) analyse the transcriptional changes of transcription factors and kinases to flubendazole, in order to identify regulatory factors that may have an important role in the drug response of *C. neoformans* to flubendazole. This strategy should provide insights that can be used to develop novel antifungal agents against *Cryptococcus*.

4.2 Methods

4.2.1 Strains, culture and drugs

Fungal strains used in this study are described below. Strains were maintained as glycerol stocks stored at -80 °C and grown on sabouraud dextrose agar (SDA) for 48 h at 30 °C before use. Flubendazole and mebendazole (Sigma-Aldrich, MO, USA) were prepared to a stock solution of 2 mg/mL in dimethyl sulfoxide (DMSO). Fluconazole (Cayman Chemical, MI, USA) was made to 12.8 mg/mL in DMSO.

For microscopy analysis, a *C. neoformans* strain with β-tubulin fluorescently-tagged with GFP (strain LK128) used. Strain LK128 was made by Assistant Professor Lukasz Kozubowski (Clemson University, USA), and with permission, kindly provided by Dr. Connie Nichols (Duke University, USA) and Anna Floyd-Averette (Duke University, USA). The construction of strain LK128 is detailed by Kozubowski *et al*. (2010) [345]. Briefly, a plasmid containing the nourseothricin (NAT)-resistance marker and β-tubulin-encoding sequence (gene CNAG_01840) was constructed using vector plasmid pCN19. This generated pLKB37, which was then biolistically transformed into the background strain *C. neoformans* var. *neoformans* serotype D strain KN99a and screened via microscopy [345]. *C. neoformans* strain H99 (Carter Lab strain collection, University of Sydney) was additionally used for comparative purposes as H99 is a clinical strain originally sourced from the United States of America, and is recognised as the global type strain for *C. neoformans*.

To characterise the role of transcription factors in response to flubendazole, transcription factor mutant strains CNAG_03229 (*YOX101*), CNAG_07464 (*MBS1*), CNAG_01438 (*MBS2*), CNAG_00239 (*YAP1*), CNAG_07924 (*MCM1*), CNAG_05176 (*HOB3*) and CNAG_04586 (*HOB7*) were acquired from Bahn's 2015 *C. neoformans* transcription factor mutant library [322]. The construction of *C. neoformans* transcription factor mutants were completed in the *C. neoformans* serotype A H99S strain background and are detailed by Jung *et al*. (2015) [322]. Briefly, overlap PCR and NAT-split marker/double-joint PCR strategies were utilised to generate gene-disruption cassettes comprised of signature-tagged sequences and the NAT-resistance marker. Biolistic transformation was used to introduce gene-disruption cassettes combined with gold microcarrier beads into H99S strains, which were screened via PCR and Southern blot analysis. This produced two H99S mutant strains, made via two different methods, for every transcription factor.

4.2.2 Spot plate assays

Spot plate assays are a fast and sensitive method, routinely used in yeast research to understand how cells respond to inhibitory agents. Cultures were grown overnight in yeast peptone dextrose (YPD) broth (pH 7) to exponential phase at 30 °C, 200 rpm. Cultures were diluted to 1 x 10^6 cells/mL using a haemocytometer and serially diluted 10-fold from 10^6 to 10^1 in PBS. Aliquots (5 µL) of each dilution were spotted onto YPD agar (pH 7) supplemented with flubendazole (0.156 or 0.195 µg/mL), mebendazole (0.156 or 0.195 µg/mL) or fluconazole (8 or 10 µg/mL). All plates were incubated at 30 °C and photographed daily for 5 days.

4.2.3 Microscopy imaging and analysis

To observe the morphological effects of flubendazole on *Cryptococcus* cells, cells grown to exponential phase were treated with or without flubendazole and observed at 24 and 48 h post-treatment. First, for each strain a broth culture was grown overnight in Yeast Nitrogen Base (YNB, pH 7; Sigma-Aldrich, St. Louis, MO, USA) media at 37 °C with shaking (240 rpm). After 16 - 17 h, the culture was sub-cultured to 1 x 10^6 cells/mL in fresh YNB media (total volume 50 mL) and returned to the shaking incubator for 3 h. After 3 h, 15 mL aliquots of cultures were taken for control and treatment. 'Treatment' cultures were treated with 100 µg/mL flubendazole to the desired final concentration (0.02 or 0.04 µg/mL). At 24 and 48 h post-treatment, a 1 mL aliquot of cells was collected, pelleted, washed twice with 1 mL phosphate buffer saline (PBS) and resuspended in PBS for imaging. Cells were visualised using a 100x objective lens (Nikon 100x NA 1.45 Plan Apo **λ**) with 1.520 immersion oil, on a Nikon eclipse Ti inverted microscope at the Microbial Imaging Facility, University of Technology Sydney. The NIS-Elements AR program was used to capture live images on the phase contrast and GFP channel, with 11 Z-stacks. Figures of microscopy images were generated using OMERO.figure (version v4.0.2).

To analyse the budding activity of *Cryptococcus* cells, regions of interest (ROIs) for each cluster of cells were manually hand drawn on the phase image, using the image processing program ImageJ (version 2.0.0) (Figure 4.1A). To count the number of cells in a cluster, clusters were segmented using seed-based distance transformed watershed segmentation in ImageJ. Watershed segmentation is an image analysis technique that effectively separates touching or joined objects in a binary image. In preparation for watershed segmentation, a Euclidean distance map was calculated for each cluster ROI. The distance map measures the distance from each pixel in the cluster to the closest border of the ROI. The maxima of the distance map were used as seed points (which in this case is usually the centre of a cell). This distance transform was then inverted and used in addition to seed points (as markers), to enable the application of marker-controlled watershed via the MorphoLibJ plugin to

create a grayscale image that can be segmented as shown in Figure 4.1B [346]. This generates a list of cell ROIs for each cluster allowing each cell to be assigned to unique clusters.

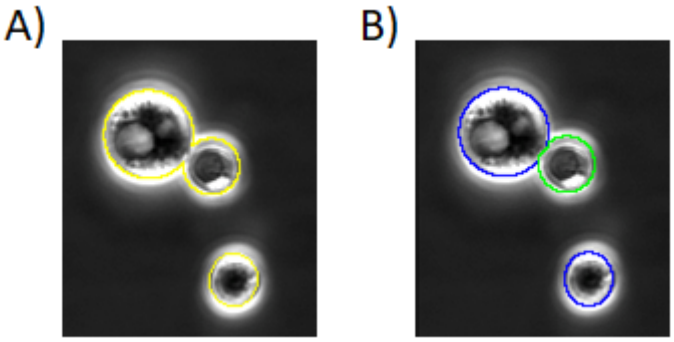

Figure 4.1. Image processing in preparation for image analyses using ImageJ.Images show a phase image of *Cryptococcus neoformans* budding (2 cells attached) and non-budding (singular). (A and B) Images show regions of interest (ROIs) outlined in yellow and ROIs segmented via seed-based distance transformed watershed segmentation, respectively.

In this study, tubulin or microtubule structures are referred to as 'strings' owing to the string-like structures observed using the microscope. To identify string structures in the GFP channel, the following protocol was applied for each cell ROI and each slice in the Z-stack. A white top hat transformation was performed on the GFP channel to enhance string-like features (MorhphoLibJ, structuring element disk radius of 5 pixels). White top hat is a grayscale morphological filter that enhances bright structures and therefore facilitate efficient segmentation. The maximum display range was adjusted to four times the 97th percentile of the intensity distribution to convert the 16-bit image to an 8-bit image. The ridge detection plugin was used to detect ridges (lines) within images [347]. This created ROIs for each filament from which statistics such as length, width and GFP-intensity were recorded. Figure 4.2 demonstrates the application of white top hat and ridge detection.

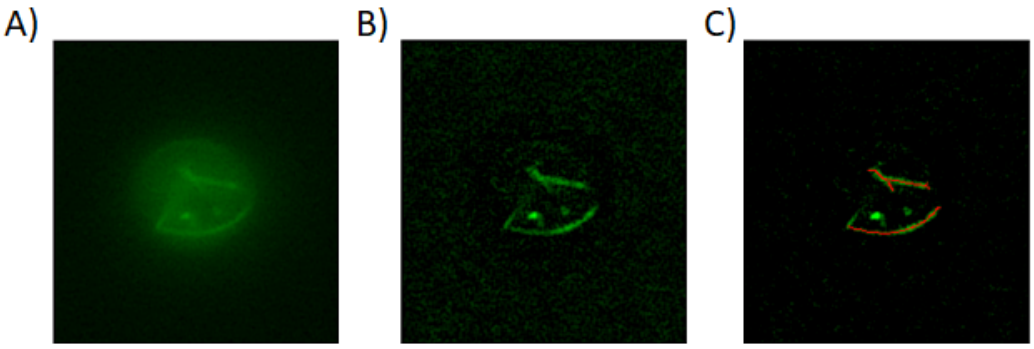

Figure 4.2. Image processing of GFP-tagged β-tubulin in *C. neoformans* using ImageJ.(A) A raw image of a single cell of *C. neoformans* on the GFP channel showing defined string-like structures. (B) A processed image of cell with enhanced visualisation of string-like structures after white top hat application. (C) The detection of visually-enhanced, string-like structures, outlined in red lines, using ridge detection.

Analysis of cell morphologies, including roundness and cell clustering, were performed using FIJI [348], Matplotlib (version 3.0.3, Hunter *et al*. 2007) and Python (version 3.5; van Rossum 1995) with the assistance of Dr Christian Evenhuis. Cell roundness was calculated as a ratio between the major and perpendicular minor axis of the cell. Parameters for cell roundness were set to allow direct comparisons between the wild-type and the treatment samples, and these parameters were adapted from Salvatier *et al*. (2016) [349]. Cells were also analysed on the event of the cells being in singular formation or clustering. To analyse these events (singular or clustered cells), populations for each event were counted in the wild-type and treatment samples and modelled against a custom distribution adapted from the discrete lognormal distribution, as described by Bi *et al*. (2001) [350].

4.3 Results

4.3.1 Qualitative and quantitative analysis of the morphological effects of flubendazole on *Cryptococcus*

Evidence described in the previous chapter suggested that flubendazole may target tubulin in *Cryptococcus*. To visualise morphological changes in tubulin in response to flubendazole, a *Cryptococcus* strain expressing GFP-tagged β-tubulin (strain LK128) was utilised in this study. Broth cultures of LK128 were grown in the presence or absence of flubendazole for 24 and 48 h and GFP localisation was visualised by fluorescence microscopy. In untreated control cells, GFP-tagged β-tubulin appeared predominantly as well-defined string-like structures at 24 and 48 h (Figure 4.3), as observed in other studies of untreated *C. neoformans* tubulin [321]. Under normal conditions (no flubendazole treatment), cells exhibited abundant GFP-tagged β-tubulin with up to 13 'strings' detected per cell, with a total added length of up to 10-14 μM (Figures 4.4A and 4.4B). In cells treated with flubendazole, however, GFP-tagged β-tubulin appeared scattered and dispersed within the cell with no defined or organised structures (Figure 4.3). Both the frequency and the total added length of detectable GFP-tagged β-tubulin 'strings' were substantially reduced while there was an increased number of cells with no GFP-tagged β-tubulin (Figures 4.4A and 4.4B). These results indicate that tubulin morphology and dynamics in *C. neoformans* became disrupted in response to flubendazole treatment. This conclusion was supported by the consistency in results observed using two different quantitative measures of GFP-tagged β-tubulin (Figures 4.4A and 4.4B).

Consistent with the observed changes in GFP morphology and localisation patterns, the distribution of mean intensity of fluorescence in flubendazole treated and untreated *C. neoformans* expressing β-tubulin-GFP revealed unique profiles (Figure 4.4C, Table 4.1). In untreated cells, approximately 3% of cells fluoresced brighter than the rest of the cell population at 24 and 48 h (Table 4.1). In flubendazole-treated *C. neoformans* expressing β-tubulin-GFP cells however, this proportion of cells substantially increased to approximately 40%, suggesting flubendazole may be inducing the expression of β-tubulin in *C. neoformans* (Table 4.1). To evaluate the magnitude of increased fluorescent intensity found in flubendazole-treated cells, the total signal of fluorescence intensity of flubendazole-treated cells was deconstructed into cells that fluoresced to a similar extent to the control cells versus cells that fluoresced brighter than the control cells (Figure 4.4C). An approximate two-fold difference in increased intensity was identified in cells at 24 (median 1.95%, 95% credible interval [1.85, 2.10]) and 48 h (median 1.83%, 95% credible interval [1.73, 1.84]). These results demonstrate that flubendazole treatment results in a distinct fluorescence intensity profile in *C. neoformans* cells, characterised by a

two-fold increase in fluorescent intensity detected in about 40% of flubendazole treated cells. This increase in intensity may reflect a disturbance of β-tubulin dynamics caused by flubendazole.

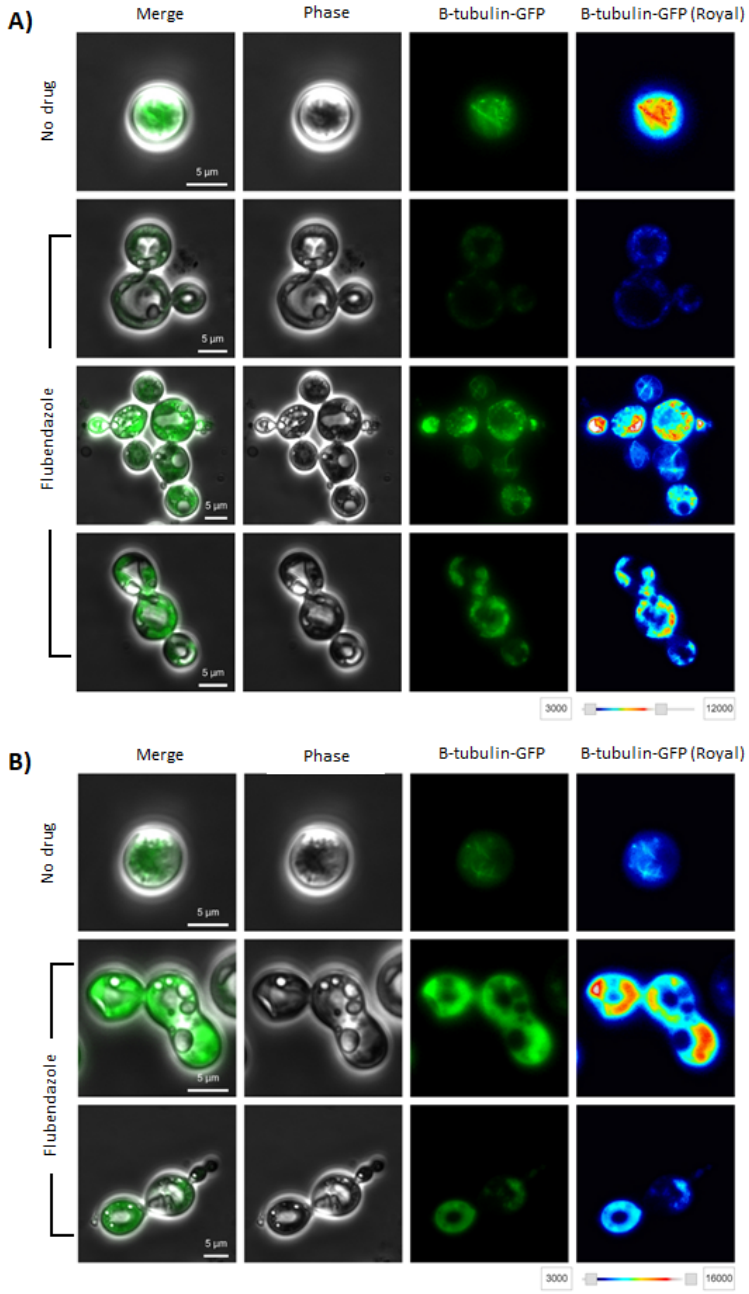

Figure 4.3. Representative images of *C. neoformans* expressing β-tubulin-GFP in the presence and absence of flubendazole.(A and B) Flubendazole treated and untreated *C. neoformans* expressing β-tubulin-GFP are shown at 24 and 48 h, respectively (Scale bar: 5 µm). Phase contrast images show flubendazole treated cells with abnormal cellular morphology and budding. The GFP channel shows abnormal β-tubulin-GFP in flubendazole-treated cells. These were observed to be less well-defined tubulin 'strings'. While some treated cells had reduced fluorescence, others were greatly increased as shown in the second row at 28 h. To enhance the visualisation of β-tubulin-GFP and degree of fluorescent intensity, an alternate channel (Royal) was additionally applied using OMERO.figure (version v4.0.2). A rainbow colour scale is shown, with warmer colours indicating a higher level of fluorescent intensity detected.

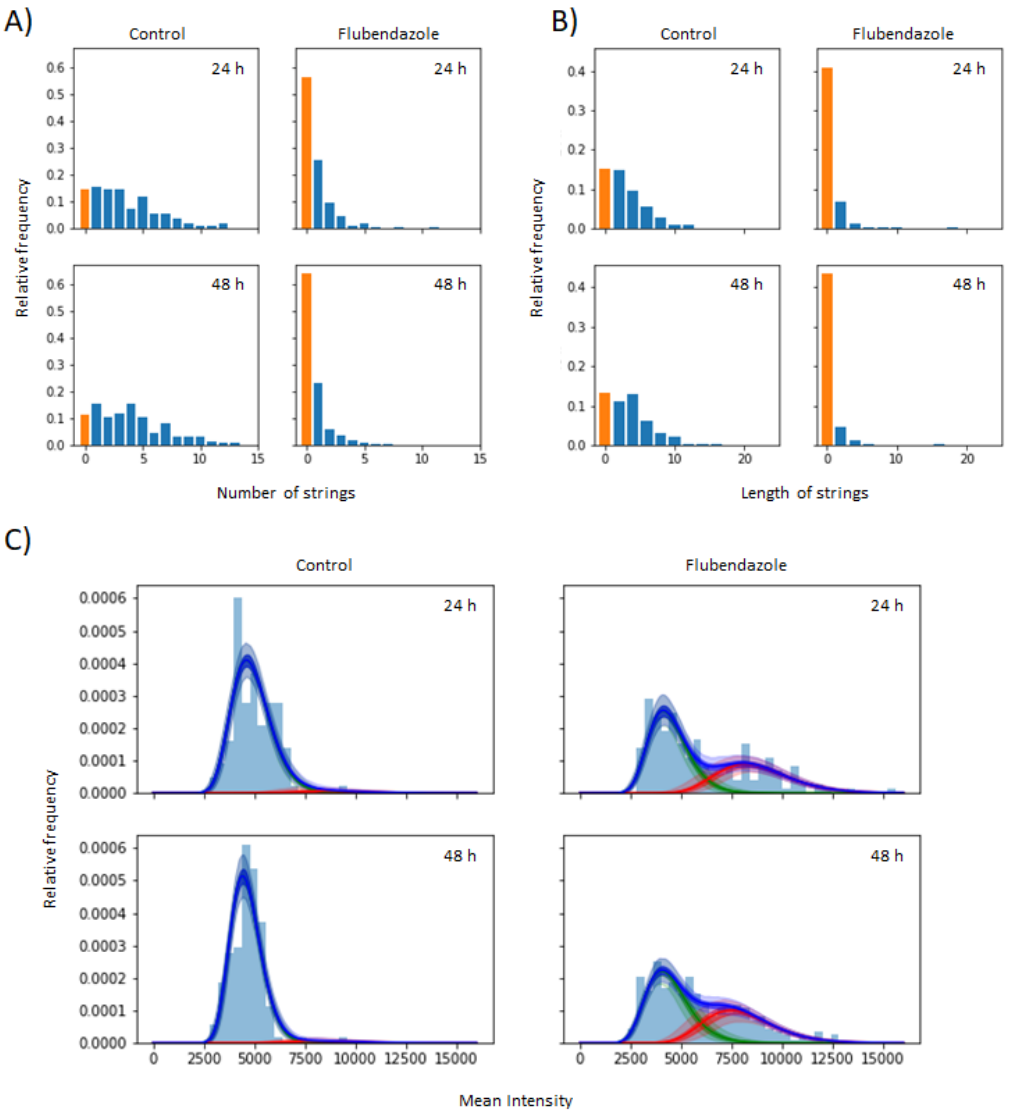

Figure 4.4. Analyses of GFP-tagged β-tubulin in flubendazole treated and untreated *C. neoformans* strain LK128.All cells within ten fields of view were outlined using ImageJ (version 2.0.0) prior to analysis. (A) The distribution of GFP-tagged β-tubulin strings expressed in terms of relative frequency. (B) The distribution of the length of GFP-tagged β-tubulin expressed in terms of relative frequency (x-axis: length in µM). Orange bars in A) and B) highlight the proportion of cells with undetected β-tubulin-GFP structures. (C) The distribution of mean intensity of GFP per cell. The blue line represents the total signal detected, and is made up of two components: one that fluoresces similarly to the control (green line) and one that fluoresces brighter (red line). Untreated *C. neoformans* strain LK128 display an abundance of GFP-tagged β-tubulin in cells, with up to 13 string-like structures detected per cell. Flubendazole treatment resulted in a reduction in the number of string-like structures and a simultaneous increase in the number of cells with no GFP-tagged β-tubulin. A similar observation was found in the summation of the total length of detected string-like structures in each cell. The quantity of GFP-tagged β-tubulin as a measure of total length was reduced following flubendazole treatment, with an increased number of cells with no GFP-tagged β-tubulin. Quantification of the mean intensity of *C. neoformans* strain LK128 show that treated a proportion of the population of treated cells fluoresce brighter compared to untreated cells.

Table 4.1. Percentage of highly fluorescent cells with their 95% credible intervals.

	Median (%)	Range of uncertainty (95% credible intervals)
Control 24 h	2.94	[0.18, 8.13]
Control 48 h	2.63	[0.18, 8.13]
Treatment 24 h	39.51	[29.90,49.37]
Treatment 48 h	42.21	[29.49, 56.00]

In addition to changes in tubulin dynamics, changes in the gross cell morphology of *C. neoformans* were observed. Untreated cells were observed to be predominantly solitary, round and unbudded consistently at 24 and 48 h, with a minority budded in pairs (Figure 4.5). This cell morphology is consistent with *C. neoformans* cells entering or at stationary phase. Comparing flubendazole-treated and untreated cells, the proportion of single and unbudded cells was significantly reduced with flubendazole treatment, with a concomitant increase in the proportion of cells budded with one or two daughter cells (Figure 4.6). In addition, multi-budded cells, where four or more cells are attached, were uniquely observed with flubendazole treatment (Figures 4.5 and 4.6).

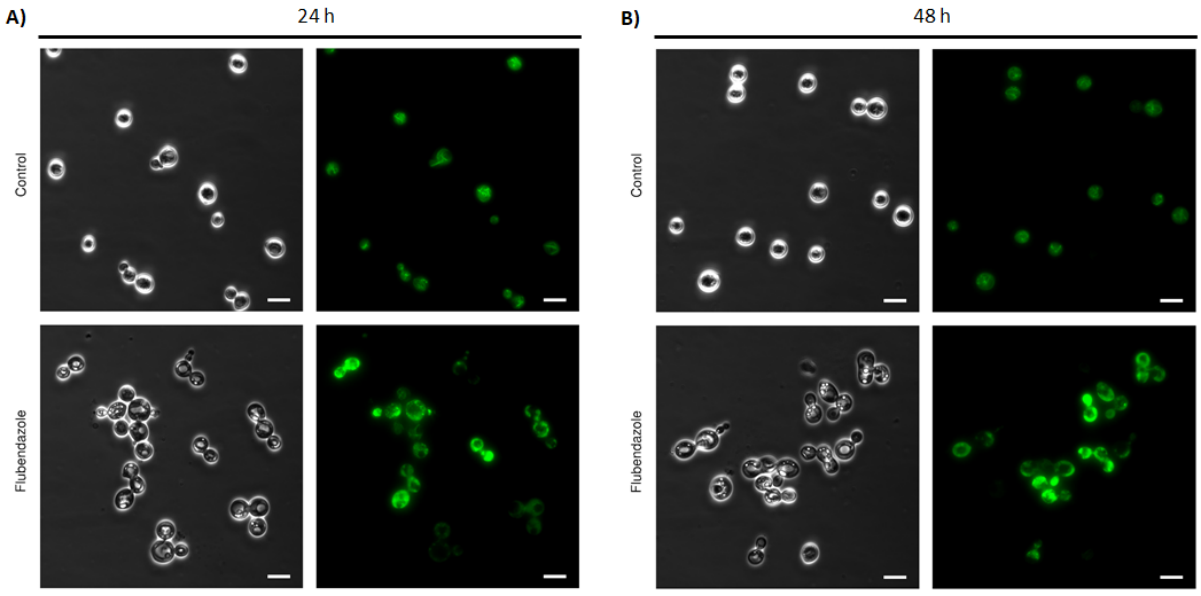

Figure 4.5. Morphological changes in *C. neoformans* cells expressing GFP-tagged β-tubulin in response to flubendazole.Cells were grown to exponential phase in YNB media at 37 °C and were either left untreated or treated with flubendazole (0.02 µg/mL). (A and B) Cells were imaged on a Nikon eclipse Ti inverted microscope at 24 and 48 h, respectively. Scale bar: 10 µm. At 24 and 24 h, untreated cells are predominantly unbudded with GFP-tagged β-tubulin visibly present as string-like structures. Flubendazole-treated cells are predominantly occur as budded cells with at least one or two daughter cells, with aberrant GFP-tagged β-tubulin morphology compared to untreated cells. Cells were also observed to be less round compared to untreated cells, with some cells showing an indented nucleus. These observations were consistent between 24 and 48 h and suggest flubendazole treatment results in abnormal cell morphology characterised by aberrant GFP-tagged β-tubulin and compromised cell shape integrity.

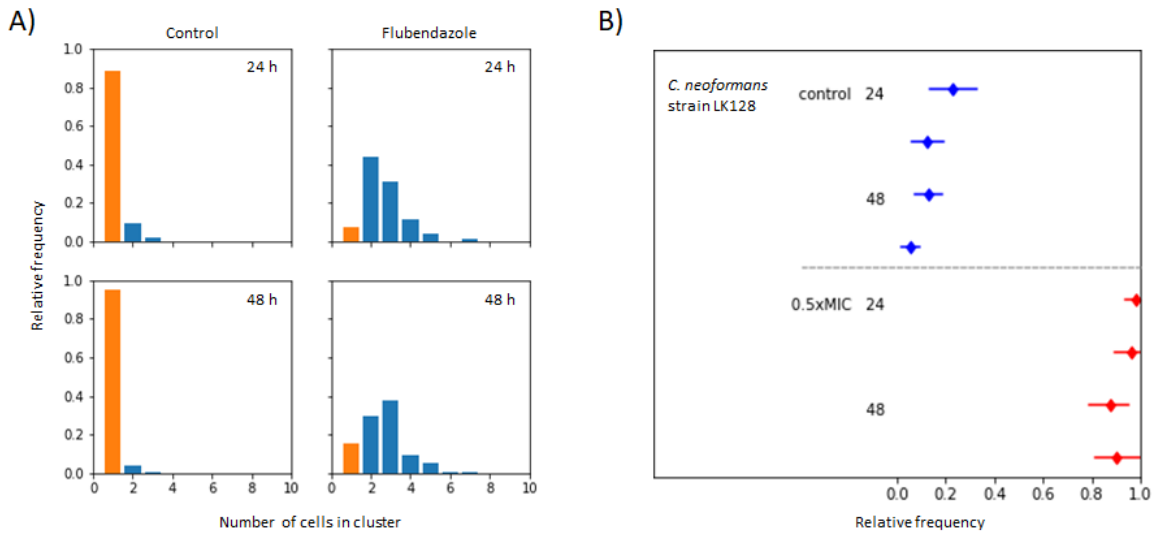

Figure 4.6. Analyses of cell clustering in flubendazole treated and untreated *C. neoformans* cells.All cells within ten fields of view were outlined using ImageJ (version 2.0.0) prior to analysis. (A) Distribution plots of cell clustering flubendazole treated and untreated *C. neoformans* cells strain LK128, expressed in terms of relative frequency. Orange bars highlight the proportion of unbudded cells. (B) Statistical analysis of cell clustering in *C. neoformans* strain LK128 in the presence or absence of flubendazole. The degree of clustering is expressed in terms of a percentage distribution of cells that were clustering (0.0 represents 0% clustering and 1.0 represents 100% cell clustering). Flubendazole treated and untreated cultures are represented in red and blue lines, respectively. Diamond icons denote the median and the length of a line shows the 95% credible interval range. The two data points represent two biological replicates. In *C. neoformans* strain LK128, cell clustering is significantly present following flubendazole treatment.

In addition to abnormal budding, microscopy images revealed cells treated with flubendazole displayed aberrant cell shape. To measure this qualitative feature, the degree of roundness of each cell was quantified and the results are depicted in Figure 4.7. In the absence of flubendazole, cells appear predominantly round in shape at 24 and 48 h (Figure 4.7A). Following flubendazole treatment, cells appear significantly less round (Figure 4.7B). These results demonstrate that cell shape was compromised in the presence of flubendazole, in addition to the abnormal budding observed in Figures 4.5 and 4.6. Overall, these results suggest that flubendazole inhibits *C. neoformans* via a mechanism that involves targeting β-tubulin and compromising its ability to form microtubule structures within a cell. Treated cells display abnormal budding phenotypes, which may reflect an impairment of cell cycle progression and cytokinesis.

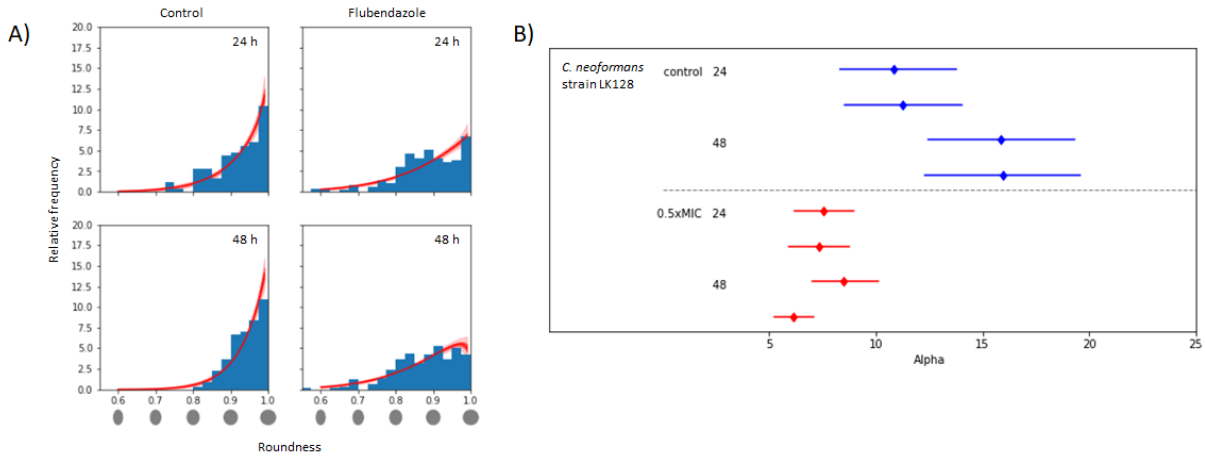

Figure 4.7. Cell shape analyses in flubendazole-treated and -untreated *C. neoformans* strain LK128.All cells within ten fields of view were outlined using ImageJ (version 2.0.0) prior to analysis. (A) The distribution of the roundness of *C. neoformans* expressing β-tubulin-GFP, expressed in terms of relative frequency. The x-axis is a scale for cell roundness, with scores closer to 1.0 denoting cells that are more round and scores less than 1.0 denoting cells that are less round and more oval in shape. The red line represents the differences in statistical significance between treated and untreated cells. (B) A statistical representation of the degree of roundness in *C. neoformans* strain LK128, expressed in terms of alpha. The lower the value of alpha (x-axis), the less round cells are. Flubendazole treated and untreated samples are represented by red and blue lines, respectively. Diamond icons denote the median and the length of a line shows the 95% credible interval range. Under normal circumstances, untreated cells are round in shape at 24 and 48 h. The two data points represent two biological replicates. Following flubendazole treatment, *C. neoformans* strain LK128 became significantly less round in shape at 24 and 48 h, suggesting cell shape integrity is compromised.

4.3.2 Differential expression of transcription factors and kinases

Transcription factors and kinases play an important role in regulating the cell response to a stimulus, and therefore represent targets that may be exploited in or inform, antifungal drug discovery efforts. To explore changes to the transcriptional landscape of signalling genes effected by flubendazole, the differential expression of transcription factors and kinases from the RNA-Seq data (Chapter 3) was extracted and further investigated. At 12 h, a total of 127 transcription factors and kinases were significantly differentially expressed between flubendazole treated and untreated cells (Figure 4.8, Appendix Tables S6.2.1 and Appendix Table S6.2.2).

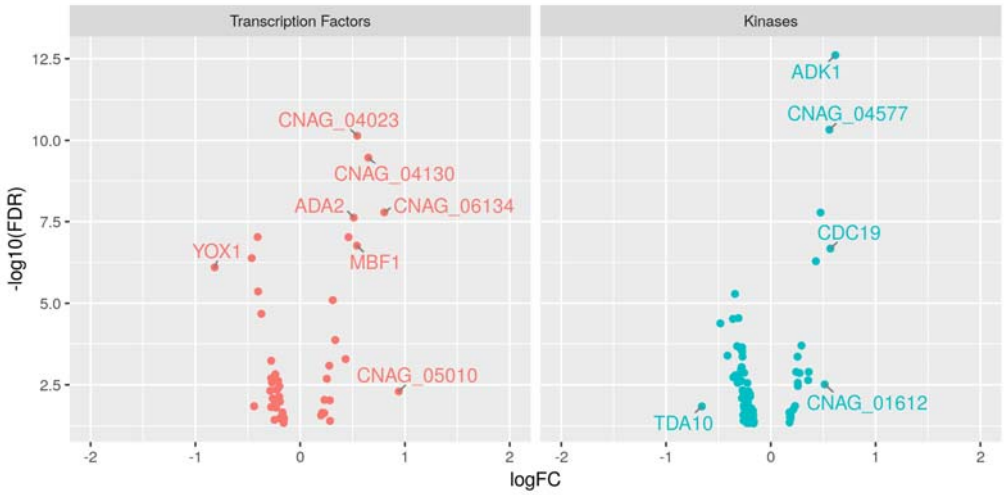

Figure 4.8. Transcription factors and kinases differentially expressed following flubendazole treatment.Genes with an adjusted p-value of less than 0.05 are separated by -$\log_{10}$ (FDR) (y-axis) and logFC (x-axis). Genes with a logFC greater than 0.5 or less than -0.5 are labelled with the Cryptococcus ID gene name, or S. cerevisiae ID gene name where there is orthology. This network was generated using R software (version 3.4.4). logFC: log fold-change. FDR: false discovery rate.

In this dataset, a large number of kinase-encoding genes were differentially expressed following flubendazole treatment (n = 78; Appendix Table S6.2.2). Of these genes, 22 had significantly increased expression while 56 others had significantly decreased expression. Almost all genes were functionally annotated with known orthologues in *S. cerevisiae*, with only three genes encoding hypothetical or uncharacterised kinases. Genes with the most significantly increased expression included adenylate kinase precursor *ADK1* (CNAG_02007, log FC 0.62) and pyruvate kinase *CDC19/PYK2* (CNAG_01820, log FC 0.57) which are involved in purine and pyruvate metabolism respectively. In contrast, the gene with the most significantly decreased expression was probable ATP-dependent kinase *TDA10* (CNAG_07779, log FC -0.65). A number of kinases with significantly decreased expression are involved in cell cycle function. These included cyclin-dependent kinase 1 *CDC28* (CNAG_01664, log FC -0.27), mitosis inhibitor protein kinase *SWE1* (CNAG_03369, log FC -0.34), checkpoint serine/threonine-protein kinase *BUB1* (CNAG_03184, log FC -0.31) and serine/threonine-protein kinase *MPS1* (CNAG_06697, log FC -0.25).

Of the 49 transcription factor genes found significantly differentially expressed, 18 had increased expression and 31 had decreased expression (Appendix Table S6.2.1). Unlike the list of kinases, more than half of the genes in this subset (n = 29) encoded uncharacterised or hypothetical proteins. The gene with the most significantly decreased expression was *YOX101* (CNAG_03229, log FC -0.82), which encodes cell cycle regulator *YOX1* in *S. cerevisiae*. Other cell cycle-related transcription factors that had decreased transcripts included *MBS2* (CNAG_01438, log FC -0.28) and *MBS1* (CNAG_07464, log

FC -0.25), which are orthologous to *MBP1/SWI6* and *MBP1* in *S. cerevisiae* respectively. In contrast, the gene with the most significantly increased expression was *C. neoformans* gene *ZFC7* (CNAG_05010, log FC 0.94) which encodes a hypothetical protein.

4.3.3 *C. neoformans YOX101Δ* exhibit decreased susceptibility in response to flubendazole

Due to a limited amount of time available, an extensive analysis of differentially expressed transcription factors and kinases could not be achieved. Therefore, this study chose to characterise the potential role of *YOX101*. This gene was selected on the basis that it was the most significantly differentially expressed transcription factor with both a clear *S. cerevisiae* homolog and a low false discovery rate (FDR) value. In addition, it is a cell-cycle regulator which is consistent with previous RNA-Seq data (Chapter 3), and the lab had access to a knockout mutant through Bahn's transcription factor knockout library (which was not the case for kinases).

Yox1p is a transcriptional repressor that binds to Mcm1 to suppress the expression of cell-cycle genes [351, 352]. Given its role in regulating the expression of cell-cycle genes, the decreased expression of *YOX101* in flubendazole-treated *C. neoformans* cells would appear to be consistent with the down-regulation of cell cycle and cell division genes and aberrant cell division morphology observed in transcriptomic and microscopy data. However, it remains unknown whether the significant suppression of *YOX1* transcripts in flubendazole-treated cells was a mechanism enabling cells to cope with flubendazole or a side-effect detrimental to cell viability. In response to antifungal drugs amphotericin B, 5-flucytosine and fluconazole, *yox101Δ* had been observed to be phenotypically indistinguishable to wild-type [322]. To determine if this also held for flubendazole, *yox101Δ* strains sourced from the same authors were used in spot plate assays. Both *yox101Δ* and H99S strains were cultured in liquid media, and spotted onto YPD agar containing flubendazole. Under no drug conditions, wild-type *C. neoformans* background strain H99S was viable (Figure 4.9). Under flubendazole treatment conditions, H99S was progressively less viable in a concentration-dependent manner with less growth observed at 4x MIC and growth almost abolished at 5 x MIC (Figure 4.9). *yox101Δ* grew to the same extent as untreated H99S on the no-drug plate, suggesting Yox101 is not essential for growth under normal conditions. This is consistent with a *S. cerevisiae* study that demonstrated the *S. cerevisiae* cells lacking Yox1p were viable [351]. On agar plates containing flubendazole, however, growth of *yox101Δ* was observed at concentrations that inhibited H99S wild-type cells. This indicates *yox101Δ* were less susceptible to flubendazole, suggesting the absence of *YOX101* may provide a survival advantage when cryptococcal cells are challenged with inhibitory concentrations of flubendazole.

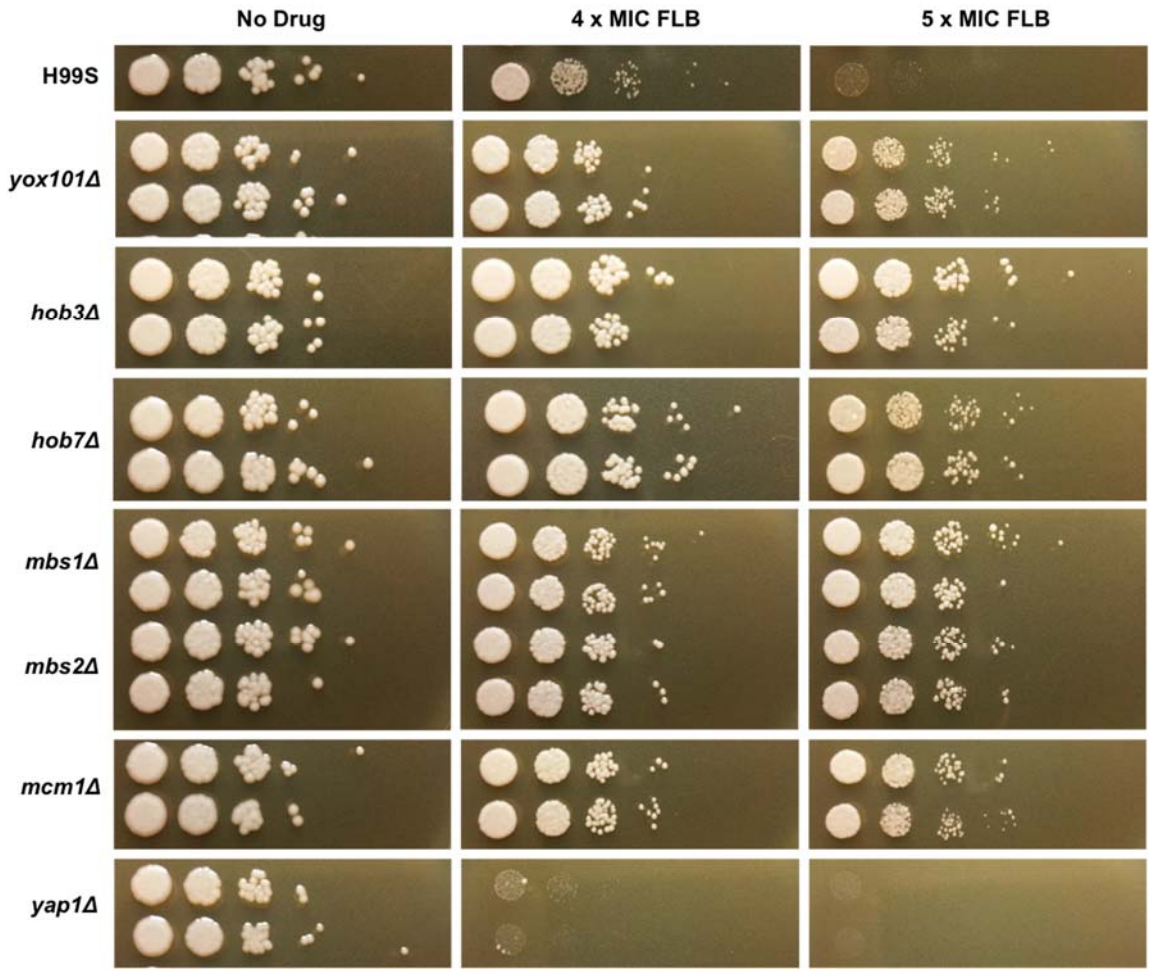

Figure 4.9. Spot assay of a series of transcription factor knockout strains in the presence of flubendazole.Cell cultures were grown in YPD broth overnight and serially diluted 10-fold from 1 x 10^6 cells/mL. A 5 µL aliquot of each dilution was spotted onto drug-free YPD agar or YPD agar containing flubendazole (FLB) and incubated at 30 °C. Two separate knockout strains were tested for each gene. Images shown were taken following 2 days of incubation. All strains were viable on drug-free YPD agar. The growth of H99S was visibly reduced on YPD agar containing FLB at 4x MIC, and abolished at 5x MIC. The knockout strains *yox101Δ, mbs1Δ, mbs2Δ, mcm1Δ, hob3Δ* and *hob7Δ* were viable on YPD agar containing FLB at 4x and 5x MIC, demonstrating substantially decreased susceptibility to FLB compared to H99S. The growth of knockout strain *yap1Δ* was almost abolished at 4x MIC FLB and completely abolished at 5x MIC. This demonstrates the importance of a functioning stress response in *C. neoformans* when treated with FLB.

4.3.4 Further investigation into the role of transcription factors in flubendazole sensitivity

To further assess the reduced susceptibility to flubendazole in *yox101Δ*, other knockout mutants of transcription factors closely associated with or functionally related to YOX101 were challenged with flubendazole (Table 4.1). In *S. cerevisiae*, Yox1p represses the activation of G1/S cell-cycle regulation genes, which depends on Yox1p interacting with transcription factor Mcm1 and transcription factor complexes Swi4-Swi6 (SBF; Swi4/Swi6-dependent cell cycle box-binding factor) and Mbp1-Swi6 (MBF; MluI cell cycle box –binding factor) (Figure 4.10, Table 4.2) [313, 351, 352]. *SWI4* and *MBP1* are orthologous to *C. neoformans MBS1*, while *SWI6* is orthologous to *C. neoformans MBS2*. *S. cerevisiae MCM1* and *C. neoformans MCM1* are orthologous and share the same gene name. On spot plates containing flubendazole, *mbs1Δ*, *mbs2Δ* and *mcm1Δ* strains displayed decreased susceptibility to flubendazole compared to H99S (Figure 4.9). These results collectively support previous phenotypic observations for *yox101Δ* and provide evidence to support the interacting relationships known between the gene products.

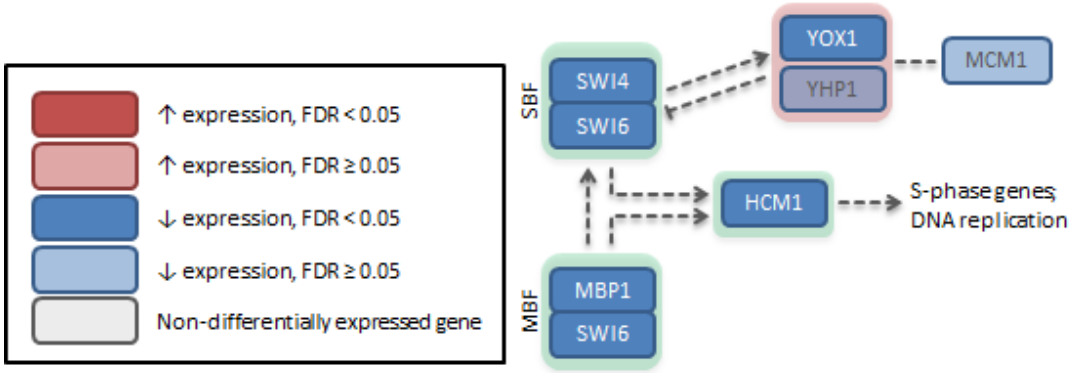

Figure 4.10. Schematic image of interactions between transcription factors Yox1, Yhp1, Mcm1, Swi4, Swi6, Mbp1 and Hcm1.Genes are shown as Saccharomyces cerevisiae orthologs inside rectangular objects, with dark red or dark blue shading indicating significantly increased or decreased expression (FDR < 0.05), respectively. Light red or light blue shading indicates genes that were differentially expressed but this was not statistically significant (FDR > 0.05). Light grey indicates genes that were not differentially expressed in this dataset. Dashed lines show a form of interaction, with pointed arrowheads and blunted ends indicating activation and inhibition, respectively. Transcription factors outlined in green or red indicate transcriptional activators or repressors, respectively. The expression data are listed in Table 4.2. SBF: Swi4/Swi6-dependent cell cycle box-binding factor; MBF: MluI cell cycle box-binding factor. Generated using [313, 351, 353] and the *S. cerevisiae* cell cycle KEGG pathway (KEGG Entry ID: sce04111) (https://www.genome.jp/kegg-bin/show_pathway?sce04111) [354].

Table 4.2. *S. cerevisiae* and *C. neoformans* orthologs of *YOX101* and associated transcription factors.

S. cerevisiae		*C. neoformans*		logFC[1]	FDR[2]	Notes[3]
YOX1	YML027W	YOX101	CNAG_03229	-0.81576	7.93E-07	Binds to Mcm1p and early Cell-cycle Boxes (ECBs) in the promoters of cell cycle-regulated genes expressed in M/G1; DNA synthesis/repair
YHP1	YDR451C	HOB7	CNAG_04586	-0.11566	0.149955	Yox1 paralog; cytokinesis, DNA synthesis/repair, cell wall synthesis
YHP1	YDR451C	HOB3	CNAG_05176	-0.40113	4.36E-06	
HCM1	YCR065W	HCM1	CNAG_03116	0.200635	0.027032	Forkhead transcription factor 3; cell wall and plasma membrane synthesis, mitosis and spindle function
HCM1	YCR065W	HCM101	CNAG_03212	-0.16625	0.028441	
MBP1; SWI4	YDL056W	MBS1	CNAG_07464	-0.24552	0.036985	Mbp1 is a component of the Swi6-Mbp1 (MBF) complex; Swi4 is a component of the Swi4-Swi6 (SBF) complex, that is involved in cell wall synthesis, DNA synthesis/repair, polarized growth, cell cycle regulation
MBP1; SWI6	YDL056W	MBS2	CNAG_01438	-0.2764	0.00059	Component of the Swi6-Mbp1 (MBF) complex; DNA synthesis/repair, cell wall synthesis
MCM1	YMR043W	MCM1	CNAG_07924	-0.1218476	0.169695	DNA replication initiation

[1] logFC: log fold-change

[2] FDR: false discovery rate

[1, 2] Data obtained from Chapter 3

[3] Information sourced from [355, 356]

YAP1 is a transcription factor that is responsible for the signalling and transcription of oxidative stress-responsive genes to modulate of levels oxidative stress [357, 358]. Although not differentially expressed in this dataset, *yap1Δ* was analysed to probe the mechanism of action of flubendazole in the context of oxidative stress in *C. neoformans*. Under normal (no-drug) conditions, *yap1Δ* grew to the same extent as H99S. On agar plates containing flubendazole, the growth of *yap1Δ* was substantially reduced at 4x MIC and abolished at 5x MIC. These results suggest that flubendazole treatment may be inducing oxidative stress in *C. neoformans* cells, which is detrimental to cell viability in the absence of Yap1.

Mebendazole is analogous to flubendazole and was recently reported to have antifungal activity against *C. neoformans* [164]. As mebendazole also belongs to the benzimidazole family of anti-parasitic agents, selected transcription factor mutants were challenged with mebendazole as well as the antifungal agent fluconazole. The knockout strains *yox101Δ*, *mbsΔ*, *mbs2Δ*, *mcm1Δ, hob3Δ* and *hob7Δ* were viable in the presence of mebendazole and growth was observed to be better compared to H99S (Figure 4.11). They were also observed to perform better in the presence of mebendazole compared to flubendazole. Most of the knockout strains also had elevated resistance to fluconazole (Figure 4.11). The growth of *yap1Δ* cells was almost abolished at 4x and 5x MIC flubendazole or mebendazole. This is consistent with the data generated following exposure of *yap1Δ* cells to flubendazole, indicating that all of these antifungal agents are inducing oxidative stress-like responses in *C. neoformans,* which may have a role in their antifungal mechanism of action. Overall, these results show consistency between the two benzimidazole agents.

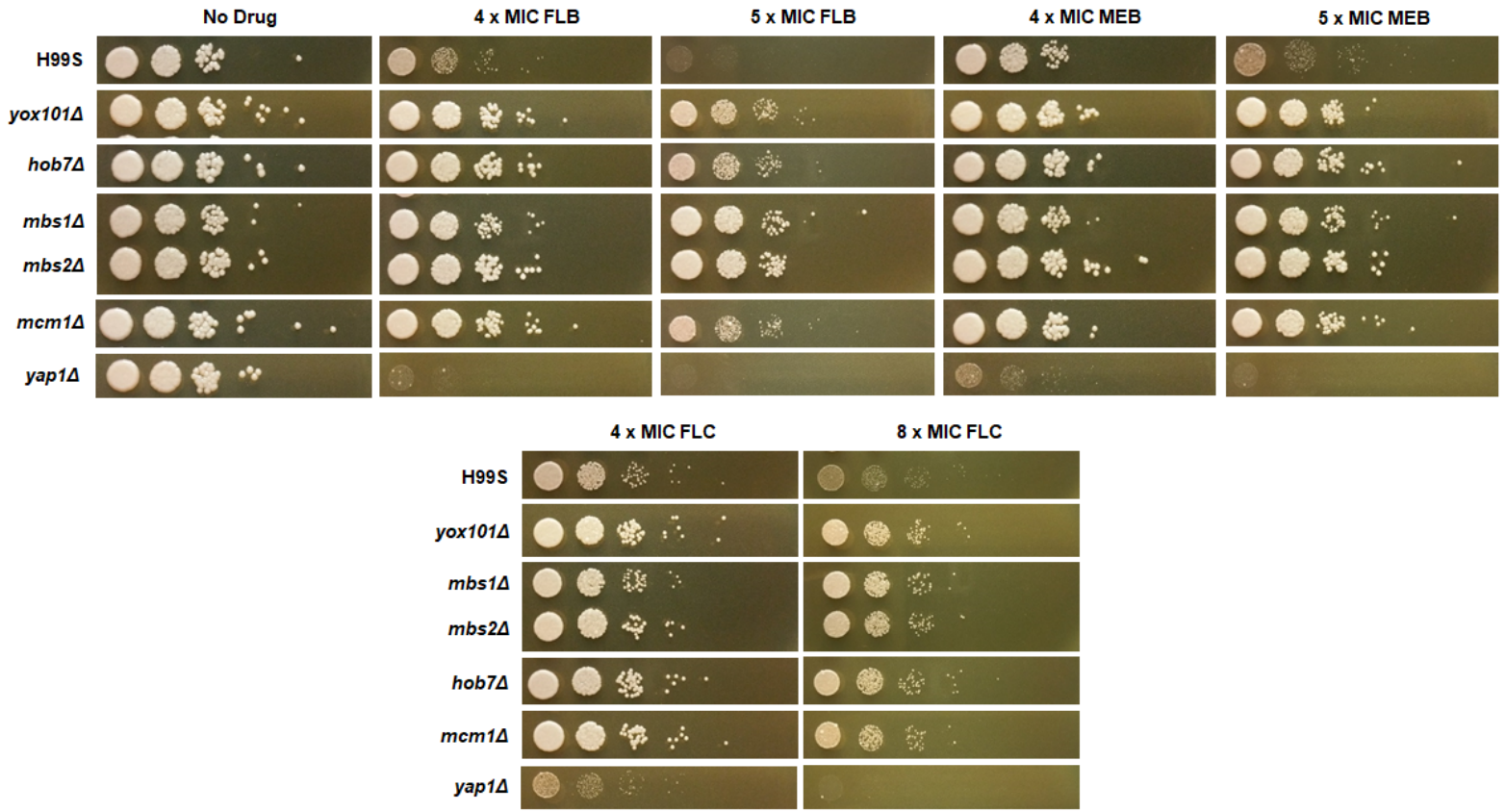

Figure 4.11. Spot assay of transcription factor knockout strains in the presence of flubendazole, mebendazole and fluconazole. Cell cultures were grown in YPD media overnight and serially diluted 10-fold from 1 x 10^6 cells/mL. A 5 µL aliquot of each dilution was spotted onto drug-free YPD agar or YPD agar containing flubendazole (FLB), mebendazole (MEB) or fluconazole (FLC), and incubated at 30 °C. One of two knockout strains were tested for each gene. Images shown were taken at day 2. All strains were viable on drug-free YPD agar. The growth of H99S was visibly reduced on YPD agar containing FLB at 4x MIC, and abolished at 5x MIC. The knockout strains *yox101Δ, mbs1Δ, mbs2Δ, mcm1Δ, hob3Δ* and *hob7Δ* were viable on YPD agar containing FLB at 4x and 5x MIC, demonstrating substantially decreased susceptibility to FLB compared to H99S. The growth of knockout strain yap1Δ was almost abolished at 4x MIC FLB and completely abolished at 5x MIC. This demonstrates the importance of a functioning stress response in *C. neoformans* when treated with FLB.

4.3.5 Flubendazole induces similar phenotypic changes in *yox101Δ* and wild-type strains

Previous microscopy work in this chapter revealed that *C. neoformans* cells treated with flubendazole had abnormal gross cellular morphology and disrupted tubulin morphology. Phenotypic work in *yox101Δ* showed decreased susceptibility to flubendazole on solid media compared to wild-type strain. In attempt to clarify the role of *YOX101* in response to flubendazole in *C. neoformans*, a microscopic analysis of knockout strain *yox101Δ* was performed.

As the *yox101* knockout mutant does not harbour fluorescently tagged tubulin, fluorescent analysis of changes in tubulin morphology in the presence of flubendazole could not be conducted. Under light microscopy, treated *yox101* cells appeared predominantly solitary, round and unbudded at 24 and 48 h, with a minority budded in pairs (Figures 4.12A and 4.12B). Following flubendazole treatment, *yox101Δ* cells displayed an increased number of budded and multi-budded cells, similar to treated H99S cells (Figures 4.12B-D). In addition, a comparative analysis of the degree of roundness of flubendazole treated and untreated *yox101Δ* cells found treated *yox101Δ* cells were distinctly and significantly less round compared to untreated cells (Figure 4.13A and 4.13B). These results are consistent with the data previously obtained using *C. neoformans* expressing β-tubulin-GFP (Figures 4.5 – 4.7) and suggest that flubendazole leads to defective cytokinesis and aberrant cell division in *Cryptococcus* regardless of *YOX101* status.

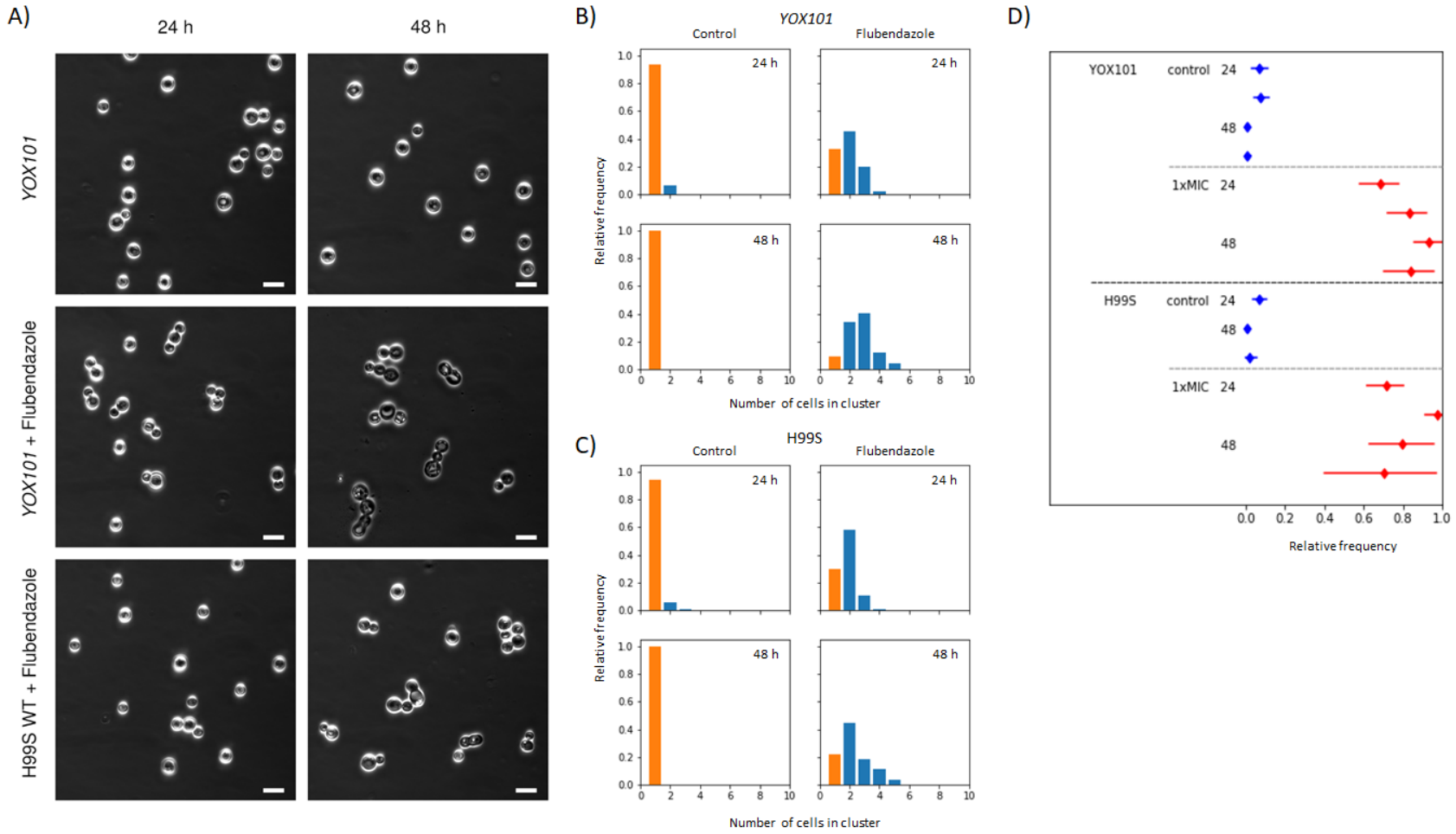

Figure 4.12. Morphological changes in *yox101Δ* cells in the presence or absence of flubendazole.H99S and *yox101Δ* cell cultures were grown overnight in YNB media and treated with 0.04 µg/mL flubendazole. Cells were imaged at 24 and 48 h on a Nikon eclipse Ti inverted microscope. (A) Microscopy images of *yox101Δ* and H99S cells treated with flubendazole (scale bar: 10 µm). In the presence of flubendazole, *yox101Δ* cells were observed to be affected similarly to H99S wild-type (WT), with cells mostly budding compared to untreated cells. (B and C) The distribution of the number of cells in a cluster expressed in

terms of relative frequency in *YOX101* and H99S, respectively. Orange bars highlight the proportion of unbudded cells. In both *yox101Δ* and H99S, flubendazole treatment resulted in a reduced proportion unbudded cells and an increased population of budding cells. Multi-budded cells, where three or more cells were attached, were also observed following treatment. (D) Statistical analysis of cell clustering in *yox101Δ* and H99S cells in the presence or absence of flubendazole. The degree of clustering expressed in terms of a percentage distribution of cells that were clustering (0.0 represents 0% clustering and 1.0 represents 100% cell clustering). Flubendazole treated and untreated cultures are represented with red and blue lines, respectively. Diamond icons denote the median and the length of a line shows the 95% credible interval range. The two data points represent two biological replicates. One H99S replicate in the 24 h control is unavailable due to unusable imaging data. In *yox101Δ* and H99S cells, significant cell clustering is present following flubendazole treatment compared to untreated cultures, which remain predominantly unbudded or not clustered.

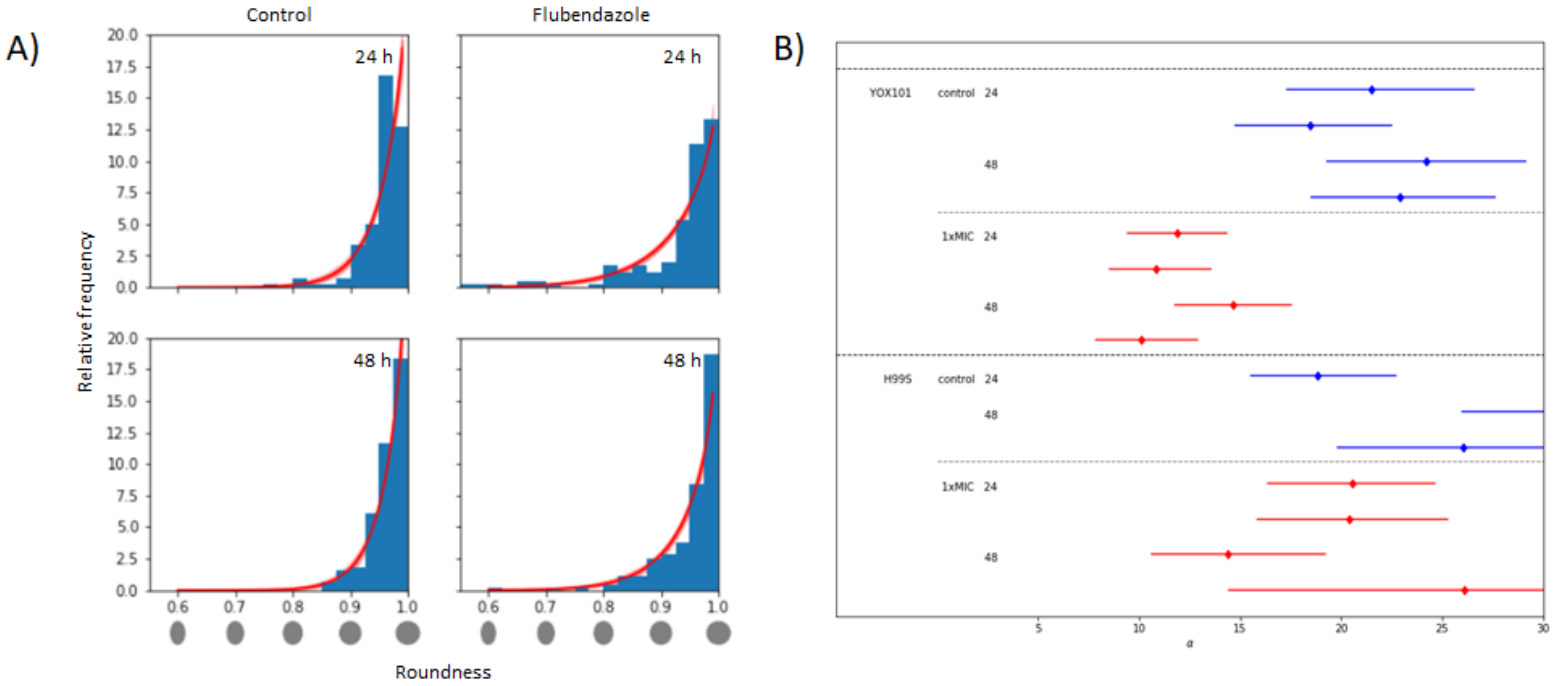

Figure 4.13. Cell shape analyses in flubendazole treated and untreated *yox101Δ* cells.

All cells within ten fields of view were outlined using ImageJ (version 2.0.0) prior to analysis. (A) The distribution of the roundness of *yox101Δ* cells expressed in terms of relative frequency. The x-axis is a scale for cell roundness, with scores closer to 1.0 denoting cells that are more round and scores less than 1.0 denoting cells that are less round and more oval in shape. The red line represents the differences in statistical significance between treated and untreated cells. (B) A statistical representation of the degree of roundness of *yox101Δ* cells, expressed in terms of alpha. The lower the value of alpha (x-axis), the less round cells are. The higher the value of alpha, the more round cells are and the greater the range of minimal changes being observed. Flubendazole treated and untreated samples are represented in red and blue lines, respectively. Diamond icons denote the median and the length of a line shows the 95% credible interval range. The two data points represent two biological replicates. One H99S replicate in the 24 h control is unavailable due to unusable imaging data. In Under normal circumstances, untreated cells are round in shape at 24 and 48 h. Following flubendazole treatment, *yox101Δ* cells become significantly less round in shape at 24 and 48 h compared to H99S wild-type, suggesting cell shape integrity is compromised.

4.4 Discussion

4.4.1 Flubendazole induces abnormal cell morphology and disturbed microtubules in *C. neoformans*

The RNA-Seq data presented in Chapter 3 suggested that tubulin may be a target of flubendazole, and multiple DNA- and cell division-related genes were down-regulated following exposure to flubendazole. To validate these observations, fluorescent microscopy was used to visualise changes to cell morphology in flubendazole-treated *C. neoformans* cells expressing β-tubulin-GFP. Imaging analyses revealed that a substantial proportion of treated cells had no microtubules filament structures, while other cells displayed scattered or fragmented β-tubulin-GFP and had an increased level of fluorescent intensity. These results may suggest that the addition of flubendazole causes a disruption in the assembly of microtubules and increased levels of tubulin proteins in cells. This is consistent with the increased levels of tubulin transcripts observed in Chapter 3, and could be a homeostatic response by the cell to increase tubulin production to compensate for microtubule breakdown or decreased tubulin turnover. This disruption of microtubule formation is consistent with recent studies in yeasts and mammalian cell lines that report a disruption of microtubular dynamics and networks caused by flubendazole or other microtubule-disturbing agents including benomyl, nocodazole and methyl benzimidazole carbamate [321, 359-361]. In a recent study investigating the inhibitory effects of flubendazole on melanoma cells, the authors found irregular microtubules and disorganised microtubule networks, accompanied by a decrease in microtubule density in flubendazole-treated cells [361]. Interestingly, a comparative study of mitotic division between ascomycete *C. albicans* and basidiomycete *C. neoformans* found that microtubules structures were similarly affected (shortened, misaligned and disorientated) when treated with nocodazole [321]. In the current study the length of microtubule structures was shortened compared to untreated cells in *C. neoformans,* however, flubendazole was not effective in inhibiting the growth of *C. albicans* at concentrations as high as 40 μg/mL (Chapter 2).

Microtubules are essential for chromosome segregation and the disruption of microtubule function is detrimental to cell division and cell viability [320, 360]. In addition to abnormal tubulin morphology (Figures 4.3 and 4.4), abnormal cell morphology was also observed in cells treated with flubendazole (Figures 4.5 and 4.6). Following flubendazole treatment, there was an increased number of budded cells, including multi-budded cell clusters, which were significantly less round in shape compared to untreated cells (Figure 4.7). The substantially increased number of budded cells in flubendazole-treated cell cultures may suggest that flubendazole exposure does not inhibit budding, but rather prevents actively budding cells from exiting mitosis, causing cells to fail cytokinesis and remain

attached to the parent cell. Similar findings were reported by Altamirano *et al.* (2017) who observed that *C. neoformans* cells treated with fluconazole, a widely used antifungal drug, displayed abnormal budding and defective cytokinesis [101]. A contrasting difference however, is that Altamirano *et al.* (2017) reported that fluconazole treatment inhibited cell budding, whereas flubendazole used in this study did not [101]. This may be explained by the differing modes of actions of flubendazole and fluconazole. Fluconazole inhibits the biosynthesis of ergosterol, which is an integral component of the fungal cell wall and cell membrane. Therefore, the targeting of ergosterol by fluconazole may impact the ability of cells exposed to the drug to grow or bud. In other studies, abnormal or irregular cell morphologies have also been reported in *Cryptococcus* following treatment with specific microtubule inhibitors [164, 362]. This indicates that the morphological changes observed in this study may not be unique to flubendazole.

4.4.2 The potential role of cell-cycle regulator *YOX101* in response to flubendazole

In this study, the treatment of cells with flubendazole resulted in the differential expression of a list of transcription factors in *C. neoformans*. Within this list, *YOX101* was the most significantly down-regulated and was chosen to investigate further to determine its significance in the response of *C. neoformans* to flubendazole. *YOX101* is a transcription factor belonging to the homeobox family. This family of transcription factors is characterised by a 180 bp sequence region that encodes a 60 amino acid long DNA-binding domain [363]. Transcription factors that contain this homeodomain are responsible for many cellular processes and biological functions but mainly partake in the transcriptional regulation of developmental genes [363, 364]. *YOX101* functions as a transcriptional repressor of cell cycle genes and is orthologous to *YOX1* in *S. cerevisiae*. In *S. cerevisiae*, Yox1p competitively binds to Mcm1p to form a complex that interacts with and represses two transcription factor complexes SBF (Swi4/Swi6-dependent cell cycle box-binding factor) and MBF (MluI cell cycle box–binding factor) [313, 351, 352, 365]. SBF and MBF are DNA-binding heterodimers comprised of Swi4-Swi6 and Mbp1-Swi6 respectively, with Swi4 and Mbp1 being the DNA-binding component and Swi6 acting as a co-regulator [366, 367]. The two transcription factor complexes are important for the periodic activation and expression of over 200 cell cycle genes and cell cycle progression [367-369]. SBF regulates the expression of genes involved in budding, and cell wall biosynthesis, while MBF regulates the expression of genes involved in DNA synthesis, replication and repair [367, 368]. The repression of these complexes by *Yox1* leads to the transcriptional repression of early cell cycle genes. The significance of *Yox1* and its paralog *Yhp1*, has been demonstrated by Pramila *et al*. (2002) using a *yox1yhp1* double mutant to assess cell cycle regulation [351]. The study revealed the absence of both *Yox1* and *Yhp1* resulted in an increased expression of a set of twenty-eight genes and their periodic expression was abolished indicating disrupted cell-cycle regulation [351].

The decreased expression of the *YOX101* gene this data does not appear to be a specific response to flubendazole in *C. neoformans*. In a similar study, Pang *et al*. (2017) profiled the transcriptional response of *C. neoformans* to amphotericin B (AMB) alone and in combination with iron chelator lactoferrin (LF) using RNA-Seq technology [178]. The expression of *YOX1* was significantly reduced under both drug treatments (AMB alone: log FC -0.51, adjusted p-value = 1.3E-0.5; AMB + LF (log FC -0.55, adjusted p-value = 4.9E-0.5), which agrees with the data in the current study.

The deletion of the *YOX101* gene in *C. neoformans* led to a decreased susceptibility to flubendazole observed on solid agar media, suggesting that down-regulation of the YOX1 gene may be a responsive mechanism to cope with flubendazole treatment. This phenotype of *C. neoformans yox1Δ* is unique and has not been previously reported. In their extensive effort to characterise the phenotypic traits of over 150 transcription factors, Jung *et al* (2015) found the deletion of *YOX1* had minimal impact on the viability of *C. neoformans* and with the exception of increased susceptibility to heavy metal-inducer cadmium sulfate and osmotic stress-inducer *tert*-butyl hydroperoxide, found the deletion of *YOX101* did not impair cell viability in the presence of cell wall, genotoxic, endoplasmic reticulum and other oxidative stresses and did not affect susceptibility to the antifungal drugs amphotericin B, fluconazole and 5-flucytosine [322]. While the current study did not test amphotericin B and 5-flucytosine, y*ox101Δ* demonstrated increased tolerance to fluconazole relative to H99S control. However, the concentration of fluconazole used by Jung *et al*. (14 and 16 µg/mL) was in higher than the concentration used in this study (8 and 10 µg/mL) making it difficult to make a meaningful comparison between these studies.

Microscopic imaging analyses revealed *yox101Δ* cells treated with flubendazole developed an altered cell morphology characterised by abnormal budding (Figure 4.12). These observations were similar to morphological defects in flubendazole-treated H99S wild-type cells, demonstrating that the absence of Yox101 alone does not wholly account for the morphological changes induced by flubendazole. This is consistent with the major functions of Yox101, relating to the synthesis and repair of DNA, and the regulation of cell cycle genes [351]. Interestingly, despite the morphological defects induced by flubendazole, *yox1Δ* cells are less susceptible to the drug and are able to proliferate even though they do not appear to undergo cell cycle normally (Figure 4.9).

The investigation of *YOX101* in this study provides a degree of validation to the RNA-Seq data obtained in Chapter 3. The significantly reduced expression of *YOX101* following flubendazole treatment may or may not have been a coping mechanism to sustain survival. However, spot plate assays demonstrated that the deletion of the *YOX1* gene enabled growth and improved survival fitness compared to H99S suggesting that the suppression of the gene was a coping mechanism in response

to flubendazole. While this result discourages the targeting *YOX101* in an antifungal capacity, it demonstrates that there are opportunities to target proteins other than tubulin such as transcription factors. Targeting non-tubulin targets that result in increased susceptibility to flubendazole, as shown by *yap1Δ* (Figure 4.9), could greatly benefit antifungal drug discovery ventures. Further antifungal drug development will be substantially aided by the availability of the *C. neoformans* transcription factor and kinase knockout libraries, as well as comprehensive phenotypic and genetic data [322, 333].

4.4.3 Future directions

The investigation of *YOX101* in this chapter helps to validate part of the RNA-Seq data obtained in Chapter 3. A comprehensive validation of the RNA-Seq dataset using quantitative PCR (qPCR) would provide additional confidence for subsequent studies that use this dataset. Furthermore, since not all gene transcripts are necessarily translated into functional proteins, a proteomic assessment of flubendazole-treated *C. neoformans* cells could be used to provide orthogonal evidence to support, or challenge, the results interpreted from the RNA-Seq data. Further studies may aim to investigate transcription factors and kinases in *C. neoformans* as potential targets for future antifungal drug discovery. A list of transcription factors and kinases which are significantly differentially expressed in response to flubendazole, are provided from this study. This can aid further efforts in the development of specific inhibitors of transcription factors and kinases.

In this study, the *yox1Δ* mutant was observed with similar morphological defects as the wild-type strain, despite having a decreased susceptibly to flubendazole. This suggests that there are other factors or targets involved in the mechanism of flubendazole and this remains an area to be explored. One possibility is the direct involvement of tubulin and its dynamics being disrupted by flubendazole, as it is a critical component of cellular structure. The relationship between Yox101 and tubulin in *C. neoformans*, in the context of flubendazole treatment, was an aspect that was not elucidated by the experiments of this study. A visualisation of tubulin within *yox1Δ* cells in the presence of flubendazole may be able to address this hypothesis.

Chapter 5: Final discussion

With the repertoire of antifungal drugs available to treat cryptococcal meningitis critically limited, drug repurposing offers immense promise as an approach to fast-track antifungal drug discovery. Using such an approach, this thesis identified the anthelmintic benzimidazole drug, flubendazole, as having potent fungicidal activity against *Cryptococcus* spp. The antifungal activity of flubendazole was comprehensively characterised and was found to target *Cryptococcus* spp., and was not effective against important human fungal pathogens *Candida* and *Aspergillus*. The antifungal activity of flubendazole was fungicidal and it inhibited members within all eight species groups that currently make up the *Cryptococcus* species complex. Importantly, flubendazole was able to equally inhibit strains of *Cryptococcus* that were susceptible or resistant to fluconazole, a widely used antifungal drug. Unfortunately, flubendazole did not synergise with standard antifungal drugs. However, as it was found to produce an additive/indifferent effect in combination, flubendazole could still be used to lower the dose of other drugs in combinational drug therapies and could help deter the development of resistance.

In an exploratory study to understand the antifungal mechanism of action of flubendazole, a combination of imaging and transcriptomic analyses found that tubulin dynamics and microtubule structures were affected in flubendazole-treated cells. This was indicated by a substantial reduction in abundance and size of microtubule 'string-like' structures, observed concomitantly with diffused or fragmented GFP-tagged tubulin, and an increased average fluorescent intensity in treated cells. These data support the hypothesis that tubulin is a likely target of flubendazole in *C. neoformans*, which is consistent with the described target of other benzimidazole agents in parasites [267, 370]. Furthermore, abnormal budding in treated cells suggested that fundamental cellular processes pertaining to cell division were disrupted following flubendazole treatment. This validated the transcriptional data that revealed a dysregulation of genes involved in DNA replication, sister chromatid segregation, mismatch repair and cellular detoxification. A specific investigation into a subset of the RNA-Seq data identified transcriptional cell-cycle gene repressor *YOX101* with significantly reduced transcript levels in response to flubendazole treatment. A *yox101Δ* strain had decreased susceptibility to flubendazole compared to the wild-type strain, and this phenotype was shared with knockout strains of *YOX101* paralogs and interacting partners.

5.1 Flubendazole – challenges and opportunities for use as a systemic antifungal therapy

Flubendazole is primarily an anti-parasitic drug that is currently used to treat nematodes that cause gastrointestinal parasitic infections in humans and animals [371]. It is well tolerated with lack of evidence of serious adverse side effects in healthy volunteers, patients undergoing anti-helminthic treatment and in mice experimentally treated with flubendazole [203, 205-207]. In recent years, flubendazole has been the subject of multiple studies investigating its potential for repurposing in therapeutic fields other than its prescribed original indication. This includes the treatment of various types of cancers and other parasitic and filarial worm infections such as onchocerciasis [196, 210-212, 223, 371-374], highlighting the diversity of biological activity of flubendazole. Contributing to this, this thesis describes the antifungal activity of flubendazole and highlights its potential application in an antifungal context. At the start of this thesis, flubendazole was shown to have previously undescribed activity against *Cryptococcus* spp., and since then two other studies have reported the antifungal activities of flubendazole, supporting its potential application in cryptococcal infections [164, 208].

While this opens new opportunities and areas of research for antifungal drug discovery, it is important to note that the formulation of flubendazole currently used to treat gastrointestinal parasites does not enable direct application for cryptococcal meningitis. This is largely due to the poor solubility of flubendazole, which consequently means its systemic bioavailability is limited [375]. While suitable for gastrointestinal infections, flubendazole needs to be systemically available, and accumulate to clinically relevant and therapeutic levels in the brain to treat cryptococcal meningitis. Reformulating flubendazole may improve bioavailability and efforts have been made in this regard for both anti-parasitic and antifungal purposes [208, 372]. In uninfected rats and jirds (rodents), flubendazole formulated as an aqueous hydroxypropyl-b-cyclodextrin suspension displayed superior systemic exposure compared to formulations as an aqueous carboxymethyl cellulose suspension and a Tween 80-based suspension [372]. A popular formulation is the use of amorphous solid dispersion. This is a strategy where the bioavailability of a drug is improved by using an inert, solid state carrier or medium to enhance the rate and extent of dissolution of the drug in the body [376]. Tweats *et al*. (2015) tested the genotoxicity of an amorphous solid dispersion formulation of flubendazole produced by Abbot Laboratories and determined that it posed minimal carcinogenic risk to patients in the context of short-term dosing [377]. However, when Nixon *et al*. (2018) tested an amorphous solid drug nanodispersion formulation of flubendazole developed by Janssen Pharmaceuticals in a murine model of cryptococcal meningitis they found that although the formulation was orally bioavailable, it was only able to delay (not inhibit) fungal brain burden in mice [208].

Very recently, Lachau-Durand *et al*. (2019) conducted a series of preclinical safety studies on an amorphous solid dispersion formulation of flubendazole for the treatment of onchocerciasis. This included an *in vivo* assessment of oral bioavailability and toxicology in dogs, rats and jirds. Unfortunately, the study was unable to successfully determine a safe and efficacious regimen that would clinically benefit patients [378]. It is unclear whether the formulation of flubendazole in this study was identical to the formulation tested by Nixon *et al*. (2018). While formulation may require additional work to optimise therapeutic effect, flubendazole may still be considered a promising lead for future antifungal drug development. Furthermore, as the preclinical studies were conducted in the context of treating parasites, re-evaluation will be necessary in the context of treating cryptococcal infection.

The establishment of flubendazole as a potent antifungal offers a chemical scaffold for future medicinal chemistry studies. Such studies would aim to find a compound or series of compounds that retain their anti-cryptococcal activity and have no or minimal toxicity. The data provided in this thesis may help support initiatives aimed to further develop formulations of flubendazole that achieve therapeutic concentrations without toxicity, or the development of new antifungal drugs in general. The latter could involve pursuing non-tubulin fungal targets that are uncovered by further analyses of the transcriptomic data. Further studies could aim to modulate the chemical structure of flubendazole to enhance its activity against non-tubulin targets, or explore drug combination strategies in order to achieve more potent antifungal activity with minimal toxicity. Flubendazole has been shown to inhibit tumour growth by inducing apoptosis via the transcription factor p53 in neuroblastoma cells, highlighting its potential for affecting non-tubulin targets in a cell [211].

5.2 Medicinal chemistry to optimise and expand the spectrum of antifungal activity of flubendazole

While the antifungal activity of flubendazole so far appears limited to *Cryptococcus* spp. [379], it may be possible that it can be pharmacologically modified to broaden its antifungal spectrum of activity to combat other medically important fungal pathogens. Importantly, benzimidazole derivatives have been developed and shown to have efficacy against *Candida* and *Aspergillus* spp. Chandrika *et al*. (2016) demonstrated that modifying the length of the alkyl chain of a benzimidazole influenced antifungal activity against *Candida* and *Aspergillus* spp. [380]. In addition, developing derivatives of benzimidazole can lead to new targets that are distinct from tubulin [381]. This was the case for benzimidazole derivative EMC120B12, which inhibited the growth of pathogenic species of *Candida* and was found to target the ergosterol biosynthesis pathway [381], and a neomycin b-bisbenzimidazole that did not inhibit the ergosterol biosynthesis pathway but induced toxic levels of

reactive oxygen species in *C. albicans* [382]. Although modifying flubendazole will require new preclinical and clinical studies to evaluate potential differences in safety and toxicity profiles, this approach may still be faster and less expensive than developing a new entity drug with no pre-established data.

Future studies may aim to further investigate tubulin as an antifungal target. *S. cerevisiae* tubulins share approximately 75% amino acid sequence identity to animal tubulin, while *C. neoformans* has 90% amino acid sequence identity to human β-tubulin [208, 218, 219]. The high sequence homology shared by fungal yeast and mammalian tubulins may raise concerns pertaining to target (tubulin) specificity in humans. However, there may be small differences in tubulin sequence that although subtle, can affect the structure and function of microtubules [383]. These differences will be better understood when crystal structures of fungal tubulin proteins have been achieved, which can facilitate structure-activity relationship docking studies to inform possible target sites with minimal adverse effects [208].

5.3 Systems biology analysis enables a holistic view of the drug response

Technologies that enable the study of biology at the systems level have become increasingly popular in yeast research. The generation of large, comprehensive 'omics-based datasets produced over multiple time points allows dynamic changes in fungal biology to be studied. This approach has been particularly helpful in assessing how fungi respond to inhibitory drugs [177, 178]. In this study, the use of RNA-Seq technology in combination with a multi-time point design proved to be a valuable approach in exploring the mechanistic action of flubendazole in *C. neoformans* as well as the biological response of *C. neoformans* to the drug. The RNA-Seq data generated in this study found evidence to support tubulin as the fungal target of flubendazole in *C. neoformans*, but also revealed a wide range of peripheral biological responses that provide a global view of the effects of the drug. Many of these responses likely represent the downstream effects of disrupting tubulin function, lending additional support for tubulin as the primary drug target.

Interestingly, the adoption of a multi-time point experimental design provided some additional and somewhat unexpected insights in understanding the effects of flubendazole on *C. neoformans*. The data revealed that minimal transcriptional changes occurred in the first two time points, meaning that a full 12 h of drug treatment was required to observe the bulk of the transcriptional response to the drug. While this limited the potential to detect dynamic transcriptional changes over time in the current data set, it suggests that, under the experimental conditions of this study, flubendazole elicits a non-acute antifungal effect, reflected by a delayed transcriptional response. This finding would not

have otherwise been apparent without the multi-time point approach, and highlights the difficulties associated with experimental design when selecting time points to study a critical response window (of time) that will provide the most meaningful biological data.

One limitation to the analysis of the RNA-Seq data is that changes the number gene transcript do not necessarily reflect the production of final protein products, which can only be inferred. This is further complicated by evidence that *Cryptococcus* genes are rich in introns and alternative splicing can occur, suggesting a capacity for redundancy in transcripts within cells [384, 385]. One strategy that can be used to validate RNA-Seq data is to conduct a proteomic analysis and then compare the two datasets. While requiring considerable resources, this evaluation provides confidence that genes with transcriptional changes do have biological significance. It is noted however, that the application of proteomics to validate RNA-Seq data in *C. neoformans* may be limited by the lack of a well-annotated genome in *C. neoformans*.

5.4 Conclusions

Screening libraries of FDA-approved compounds offers new possibilities to find compounds that may have hidden and undescribed therapeutic activities and can be harnessed to address unmet medical needs. The work generated from this thesis demonstrates how a candidate compound may be found and validated, although ensuing studies may still be complex and require effort to bring it to market. Regardless of whether a drug can be directly repurposed with a new antifungal indication, or additional modification and optimisation work is required, any progress in antifungal drug discovery is useful given the longstanding lack of currently available antifungal drugs. Therefore, continued efforts in finding candidate compounds that may be repurposed as antifungal drugs or act as leads for antifungal drug development programs are warranted.

This thesis concludes that high-throughput screening methodologies using FDA-approved drugs are valuable approaches to kick-start drug discovery efforts. This is demonstrated by the discovery of the anti-parasitic drug flubendazole as an FDA-approved compound with novel antifungal activity against *Cryptococcus*. Flubendazole showed potent antifungal activity against *Cryptococcus* spp., with RNA-Seq and microscopy evidence supporting tubulin as the primary target. Careful attention to optimisation and replication provided robust transcriptomic data, producing a profile of the response that was relatively easy to interpret and made sense from a biological perspective. This robust data set enables future studies to use, benefit and build on the current body of work for additional drug discovery ventures such as drug synergy. It also provides data for further investigation of transcription factors and kinases in *C. neoformans* as an untapped resource of potential antifungal targets.

Chapter 6: Appendix

6.1 Chapter 3 Supplementary Material

Supplementary Table S6.1.1. List of genes differentially expressed comparing flubendazole treated and untreated cells at 6 h (FLBvsCTRL.6h).

Gene ID	logFC[1]	FDR[2]	Broad gene name	Sc[3]	Sc ortholog descriptions
CNAG_02300	0.762982	0.027203	hypothetical protein		
CNAG_06853	0.556193	0.049198	hypothetical protein		
CNAG_01077	0.548004	0.007991	hypothetical protein		
CNAG_00149	0.534396	0.000787	NADH dehydrogenase (ubiquinone) 1 alpha		
CNAG_01113	0.418059	0.007991	hypothetical protein		
CNAG_01070	0.414434	0.038996	class II aldolase/adducin family protein		
CNAG_01396	0.367899	0.013376	protein SUS1	SUS1	Transcription and mRNA export factor SUS1
CNAG_06935	0.324867	0.020158	isochorismatase hydrolase		
CNAG_06870	0.294635	0.013658	hypothetical protein		
CNAG_01007	-0.29723	0.012406	C2 domain-containing protein		
CNAG_05872	-0.30491	0.006936	endopeptidase		
CNAG_01464	-0.91375	4.07E-06	nitric oxide dioxygenase	YHB1	Flavohemoprotein

[1] logFC: log fold-change

[2] FDR: false discovery rate (adjusted p-value < 0.05)

[3] Sc: *Saccharomyces cerevisiae*

Supplementary Table S6.1.2. List of genes differentially expressed comparing flubendazole treated and untreated cells at 8 h (FLBvsCTRL.8h).

Gene ID	logFC[1]	FDR[2]	Broad gene name	Sc[3]	Sc ortholog descriptions
CNAG_04245	1.300853	1.65E-05	chitinase		
CNAG_04183	1.152026	0.00011	hypothetical protein		
CNAG_02300	1.145195	1.02E-05	hypothetical protein		
CNAG_07842	0.74402	0.045313	hypothetical protein		
CNAG_05660	0.740355	0.000229	hypothetical protein		
CNAG_03516	0.724355	0.001139	hypothetical protein		
CNAG_02850	0.706993	0.003982	glucan endo-1,3-alpha-glucosidase agn1		
CNAG_06205	0.70388	0.000287	hypothetical protein		
CNAG_04553	0.649188	0.001122	hypothetical protein		
CNAG_06172	0.648047	0.030557	transketolase		
CNAG_06245	0.612094	0.015181	hypothetical protein		
CNAG_00854	0.581372	0.037638	C-8 sterol isomerase	ERG2	C-8 sterol isomerase
CNAG_03037	0.562179	0.000941	hypothetical protein		
CNAG_07836	0.55367	0.035625	NAD binding dehydrogenase family protein		
CNAG_01023	0.55285	0.008807	cohesin complex subunit SCC1		
CNAG_00799	0.544258	0.014284	cellulase		
CNAG_06853	0.541125	0.027397	hypothetical protein		
CNAG_07448	0.535058	0.036474	urea transporter	DUR3	Urea active transporter
CNAG_04469	0.511285	0.041634	4-aminobutyrate transaminase		
CNAG_07756	0.507531	0.000139	cell division control protein	CDC20	APC/C activator protein CDC20
CNAG_00930	0.503335	0.014284	argininosuccinate synthase	ARG1	Argininosuccinate synthase
CNAG_00194	0.491524	0.035309	hypothetical protein		
CNAG_01827	0.475664	0.011453	hypothetical protein		
CNAG_01113	0.448919	0.000664	hypothetical protein		
CNAG_02830	0.446879	0.019944	delta24(24(1))-sterol reductase	ERG4	Delta(24(24(1)))-sterol reductase
CNAG_06102	0.427752	0.037638	ADP,ATP carrier protein		

CNAG_02577	0.425196	0.04691	oxidoreductase	SCS7	Ceramide very long chain fatty acid hydroxylase SCS7
CNAG_06920	0.423207	0.000663	ubiquitin carboxyl-terminal hydrolase 10	UBP3	Ubiquitin carboxyl-terminal hydrolase 3
CNAG_01889	0.415478	0.008807	glutathione S-transferase		
CNAG_02918	0.399243	0.028089	acetyl-CoA C-acetyltransferase	ERG10	Acetyl-CoA acetyltransferase
CNAG_01881	0.389096	0.004184	molecular chaperone GrpE	MGE1	GrpE protein homolog, mitochondrial precursor
CNAG_04080	0.384973	0.004398	3-hydroxyanthranilate 3,4-dioxygenase	BNA1	3-hydroxyanthranilate 3,4-dioxygenase
CNAG_05573	0.357223	0.028089	cytochrome c oxidase assembly protein subunit 17	COX17	Cytochrome c oxidase copper chaperone
CNAG_04062	0.348952	0.012443	ribosome biogenesis protein ENP2	ENP2	Ribosome biogenesis protein ENP2
CNAG_07671	0.343598	0.027397	hypothetical protein		
CNAG_07778	0.34147	0.000171	translation initiation factor 2 subunit 1	SUI2	Eukaryotic translation initiation factor 2 subunit alpha
CNAG_04899	0.33691	0.042479	cytoplasmic protein		
CNAG_03735	0.333187	0.009396	hypothetical protein		
CNAG_06367	0.331307	0.008807	U3 small nucleolar RNA-associated protein 3	SAS10	Something about silencing protein 10
CNAG_03790	0.325917	0.011653	hypothetical protein		
CNAG_03951	0.3237	0.010485	hypothetical protein		
CNAG_04082	0.315751	0.030828	proline-tRNA ligase	YHR020W	Putative proline--tRNA ligase YHR020W
CNAG_05018	0.314637	0.049821	hypothetical protein		
CNAG_02552	0.307597	0.046491	Transketolase		
CNAG_03242	0.307565	0.008807	solute carrier family 25 (peroxisomal adenine nucleotide transporter), member 17		
CNAG_03453	0.300192	0.030647	kinesin family member 11	KIP1	Kinesin-like protein KIP1
CNAG_05618	0.297889	0.036474	cleft lip and palate associated transmembrane protein		
CNAG_01701	0.289478	0.014284	integral membrane protein	RTA1	Protein RTA1
CNAG_04023	0.289429	0.034107	hypothetical protein		
CNAG_07998	0.27827	0.044195	hypothetical protein		

CNAG_01781	0.254787	0.039902	hypothetical protein		
CNAG_02566	0.239199	0.028884	hepatocyte nuclear factor	FKH2	Fork head protein homolog 2
CNAG_03815	0.238651	0.04691	hypothetical protein		
CNAG_04961	0.23367	0.021041	orotidine 5'-phosphate decarboxylase	URA3	Orotidine 5'-phosphate decarboxylase
CNAG_02115	0.233589	0.030343	nonhistone protein 6	HMO1	High mobility group protein 1
CNAG_02898	0.232693	0.043442	RNA-binding protein 8A		
CNAG_05657	0.227838	0.04317	cytoplasmic protein		
CNAG_01155	-0.24421	0.049821	glycerol kinase	GUT1	Glycerol kinase
CNAG_01987	-0.26467	0.030557	carbohydrate binding protein	MNL1	ER degradation-enhancing alpha-mannosidase-like protein 1 precursor
CNAG_06090	-0.27359	0.006116	hypothetical protein		
CNAG_04746	-0.2744	0.008807	hypothetical protein	NCA2	Nuclear control of ATPase protein 2
CNAG_04970	-0.2752	0.034216	hypothetical protein		
CNAG_01496	-0.28108	0.026276	protein phosphatase 5	PPT1	Serine/threonine-protein phosphatase T
CNAG_01584	-0.28545	0.037638	hydrolase		
CNAG_02532	-0.29464	0.049821	D-amino-acid oxidase		
CNAG_03685	-0.29596	0.004527	hypothetical protein		
CNAG_05178	-0.30884	0.041992	hypothetical protein		
CNAG_03187	-0.30978	0.028884	protoporphyrinogen oxidase	HEM14	Protoporphyrinogen oxidase
CNAG_02658	-0.30984	0.049788	hypothetical protein		
CNAG_04187	-0.31087	0.014284	GPI-anchored wall transfer protein 1	GWT1	GPI-anchored wall transfer protein 1
CNAG_01007	-0.317	0.001967	C2 domain-containing protein		
CNAG_06868	-0.32421	0.046491	phosphopyruvate hydratase		
CNAG_00499	-0.32696	0.019944	solute carrier family 25 (mitochondrial carnitine/acylcarnitine transporter), member 20/29	CRC1	Mitochondrial carnitine carrier
CNAG_06901	-0.33067	0.04317	UDP-N-acetylglucosamine-dolichyl-phosphate N-acetylglucosaminephosphotransferase	ALG7	UDP-N-acetylglucosamine--dolichyl-phosphate N-acetylglucosaminephosphotransferase
CNAG_00036	-0.33378	0.019944	Sec14 cytosolic factor	SEC14	SEC14 cytosolic factor

CNAG_00732	-0.33388	0.019292	hypothetical protein		
CNAG_06771	-0.33536	0.013242	hypothetical protein		
CNAG_05872	-0.33984	0.000283	Endopeptidase		
CNAG_03564	-0.36806	0.01129	hypothetical protein		
CNAG_06334	-0.37009	0.008807	hypothetical protein		
CNAG_01387	-0.37719	0.008021	hypothetical protein		
CNAG_05119	-0.37994	0.000139	GabA permease	TPO5	Polyamine transporter TPO5
CNAG_06064	-0.39539	0.000776	hypothetical protein		
CNAG_06286	-0.39871	0.026276	hypothetical protein		
CNAG_04275	-0.40391	0.008807	metalloendopeptidase		
CNAG_06668	-0.40591	0.017039	mitochondrial protein	RCF2	Respiratory supercomplex factor 2, mitochondrial
CNAG_04886	-0.41354	0.000664	hypothetical protein		
CNAG_03002	-0.45352	0.042479	hypothetical protein		
CNAG_02069	-0.4561	0.000171	hypothetical protein		
CNAG_02263	-0.45982	0.000558	hypothetical protein		
CNAG_02815	-0.47065	0.000941	glycerol-3-phosphate dehydrogenase	GUT2	Glycerol-3-phosphate dehydrogenase, mitochondrial precursor
CNAG_00834	-0.47503	0.003166	phosphatidylserine decarboxylase		
CNAG_02006	-0.47578	0.000348	protein N-terminal amidase	NTA1	Protein N-terminal amidase
CNAG_07551	-0.48699	0.000558	hypothetical protein		
CNAG_04951	-0.53242	0.019292	3-deoxy-7-phosphoheptulonate synthase	ARO3	Phospho-2-dehydro-3-deoxyheptonate aldolase, phenylalanine-inhibited
CNAG_01212	-0.55903	8.59E-05	hypothetical protein		
CNAG_07309	-0.65631	0.000553	mRNA surveillance protein pelota	DOM34	Protein DOM34
CNAG_02864	-1.05581	0.003982	hypothetical protein		

[1] logFC: log fold-change

[2] FDR: false discovery rate (adjusted p-value < 0.05)

[3] Sc: *Saccharomyces cerevisiae*

Supplementary Table S6.1.3. List of drug transporters from FLBvsCTRL.12h.

Gene ID	logFC[1]	FDR[2]	Broad gene name	Sc[3] ortholog	Sc ortholog descriptions
CNAG_00898	0.664618	0.1065581	multidrug efflux pump		
CNAG_00730	0.25927	0.0034284	ATP-binding cassette transporter	AUS1; PDR10;	ATP-dependent permease AUS1; ATP-dependent
CNAG_03215	0.187869	0.3358236	hypothetical protein	AQR1; QDR1;	Probable transporter AQR1; Quinidine resistance
CNAG_04414	0.163815	0.1160357	multidrug resistance protein fnx1	VBA1	Vacuolar basic amino acid transporter 1
CNAG_04098	0.134176	0.331949	ATP-binding cassette, subfamily G	AUS1; PDR10;	ATP-dependent permease AUS1; ATP-dependent
CNAG_05994	0.03527	0.8329256	multidrug transporter		
CNAG_02430	0.031021	0.7798561	ABC transporter ABCC.6	BPT1; NFT1;	Bile pigment transporter 1; ABC transporter NFT1;
CNAG_06348	0.004519	0.9758772	ABC transporter PMR5	AUS1; PDR10;	ATP-dependent permease AUS1; ATP-dependent
CNAG_00796	0.004223	0.9787791	ATP-binding cassette, subfamily B	STE6	Alpha-factor-transporting ATPase
CNAG_07799	-0.00471	0.971034	ABC transporter	AUS1; PDR10;	ATP-dependent permease AUS1; ATP-dependent
CNAG_06338	-0.01604	0.8693864	ABC transporter PMR5	AUS1; PDR10;	ATP-dependent permease AUS1; ATP-dependent
CNAG_03845	-0.02809	0.7878359	multidrug resistance protein fnx1		
CNAG_04714	-0.03147	0.7170899	MFS multidrug transporter protein		
CNAG_04720	-0.03566	0.6936847	GTPase activating protein	MDR1	GTPase-activating protein GYP2
CNAG_05616	-0.07153	0.4335522	ABC transporter		
CNAG_02527	-0.11081	0.3120553	multidrug transporter		
CNAG_05470	-0.12403	0.1567916	ABC transporter family protein	YOL075C	Uncharacterized ABC transporter ATP-binding
CNAG_04546	-0.13477	0.4399505	multidrug transporter	TPO4	Polyamine transporter 4
CNAG_00869	-0.15019	0.128089	ATP-binding cassette transporter	AUS1; PDR10;	ATP-dependent permease AUS1; ATP-dependent
CNAG_06909	-0.19749	0.01508546	ABC transporter family protein		
CNAG_07431	-0.21531	0.004386292	MATE family multidrug resistance	YDR338C	Uncharacterized transporter YDR338C
CNAG_05718	-0.23513	0.1190144	multidrug resistance protein fnx1		

[1] logFC: log fold-change

[2] FDR: false discovery rate (adjusted p-value < 0.05)

[3] Sc: *Saccharomyces cerevisiae*

Supplementary Table S6.1.4. List of genes differentially expressed comparing flubendazole treated cells at 6 and 8 h (FLB.8vs6).

Gene ID	logFC[1]	FDR[2]	Broad gene name	Sc[3]	Sc ortholog descriptions
CNAG_04523	0.852061	0.011268	glyceraldehyde-3-phosphate dehydrogenase, type I		
CNAG_05767	0.567122	9.83E-08	hypothetical protein		
CNAG_07736	0.531869	0.0106	glucan endo-1,3-alpha-glucosidase agn1		
CNAG_01076	0.529151	0.034644	4-aminobutyrate aminotransferase	UGA1	4-aminobutyrate aminotransferase
CNAG_05653	0.508199	0.004797	malate synthase A	DAL7; MLS1	Malate synthase 2, glyoxysomal; Malate synthase 1, glyoxysomal
CNAG_01946	0.47296	0.004745	allantoate permease		
CNAG_01262	0.4631	4.54E-06	guanine nucleotide-binding protein subunit beta	STE4	Guanine nucleotide-binding protein subunit beta
CNAG_02759	0.4553	0.000628	hypothetical protein		
CNAG_04869	0.438045	0.00596	carboxylesterase		
CNAG_07695	0.436608	0.010684	gamma-aminobutyric acid transporter		
CNAG_01562	0.429412	0.026819	hypothetical protein		
CNAG_01272	0.421542	0.0137	hypothetical protein		
CNAG_05312	0.396353	0.044606	hypothetical protein		
CNAG_07756	0.386847	0.004546	cell division control protein	CDC20	APC/C activator protein CDC20
CNAG_05911	0.386188	0.032674	hypothetical protein		
CNAG_04861	0.348103	0.004797	transglycosylase SLT domain-containing protein		
CNAG_03453	0.341732	0.003814	kinesin family member 11	KIP1	Kinesin-like protein KIP1
CNAG_01334	0.334076	0.007114	hypothetical protein		
CNAG_03068	0.332543	0.00729	hypothetical protein		
CNAG_05130	0.298823	0.010684	hypothetical protein	QDR3	Quinidine resistance protein 3
CNAG_06902	0.279012	0.034629	hypothetical protein		
CNAG_02724	0.277705	0.013706	hypothetical protein		
CNAG_02661	0.257656	0.034629	hypothetical protein		
CNAG_05632	0.254046	0.044398	hypothetical protein		

CNAG_06118	0.251955	0.040422	hypothetical protein		
CNAG_03212	0.234935	0.033231	forkhead domain-containing protein	HCM1	Forkhead transcription factor HCM1
CNAG_04351	-0.25721	0.044398	methylmalonate-semialdehyde dehydrogenase (acylating)		
CNAG_04313	-0.26443	0.02611	NADPH2 dehydrogenase	OYE2; OYE3	NADPH dehydrogenase 2; NADPH dehydrogenase 3
CNAG_00676	-0.26798	0.023798	ESCRT-I complex subunit VPS28	VPS28	Vacuolar protein sorting-associated protein 28
CNAG_06090	-0.27827	0.002317	hypothetical protein		
CNAG_04206	-0.28663	0.034072	hypothetical protein		
CNAG_00920	-0.29079	0.046642	YjeF family protein	YNL200C	NAD(P)H-hydrate epimerase
CNAG_04443	-0.29233	0.0287	hypothetical protein		
CNAG_00605	-0.30165	0.006212	cytoplasmic protein	YML131W	Uncharacterized membrane protein YML131W
CNAG_05839	-0.30341	0.005301	cytochrome c oxidase subunit 6b	COX12	Cytochrome c oxidase subunit 6B
CNAG_03861	-0.30529	0.046642	cytochrome c oxidase subunit 5a	COX6	Cytochrome c oxidase subunit 6, mitochondrial precursor
CNAG_06064	-0.31445	0.010684	hypothetical protein		
CNAG_02006	-0.32289	0.037471	protein N-terminal amidase	NTA1	Protein N-terminal amidase
CNAG_03709	-0.33809	0.003814	hypothetical protein		
CNAG_05317	-0.34119	0.004745	phytanoyl-CoA dioxygenase family protein		
CNAG_03679	-0.34221	0.003814	hypothetical protein		
CNAG_02226	-0.34554	0.034633	hypothetical protein		
CNAG_00038	-0.34883	0.000204	alcohol dehydrogenase		
CNAG_01947	-0.36957	0.037046	2,4-dienoyl-CoA reductase		
CNAG_00932	-0.3778	0.000204	hypothetical protein	YMR090W	UPF0659 protein YMR090W
CNAG_01954	-0.38024	0.02611	aldo-keto reductase		
CNAG_07690	-0.38372	0.017947	hypothetical protein		
CNAG_05842	-0.38797	0.032674	cytochrome P450		
CNAG_00475	-0.43085	0.000204	WSC domain-containing protein		

CNAG_02203	-0.43902	0.000321	karyopherin/importin that interacts with the nuclear pore complex	PSE1	Importin subunit beta-3
CNAG_03215	-0.46462	0.046555	hypothetical protein	AQR1; QDR1; QDR2	Probable transporter AQR1; Quinidine resistance protein 1; Quinidine resistance protein 2
CNAG_07309	-0.46714	0.034629	mRNA surveillance protein pelota	DOM34	Protein DOM34
CNAG_02347	-0.52039	0.008108	hypothetical protein		
CNAG_04981	-0.58869	0.040071	catalase		
CNAG_06440	-0.60343	0.004797	DNA dependent ATPase		
CNAG_05658	-0.71473	0.044606	L-iditol 2-dehydrogenase		
CNAG_06298	-1.03077	0.003814	hypothetical protein		
CNAG_06404	-1.07997	0.002073	hypothetical protein		
CNAG_06207	-2.11843	6.11E-25	hypothetical protein		

[1] logFC: log fold-change

[2] FDR: false discovery rate (adjusted p-value < 0.05)

[3] Sc: *Saccharomyces cerevisiae*

Supplementary Table S6.1.5. Expression data for genes in Figure 3.7.

Gene ID	Sc[1] ortholog	Description	logFC[2]	FDR[3]
Oxidative stress-related				
CNAG_01019	SOD1	Superoxide dismutase [Cu-Zn]	0.604878	3.65E-06
CNAG_04388	SOD2	Superoxide dismutase [Mn], mitochondrial precursor	0.6163	2.62E-07
CNAG_03482	TSA1	Peroxiredoxin TSA1	0.563644	1.93E-05
CNAG_07032	AHP1	Peroxiredoxin type-2	0.741467	5.27E-13
CNAG_02292	CCS1	Superoxide dismutase 1 copper chaperone	0.274688	0.00137
CNAG_06917	PRX1	Mitochondrial peroxiredoxin PRX1	0.303006	0.028273
CNAG_02503	GPX2	Glutathione peroxidase 2	0.529407	2.20E-10
CNAG_05847	TRR1	Thioredoxin reductase 1	0.804008	1.92E-08
CNAG_02399	GLR1	Glutathione reductase	0.587167	3.52E-10
CNAG_03795	OGG1	N-glycosylase/DNA lyase	0.454235	3.64E-07
CNAG_02801	TRX3	Thioredoxin-3, mitochondrial precursor	0.735843	1.82E-12
CNAG_00654	SRX1	Sulfiredoxin	0.381706	0.001466
Cytoskeletal network				
CNAG_03787	TUB1/TUB3	Tubulin alpha-1 chain; Tubulin alpha-3 chain	0.394257	0.000447
CNAG_01840	TUB2	Tubulin beta chain	0.107992	0.436124
CNAG_01110	RBL2	Tubulin-specific chaperone A	-0.0671	0.546655
CNAG_03702	ALF1	Tubulin-specific chaperone B	-0.0182	0.900673
Gamma-tubulin complex				
CNAG_06914	TUB4	Tubulin gamma chain	-0.17243	0.107377
CNAG_00300	SPC97	Spindle pole body component SPC97	-0.31395	0.003718
CNAG_01566	SPC98	Spindle pole body component SPC98	-0.37974	0.007457
CNAG_00483	ACT1	Actin	0.62148	1.27E-05
CNAG_05701	TPM1	Tropomyosin-1	0.371634	0.00095
CNAG_00584	PFY1	Profilin	0.488801	4.86E-06
CNAG_01402	ARP3	Actin-related protein 3	0.345021	5.13E-05

CNAG_02094	ARC35	Actin-related protein 2/3 complex subunit 2	-0.28133	0.000542
CNAG_05878	ARC40	Actin-related protein 2/3 complex subunit 1	0.357162	0.000549
CNAG_01918	BUD6	Bud site selection protein 6	-0.20088	0.006705
Cytokinesis				
CNAG_05925	CDC3	Cell division control protein 3	-0.20379	0.012442
CNAG_01373	CDC10	Cell division control protein 10	-0.23081	0.022804
CNAG_02196	CDC11	Cell division control protein 11	-0.2925	0.003408
CNAG_01740	CDC12	Cell division control protein 12	-0.07808	0.452754
CNAG_02675	HSL1	Probable serine/threonine-protein kinase HSL1	-0.28709	0.000255
CNAG_02829	HSL7	Protein arginine N-methyltransferase HSL7	-0.37174	1.55E-06
Chromosome segregation				
DASH complex				
CNAG_02082	DAD1	DASH complex subunit DAD1	-0.34431	0.000446
CNAG_00327	DAD2	DASH complex subunit DAD2	-0.42485	0.003862
CNAG_02291	DAM1	DASH complex subunit DAM1	-0.32419	0.000398
CNAG_01325	SPC19	DASH complex subunit SPC19	-0.39223	0.005462
CNAG_01736	DAD4	DASH complex subunit DAD4	0.10607	0.401928
CNAG_03835	DAD3	DASH complex subunit DAD3	-0.19072	0.082007
Ndc80 complex				
CNAG_07635	NDC80	Kinetochore protein NDC80	-0.38781	0.000581
CNAG_00680	NUF2	Kinetochore protein NUF2	-0.4236	0.001924
Condensin compex				
CNAG_00681	YCG1	Condensin complex subunit 3	-0.47554	1.09E-05
CNAG_01959	YCS4	Condensin complex subunit 1	-0.34631	0.001303
CNAG_03148	SMC2	Structural maintenance of chromosomes protein 2	-0.34877	0.000286
CNAG_07627	SMC4	Structural maintenance of chromosomes protein 4	-0.16908	0.130862
CNAG_04936	BRN1	Condensin complex subunit 2	-0.14416	0.07587641

Cohesion complex					
	CNAG_03767	SMC1	Structural maintenance of chromosomes protein 1	-0.37174	5.15E-06
	CNAG_00812	IRR1	Cohesin subunit SCC3	-0.33418	0.000236
	CNAG_01023	SCC1	Cohesin complex subunit SCC1	0.865202	1.39E-09
	CNAG_01167	SMC3	Structural maintenance of chromosomes protein 3	0.061478	0.519688
Alternative Replication Factor C complex					
	CNAG_06408	DCC1	sister chromatid cohesion protein DCC1	-0.35377	0.001245
	CNAG_03526	CTF8	chromosome transmission fidelity protein 8	-0.42648	0.000574
	CNAG_05374	CTF18	Chromosome transmission fidelity protein 18	-0.32053	0.000408
Spindle assembly checkpoint					
	CNAG_06697	MPS1	Serine/threonine-protein kinase MPS1	-0.2479	0.021881
	CNAG_04824	MAD1	Spindle assembly checkpoint component MAD1	-0.16274	0.049348
	CNAG_07756	CDC20	APC/C activator protein CDC20	0.43221	1.42E-05
	CNAG_03184	BUB1	Checkpoint serine/threonine-protein kinase BUB1	-0.3068	0.001554
	CNAG_02267	BUB3	Cell cycle arrest protein BUB3	-0.25482	0.002275
	CNAG_07463	ESP1	Separin	-0.21043	0.027251
	CNAG_01638	MAD2	Mitotic spindle checkpoint component MAD2	-0.05499	0.555338
	CNAG_06087	SPC105	Kinetochore protein Spc7/SPC105	-0.30781	0.000195
	CNAG_04648	PDS1	Sister chromatid cohesion protein PDS5	-0.36747	6.20E-05
Others					
	CNAG_04648	PDS5	Sister chromatid cohesion protein PDS5	-0.36747	6.20E-05
	CNAG_00545	SCC2	Cohesin loading factor subunit SCC2	-0.1097	0.201551
Prefoldin Complex					
	CNAG_05107	GIM3	Prefoldin subunit 4	0.265181	0.032839
	CNAG_00510	GIM4	Prefoldin subunit 2	-0.26102	0.004622
	CNAG_01899	GIM5	Prefoldin subunit 5	-0.20788	0.043909
	CNAG_05483	YKE2	Prefoldin subunit 6	-0.01381	0.904492
	CNAG_00987	PAC10	Prefoldin subunit 3	-0.07878	0.502754

DNA replication/metabolic processes

SMC5-SMC6 complex				
CNAG_06860	SMC5	Structural maintenance of chromosomes protein 5	-0.19975	0.030085
CNAG_01276	SMC6	Structural maintenance of chromosomes protein 6	-0.27479	0.03865
CNAG_05359	NSE1	Non-structural maintenance of chromosomes element 1	-0.40998	0.000214
CNAG_02491	NSE4	Non-structural maintenance of chromosome element 4	-0.39336	0.009425
Origin recognition complex				
CNAG_02195	ORC1	Origin recognition complex subunit 1	-0.24857	0.017198
CNAG_07162	ORC2	Origin recognition complex subunit 2	-0.32821	0.000871
CNAG_06183	ORC4	Origin recognition complex subunit 4	-0.16502	0.038071
CNAG_00310	ORC5	Origin recognition complex subunit 5	-0.17339	0.033395
MCM2-7 complex				
CNAG_03341	MCM2	DNA replication licensing factor MCM2	-0.22265	0.007221
CNAG_00099	MCM3	DNA replication licensing factor MCM3	-0.17943	0.056811
CNAG_06182	MCM4	DNA replication licensing factor MCM4	-0.43242	1.08E-05
CNAG_04052	MCM5	Minichromosome maintenance protein 5	-0.26001	0.011427
CNAG_03962	MCM6	DNA replication licensing factor MCM6	-0.24927	0.004349
CNAG_05825	MCM7	DNA replication licensing factor MCM7	-0.29452	0.000113
Replication factor C complex				
CNAG_07539	RFC1	Replication factor C subunit 1	-0.32538	0.00019
CNAG_05409	RFC2	Replication factor C subunit 2	-0.45432	2.89E-05
CNAG_06333	RFC3	Replication factor C subunit 3	-0.2171	0.009899
CNAG_03332	RFC4	Replication factor C subunit 4	-0.28063	0.003272
CNAG_03956	RFC5	Replication factor C subunit 5	-0.2422	0.016508
DNA polymerase (II) epsilon				
CNAG_02654	POL2	DNA polymerase epsilon catalytic subunit A	-0.71875	2.31E-19
CNAG_06634	DPB2	DNA polymerase epsilon subunit B	-0.51451	6.03E-08
CNAG_07904	DPB4	DNA polymerase epsilon subunit D	0.137236	0.08371

DNA polymerase delta				
CNAG_02563	POL3	DNA polymerase delta catalytic subunit	-0.33951	0.003521
CNAG_06725	POL31	DNA polymerase delta small subunit	-0.33807	0.000326
DNA polymerase (I) alpha				
CNAG_06607	POL1	DNA polymerase alpha catalytic subunit A	-0.50613	4.64E-09
CNAG_06142	POL12	DNA polymerase alpha subunit B	-0.46742	1.93E-08
CNAG_02385	PRI1	DNA primase small subunit	-0.68537	8.44E-11
CNAG_04742	PRI2	DNA primase large subunit	-0.60429	2.86E-07
DNA topoisomerases				
CNAG_04190	TOP1	DNA topoisomerase 1	0.215792	0.006154
CNAG_00377	TOP2	DNA topoisomerase 2	-0.25556	0.005608
CNAG_04600	TOP3	DNA topoisomerase 3	0.0992	0.300211
Replication protein A complex				
CNAG_01144	RFA1	Replication factor A protein 1	-0.67433	1.13E-13
CNAG_01316	RFA2	Replication factor A protein 2	-0.1529	0.107256
CNAG_03813	RFA3	Replication factor A3	0.29111	0.00034
FACT complex				
CNAG_01726	SPT16	FACT complex subunit SPT16	-0.27219	0.005231
CNAG_05661	POB3	FACT complex subunit POB3	-0.29649	0.000646
Histones				
CNAG_06747	HTA1; HTA2	Histone H2A.1; Histone H2A.2	-0.83315	3.02E-14
CNAG_06746	HTB1; HTB2	Histone H2B.1; Histone H2B.2	-0.8281	7.30E-16
CNAG_04828	HHT1; HHT2	Histone H3; Histone H3	0.196391	0.05911
CNAG_01648	HHF1; HHF2	Histone H4; Histone H4	-0.63729	2.97E-13
CNAG_04168	HHO1	Histone H1	-0.71409	4.32E-21
Mismatch repair				
CNAG_02682	MSH1	DNA mismatch repair protein MSH1, mitochondrial precursor	-0.31365	0.000102
CNAG_00770	MSH2	DNA mismatch repair protein MSH2	-0.28184	0.000907

	CNAG_01642	MSH3	DNA mismatch repair protein MSH3	-0.19376	0.014916
	CNAG_05201	MSH4	MutS protein homolog 4	0.254645	0.026416
	CNAG_00550	MSH5	MutS protein homolog 5	-0.39681	8.14E-05
	CNAG_01916	MSH6	DNA mismatch repair protein MSH6	-0.26215	0.004149
	CNAG_02073	MLH1	DNA mismatch repair protein MLH1	-0.22833	0.00234
	CNAG_01037	MLH3	DNA mismatch repair protein MLH3	-0.17484	0.047497
	CNAG_07599	PMS1	DNA mismatch repair protein PMS1	-0.17549	0.074351
	CNAG_06793	EXO1	Exodeoxyribonuclease 1	-0.36893	5.14E-06
Others					
	CNAG_06342	AOS1	DNA damage tolerance protein RHC31	-0.43488	1.93E-05
	CNAG_05896	UBA2	Ubiquitin-activating enzyme E1-like	-0.33257	3.90E-05
	CNAG_06079	POL30	Proliferating cell nuclear antigen	-0.31408	0.001003
	CNAG_01531	SRS2	ATP-dependent DNA helicase SRS2	-0.46434	9.85E-08
	CNAG_02115	HMO1	High mobility group protein 1	0.302437	9.41E-06
	CNAG_03682	FPR1	FK506-binding protein 1	0.563131	6.64E-08
	CNAG_01839	ESS1	Peptidyl-prolyl cis-trans isomerase ESS1	0.339786	7.39E-06
	CNAG_00085	ASF1	Histone chaperone ASF1	-0.39258	0.00041
	CNAG_03723	ARP8	Actin-like protein ARP8	-0.21142	0.008557
	CNAG_07924	MCM1	Pheromone receptor transcription factor	-0.12185	0.169695
	CNAG_02406	CDC45	Cell division control protein 45	-0.6023	1.60E-11
	CNAG_02823	SGS1	ATP-dependent helicase SGS1	-0.16914	0.040373
	CNAG_04278	CDC9	DNA ligase 1 precursor	-0.51437	9.19E-08
	CNAG_04662	CTF4	DNA polymerase alpha-binding protein	-0.21572	0.020372
	CNAG_02138	DNA2	DNA replication ATP-dependent helicase/nuclease DNA2	-0.48377	6.65E-08

[1] Sc: *Saccharomyces cerevisiae*

[2] logFC: log fold-change

[3] FDR: false discovery rate (adjusted p-value < 0.05)

6.2 Chapter 4 Supplementary Material

Supplementary Table S6.2.1. List of significantly differentially expressed transcription factors at FLBvsCTRL.12h.

Gene ID	logFC	FDR	Broad gene name	Sc ortholog	Sc ortholog description	TF Class[a]	Cn gene name[a]	Description[a]
CNAG_05010	0.941191	0.005026	hypothetical protein			C2H2 zinc finger	ZFC7	hypothetical protein
CNAG_06134	0.802909	1.65E-08	hypothetical protein			bZIP	BZP1(HXL1)	hypothetical protein
CNAG_04130	0.650673	3.38E-10	hypothetical protein			Not defined		hypothetical protein
CNAG_04023	0.54426	7.22E-11	hypothetical protein			Not defined		hypothetical protein
CNAG_04637	0.541632	1.73E-07	multiprotein-bridging factor 1	MBF1	Multiprotein-bridging factor 1	Helix-turn-helix type 3	MBF1	multiprotein-bridging factor 1
CNAG_01626	0.511163	2.39E-08	transcriptional adapter 2-alpha	ADA2	Transcriptional adapter 2	Myb	ADA2	transcriptional adapter 2-alpha
CNAG_03790	0.461531	9.48E-08	hypothetical protein			Not defined		hypothetical protein
CNAG_02516	0.433574	0.000521	hypothetical protein			bHLH	HLH5	hypothetical protein
CNAG_02671	0.335066	0.000138	pre-mRNA-splicing factor CEF1	CEF1	Pre-mRNA-splicing factor CEF1	Myb		pre-mRNA-splicing factor CEF1
CNAG_01317	0.311153	8.00E-06	hypothetical protein			bHLH		hypothetical protein
CNAG_01858	0.285507	0.039576	hypothetical protein			Homeodomain-like	HOB2	hypothetical protein

CNAG_05170	0.283522	0.009393	hypothetical protein			Not defined	PIP2	hypothetical protein
CNAG_04864	0.27766	0.000829	iron regulator 1			Not defined	CIR1	iron regulator 1
CNAG_05311	0.254203	0.002076	arsenite-resistant protein ASR2			Not defined		arsenite-resistant protein ASR2
CNAG_05940	0.232012	0.009117	hypothetical protein			Not defined	ZFC3	hypothetical protein
CNAG_00871	0.230925	0.022881	hypothetical protein			bZIP	CLR3	hypothetical protein
CNAG_04878	0.210607	0.022379	hypothetical protein			Zn2Cys6	FZC1	hypothetical protein
CNAG_03116	0.200635	0.027032	forkhead transcription factor 3			Winged helix repressor DNA-binding	HCM1	forkhead transcription factor 3
CNAG_03431	-0.1552	0.035399	nuclear protein	YJL206C	Putative transcriptional regulatory protein YJL206C	Zn2Cys6	FZC48	nuclear protein
CNAG_04774	-0.15722	0.030924	nuclear protein			Zn2Cys6	FZC26	nuclear protein
CNAG_04398	-0.158	0.045783	specific RNA polymerase II transcription factor	ARO80	Transcriptional activator ARO80	Zn2Cys6	ARO80	specific RNA polymerase II transcription factor
CNAG_03212	-0.16625	0.028441	forkhead domain-containing protein	HCM1	Forkhead transcription factor HCM1	Winged helix repressor DNA-binding	HCM101	forkhead domain-containing protein
CNAG_03409	-0.16813	0.021842	osomolarity two-component system,	SKN7	Transcription factor SKN7	Winged helix repressor DNA-binding	SKN7	osomolarity two-component

			response regulator SKN7					system, response regulator SKN7
CNAG_06751	-0.17565	0.035609	hypothetical protein			bHLH	HLH3	hypothetical protein
CNAG_00514	-0.19269	0.010265	hypothetical protein			Not defined	GAT6	hypothetical protein
CNAG_04807	-0.19315	0.032737	hypothetical protein			Not defined	FZC8	hypothetical protein
CNAG_03849	-0.19763	0.00353	nuclear protein	ASG1	Activator of stress genes 1	Zn2Cys6	ASG1	nuclear protein
CNAG_02134	-0.2	0.007243	hypothetical protein	RSC8	Chromatin structure-remodeling complex protein RSC8	Myb		hypothetical protein
CNAG_02698	-0.21024	0.002403	hypothetical protein			SGT1		hypothetical protein
CNAG_06425	-0.21505	0.010279	fungal specific transcription factor	PPR1	Pyrimidine pathway regulatory protein 1	Zn2Cys6	PPR1	fungal specific transcription factor
CNAG_06156	-0.22043	0.004395	hypothetical protein			Zn2Cys6	FZC7	hypothetical protein
CNAG_05112	-0.22671	0.004497	hypothetical protein	TEA1	TY1 enhancer activator	Zn2Cys6	FZC42	hypothetical protein
CNAG_06188	-0.22922	0.015732	hypothetical protein			Zn2Cys6	FZC15	hypothetical protein
CNAG_04836	-0.23658	0.001505	nuclear protein			Zn2Cys6	FZC10	nuclear protein
CNAG_07464	-0.24552	0.036985	transcription factor	MBP1	Transcription factor MBP1	APSES	MBS1	transcription factor
CNAG_03366	-0.24664	0.009271	hypothetical protein			C2H2 zinc finger	ZNF2	hypothetical protein

CNAG_03561	-0.26204	0.002352	hypothetical protein			Zn2Cys6	FZC33	hypothetical protein
CNAG_03279	-0.26241	0.008232	hypothetical protein			Zn2Cys6	CCD4	hypothetical protein
CNAG_06483	-0.26896	0.002693	hypothetical protein			Zn2Cys6	FZC25	hypothetical protein
CNAG_01438	-0.2764	0.00059	transcription factor	MBP1; SWI6	Transcription factor MBP1; Regulatory protein SWI6	APSES	MBS2	transcription factor
CNAG_04263	-0.27688	0.001998	hypothetical protein			bZIP	BZP2	hypothetical protein
CNAG_00896	-0.27719	0.015071	transcription factor			Zn2Cys6	FZC34	transcription factor
CNAG_05538	-0.28588	0.004801	hypothetical protein	JJJ1	J protein JJJ1	Not defined	JJJ1	hypothetical protein
CNAG_05153	-0.36986	2.10E-05	hypothetical protein			HMG	GAT5	hypothetical protein
CNAG_05176	-0.40113	4.36E-06	hypothetical protein			Homeodomain-like	HOB3	hypothetical protein
CNAG_00883	-0.40565	9.38E-08	transcription factor			Zn2Cys6		transcription factor
CNAG_03894	-0.43959	0.014176	hypothetical protein			Zn2Cys6	PDR802	hypothetical protein
CNAG_03183	-0.46249	4.15E-07	nuclear protein			Zn2Cys6	FZC24	nuclear protein
CNAG_03229	-0.81576	7.93E-07	specific transcriptional repressor			Homeodomain-like	YOX101	specific transcriptional repressor

logFC: log fold-change; FDR: false discovery rate; Sc: *S. cerevisiae*; Cn: *C. neoformans*; TF: transcription factor

[a] Information from Jung *et al*. 2015 [322]

Supplementary Table S6.2.2. List of significantly differentially expressed kinases at FLBvsCTRL.12h.

Gene ID	logFC	FDR	Broad gene name	Sc orthologs	Sc ortholog descriptions
CNAG_02007	0.615561	2.47E-13	adenylate kinase 1	ADK1	Adenylate kinase precursor
CNAG_01820	0.568628	2.12E-07	pyruvate kinase	CDC19; PYK2	Pyruvate kinase 1; Pyruvate kinase 2
CNAG_04577	0.559275	4.71E-11	nucleoside-diphosphate kinase		
CNAG_01612	0.513863	0.00307	CAMK/CAMKL protein kinase		
CNAG_05935	0.474553	1.68E-08	UMP-CMP kinase	URA6	Uridylate kinase
CNAG_01250	0.429873	5.17E-07	tRNA ligase	TRL1	tRNA ligase
CNAG_02285	0.361613	0.001282	nucleoside diphosphate kinase	YNK1	Nucleoside diphosphate kinase
CNAG_03358	0.356076	0.002306	phosphoglycerate kinase	PGK1	Phosphoglycerate kinase
CNAG_01364	0.292265	0.000203	guanylate kinase	GUK1	Guanylate kinase
CNAG_02799	0.274332	0.001384	dihydroxyacetone kinase	DAK2	Dihydroxyacetone kinase 2
CNAG_04162	0.258186	0.003429	AGC/PKA protein kinase		
CNAG_02202	0.257252	0.002744	adenylylsulfate kinase	MET14	Adenylyl-sulfate kinase
CNAG_00769	0.255089	0.000441	STE/STE7 protein kinase	PBS2	MAP kinase kinase PBS2
CNAG_02459	0.241272	0.001282	Atypical/ABC1/ABC1-A protein	COQ8	Atypical kinase COQ8, mitochondrial precursor
CNAG_07427	0.230712	0.013968	CK1/CK1/CK1-D protein kinase	HRR25	Casein kinase I homolog HRR25
CNAG_02531	0.214655	0.017857	CMGC/MAPK protein kinase	FUS3	Mitogen-activated protein kinase FUS3
CNAG_06174	0.188723	0.026375	PEK/GCN2 protein kinase	GCN2	eIF-2-alpha kinase GCN2
CNAG_05965	0.188722	0.033024	hypothetical protein		
CNAG_03791	0.183865	0.024457	CAMKK/ELM protein kinase	SAK1	SNF1-activating kinase 1
CNAG_02897	0.181975	0.03076	inositol hexaphosphate kinase 1	KCS1	Inositol hexakisphosphate kinase 1
CNAG_02542	0.178987	0.044359	fructosamine kinase		
CNAG_06490	0.177166	0.021877	CAMK/CAMKL protein kinase	YPL150W	Putative serine/threonine-protein kinase YPL150W
CNAG_05200	-0.16196	0.040515	pyridoxal kinase	BUD16	Putative pyridoxal kinase BUD16
CNAG_05694	-0.1635	0.040186	CMGC/CK2 protein kinase	CKA1; CKA2	Casein kinase II subunit alpha; Casein kinase II subunit alpha'
CNAG_05558	-0.16364	0.047328	CAMK/CAMKL/Kin4 protein kinase	FRK1	Fatty acyl-CoA synthetase and RNA processing-associated kinase 1

CNAG_01988	-0.16763	0.027135	bacteriophytochrome histidine kinase	SLN1	Osmosensing histidine protein kinase SLN1
CNAG_04316	-0.16933	0.019745	NAD kinase	UTR1	NAD(+) kinase
CNAG_00636	-0.17561	0.035609	CDC7 protein kinase	CDC7	Cell division control protein 7
CNAG_04678	-0.17622	0.024102	AGC/Akt protein kinase	YPK1; YPK2	Serine/threonine-protein kinase YPK1; Serine/threonine-protein kinase YPK2/YKR2
CNAG_03567	-0.17731	0.020614	AGC/NDR/NDR protein kinase	CBK1	Serine/threonine-protein kinase CBK1
CNAG_06445	-0.18596	0.025821	CMGC/CDK/CDK7 protein kinase	KIN28	Serine/threonine-protein kinase KIN28
CNAG_00405	-0.18677	0.016246	STE/STE20/YSK protein kinase	KIC1	Serine/threonine-protein kinase KIC1
CNAG_03701	-0.18887	0.024508	3-phosphoshikimate 1-carboxyvinyltransferase	ARO1	Pentafunctional AROM polypeptide
CNAG_03367	-0.19502	0.024814	uridine kinase	URK1	Uridine kinase
CNAG_00388	-0.19577	0.021061	1-phosphatidylinositol-4-phosphate 5-kinase	MSS4	Probable phosphatidylinositol 4-phosphate 5-kinase MSS4
CNAG_02947	-0.1978	0.007196	SCYL protein kinase	SCY1	Protein kinase-like protein SCY1
CNAG_03355	-0.19799	0.028151	hypothetical protein		
CNAG_07408	-0.1981	0.015756	STE/STE20/PAKA protein kinase	CLA4; SKM1	Serine/threonine-protein kinase CLA4; Serine/threonine-protein kinase SKM1
CNAG_06193	-0.19847	0.006056	CMGC/RCK protein kinase	IME2	Meiosis induction protein kinase IME2/SME1
CNAG_02859	-0.20127	0.017995	NADH kinase	POS5	NADH kinase POS5, mitochondrial precursor
CNAG_03137	-0.20223	0.046063	CMGC/CDK protein kinase		
CNAG_06730	-0.21217	0.004983	CMGC/GSK protein kinase	RIM11	Serine/threonine-protein kinase RIM11/MSD1
CNAG_05386	-0.21222	0.007465	glutamate 5-kinase	PRO1	Glutamate 5-kinase
CNAG_00415	-0.21889	0.010213	CMGC/CDK protein kinase		
CNAG_05771	-0.22036	0.03058	serine/threonine-protein kinase TEL1	TEL1	Serine/threonine-protein kinase TEL1

CNAG_04335	-0.22398	0.00279	phosphatidylinositol 4-kinase	STT4	Phosphatidylinositol 4-kinase STT4
CNAG_00877	-0.22484	0.04362	adenylate kinase	ADK2	GTP:AMP phosphotransferase, mitochondrial
CNAG_02389	-0.2249	0.021881	AGC protein kinase		
CNAG_01907	-0.22779	0.046118	PLK/PLK1 protein kinase	CDC5	Cell cycle serine/threonine-protein kinase CDC5/MSD2
CNAG_01845	-0.23373	0.006207	AGC/PKC protein kinase	PKC1	Protein kinase C-like 1
CNAG_06697	-0.2479	0.021881	TTK protein kinase	MPS1	Serine/threonine-protein kinase MPS1
CNAG_01285	-0.25011	0.00824	Aur protein kinase	IPL1	Spindle assembly checkpoint kinase
CNAG_00782	-0.2547	0.016042	STE/STE20/Fray protein kinase		
CNAG_01165	-0.25477	0.00136	D-erythro-sphingosine kinase	LCB4; LCB5	Sphingoid long chain base kinase 4; Sphingoid long chain base kinase 5
CNAG_07377	-0.25789	0.013639	transformation/transcription domain-associated protein	TRA1	Transcription-associated protein 1
CNAG_03167	-0.26036	0.03885	CAMK/CAMKL/Chk1 protein kinase	CHK1	Serine/threonine-protein kinase CHK1
CNAG_01704	-0.26364	0.026256	serine/threonine protein kinase		
CNAG_01664	-0.26492	0.005293	CMGC/CDK/CDC2 protein kinase	CDC28	Cyclin-dependent kinase 1
CNAG_02866	-0.27032	0.004572	pantothenate kinase	CAB1	Pantothenate kinase CAB1
CNAG_04156	-0.27072	0.00044	homoserine kinase	THR1	Homoserine kinase
CNAG_05549	-0.27343	0.000308	CMGC/CDK protein kinase	SGV1	Serine/threonine-protein kinase BUR1
CNAG_04191	-0.2745	0.000229	SCYL protein kinase	CEX1	Cytoplasmic export protein 1
CNAG_02194	-0.276	0.008109	AGC/NDR protein kinase	DBF2; DBF20	Cell cycle protein kinase DBF2; Serine/threonine-protein kinase DBF20
CNAG_03946	-0.27817	0.000913	galactokinase		
CNAG_01162	-0.2789	0.002428	hypothetical protein		
CNAG_05274	-0.28399	0.001056	STE/STE20/YSK protein kinase		

CNAG_02675	-0.28709	0.000255	CAMK/CAMKL/GIN4 protein kinase	HSL1	Probable serine/threonine-protein kinase HSL1
CNAG_03184	-0.3068	0.001554	BUB protein kinase	BUB1	Checkpoint serine/threonine-protein kinase BUB1
CNAG_02962	-0.30897	2.85E-05	CMGC/DYRK/PRP4 protein kinase		
CNAG_01333	-0.31695	0.002748	Haspin protein kinase		
CNAG_03290	-0.32239	0.000211	STE/STE20/YSK protein kinase		
CNAG_03369	-0.33979	0.001622	Wee protein kinase	SWE1	Mitosis inhibitor protein kinase SWE1
CNAG_04108	-0.34211	5.18E-06	pyruvate dehydrogenase kinase	PKP1	[Pyruvate dehydrogenase (acetyl-transferring)] kinase 1, mitochondrial precursor
CNAG_01730	-0.35847	0.001868	STE/STE7/MEK1 protein kinase		
CNAG_04272	-0.36171	3.01E-05	CAMK/CAMK1 protein kinase		
CNAG_02847	-0.41398	0.00041	thymidylate kinase	CDC8	Thymidylate kinase
CNAG_04221	-0.48171	4.13E-05	6-phosphofructo-2-kinase/fructose-2,6-	FBP26	Fructose-2,6-bisphosphatase
CNAG_07779	-0.65825	0.014318	D-glycerate 3-kinase	TDA10	Probable ATP-dependent kinase TDA10

logFC: log fold-change; FDR: false discovery rate; Sc: *S. cerevisiae.*

Chapter 7: References

1. Menzin J, Meyers JL, Friedman M, Perfect JR, Langston AA, Danna RP, et al. Mortality, length of hospitalization, and costs associated with invasive fungal infections in high-risk patients. American Journal of Health-System Pharmacy. 2009;66(19):1711-7.

2. Menzin J, Meyers JL, Friedman M, Korn JR, Perfect JR, Langston AA, et al. The economic costs to United States hospitals of invasive fungal infections in transplant patients. American journal of infection control. 2011;39(4):e15-20. Epub 2010/10/22. doi: 10.1016/j.ajic.2010.06.009. PubMed PMID: 20961657.

3. Dodds Ashley E, Drew R, Johnson M, Danna R, Dabrowski D, Walker V, et al. Cost of invasive fungal infections in the era of new diagnostics and expanded treatment options. Pharmacotherapy. 2012;32(10):890-901. Epub 2012/10/04. doi: 10.1002/j.1875-9114.2012.01124. PubMed PMID: 23033228.

4. Balada-Llasat J, Rosenthal N, Hasbun R, Zimmer L, Ginocchio CC, Duff S, et al. Cost of managing meningitis and encephalitis among adult patients in the United States of America. International Journal of Infectious Diseases. 2018;71:117-21.

5. Wilson LS, Reyes CM, Stolpman M, Speckman J, Allen K, Beney J. The direct cost and incidence of systemic fungal infections. Value Health. 2002;5(1):26-34. Epub 2002/03/05. doi: 10.1046/j.1524-4733.2002.51108.x. PubMed PMID: 11873380.

6. Benedict K, Jackson BR, Chiller T, Beer KD. Estimation of Direct Healthcare Costs of Fungal Diseases in the United States. Clinical Infectious Diseases. 2018:ciy776-ciy. doi: 10.1093/cid/ciy776.

7. Bitar D, Lortholary O, Strat YL, Nicolau J, Coignard B, Tattevin P, et al. Population-Based Analysis of Invasive Fungal Infections, France, 2001–2010. Emerging Infectious Disease journal. 2014;20(7):1163. doi: 10.3201/eid2007.140087.

8. Park BJ, Wannemuehler KA, Marston BJ, Govender N, Pappas PG, Chiller TM. Estimation of the current global burden of cryptococcal meningitis among persons living with HIV/AIDS. AIDS. 2009;23(4):525-30. doi: 10.1097/QAD.0b013e328322ffac.

9. Chapman N, Doubell A, Oversteegen L, Chowdhary V, Rugarabamu G, Zanetti R, et al. Neglected disease research and development: reflecting on a decade of global investment. Policy Cures Research. 2017.

10. Merry M, Boulware DR. Cryptococcal Meningitis Treatment Strategies Affected by the Explosive Cost of Flucytosine in the United States: A Cost-effectiveness Analysis. Clinical infectious diseases : an official publication of the Infectious Diseases Society of America. 2016;62(12):1564-8. Epub 2016/03/25. doi: 10.1093/cid/ciw151. PubMed PMID: 27009249; PubMed Central PMCID: PMCPMC4885648.

11. Pyrgos V, Seitz AE, Steiner CA, Prevots DR, Williamson PR. Epidemiology of cryptococcal meningitis in the US: 1997–2009. PloS one. 2013;8(2):e56269. doi: 10.1371/journal.pone.0056269.

12. Rajasingham R, Rhein J, Klammer K, Musubire A, Nabeta H, Akampurira A, et al. Epidemiology of meningitis in an HIV-infected Ugandan cohort. Am J Trop Med Hyg. 2015;92(2):274-9. Epub

2014/11/12. doi: 10.4269/ajtmh.14-0452. PubMed PMID: 25385864; PubMed Central PMCID: PMCPMC4347329.

13. Jarvis JN, Meintjes G, Williams A, Brown Y, Crede T, Harrison TS. Adult meningitis in a setting of high HIV and TB prevalence: findings from 4961 suspected cases. BMC Infectious Diseases. 2010;10:67-. doi: 10.1186/1471-2334-10-67. PubMed PMID: PMC3161361.

14. Reniers G, Slaymaker E, Nakiyingi-Miiro J, Nyamukapa C, Crampin AC, Herbst K, et al. Mortality trends in the era of antiretroviral therapy: evidence from the Network for Analysing Longitudinal Population based HIV/AIDS data on Africa (ALPHA). AIDS (London, England). 2014;28 Suppl 4(4):S533-S42. Epub 2014/11/20. doi: 10.1097/QAD.0000000000000496. PubMed PMID: 25406756.

15. Montaner JSG, Lima VD, Harrigan PR, Lourenço L, Yip B, Nosyk B, et al. Expansion of HAART Coverage Is Associated with Sustained Decreases in HIV/AIDS Morbidity, Mortality and HIV Transmission: The "HIV Treatment as Prevention" Experience in a Canadian Setting. PloS one. 2014;9(2):e87872. doi: 10.1371/journal.pone.0087872.

16. Boulware DR, Meya DB, Muzoora C, Rolfes MA, Huppler Hullsiek K, Musubire A, et al. Timing of antiretroviral therapy after diagnosis of cryptococcal meningitis. The New England journal of medicine. 2014;370(26):2487-98. doi: 10.1056/NEJMoa1312884. PubMed PMID: 24963568.

17. Touma M, Rasmussen LD, Martin-Iguacel R, Engsig FN, Stærke NB, Stærkind M, et al. Incidence, clinical presentation, and outcome of HIV-1-associated cryptococcal meningitis during the highly active antiretroviral therapy era: a nationwide cohort study. Clinical epidemiology. 2017;9:385-92. doi: 10.2147/CLEP.S135309. PubMed PMID: 28790866.

18. Cabello Úbeda A, Fortes Alen J, Gadea I, Mahillo I, Górgolas M, Fernández Guerrero ML. Cryptococcal meningoencephalitis. Epidemiology and mortality risk factors in pre- and post-HAART era. Medicina Clínica (English Edition). 2016;146(9):397-401. doi: https://doi.org/10.1016/j.medcle.2016.06.030.

19. Limper AH, Adenis A, Le T, Harrison TS. Fungal infections in HIV/AIDS. The Lancet Infectious Diseases. 2017;17(11):e334-e43.

20. Perfect JR, Bicanic T. Cryptococcosis diagnosis and treatment: What do we know now. Fungal Genetics and Biology. 2015;78:49-54. doi: https://doi.org/10.1016/j.fgb.2014.10.003.

21. Rajasingham R, Smith RM, Park BJ, Jarvis JN, Govender NP, Chiller TM, et al. Global burden of disease of HIV-associated cryptococcal meningitis: an updated analysis. Lancet Infectious Diseases. 2017;17(8):873-81. doi: 10.1016/s1473-3099(17)30243-8.

22. Phillips AN, Stover J, Cambiano V, Nakagawa F, Jordan MR, Pillay D, et al. Impact of HIV Drug Resistance on HIV/AIDS-Associated Mortality, New Infections, and Antiretroviral Therapy Program Costs in Sub-Saharan Africa. The Journal of infectious diseases. 2017;215(9):1362-5. Epub 2017/02/17. doi: 10.1093/infdis/jix089. PubMed PMID: 28329236.

23. Perfect JR, Dismukes WE, Dromer F, Goldman DL, Graybill JR, Hamill RJ, et al. Clinical practice guidelines for the management of cryptococcal disease: 2010 update by the Infectious Diseases Society of America. Clinical Infectious Diseases. 2010;50(3):291-322. doi: 10.1086/649858.

24. Springer DJ, Chaturvedi V. Projecting global occurrence of Cryptococcus gattii. Emerging infectious diseases. 2010;16(1):14-20. Epub 2009/12/25. doi: 10.3201/eid1601.090369. PubMed PMID: 20031037; PubMed Central PMCID: PMCPMC2874352.

25. Velagapudi R, Hsueh YP, Geunes-Boyer S, Wright JR, Heitman J. Spores as infectious propagules of *Cryptococcus neoformans*. Infection and Immunity. 2009;77(10):4345-55. doi: 10.1128/iai.00542-09.

26. Levitz SM. The Ecology of Cryptococcus neoformans and the Epidemiology of Cryptococcosis. Reviews of Infectious Diseases. 1991;13(6):1163-9. doi: 10.1093/clinids/13.6.1163.

27. Kronstad JW, Attarian R, Cadieux B, Choi J, D'Souza CA, Griffiths EJ, et al. Expanding fungal pathogenesis: *Cryptococcus* breaks out of the opportunistic box. Nature Reviews Microbiology. 2011;9(3):193-203.

28. Chen SC-A, Meyer W, Sorrell TC. Cryptococcus gattii Infections. Clinical microbiology reviews. 2014;27(4):980-1024. doi: 10.1128/cmr.00126-13.

29. Chen SC-A, Slavin MA, Heath CH, Playford EG, Byth K, Marriott D, et al. Clinical manifestations of *Cryptococcus gattii* infection: determinants of neurological sequelae and death. Clinical Infectious Diseases. 2012;55(6):789-98. doi: 10.1093/cid/cis529.

30. Harris JR, Lockhart SR, Sondermeyer G, Vugia DJ, Crist MB, D'Angelo MT, et al. *Cryptococcus gattii* Infections in multiple states outside the US Pacific Northwest. Emerging infectious diseases. 2013;19(10):1621-7. Epub 2013/09/21. doi: 10.3201/eid1910.130441. PubMed PMID: 24050410.

31. Lizarazo J, Escandón P, Agudelo CI, Firacative C, Meyer W, Castañeda E. Retrospective Study of the Epidemiology and Clinical Manifestations of Cryptococcus gattii Infections in Colombia from 1997–2011. PLOS Neglected Tropical Diseases. 2014;8(11):e3272. doi: 10.1371/journal.pntd.0003272.

32. Stephen C, Lester S, Black W, Fyfe M, Raverty S. Multispecies outbreak of cryptococcosis on southern Vancouver Island, British Columbia. Canadian Veterinary Journal. 2002;43(10):792-4. Epub 2002/10/25. PubMed PMID: 12395765; PubMed Central PMCID: PMC339618.

33. MacDougall L, Kidd SE, Galanis E, Mak S, Leslie MJ, Cieslak PR, et al. Spread of *Cryptococcus gattii* in British Columbia, Canada, and detection in the Pacific Northwest, USA. Emerging infectious diseases. 2007;13(1):42.

34. Malik R, Krockenberger M, Cross G, Doneley R, Madill D, Black D, et al. Avian cryptococcosis. Medical Mycology. 2003;41(2):115-24.

35. Johnston SA, Voelz K, May RC. Cryptococcus neoformans thermotolerance to avian body temperature is sufficient for extracellular growth but not intracellular survival in macrophages. Scientific reports. 2016;6:20977.

36. Littman M, Borok R. Relation of the pigeon to cryptococcosis: natural carrier state, heat resistance and survival of *Cryptococcus neoformans*. Mycopathologia et Mycologia Applicata. 1968;35(3-4):329-45. doi: 10.1007/bf02050749.

37. Hull CM, Heitman J. Genetics of *Cryptococcus neoformans*. Annual review of genetics. 2002;36:557-615. Epub 2002/11/14. doi: 10.1146/annurev.genet.36.052402.152652. PubMed PMID: 12429703.

38. Chaturvedi V, Chaturvedi S. *Cryptococcus gattii*: a resurgent fungal pathogen. Trends in Microbiology. 2011;19(11):564-71. doi: http://dx.doi.org/10.1016/j.tim.2011.07.010.

39. Lin X, Heitman J. The Biology of the Cryptococcus neoformans Species Complex. Annual Review of Microbiology. 2006;60(1):69-105. doi: 10.1146/annurev.micro.60.080805.142102.

40. Hagen F, Khayhan K, Theelen B, Kolecka A, Polacheck I, Sionov E, et al. Recognition of seven species in the *Cryptococcus gattii*/*Cryptococcus neoformans* species complex. Fungal Genetics and Biology. 2015;78(Supplement C):16-48. doi: 10.1016/j.fgb.2015.02.009.

41. George IA, Spec A, Powderly WG, Santos CAQ. Comparative Epidemiology and Outcomes of Human Immunodeficiency virus (HIV), Non-HIV Non-transplant, and Solid Organ Transplant Associated Cryptococcosis: A Population-Based Study. Clinical Infectious Diseases. 2018;66(4):608-11. doi: 10.1093/cid/cix867.

42. Shaheen AA, Somayaji R, Myers R, Mody CH. Epidemiology and trends of cryptococcosis in the United States from 2000 to 2007: A population-based study. International journal of STD & AIDS. 2018;29(5):453-60. Epub 2017/10/04. doi: 10.1177/0956462417732649. PubMed PMID: 28971712.

43. Bratton EW, El Husseini N, Chastain CA, Lee MS, Poole C, Stürmer T, et al. Comparison and temporal trends of three groups with cryptococcosis: HIV-infected, solid organ transplant, and HIV-negative/non-transplant. PloS one. 2012;7(8):e43582.

44. Hajjeh RA, Conn LA, Stephens DS, Baughman W, Hamill R, Graviss E, et al. Cryptococcosis: population-based multistate active surveillance and risk factors in Human Immunodeficiency Virus—infected persons. Journal of Infectious Diseases. 1999;179(2):449-54. doi: 10.1086/314606.

45. Speed B, Dunt D. Clinical and host differences between infections with the two varieties of *Cryptococcus neoformans*. Clinical Infectious Diseases. 1995;21(1):28-34. doi: 10.1093/clinids/21.1.28.

46. Pappas PG, Alexander BD, Andes DR, Hadley S, Kauffman CA, Freifeld A, et al. Invasive fungal infections among organ transplant recipients: results of the Transplant-Associated Infection Surveillance Network (TRANSNET). Clinical Infectious Diseases. 2010;50(8):1101-11. Epub 2010/03/12. doi: 10.1086/651262. PubMed PMID: 20218876.

47. Fisher D, Burrow J, Lo D, Currie B. *Cryptococcus neoformans* in tropical northern Australia: predominantly variant *gattii* with good outcomes. Australian and New Zealand Journal of Medicine. 1993;23(6):678-82. Epub 1993/12/01. PubMed PMID: 8141697.

48. Ellis DH. *Cryptococcus neoformans* var. *gattii* in Australia. Journal of Clinical Microbiology. 1987;25(2):430-1. Epub 1987/02/01. PubMed PMID: 3546370; PubMed Central PMCID: PMC265916.

49. Sorrell TC. *Cryptococcus neoformans* variety *gattii*. Medical Mycology. 2001;39(2):155-68. doi: doi:10.1080/mmy.39.2.155.168. PubMed PMID: 11346263.

50. Kwon-Chung KJ, Bennett JE. High prevalence of *Cryptococcus neoformans* var. *gattii* in tropical and subtropical regions. Zentralblatt für Bakteriologie, Mikrobiologie und Hygiene. 1984;257(2):213-8. Epub 1984/07/01. PubMed PMID: 6207684.

51. Chen S, Sorrell T, Nimmo G, Speed B, Currie B, Ellis D, et al. Epidemiology and host- and variety-dependent characteristics of infection due to *Cryptococcus neoformans* in Australia and New Zealand. Clinical Infectious Diseases. 2000;31(2):499-508. doi: 10.1086/313992.

52. Galanis E, MacDougall L. Epidemiology of *Cryptococcus gattii*, British Columbia, Canada, 1999-2007. Emerging infectious diseases. 2010;16(2):251-7.

53. Fyfe M, MacDougall L, Romney M, Starr M, Pearce M, Mak S, et al. Cryptococcus gattii infections on Vancouver Island, British Columbia, Canada: emergence of a tropical fungus in a temperate environment. Can Commun Dis Rep. 2008;34(6):1-12.

54. Datta K, Bartlett KH, Baer R, Byrnes E, Galanis E, Heitman J, et al. Spread of *Cryptococcus gattii* into Pacific Northwest region of the United States. Emerging infectious diseases. 2009;15(8):1185-91.

55. Dixit A, Carroll SF, Qureshi ST. *Cryptococcus gattii*: an emerging cause of fungal disease in North America. Interdisciplinary Perspectives on Infectious Diseases. 2009;2009:1-13. doi: 10.1155/2009/840452.

56. Chowdhary A, Randhawa HS, Boekhout T, Hagen F, Klaassen CH, Meis JF. Temperate climate niche for *Cryptococcus gattii* in Northern Europe. Emerging infectious diseases. 2012;18(1):172-3.

57. Byrnes EJ, III, Li W, Lewit Y, Ma H, Voelz K, Ren P, et al. Emergence and pathogenicity of highly virulent *Cryptococcus gattii* genotypes in the northwest United States. PLoS Pathogens. 2010;6(4):e1000850. doi: 10.1371/journal.ppat.1000850.

58. Harris JR, Lockhart SR, Debess E, Marsden-Haug N, Goldoft M, Wohrle R, et al. Cryptococcus gattii in the United States: Clinical Aspects of Infection With an Emerging Pathogen. Clinical Infectious Diseases. 2011;53(12):1188-95. doi: 10.1093/cid/cir723.

59. Ngamskulrungroj P, Chang Y, Sionov E, Kwon-Chung KJ. The Primary Target Organ of Cryptococcus gattii Is Different from That of Cryptococcus neoformans in a Murine Model. mBio. 2012;3(3). doi: 10.1128/mBio.00103-12.

60. Hagen F, Assen Sv, Luijckx GJ, Boekhout T, Kampinga GA. Activated dormant Cryptococcus gattii infection in a Dutch tourist who visited Vancouver Island (Canada): a molecular epidemiological approach. Medical Mycology. 2010;48(3):528-31. doi: doi:10.3109/13693780903300319. PubMed PMID: 19824880.

61. Bauer M, Wickenhauser C, Haak A, Pazaitis N, Siebolts U, Mawrin C, et al. Case report: A fatal case of cryptococcosis in an immunocompetent patient due to Cryptococcus deuterogattii (AFLP6/VGII). JMM Case Reports. 2018.

62. Gray KC, Palacios DS, Dailey I, Endo MM, Uno BE, Wilcock BC, et al. Amphotericin primarily kills yeast by simply binding ergosterol. Proceedings of the National Academy of Sciences. 2012;109(7):2234-9.

63. Finkelstein A, Holz R. Aqueous pores created in thin lipid membranes by the polyene antibiotics nystatin and amphotericin B. Membranes. 1973;2:377.

64. Cass A, Finkelstein A, Krespi V. The ion permeability induced in thin lipid membranes by the polyene antibiotics nystatin and amphotericin B. The journal of general physiology. 1970;56(1):100-24.

65. Loyse A, Dromer F, Day J, Lortholary O, Harrison TS. Flucytosine and cryptococcosis: time to urgently address the worldwide accessibility of a 50-year-old antifungal. Journal of Antimicrobial Chemotherapy. 2013;68(11):2435-44. doi: 10.1093/jac/dkt221.

66. Ashley ESD, Lewis R, Lewis JS, Martin C, Andes D. Pharmacology of systemic antifungal agents. Clinical Infectious Diseases. 2006;43(Supplement 1):S28-S39. doi: 10.1086/504492.

67. Vermes A, Guchelaar HJ, Dankert J. Flucytosine: a review of its pharmacology, clinical indications, pharmacokinetics, toxicity and drug interactions. The Journal of antimicrobial chemotherapy. 2000;46(2):171-9. Epub 2000/08/10. PubMed PMID: 10933638.

68. Day JN, Chau TTH, Wolbers M, Mai PP, Dung NT, Mai NH, et al. Combination Antifungal Therapy for Cryptococcal Meningitis. New England Journal of Medicine. 2013;368(14):1291-302. doi: doi:10.1056/NEJMoa1110404. PubMed PMID: 23550668.

69. Rajasingham R, Rolfes MA, Birkenkamp KE, Meya DB, Boulware DR. Cryptococcal meningitis treatment strategies in resource-limited settings: a cost-effectiveness analysis. PLoS Medicine. 2012;9(9):e1001316. doi: 10.1371/journal.pmed.1001316.

70. Meiring S, Fortuin-de Smidt M, Kularatne R, Dawood H, Govender NP, Germs SA. Prevalence and hospital management of amphotericin B deoxycholate-related toxicities during treatment of HIV-associated cryptococcal meningitis in South Africa. PLOS Neglected Tropical Diseases. 2016;10(7):e0004865. doi: 10.1371/journal.pntd.0004865.

71. Mourad A, Perfect JR. Tolerability profile of the current antifungal armoury. Journal of Antimicrobial Chemotherapy. 2018;73(suppl_1):i26-i32. doi: 10.1093/jac/dkx446.

72. Bicanic T, Bottomley C, Loyse A, Brouwer AE, Muzoora C, Taseera K, et al. Toxicity of amphotericin B deoxycholate-based induction therapy in patients with HIV-associated cryptococcal meningitis. Antimicrobial agents and chemotherapy. 2015;59(12):7224-31.

73. Yang H, Chaudhari P, Zhou ZY, Wu EQ, Patel C, Horn DL. Budget impact analysis of liposomal amphotericin B and amphotericin B lipid complex in the treatment of invasive fungal infections in the United States. Applied health economics and health policy. 2014;12(1):85-93. Epub 2014/01/05. doi: 10.1007/s40258-013-0072-7. PubMed PMID: 24385260.

74. Kneale M, Bartholomew JS, Davies E, Denning DW. Global access to antifungal therapy and its variable cost. Journal of Antimicrobial Chemotherapy. 2016;71(12):3599-606. doi: 10.1093/jac/dkw325.

75. Loyse A, Thangaraj H, Easterbrook P, Ford N, Roy M, Chiller T, et al. Cryptococcal meningitis: improving access to essential antifungal medicines in resource-poor countries. The Lancet infectious diseases. 2013;13(7):629-37.

76. Molloy SF, Chiller T, Greene GS, Burry J, Govender NP, Kanyama C, et al. Cryptococcal meningitis: A neglected NTD? PLOS Neglected Tropical Diseases. 2017;11(6):e0005575. doi: 10.1371/journal.pntd.0005575.

77. Harsanyi A, Conte A, Pichon L, Rabion A, Grenier S, Sandford G. One-Step Continuous Flow Synthesis of Antifungal WHO Essential Medicine Flucytosine Using Fluorine. Organic Process Research & Development. 2017;21(2):273-6. doi: 10.1021/acs.oprd.6b00420.

78. Rothe C, Sloan DJ, Goodson P, Chikafa J, Mukaka M, Denis B, et al. A Prospective Longitudinal Study of the Clinical Outcomes from Cryptococcal Meningitis following Treatment Induction with 800 mg Oral Fluconazole in Blantyre, Malawi. PloS one. 2013;8(6):e67311. doi: 10.1371/journal.pone.0067311.

79. Bicanic T, Harrison T, Niepieklo A, Dyakopu N, Meintjes G. Symptomatic relapse of HIV-associated cryptococcal meningitis after initial fluconazole monotherapy: the role of fluconazole resistance and immune reconstitution. Clinical Infectious Diseases. 2006;43(8):1069-70. doi: 10.1086/507895.

80. Pasquier E, Kunda J, De Beaudrap P, Loyse A, Temfack E, Molloy SF, et al. Long-term Mortality and Disability in Cryptococcal Meningitis: A Systematic Literature Review. Clinical Infectious Diseases. 2017;66(7):1122-32.

81. Goldberg DW, Tenforde MW, Mitchell HK, Jarvis JN, editors. Neurological sequelae of adult meningitis in Africa: A systematic literature review. Open forum infectious diseases; 2017: Oxford University Press US.

82. Butts A, DiDone L, Koselny K, Baxter BK, Chabrier-Rosello Y, Wellington M, et al. A repurposing approach identifies off-patent drugs with fungicidal cryptococcal activity, a common structural chemotype, and pharmacological properties relevant to the treatment of cryptococcosis. Eukaryotic Cell. 2013;12(2):278-87. doi: 10.1128/EC.00314-12.

83. Shapiro RS, Robbins N, Cowen LE. Regulatory circuitry governing fungal development, drug resistance, and disease. Microbiology and Molecular Biology Reviews. 2011;75(2):213-67.

84. Sionov E, Lee H, Chang YC, Kwon-Chung KJ. Cryptococcus neoformans Overcomes Stress of Azole Drugs by Formation of Disomy in Specific Multiple Chromosomes. PLOS Pathogens. 2010;6(4):e1000848. doi: 10.1371/journal.ppat.1000848.

85. Chong HS, Dagg R, Malik R, Chen S, Carter D. *In vitro* susceptibility of the yeast pathogen *Cryptococcus* to fluconazole and other azoles varies with molecular genotype. Journal of Clinical Microbiology. 2010;48(11):4115-20. doi: 10.1128/jcm.01271-10.

86. Herkert P, Hagen F, de Oliveira Salvador G, Gomes R, Ferreira M, Vicente V, et al. Molecular characterisation and antifungal susceptibility of clinical Cryptococcus deuterogattii (AFLP6/VGII) isolates from Southern Brazil. Eur J Clin Microbiol Infect Dis. 2016;35(11):1803-10.

87. Espinel-Ingroff A, Chowdhary A, Cuenca-Estrella M, Fothergill A, Fuller J, Hagen F, et al. *Cryptococcus neoformans-Cryptococcus gattii* species complex: an international study of wild-type susceptibility endpoint distributions and epidemiological cutoff values for amphotericin B and flucytosine. Antimicrobial Agents Chemotherapy. 2012;56(6):3107-13. Epub 2012/03/07. doi: 10.1128/aac.06252-11. PubMed PMID: 22391546; PubMed Central PMCID: PMCPMC3370763.

88. Li M, Liao Y, Chen M, Pan W, Weng L. Antifungal susceptibilities of *Cryptococcus* species complex isolates from AIDS and non-AIDS patients in Southeast China. Brazilian Journal of Infectious Diseases. 2012;16(2):175-9. Epub 2012/05/04. PubMed PMID: 22552461.

89. Pfaller MA, Messer SA, Jones RN, Castanheira M. Antifungal susceptibilities of Candida, Cryptococcus neoformans and Aspergillus fumigatus from the Asia and Western Pacific region: data from the SENTRY antifungal surveillance program (2010-2012). J Antibiot. 2015;68(9):556-61. doi: 10.1038/ja.2015.29.

90. Nyazika TK, Herkert PF, Hagen F, Mateveke K, Robertson VJ, Meis JF. In vitro antifungal susceptibility profiles of Cryptococcus species isolated from HIV-associated cryptococcal meningitis patients in Zimbabwe. Diagnostic Microbiology and Infectious Disease. 2016;86(3):289-92. doi: https://doi.org/10.1016/j.diagmicrobio.2016.08.004.

91. Smith KD, Achan B, Hullsiek KH, McDonald TR, Okagaki LH, Alhadab AA, et al. Increased antifungal drug resistance in clinical isolates of *Cryptococcus neoformans* in Uganda. Antimicrobial agents and chemotherapy. 2015;59(12):7197-204. doi: 10.1128/AAC.01299-15.

92. Govender NP, Patel J, van Wyk M, Chiller TM, Lockhart SR. Trends in antifungal drug susceptibility of *Cryptococcus neoformans* isolates obtained through population-based surveillance in South Africa in 2002-2003 and 2007-2008. Antimicrobial agents and chemotherapy. 2011;55(6):2606-11. Epub 2011/03/30. doi: 10.1128/aac.00048-11. PubMed PMID: 21444707; PubMed Central PMCID: PMCPMC3101403.

93. Pfaller M, Messer S, Boyken L, Rice C, Tendolkar S, Hollis R, et al. Global trends in the antifungal susceptibility of *Cryptococcus neoformans* (1990 to 2004). Journal of Clinical Microbiology. 2005;43(5):2163-7.

94. Sar B, Monchy D, Vann M, Keo C, Sarthou JL, Buisson Y. Increasing in vitro resistance to fluconazole in Cryptococcus neoformans Cambodian isolates: April 2000 to March 2002. Journal of Antimicrobial Chemotherapy. 2004;54(2):563-5. doi: 10.1093/jac/dkh361.

95. Hsueh PR, Lau YJ, Chuang YC, Wan JH, Huang WK, Shyr JM, et al. Antifungal susceptibilities of clinical isolates of *Candida* species, *Cryptococcus neoformans*, and *Aspergillus* species from Taiwan: surveillance of multicenter antimicrobial resistance in Taiwan program data from 2003. Antimicrobial agents and chemotherapy. 2005;49(2):512-7. Epub 2005/01/28. doi: 10.1128/aac.49.2.512-517.2005. PubMed PMID: 15673726; PubMed Central PMCID: PMCPMC547329.

96. Chen Y-C, Chang T-Y, Liu J-W, Chen F-J, Chien C-C, Lee C-H, et al. Increasing trend of fluconazole-non-susceptible Cryptococcus neoformans in patients with invasive cryptococcosis: a 12-year longitudinal study. BMC infectious diseases. 2015;15(1):277.

97. Bongomin F, Oladele RO, Gago S, Moore CB, Richardson MD. A systematic review of fluconazole resistance in clinical isolates of Cryptococcus species. Mycoses. 2018;61(5):290-7. doi: doi:10.1111/myc.12747.

98. Revie NM, Iyer KR, Robbins N, Cowen LE. Antifungal drug resistance: evolution, mechanisms and impact. Current opinion in microbiology. 2018;45:70-6.

99. Zhang J, Li L, Lv Q, Yan L, Wang Y, Jiang Y. The Fungal CYP51s: Their Functions, Structures, Related Drug Resistance, and Inhibitors. Frontiers in microbiology. 2019;10.

100. Sionov E, Chang YC, Garraffo HM, Kwon-Chung KJ. Heteroresistance to Fluconazole in Cryptococcus neoformans Is Intrinsic and Associated with Virulence. Antimicrobial agents and chemotherapy. 2009;53(7):2804-15. doi: 10.1128/aac.00295-09.

101. Altamirano S, Fang D, Simmons C, Sridhar S, Wu P, Sanyal K, et al. Fluconazole-Induced Ploidy Change in *Cryptococcus neoformans* Results from the Uncoupling of Cell Growth and Nuclear Division. mSphere. 2017;2(3):e00205-17.

102. Stone NR, Rhodes J, Fisher MC, Mfinanga S, Kivuyo S, Rugemalila J, et al. Dynamic ploidy changes drive fluconazole resistance in human cryptococcal meningitis. The Journal of clinical investigation. 2019;129(3).

103. Chang YC, Lamichhane AK, Kwon-Chung KJ. Cryptococcus neoformans, Unlike Candida albicans, Forms Aneuploid Clones Directly from Uninucleated Cells under Fluconazole Stress. mBio. 2018;9(6):e01290-18.

104. Sionov E, Chang YC, Kwon-Chung KJ. Azole heteroresistance in Cryptococcus neoformans: emergence of resistant clones with chromosomal disomy in the mouse brain during fluconazole treatment. Antimicrobial agents and chemotherapy. 2013;57(10):5127-30.

105. Herreros E, Almela MJ, Lozano S, Gomez De Las Heras F, Gargallo-Viola D. Antifungal activities and cytotoxicity studies of six new azasordarins. Antimicrobial agents and chemotherapy. 2001;45(11):3132-9. doi: 10.1128/aac.45.11.3132-3139.2001.

106. Spitzer M, Griffiths E, Blakely KM, Wildenhain J, Ejim L, Rossi L, et al. Cross-species discovery of syncretic drug combinations that potentiate the antifungal fluconazole. Molecular systems biology. 2011;7:499. doi: 10.1038/msb.2011.31.

107. Shoham S, Levitz SM. The immune response to fungal infections. British journal of haematology. 2005;129(5):569-82. Epub 2005/05/27. doi: 10.1111/j.1365-2141.2005.05397.x. PubMed PMID: 15916679.

108. Roemer T, Krysan DJ. Antifungal Drug Development: Challenges, Unmet Clinical Needs, and New Approaches. Cold Spring Harbor Perspectives in Medicine. 2014;4(5). doi: 10.1101/cshperspect.a019703.

109. Pardridge WM. Drug transport across the blood–brain barrier. Journal of cerebral blood flow & metabolism. 2012;32(11):1959-72.

110. Shah S, Federoff HJ. Drug discovery dilemma and Cura Quartet collaboration. Drug Discovery Today. 2009;14(21):1006-10. doi: https://doi.org/10.1016/j.drudis.2009.09.007.

111. Wong CH, Siah KW, Lo AW. Estimation of clinical trial success rates and related parameters. Biostatistics. 2018:kxx069-kxx. doi: 10.1093/biostatistics/kxx069.

112. DiMasi JA, Grabowski HG, Hansen RW. Innovation in the pharmaceutical industry: new estimates of R&D costs. Journal of health economics. 2016;47:20-33.

113. Adams CP, Brantner VV. Estimating the cost of new drug development: is it really $802 million? Health Affairs. 2006;25(2):420-8. doi: 10.1377/hlthaff.25.2.420.

114. DiMasi JA, Grabowski HG. The cost of biopharmaceutical R&D: is biotech different? Managerial and Decision Economics. 2007;28(4-5):469-79.

115. DiMasi JA, Hansen RW, Grabowski HG. The price of innovation: new estimates of drug development costs. Journal of health economics. 2003;22(2):151-85. Epub 2003/02/28. doi: 10.1016/s0167-6296(02)00126-1. PubMed PMID: 12606142.

116. Paul SM, Mytelka DS, Dunwiddie CT, Persinger CC, Munos BH, Lindborg SR, et al. How to improve R&D productivity: the pharmaceutical industry's grand challenge. Nature Reviews Drug Discovery. 2010;9(3):203-14. doi: http://www.nature.com/nrd/journal/v9/n3/suppinfo/nrd3078_S1.html.

117. Morgan S, Grootendorst P, Lexchin J, Cunningham C, Greyson D. The cost of drug development: a systematic review. Health policy (Amsterdam, Netherlands). 2011;100(1):4-17. Epub 2011/01/25. doi: 10.1016/j.healthpol.2010.12.002. PubMed PMID: 21256615.

118. Van Norman GA. Drugs, Devices, and the FDA: Part 1: An Overview of Approval Processes for Drugs. JACC: Basic to Translational Science. 2016;1(3):170-9. doi: https://doi.org/10.1016/j.jacbts.2016.03.002.

119. Thomas DW, Burns J, Audette J, Carroll A, Dow-Hygelund C, Hay M. Clinical Development Success Rates 2006-2015. San Diego, California: Biomedtracker; 2016.

120. Getz KA, Wenger J, Campo RA, Seguine ES, Kaitin KI. Assessing the Impact of Protocol Design Changes on Clinical Trial Performance. American Journal of Therapeutics. 2008;15(5):450-7. doi: 10.1097/MJT.0b013e31816b9027. PubMed PMID: 00045391-200809000-00007.

121. Mullard A. 2017 FDA drug approvals. Nature Publishing Group; 2018.

122. Ashburn TT, Thor KB. Drug repositioning: identifying and developing new uses for existing drugs. Nature Reviews Drug Discovery. 2004;3(8):673-83.

123. Nosengo N. Can you teach old drugs new tricks? Nature News. 2016;534(7607):314.

124. Butts A, Krysan DJ. Antifungal drug discovery: something old and something new. PLoS Pathogens. 2012;8(9):e1002870.

125. Miller CP. Increasing Market Exclusivity for New Drugs, the Cure for What Ails Us? Patent Highlight. ACS Publications; 2012.

126. Hathaway C, Manthei J, Scherer C. Exclusivity Strategies in the United States and European Union. The Food and Drug Law Institute: Update. 2009;3:34-9.

127. Pushpakom S, Iorio F, Eyers PA, Escott KJ, Hopper S, Wells A, et al. Drug repurposing: progress, challenges and recommendations. Nature Reviews Drug Discovery. 2019;18(1):41.

128. Prasad V, Mailankody S. Research and Development Spending to Bring a Single Cancer Drug to Market and Revenues After Approval. JAMA Intern Med. 2017;177(11):1569-75. Epub 2017/09/12. doi: 10.1001/jamainternmed.2017.3601. PubMed PMID: 28892524; PubMed Central PMCID: PMCPMC5710275.

129. Paavola A. Big pharma backs off superbug: Why 5 drugmakers bailed on antibiotic research: Becker's Hospital Review; 2018 [cited 2019 April 1]. Available from: https://www.beckershospitalreview.com/pharmacy/big-pharma-backs-off-superbug-why-5-drugmakers-bailed-on-antibiotic-research.html.

130. Hu C. Pharmaceutical companies are backing away from a growing threat that could kill 10 million people a year by 2050: Business Insider Australia; 2018 [cited 2019 April 1]. Available from: https://www.businessinsider.com.au/major-pharmaceutical-companies-dropping-antibiotic-projects-superbugs-2018-7?r=US&IR=T.

131. Wanted: a reward for antibiotic development. Nature Biotechnology. 2018;36:555. doi: 10.1038/nbt.4193.

132. Tillotson J, Tillotson GS. The regulatory pathway for antifungal drugs: a US perspective. Clinical Infectious Diseases. 2015;61(suppl_6):S678-S83.

133. FDA. GENERATING ANTIBIOTIC INCENTIVES NOW.

134. Luepke KH, Suda KJ, Boucher H, Russo RL, Bonney MW, Hunt TD, et al. Past, present, and future of antibacterial economics: increasing bacterial resistance, limited antibiotic pipeline, and societal implications. Pharmacotherapy: The Journal of Human Pharmacology and Drug Therapy. 2017;37(1):71-84.

135. FDA. Guidance for Industry Expedited Programs for Serious Conditions – Drugs and Biologics. 2014.

136. FDA. Limited Population Pathway for Antibacterial

and Antifungal Drugs Guidance for Industry. 2018.

137. Espinel-Ingroff A. Novel antifungal agents, targets or therapeutic strategies for the treatment of invasive fungal diseases: a review of the literature (2005-2009). Revista iberoamericana de micologia. 2009;26(1):15-22. Epub 2009/05/26. doi: 10.1016/s1130-1406(09)70004-x. PubMed PMID: 19463273.

138. Chaturvedi AK, Hameed RS, Wozniak KL, Hole CR, Wager CML, Weintraub ST, et al. Vaccine-mediated immune responses to experimental pulmonary Cryptococcus gattii infection in mice. PloS one. 2014;9(8):e104316.

139. Chow S-K, Casadevall A. Evaluation of Cryptococcus neoformans galactoxylomannan–protein conjugate as vaccine candidate against murine cryptococcosis. Vaccine. 2011;29(10):1891-8.

140. Rachini A, Pietrella D, Lupo P, Torosantucci A, Chiani P, Bromuro C, et al. An anti-β-glucan monoclonal antibody inhibits growth and capsule formation of Cryptococcus neoformans in vitro and exerts therapeutic, anticryptococcal activity in vivo. Infection and immunity. 2007;75(11):5085-94.

141. Oscarson S, Alpe M, Svahnberg P, Nakouzi A, Casadevall A. Synthesis and immunological studies of glycoconjugates of Cryptococcus neoformans capsular glucuronoxylomannan oligosaccharide structures. Vaccine. 2005;23(30):3961-72.

142. Nakouzi A, Zhang T, Oscarson S, Casadevall A. The common Cryptococcus neoformans glucuronoxylomannan M2 motif elicits non-protective antibodies. Vaccine. 2009;27(27):3513-8.

143. Guazzelli L, Ulc R, Rydner L, Oscarson S. A synthetic strategy to xylose-containing thioglycoside tri-and tetrasaccharide building blocks corresponding to Cryptococcus neoformans capsular polysaccharide structures. Organic & biomolecular chemistry. 2015;13(23):6598-610.

144. Larsen RA, Pappas PG, Perfect J, Aberg JA, Casadevall A, Cloud GA, et al. Phase I evaluation of the safety and pharmacokinetics of murine-derived anticryptococcal antibody 18B7 in subjects with treated cryptococcal meningitis. Antimicrobial agents and chemotherapy. 2005;49(3):952-8.

145. Hole CR, Wormley FL, Jr. Vaccine and immunotherapeutic approaches for the prevention of cryptococcosis: lessons learned from animal models. Frontiers in microbiology. 2012;3:291. Epub 2012/09/14. doi: 10.3389/fmicb.2012.00291. PubMed PMID: 22973262; PubMed Central PMCID: PMCPMC3428735.

146. Butts A, Koselny K, Chabrier-Roselló Y, Semighini CP, Brown JC, Wang X, et al. Estrogen receptor antagonists are anti-cryptococcal agents that directly bind EF hand proteins and synergize with fluconazole in vivo. MBio. 2014;5(1):e00765-13.

147. Lai Y-W, Campbell LT, Wilkins MR, Pang CNI, Chen S, Carter DA. Synergy and antagonism between iron chelators and antifungal drugs in *Cryptococcus*. International Journal of Antimicrobial Agents. 2016;48(4):388-94. doi: 10.1016/j.ijantimicag.2016.06.012.

148. Sangalli-Leite F, Scorzoni L, da Silva JdF, de Oliveira HC, de Lacorte Singulani J, Gullo FP, et al. Synergistic effect of pedalitin and amphotericin B against Cryptococcus neoformans by in vitro and in vivo evaluation. International journal of antimicrobial agents. 2016;48(5):504-11.

149. Pfaller M, Messer S, Georgopapadakou N, Martell L, Besterman J, Diekema D. Activity of MGCD290, a Hos2 histone deacetylase inhibitor, in combination with azole antifungals against opportunistic fungal pathogens. Journal of clinical microbiology. 2009;47(12):3797-804.

150. Zhai B, Zhou H, Yang L, Zhang J, Jung K, Giam C-Z, et al. Polymyxin B, in combination with fluconazole, exerts a potent fungicidal effect. Journal of Antimicrobial Chemotherapy. 2010;65(5):931-8. doi: 10.1093/jac/dkq046.

151. Sleigh SH, Barton CL. Repurposing strategies for therapeutics. Pharmaceutical Medicine. 2010;24(3):151-9.

152. Tobinick EL. The value of drug repositioning in the current pharmaceutical market. Drug News and Perspectives. 2009;22(2):119-25. Epub 2009/03/31. doi: 10.1358/dnp.2009.22.2.1303818. PubMed PMID: 19330170.

153. Bisson WH. Drug repurposing in chemical genomics: can we learn from the past to improve the future? Current topics in medicinal chemistry. 2012;12(17):1883-8. Epub 2012/11/03. PubMed PMID: 23116467.

154. Dickson M, Gagnon JP. Key factors in the rising cost of new drug discovery and development. Nature Reviews Drug Discovery. 2004;3(5):417-29.

155. Zhai B, Lin X. Recent progress on antifungal drug development. Current Pharmaceutical Biotechnology. 2011;12(8):1255-62.

156. Chong CR, Sullivan DJ. New uses for old drugs. Nature. 2007;448:645-6.

157. Roin BN. Solving the problem of new uses. Browser Download This Paper. 2013.

158. Strittmatter SM. Overcoming Drug Development Bottlenecks With Repurposing: Old drugs learn new tricks. Nature Medicine. 2014;20:590. doi: 10.1038/nm.3595.

159. Sun W, Sanderson PE, Zheng W. Drug combination therapy increases successful drug repositioning. Drug Discovery Today. 2016;21(7):1189-95. doi: https://doi.org/10.1016/j.drudis.2016.05.015.

160. Dehdashti SJ, Abbott J, Nguyen DT, McKew JC, Williamson PR, Zheng W. A high-throughput screening assay for assessing the viability of *Cryptococcus neoformans* under nutrient starvation conditions. Analytical and bioanalytical chemistry. 2013;405(21):6823-9. Epub 2013/07/03. doi: 10.1007/s00216-013-7134-4.

161. Rabjohns JLA, Park Y-D, Dehdashti J, Sun W, Henderson C, Zelazny A, et al. A high-throughput screening assay for fungicidal compounds against *Cryptococcus neoformans*. Journal of Biomolecular Screening. 2013;19(2):270-7. doi: 10.1177/1087057113496847.

162. Brown JCS, Nelson J, VanderSluis B, Deshpande R, Butts A, Kagan S, et al. Unraveling the biology of a fungal meningitis pathogen using chemical genetics. Cell. 2014;159(5):1168-87. doi: 10.1016/j.cell.2014.10.044. PubMed PMID: PMC4243055.

163. Samantaray S, Correia JN, Garelnabi M, Voelz K, May RC, Hall RA. Novel cell-based in vitro screen to identify small-molecule inhibitors against intracellular replication of Cryptococcus neoformans in macrophages. International Journal of Antimicrobial Agents. 2016;48(1):69-77. doi: 10.1016/j.ijantimicag.2016.04.018.

164. Joffe LS, Schneider R, Lopes W, Azevedo R, Staats CC, Kmetzsch L, et al. The anti-helminthic compound mebendazole has multiple antifungal effects against *Cryptococcus neoformans*. Frontiers in microbiology. 2017;8:1-14. doi: 10.3389/fmicb.2017.00535.

165. Zhai B, Wu C, Wang L, Sachs MS, Lin X. The antidepressant sertraline provides a promising therapeutic option for neurotropic cryptococcal infections. Antimicrobial agents and chemotherapy. 2012;56(7):3758-66. doi: 10.1128/aac.00212-12.

166. Rhein J, Morawski BM, Hullsiek KH, Nabeta HW, Kiggundu R, Tugume L, et al. Efficacy of adjunctive sertraline for the treatment of HIV-associated cryptococcal meningitis: an open-label dose-ranging study. Lancet Infectious Diseases. 2016;16(7):809-18. doi: 10.1016/S1473-3099(16)00074-8.

167. Santos-Gandelman J, Rodrigues ML, Machado Silva A. Future perspectives for cryptococcosis treatment. Expert Opinion on Therapeutic Patents. 2018;28(8):625-34. doi: 10.1080/13543776.2018.1503252.

168. Bradley D. Why big pharma needs to learn the three 'R's. Nature Reviews Drug Discovery. 2005;4(6):446-.

169. Schubert OT, Röst HL, Collins BC, Rosenberger G, Aebersold R. Quantitative proteomics: challenges and opportunities in basic and applied research. Nature Protocols. 2017;12:1289. doi: 10.1038/nprot.2017.040.

170. Loscalzo J, Barabasi AL. Systems biology and the future of medicine. Wiley Interdisciplinary Reviews: Systems Biology and Medicine. 2011;3(6):619-27.

171. Soon WW, Hariharan M, Snyder MP. High-throughput sequencing for biology and medicine. Molecular systems biology. 2013;9(1):640.

172. Horgan RP, Kenny LC. 'Omic'technologies: genomics, transcriptomics, proteomics and metabolomics. The Obstetrician & Gynaecologist. 2011;13(3):189-95.

173. Wang Z, Gerstein M, Snyder M. RNA-Seq: a revolutionary tool for transcriptomics. Nature Reviews Genetics. 2009;10:57. doi: 10.1038/nrg2484.

174. Ozsolak F, Milos PM. RNA sequencing: advances, challenges and opportunities. Nature reviews Genetics. 2011;12(2):87-98. Epub 2010/12/30. doi: 10.1038/nrg2934. PubMed PMID: 21191423.

175. Dong Y, Hu J, Fan L, Chen Q. RNA-Seq-based transcriptomic and metabolomic analysis reveal stress responses and programmed cell death induced by acetic acid in Saccharomyces cerevisiae. Scientific reports. 2017;7:42659. doi: 10.1038/srep42659

176. Upadhya R, Campbell LT, Donlin MJ, Aurora R, Lodge JK. Global transcriptome profile of Cryptococcus neoformans during exposure to hydrogen peroxide induced oxidative stress. PloS one. 2013;8(1):e55110.

177. Florio AR, Ferrari S, De Carolis E, Torelli R, Fadda G, Sanguinetti M, et al. Genome-wide expression profiling of the response to short-term exposure to fluconazole in Cryptococcus neoformans serotype A. BMC microbiology. 2011;11(1):97.

178. Pang CN, Lai YW, Campbell LT, Chen SC, Carter DA, Wilkins MR. Transcriptome and network analyses in Saccharomyces cerevisiae reveal that amphotericin B and lactoferrin synergy disrupt metal homeostasis and stress response. Scientific reports. 2017;7:40232. Epub 2017/01/13. doi: 10.1038/srep40232. PubMed PMID: 28079179; PubMed Central PMCID: PMCPMC5228129.

179. Dzoyem J, Kechia F, Ngaba G, Lunga P, Lohoue P. Prevalence of cryptococcosis among HIV-infected patients in Yaounde, Cameroon. African Health Sciences. 2012;12(2):129-33. doi: 10.4314/ahs.v12i2.8.

180. Jarvis JN, Bicanic T, Loyse A, Namarika D, Jackson A, Nussbaum JC, et al. Determinants of mortality in a combined cohort of 501 patients with HIV-associated cryptococcal meningitis: implications for improving outcomes. Clinical Infectious Diseases. 2014;58(5):736-45. doi: 10.1093/cid/cit794.

181. Oprea TI, Mestres J. Drug repurposing: far beyond new targets for old drugs. AAPS Journal. 2012;14(4):759-63. doi: 10.1208/s12248-012-9390-1.

182. Clinical and Laboratory Standards Insititute (CLSI). Reference method for broth dilution antifungal susceptibility testing of yeasts - Approved Standard - Third Edition M27-A3. Wayne, Pennsylvania: Clinical and Laboratory Standards Insititute (CLSI); 2008.

183. Clinical and Laboratory Standards Insititute (CLSI). Reference method for broth dilution antifungal susceptibility testing of filamentous fungi - Approved Standard - Second Edition M38-A2. Wayne, Pennsylvania: Clinical and Laboratory Standards Insititute (CLSI); 2008.

184. Espinel-Ingroff A, Fothergill A, Peter J, Rinaldi M, Walsh T. Testing conditions for determination of minimum fungicidal concentrations of new and established antifungal agents for *Aspergillus* spp.: NCCLS collaborative study. Journal of Clinical Microbiology. 2002;40(9):3204-8. doi: 10.1128/JCM.40.9.3204-3208.2002.

185. Catterall WA. Voltage-gated calcium channels. Cold Spring Harbor Perspectives Biology. 2011;3(8):a003947. doi: 10.1101/cshperspect.a003947.

186. Prole DL, Taylor CW. Identification and analysis of cation channel homologues in human pathogenic fungi. PloS one. 2012;7(8):e42404. doi: 10.1371/journal.pone.0042404.

187. Teng J, Goto R, Iida K, Kojima I, Iida H. Ion-channel blocker sensitivity of voltage-gated calcium-channel homologue Cch1 in *Saccharomyces cerevisiae*. Microbiology. 2008;154(12):3775-81. doi: 10.1099/mic.0.2008/021089-0.

188. Hong MP, Vu K, Bautos JM, Tham R, Jamklang M, Uhrig JP, et al. Activity of the calcium channel pore Cch1 is dependent on a modulatory region of the subunit Mid1 in *Cryptococcus neoformans*. Eukaryotic Cell. 2013;12(1):142-50. Epub 2012/11/24. doi: 10.1128/ec.00130-12.

189. Hong MP, Vu K, Bautos J, Gelli A. Cch1 restores intracellular Ca2+ in fungal cells during endoplasmic reticulum stress. Journal of Biological Chemistry. 2010;285(14):10951-8. Epub 2010/02/04. doi: 10.1074/jbc.M109.056218.

190. Liu M, Du P, Heinrich G, Cox GM, Gelli A. Cch1 mediates calcium entry in *Cryptococcus neoformans* and is essential in low-calcium environments. Eukaryotic Cell. 2006;5(10):1788-96. doi: 10.1128/EC.00158-06.

191. Peiter E, Fischer M, Sidaway K, Roberts SK, Sanders D. The *Saccharomyces cerevisiae* Ca2+ channel Cch1pMid1p is essential for tolerance to cold stress and iron toxicity. FEBS letters. 2005;579(25):5697-703. Epub 2005/10/15. doi: 10.1016/j.febslet.2005.09.058.

192. Liu S, Yue L, Gu W, Li X, Zhang L, Sun S. Synergistic effect of fluconazole and calcium channel blockers against resistant *Candida albicans*. PloS one. 2016;11(3):e0150859. doi: 10.1371/journal.pone.0150859.

193. Afeltra J, Vitale RG, Mouton JW, Verweij PE. Potent Synergistic In Vitro Interaction between Nonantimicrobial Membrane-Active Compounds and Itraconazole against Clinical Isolates of Aspergillus fumigatus Resistant to Itraconazole. Antimicrobial agents and chemotherapy. 2004;48(4):1335-43. doi: 10.1128/aac.48.4.1335-1343.2004.

194. Chrysant S. The ALLHAT study: results and clinical implications. QJM: An International Journal of Medicine. 2003;96(10):771-3. doi: 10.1093/qjmed/hcg123.

195. Gaggi R, Cont R, Gianni AM. Comparison among the effects of nifedipine, nimodipine and nisoldipine on the brain biogenic amines of normal or haloperidol treated rats. General Pharmacology. 1993;24(5):1091-6. doi: 10.1016/0306-3623(93)90354-Z.

196. Spagnuolo PA, Hu J, Hurren R, Wang X, Gronda M, Sukhai MA, et al. The antihelmintic flubendazole inhibits microtubule function through a mechanism distinct from Vinca alkaloids and displays preclinical activity in leukemia and myeloma. Blood. 2010;115(23):4824-33. doi: 10.1182/blood-2009-09-243055.

197. Chatterji BP, Jindal B, Srivastava S, Panda D. Microtubules as antifungal and antiparasitic drug targets. Expert Opinion on Therapeutic Patents. 2011;21(2):167-86. doi: 10.1517/13543776.2011.545349.

198. Cruz MC, Edlind T. β-Tubulin genes and the basis for benzimidazole sensitivity of the opportunistic fungus *Cryptococcus neoformans*. Microbiology. 1997;143(6):2003-8. doi: 10.1099/00221287-143-6-2003.

199. Horton J. Albendazole: a review of anthelmintic efficacy and safety in humans. Parasitology. 2000;121(7):113-32. doi: 10.1017/S0031182000007290.

200. Cruz M, Bartlett M, Edlind T. *In vitro* susceptibility of the opportunistic fungus *Cryptococcus neoformans* to anthelmintic benzimidazoles. Antimicrobial agents and chemotherapy. 1994;38(2):378-80.

201. Edlind TD, Cruz MC, inventors; Google Patents, assignee. Treatment of *Cryptococcus neoformans* infection1995.

202. Del Poeta M, Schell WA, Dykstra CC, Jones SK, Tidwell RR, Kumar A, et al. *In vitro* antifungal activities of a series of dication-substituted carbazoles, furans, and benzimidazoles. Antimicrobial agents and chemotherapy. 1998;42(10):2503-10.

203. Téllez-Girón E, Ramos MC, Dufour L, Montante M, Téllez Jr E, Rodríguez J, et al. Treatment of neurocysticercosis with flubendazole. American Journal of Tropical Medicine and Hygiene. 1984;33(4):627-31. doi: 10.4269/ajtmh.1984.33.627.

204. Cumino AC, Elissondo MC, Denegri GM. Flubendazole interferes with a wide spectrum of cell homeostatic mechanisms in *Echinococcus granulosus* protoscoleces. Parasitology Internaitonal. 2009;58(3):270-7. doi: 10.1016/j.parint.2009.03.005.

205. Feldmeier H, Bienzle U, Döhring E, Dietrich M. Flubendazole versus mebendazole in intestinal helminthic infections. Acta Tropica. 1982;39(2):185-9.

206. Lassègue A, Estavoyer J, Minazzi H, Barale T, Gillet M, Vuitton D, et al. Treatment of human alveolar echinococcosis with flubendazole. Clinical, morphological and immunological study. Gastroentérologie Clinique et Biologique. 1984;8(4):314.

207. Ceballos L, Elissondo M, Bruni SS, Denegri G, Alvarez L, Lanusse C. Flubendazole in cystic echinococcosis therapy: pharmaco-parasitological evaluation in mice. Parasitology International. 2009;58(4):354-8. doi: 10.1016/j.parint.2009.07.006.

208. Nixon GL, McEntee L, Johnson A, Farrington N, Whalley S, Livermore J, et al. Repurposing and reformulation of the antiparasitic agent flubendazole for treatment of cryptococcal meningoencephalitis, a neglected fungal disease. Antimicrobial agents and chemotherapy. 2018;62(4):e09190917. doi: 10.1128/aac.01909-17.

209. Keri RS, Hiremathad A, Budagumpi S, Nagaraja BM. Comprehensive Review in Current Developments of Benzimidazole-Based Medicinal Chemistry. Chemical biology & drug design. 2015;86(1):19-65.

210. Hou Z-J, Luo X, Zhang W, Peng F, Cui B, Wu S-J, et al. Flubendazole, FDA-approved anthelmintic, targets breast cancer stem-like cells. Oncotarget. 2015;6(8):6326.

211. Michaelis M, Agha B, Rothweiler F, Löschmann N, Voges Y, Mittelbronn M, et al. Identification of flubendazole as potential anti-neuroblastoma compound in a large cell line screen. Scientific reports. 2015;5:8202.

212. O'Neill M, Ballesteros C, Tritten L, Burkman E, Zaky WI, Xia J, et al. Profiling the macrofilaricidal effects of flubendazole on adult female Brugia malayi using RNAseq. International Journal for Parasitology: Drugs and Drug Resistance. 2016;6(3):288-96.

213. Chauhan S, Ahmed Z, Bradfute SB, Arko-Mensah J, Mandell MA, Won Choi S, et al. Pharmaceutical screen identifies novel target processes for activation of autophagy with a broad

translational potential. Nat Commun. 2015;6:8620. Epub 2015/10/28. doi: 10.1038/ncomms9620. PubMed PMID: 26503418; PubMed Central PMCID: PMCPMC4624223.

214. Salahuddin, Shaharyar M, Mazumder A. Benzimidazoles: A biologically active compounds. Arabian Journal of Chemistry. 2017;10:S157-S73. doi: https://doi.org/10.1016/j.arabjc.2012.07.017.

215. Bansal Y, Silakari O. The therapeutic journey of benzimidazoles: a review. Bioorganic & medicinal chemistry. 2012;20(21):6208-36.

216. Goode BL, Drubin DG, Barnes G. Functional cooperation between the microtubule and actin cytoskeletons. Current opinion in cell biology. 2000;12(1):63-71.

217. Kilmartin J, Adams A. Structural rearrangements of tubulin and actin during the cell cycle of the yeast Saccharomyces. The Journal of cell biology. 1984;98(3):922-33.

218. Neff NF, Thomas JH, Grisafi P, Botstein D. Isolation of the β-tubulin gene from yeast and demonstration of its essential function in vivo. Cell. 1983;33(1):211-9.

219. Schatz P, Pillus L, Grisafi P, Solomon F, Botstein D. Two functional alpha-tubulin genes of the yeast Saccharomyces cerevisiae encode divergent proteins. Molecular and cellular biology. 1986;6(11):3711-21.

220. Schatz P, Solomon F, Botstein D. Genetically essential and nonessential alpha-tubulin genes specify functionally interchangeable proteins. Molecular and Cellular Biology. 1986;6(11):3722-33.

221. Erlemann S, Neuner A, Gombos L, Gibeaux R, Antony C, Schiebel E. An extended γ-tubulin ring functions as a stable platform in microtubule nucleation. The Journal of Cell Biology. 2012;197(1):59-74. doi: 10.1083/jcb.201111123.

222. Roostalu J, Surrey T. Microtubule nucleation: beyond the template. Nature Reviews Molecular Cell Biology. 2017;18:702. doi: 10.1038/nrm.2017.75.

223. Zhou X, Liu J, Zhang J, Wei Y, Li H. Flubendazole inhibits glioma proliferation by G2/M cell cycle arrest and pro-apoptosis. Cell Death Discovery. 2018;4(1):18. doi: 10.1038/s41420-017-0017-2.

224. Chen Y, Toffaletti DL, Tenor JL, Litvintseva AP, Fang C, Mitchell TG, et al. The Cryptococcus neoformans transcriptome at the site of human meningitis. MBio. 2014;5(1):e01087-13.

225. Jung K-W, Yang D-H, Kim M-K, Seo HS, Lim S, Bahn Y-S. Unraveling fungal radiation resistance regulatory networks through the genome-wide transcriptome and genetic analyses of Cryptococcus neoformans. MBio. 2016;7(6):e01483-16.

226. Chong H, Campbell L, Padula M, Hill C, Harry E. Time-Course Proteome Analysis Reveals the Dynamic Response of Cryptococcus gattii Cells. 2012.

227. Kim D, Langmead B, Salzberg SL. HISAT: a fast spliced aligner with low memory requirements. Nature methods. 2015;12(4):357.

228. Liao Y, Smyth GK, Shi W. FeatureCounts: an efficient general purpose program for assigning sequence reads to genomic features. Bioinformatics. 2013;30(7):923-30.

229. McCarthy DJ, Chen Y, Smyth GK. Differential expression analysis of multifactor RNA-Seq experiments with respect to biological variation. Nucleic acids research. 2012;40(10):4288-97.

230. Chen Y, Lun AT, Smyth GK. From reads to genes to pathways: differential expression analysis of RNA-Seq experiments using Rsubread and the edgeR quasi-likelihood pipeline. F1000Research. 2016;5.

231. Robinson MD, McCarthy DJ, Smyth GK. edgeR: a Bioconductor package for differential expression analysis of digital gene expression data. Bioinformatics. 2010;26(1):139-40.

232. Risso D, Ngai J, Speed TP, Dudoit S. Normalization of RNA-seq data using factor analysis of control genes or samples. Nature biotechnology. 2014;32(9):896.

233. Gandolfo LC, Speed TP. RLE plots: Visualizing unwanted variation in high dimensional data. PloS one. 2018;13(2):e0191629.

234. Gagnon-Bartsch JA, Speed TP. Using control genes to correct for unwanted variation in microarray data. Biostatistics. 2012;13(3):539-52.

235. Bindea G, Mlecnik B, Hackl H, Charoentong P, Tosolini M, Kirilovsky A, et al. ClueGO: a Cytoscape plug-in to decipher functionally grouped gene ontology and pathway annotation networks. Bioinformatics. 2009;25(8):1091-3. doi: 10.1093/bioinformatics/btp101.

236. Adams J, Kelso R, Cooley L. The kelch repeat superfamily of proteins: propellers of cell function. Trends in cell biology. 2000;10(1):17-24.

237. Peeters T, Louwet W, Geladé R, Nauwelaers D, Thevelein JM, Versele M. Kelch-repeat proteins interacting with the Gα protein Gpa2 bypass adenylate cyclase for direct regulation of protein kinase A in yeast. Proceedings of the National Academy of Sciences. 2006;103(35):13034-9.

238. Gould CJ, Chesarone-Cataldo M, Alioto SL, Salin B, Sagot I, Goode BL. S. cerevisiae Kelch proteins and Bud14 form a stable 520 kDa Formin-regulatory complex that controls actin cable assembly and cell morphogenesis. Journal of Biological Chemistry. 2014:jbc. M114. 548719.

239. Hudson AM, Mannix KM, Gerdes JA, Kottemann MC, Cooley L. Targeted substrate degradation by Kelch controls the actin cytoskeleton during ring canal expansion. Development. 2019;146(1):dev169219. doi: 10.1242/dev.169219.

240. Budhwar R, Fang G, Hirsch JP. Kelch repeat proteins control yeast PKA activity in response to nutrient availability. Cell cycle. 2011;10(5):767-70.

241. Philips J, Herskowitz I. Identification of Kel1p, a kelch domain-containing protein involved in cell fusion and morphology in Saccharomyces cerevisiae. The Journal of cell biology. 1998;143(2):375-89.

242. Alomer RM, da Silva EML, Chen J, Piekarz KM, McDonald K, Sansam CG, et al. Esco1 and Esco2 regulate distinct cohesin functions during cell cycle progression. Proceedings of the National Academy of Sciences. 2017;114(37):9906-11. doi: 10.1073/pnas.1708291114.

243. Rivera-Colón Y, Maguire A, Liszczak GP, Olia AS, Marmorstein R. Molecular Basis for Cohesin Acetylation by Establishment of Sister Chromatid Cohesion N-Acetyltransferase ESCO1. Journal of Biological Chemistry. 2016:jbc. M116. 752220.

244. Kawasumi R, Abe T, Arakawa H, Garre M, Hirota K, Branzei D. ESCO1/2's roles in chromosome structure and interphase chromatin organization. Genes & development. 2017.

245. Ivanov MP, Ladurner R, Poser I, Beveridge R, Rampler E, Hudecz O, et al. The replicative helicase MCM recruits cohesin acetyltransferase ESCO2 to mediate centromeric sister chromatid cohesion. The EMBO Journal. 2018;37(15):e97150. doi: doi:10.15252/embj.201797150.

246. Lu Y, Li S, Cui Z, Dai X, Zhang M, Miao Y, et al. The cohesion establishment factor Esco1 acetylates α-tubulin to ensure proper spindle assembly in oocyte meiosis. Nucleic Acids Research. 2018;46(5):2335-46. doi: 10.1093/nar/gky001.

247. Sacristan C, Kops GJPL. Joined at the hip: kinetochores, microtubules, and spindle assembly checkpoint signaling. Trends in Cell Biology. 2015;25(1):21-8. doi: https://doi.org/10.1016/j.tcb.2014.08.006.

248. Palou R, Palou G, Quintana DG. A role for the spindle assembly checkpoint in the DNA damage response. Current Genetics. 2017;63(2):275-80. doi: 10.1007/s00294-016-0634-y.

249. Yang J, Zhang X, Feng J, Leng H, Li S, Xiao J, et al. The histone chaperone FACT contributes to DNA replication-coupled nucleosome assembly. Cell reports. 2016;14(5):1128-41.

250. Bermúdez-López M, Ceschia A, de Piccoli G, Colomina N, Pasero P, Aragón L, et al. The Smc5/6 complex is required for dissolution of DNA-mediated sister chromatid linkages. Nucleic Acids Research. 2010;38(19):6502-12. doi: 10.1093/nar/gkq546. PubMed PMID: PMC2965248.

251. Lu J, Liu Y. Deletion of Ogg1 DNA glycosylase results in telomere base damage and length alteration in yeast. The EMBO journal. 2010;29(2):398-409.

252. Pommier Y, Sun Y, Shar-yin NH, Nitiss JL. Roles of eukaryotic topoisomerases in transcription, replication and genomic stability. Nature reviews Molecular cell biology. 2016;17(11):703.

253. Fishel R, Kolodner RD. Identification of mismatch repair genes and their role in the development of cancer. Current Opinion in Genetics & Development. 1995;5(3):382-95. doi: https://doi.org/10.1016/0959-437X(95)80055-7.

254. Li G-M. Mechanisms and functions of DNA mismatch repair. Cell Research. 2007;18:85. doi: 10.1038/cr.2007.115.

255. Jun SH, Kim TG, Ban C. DNA mismatch repair system. Classical and fresh roles. The FEBS journal. 2006;273(8):1609-19. Epub 2006/04/21. doi: 10.1111/j.1742-4658.2006.05190.x. PubMed PMID: 16623698.

256. Dahal BK, Kadyrova LY, Delfino KR, Rogozin IB, Gujar V, Lobachev KS, et al. Involvement of DNA mismatch repair in the maintenance of heterochromatic DNA stability in Saccharomyces cerevisiae. PLoS genetics. 2017;13(10):e1007074.

257. Goellner EM, Putnam CD, Kolodner RD. Exonuclease 1-dependent and independent mismatch repair. DNA Repair. 2015;32:24-32. doi: https://doi.org/10.1016/j.dnarep.2015.04.010.

258. Wei K, Clark AB, Wong E, Kane MF, Mazur DJ, Parris T, et al. Inactivation of Exonuclease 1 in mice results in DNA mismatch repair defects, increased cancer susceptibility, and male and female sterility. Genes & development. 2003;17(5):603-14.

259. Sanchez-Diaz A, Nkosi PJ, Murray S, Labib K. The Mitotic Exit Network and Cdc14 phosphatase initiate cytokinesis by counteracting CDK phosphorylations and blocking polarised growth. The EMBO journal. 2012;31(17):3620-34.

260. Lee SE, Frenz LM, Wells NJ, Johnson AL, Johnston LH. Order of function of the budding-yeast mitotic exit-network proteins Tem1, Cdc15, Mob1, Dbf2, and Cdc5. Current Biology. 2001;11(10):784-8.

261. Hergovich A, Hemmings BA. Hippo signalling in the G2/M cell cycle phase: Lessons learned from the yeast MEN and SIN pathways. Seminars in cell & developmental biology. 2012;23(7):794-802. doi: https://doi.org/10.1016/j.semcdb.2012.04.001.

262. Perez AM, Finnigan GC, Roelants FM, Thorner J. Septin-Associated Protein Kinases in the Yeast Saccharomyces cerevisiae. Frontiers in cell and developmental biology. 2016;4:119-. doi: 10.3389/fcell.2016.00119. PubMed PMID: 27847804.

263. Chang M, Sionov E, Khanal Lamichhane A, Kwon-Chung KJ, Chang YC. Roles of Three Cryptococcus neoformans and Cryptococcus gattii Efflux Pump-Coding Genes in Response to Drug Treatment. Antimicrobial agents and chemotherapy. 2018;62(4):e01751-17. doi: 10.1128/AAC.01751-17. PubMed PMID: 29378705.

264. Yang ML, Uhrig J, Vu K, Singapuri A, Dennis M, Gelli A, et al. Fluconazole susceptibility in Cryptococcus gattii is dependent on the ABC transporter Pdr11. Antimicrobial agents and chemotherapy. 2016;60(3):1202-7.

265. Zhang T, Bu P, Zeng J, Vancura A. Increased heme synthesis in yeast induces a metabolic switch from fermentation to respiration even under conditions of glucose repression. Journal of Biological Chemistry. 2017;292(41):16942-54. doi: 10.1074/jbc.M117.790923.

266. Galdieri L, Zhang T, Rogerson D, Vancura A. Reduced histone expression or defect in chromatin assembly induce respiration. Molecular and Cellular Biology. 2016. doi: 10.1128/mcb.00770-15.

267. Lacey E. The role of the cytoskeletal protein, tubulin, in the mode of action and mechanism of drug resistance to benzimidazoles. International journal for parasitology. 1988;18(7):885-936.

268. Weinstein B, Solomon F. Phenotypic consequences of tubulin overproduction in Saccharomyces cerevisiae: differences between alpha-tubulin and beta-tubulin. Mol Cell Biol. 1990;10(10):5295-304. Epub 1990/10/01. PubMed PMID: 2204812; PubMed Central PMCID: PMCPMC361218.

269. Burke D, Gasdaska P, Hartwell L. Dominant effects of tubulin overexpression in Saccharomyces cerevisiae. Molecular and Cellular Biology. 1989;9(3):1049-59.

270. Bermudez VP, Maniwa Y, Tappin I, Ozato K, Yokomori K, Hurwitz J. The alternative Ctf18-Dcc1-Ctf8-replication factor C complex required for sister chromatid cohesion loads proliferating cell nuclear antigen onto DNA. Proceedings of the National Academy of Sciences. 2003;100(18):10237-42. doi: 10.1073/pnas.1434308100.

271. Mayer ML, Gygi SP, Aebersold R, Hieter P. Identification of RFC (Ctf18p, Ctf8p, Dcc1p): an alternative RFC complex required for sister chromatid cohesion in S. cerevisiae. Molecular cell. 2001;7(5):959-70.

272. Paul MR, Markowitz TE, Hochwagen A, Ercan S. Condensin Depletion Causes Genome Decompaction Without Altering the Level of Global Gene Expression in Saccharomyces cerevisiae. Genetics. 2018. doi: 10.1534/genetics.118.301217.

273. Uhlmann F. SMC complexes: from DNA to chromosomes. Nature Reviews Molecular Cell Biology. 2016;17(7):399.

274. Lazar-Stefanita L, Scolari VF, Mercy G, Muller H, Guérin TM, Thierry A, et al. Cohesins and condensins orchestrate the 4D dynamics of yeast chromosomes during the cell cycle. The EMBO journal. 2017:e201797342.

275. Miranda JL, De Wulf P, Sorger PK, Harrison SC. The yeast DASH complex forms closed rings on microtubules. Nature Structural and Molecular Biology. 2005;12(2):138.

276. Jenni S, Harrison SC. Structure of the DASH/Dam1 complex shows its role at the yeast kinetochore-microtubule interface. Science. 2018;360(6388):552-8.

277. Maure J-F, Komoto S, Oku Y, Mino A, Pasqualato S, Natsume K, et al. The Ndc80 loop region facilitates formation of kinetochore attachment to the dynamic microtubule plus end. Current biology. 2011;21(3):207-13.

278. Best HA, Matthews JH, Heathcott RW, Hanna R, Leahy DC, Coorey NV, et al. Laulimalide and peloruside A inhibit mitosis of Saccharomyces cerevisiae by preventing microtubule depolymerisation-dependent steps in chromosome separation and nuclear positioning. Mol Biosyst. 2013;9(11):2842-52. Epub 2013/09/24. doi: 10.1039/c3mb70211a. PubMed PMID: 24056987.

279. Parsons AB, Lopez A, Givoni IE, Williams DE, Gray CA, Porter J, et al. Exploring the mode-of-action of bioactive compounds by chemical-genetic profiling in yeast. Cell. 2006;126(3):611-25. Epub 2006/08/12. doi: 10.1016/j.cell.2006.06.040. PubMed PMID: 16901791.

280. Wang LL, Lee K-T, Jung K-W, Lee D-G, Bahn Y-S. The novel microtubule-associated CAP-glycine protein Cgp1 governs growth, differentiation, and virulence of Cryptococcus neoformans. Virulence. 2018;9(1):566-84. doi: 10.1080/21505594.2017.1423189.

281. Pan X, Yuan DS, Xiang D, Wang X, Sookhai-Mahadeo S, Bader JS, et al. A robust toolkit for functional profiling of the yeast genome. Molecular cell. 2004;16(3):487-96.

282. Millán-Zambrano G, Rodríguez-Gil A, Peñate X, de Miguel-Jiménez L, Morillo-Huesca M, Krogan N, et al. The Prefoldin Complex Regulates Chromatin Dynamics during Transcription Elongation. PLOS Genetics. 2013;9(9):e1003776. doi: 10.1371/journal.pgen.1003776.

283. Yadav V, Sanyal K. Sad1 Spatiotemporally Regulates Kinetochore Clustering To Ensure High-Fidelity Chromosome Segregation in the Human Fungal Pathogen Cryptococcus neoformans. mSphere. 2018;3(4). Epub 2018/07/07. doi: 10.1128/mSphere.00190-18. PubMed PMID: 29976642; PubMed Central PMCID: PMCPMC6034078.

284. Zhao Z, Liu H, Luo Y, Zhou S, An L, Wang C, et al. Molecular evolution and functional divergence of tubulin superfamily in the fungal tree of life. Scientific reports. 2014;4:6746. doi: 10.1038/srep06746

https://www.nature.com/articles/srep06746#supplementary-information.

285. Zhang L, Addla D, Ponmani J, Wang A, Xie D, Wang Y-N, et al. Discovery of membrane active benzimidazole quinolones-based topoisomerase inhibitors as potential DNA-binding antimicrobial agents. European Journal of Medicinal Chemistry. 2016;111:160-82. doi: https://doi.org/10.1016/j.ejmech.2016.01.052.

286. Gao C, Li B, Zhang B, Sun Q, Li L, Li X, et al. Synthesis and biological evaluation of benzimidazole acridine derivatives as potential DNA-binding and apoptosis-inducing agents. Bioorganic & Medicinal Chemistry. 2015;23(8):1800-7. doi: https://doi.org/10.1016/j.bmc.2015.02.036.

287. Luo Y-L, Baathulaa K, Kannekanti VK, Zhou C-H, Cai G-X. Novel benzimidazole derived naphthalimide triazoles: synthesis, antimicrobial activity and interactions with calf thymus DNA. Science China Chemistry. 2015;58(3):483-94. doi: 10.1007/s11426-014-5296-3.

288. Larsen NB, Liberti SE, Vogel I, Jørgensen SW, Hickson ID, Mankouri HW. Stalled replication forks generate a distinct mutational signature in yeast. Proceedings of the National Academy of Sciences. 2017;114(36):9665-70.

289. Winkler DD, Luger K. The Histone Chaperone FACT: Structural Insights and Mechanisms for Nucleosome Reorganization. The Journal of Biological Chemistry. 2011;286(21):18369-74. doi: 10.1074/jbc.R110.180778. PubMed PMID: PMC3099653.

290. Valieva ME, Armeev GA, Kudryashova KS, Gerasimova NS, Shaytan AK, Kulaeva OI, et al. Large-Scale ATP-Independent Nucleosome Unfolding by a Histone Chaperone. Nature structural & molecular biology. 2016;23(12):1111-6. doi: 10.1038/nsmb.3321. PubMed PMID: PMC5518926.

291. Kurat CF, Yeeles JTP, Patel H, Early A, Diffley JFX. Chromatin Controls DNA Replication Origin Selection, Lagging-Strand Synthesis, and Replication Fork Rates. Molecular Cell. 2017;65(1):117-30. doi: https://doi.org/10.1016/j.molcel.2016.11.016.

292. Herrera-Moyano E, Mergui X, García-Rubio ML, Barroso S, Aguilera A. The yeast and human FACT chromatin-reorganizing complexes solve R-loop-mediated transcription–replication conflicts. Genes & development. 2014.

293. Peng XP, Lim S, Li S, Marjavaara L, Chabes A, Zhao X. Acute Smc5/6 depletion reveals its primary role in rDNA replication by restraining recombination at fork pausing sites. PLOS Genetics. 2018;14(1):e1007129. doi: 10.1371/journal.pgen.1007129.

294. Cejka P, Plank Jody L, Dombrowski Christopher C, Kowalczykowski Stephen C. Decatenation of DNA by the S. cerevisiae Sgs1-Top3-Rmi1 and RPA Complex: A Mechanism for Disentangling Chromosomes. Molecular Cell. 2012;47(6):886-96. doi: https://doi.org/10.1016/j.molcel.2012.06.032.

295. Gonzalez-Huici V, Szakal B, Urulangodi M, Psakhye I, Castellucci F, Menolfi D, et al. DNA bending facilitates the error-free DNA damage tolerance pathway and upholds genome integrity. The EMBO Journal. 2014;33(4):327-40. doi: 10.1002/embj.201387425. PubMed PMID: PMC3983681.

296. Lia D, Reyes A, de Melo Campos JTA, Piolot T, Baijer J, Radicella JP, et al. Mitochondrial maintenance under oxidative stress depends on mitochondrially localised alpha-OGG1. J Cell Sci. 2018;131(12). Epub 2018/06/01. doi: 10.1242/jcs.213538. PubMed PMID: 29848661.

297. Claeys Bouuaert C, Keeney S. Distinct DNA-binding surfaces in the ATPase and linker domains of MutLγ determine its substrate specificities and exert separable functions in meiotic recombination and mismatch repair. PLOS Genetics. 2017;13(5):e1006722. doi: 10.1371/journal.pgen.1006722.

298. Genschel J, Kadyrova LY, Iyer RR, Dahal BK, Kadyrov FA, Modrich P. Interaction of proliferating cell nuclear antigen with PMS2 is required for MutLα activation and function in mismatch repair. Proceedings of the National Academy of Sciences. 2017;114(19):4930-5. doi: 10.1073/pnas.1702561114.

299. Goellner Eva M, Smith Catherine E, Campbell Christopher S, Hombauer H, Desai A, Putnam Christopher D, et al. PCNA and Msh2-Msh6 Activate an Mlh1-Pms1 Endonuclease Pathway Required for Exo1-Independent Mismatch Repair. Molecular Cell. 2014;55(2):291-304. doi: https://doi.org/10.1016/j.molcel.2014.04.034.

300. Ko Y-J, Yu YM, Kim G-B, Lee G-W, Maeng PJ, Kim S, et al. Remodeling of global transcription patterns of Cryptococcus neoformans genes mediated by the stress-activated HOG signaling pathways. Eukaryotic cell. 2009;8(8):1197-217.

301. Tsang CK, Liu Y, Thomas J, Zhang Y, Zheng XS. Superoxide dismutase 1 acts as a nuclear transcription factor to regulate oxidative stress resistance. Nature communications. 2014;5:3446.

302. Giles SS, Batinic-Haberle I, Perfect JR, Cox GM. Cryptococcus neoformans mitochondrial superoxide dismutase: an essential link between antioxidant function and high-temperature growth. Eukaryot Cell. 2005;4(1):46-54. Epub 2005/01/12. doi: 10.1128/ec.4.1.46-54.2005. PubMed PMID: 15643059; PubMed Central PMCID: PMCPMC544162.

303. Narasipura SD, Chaturvedi V, Chaturvedi S. Characterization of Cryptococcus neoformans variety gattii SOD2 reveals distinct roles of the two superoxide dismutases in fungal biology and virulence. Mol Microbiol. 2005;55(6):1782-800. Epub 2005/03/09. doi: 10.1111/j.1365-2958.2005.04503.x. PubMed PMID: 15752200.

304. Kajiwara K, Muneoka T, Watanabe Y, Karashima T, Kitagaki H, Funato K. Perturbation of sphingolipid metabolism induces endoplasmic reticulum stress-mediated mitochondrial apoptosis in budding yeast. Molecular microbiology. 2012;86(5):1246-61.

305. Niles BJ, Joslin AC, Fresques T, Powers T. TOR complex 2-Ypk1 signaling maintains sphingolipid homeostasis by sensing and regulating ROS accumulation. Cell Rep. 2014;6(3):541-52. Epub

2014/01/28. doi: 10.1016/j.celrep.2013.12.040. PubMed PMID: 24462291; PubMed Central PMCID: PMCPMC3985744.

306. Yamaguchi Y, Katsuki Y, Tanaka S, Kawaguchi R, Denda H, Ikeda T, et al. Protective role of the HOG pathway against the growth defect caused by impaired biosynthesis of complex sphingolipids in yeast Saccharomyces cerevisiae. Molecular microbiology. 2018;107(3):363-86.

307. Vokral I, Krizova V, Lamka J, Kubicek V, Szotáková B, Varady B, et al. Effect of flubendazole on biotransformation enzymes activities in Haemonchus contortus. Open Parasitol J. 2010;4:24-8.

308. Zhang L, Guo M, Li J, Zheng Y, Zhang S, Xie T, et al. Systems biology-based discovery of a potential Atg4B agonist (Flubendazole) that induces autophagy in breast cancer. Mol Biosyst. 2015;11(11):2860-6. Epub 2015/08/25. doi: 10.1039/c5mb00466g. PubMed PMID: 26299935.

309. Karna P, Zughaier S, Pannu V, Simmons R, Narayan S, Aneja R. Induction of reactive oxygen species (ROS)-mediated autophagy by a novel microtubule-modulating agent. Journal of Biological Chemistry. 2010:jbc. M109. 091694.

310. Krishnan N, Dickman MB, Becker DF. Proline modulates the intracellular redox environment and protects mammalian cells against oxidative stress. Free radical biology & medicine. 2008;44(4):671-81. doi: 10.1016/j.freeradbiomed.2007.10.054. PubMed PMID: PMC2268104.

311. Chen C, Wanduragala S, Becker DF, Dickman MB. Tomato QM-like protein protects Saccharomyces cerevisiae cells against oxidative stress by regulating intracellular proline levels. Applied and environmental microbiology. 2006;72(6):4001-6.

312. Chang CL, Marra G, Chauhan DP, Ha HT, Chang DK, Ricciardiello L, et al. Oxidative stress inactivates the human DNA mismatch repair system. American Journal of Physiology-Cell Physiology. 2002;283(1):C148-C54.

313. Kelliher CM, Leman AR, Sierra CS, Haase SB. Investigating Conservation of the Cell-Cycle-Regulated Transcriptional Program in the Fungal Pathogen, Cryptococcus neoformans. PLOS Genetics. 2016;12(12):e1006453. doi: 10.1371/journal.pgen.1006453.

314. Yamaguchi M, Ohkusu M, Biswas SK, Kawamoto S. Cytological study of cell cycle of the pathogenic yeast Cryptococcus neoformans. Nippon Ishinkin Gakkai Zasshi. 2007;48(4):147-52.

315. González A, Fillat MF, Lanas Á. Transcriptional regulators: valuable targets for novel antibacterial strategies. Future medicinal chemistry. 2018;10(5):541-60. doi: 10.4155/fmc-2017-0181. PubMed PMID: 29461098.

316. Dang CV, Reddy EP, Shokat KM, Soucek L. Drugging the 'undruggable' cancer targets. Nature reviews Cancer. 2017;17(8):502-8. Epub 2017/06/23. doi: 10.1038/nrc.2017.36. PubMed PMID: 28643779.

317. Cuadrado A, Manda G, Hassan A, Alcaraz MJ, Barbas C, Daiber A, et al. Transcription factor NRF2 as a therapeutic target for chronic diseases: a systems medicine approach. Pharmacological reviews. 2018;70(2):348-83.

318. Bhullar KS, Lagarón NO, McGowan EM, Parmar I, Jha A, Hubbard BP, et al. Kinase-targeted cancer therapies: progress, challenges and future directions. Molecular cancer. 2018;17(1):48.

319. Cranfill PJ, Sell BR, Baird MA, Allen JR, Lavagnino Z, de Gruiter HM, et al. Quantitative assessment of fluorescent proteins. Nature methods. 2016;13(7):557.

320. Kopecká M. Microtubules and Actin Cytoskeleton of *Cryptococcus neoformans* as Targets for Anticancer Agents to Potentiate a Novel Approach for New Antifungals. Chemotherapy. 2015;61(3):117-21.

321. Sutradhar S, Yadav V, Sridhar S, Sreekumar L, Bhattacharyya D, Ghosh SK, et al. A comprehensive model to predict mitotic division in budding yeasts. Molecular biology of the cell. 2015;26(22):3954-65.

322. Jung K-W, Yang D-H, Maeng S, Lee K-T, So Y-S, Hong J, et al. Systematic functional profiling of transcription factor networks in *Cryptococcus neoformans*. Nature communications. 2015;6:6757.

323. Ardito F, Giuliani M, Perrone D, Troiano G, Lo Muzio L. The crucial role of protein phosphorylation in cell signaling and its use as targeted therapy (Review). International journal of molecular medicine. 2017;40(2):271-80. Epub 2017/06/22. doi: 10.3892/ijmm.2017.3036. PubMed PMID: 28656226.

324. Hawkins LJ, Al-Attar R, Storey KB. Transcriptional regulation of metabolism in disease: From transcription factors to epigenetics. PeerJ. 2018;6:e5062-e. doi: 10.7717/peerj.5062. PubMed PMID: 29922517.

325. Lee TI, Young RA. Transcriptional regulation and its misregulation in disease. Cell. 2013;152(6):1237-51.

326. Ochoa D, Bradley D, Beltrao P. Evolution, dynamics and dysregulation of kinase signalling. Current opinion in structural biology. 2018;48:133-40.

327. Eglen RM, Reisine T. The current status of drug discovery against the human kinome. Assay and drug development technologies. 2009;7(1):22-43.

328. Li YH, Wang PP, Li XX, Yu CY, Yang H, Zhou J, et al. The Human Kinome Targeted by FDA Approved Multi-Target Drugs and Combination Products: A Comparative Study from the Drug-Target Interaction Network Perspective. PloS one. 2016;11(11):e0165737. doi: 10.1371/journal.pone.0165737.

329. Lambert M, Jambon S, Depauw S, David-Cordonnier MH. Targeting Transcription Factors for Cancer Treatment. Molecules (Basel, Switzerland). 2018;23(6). Epub 2018/06/21. doi: 10.3390/molecules23061479. PubMed PMID: 29921764; PubMed Central PMCID: PMCPMC6100431.

330. Gross S, Rahal R, Stransky N, Lengauer C, Hoeflich KP. Targeting cancer with kinase inhibitors. The Journal of clinical investigation. 2015;125(5):1780-9.

331. Lazo JS, Sharlow ER. Drugging Undruggable Molecular Cancer Targets. Annual Review of Pharmacology and Toxicology. 2016;56(1):23-40. doi: 10.1146/annurev-pharmtox-010715-103440. PubMed PMID: 26527069.

332. Youn J-Y, Friesen H, Ba ANN, Liang W, Messier V, Cox MJ, et al. Functional analysis of kinases and transcription factors in Saccharomyces cerevisiae using an integrated overexpression library. G3: Genes, Genomes, Genetics. 2017;7(3):911-21.

333. Lee K-T, So Y-S, Yang D-H, Jung K-W, Choi J, Lee D-G, et al. Systematic functional analysis of kinases in the fungal pathogen Cryptococcus neoformans. Nature communications. 2016;7:12766.

334. Lev S, Kaufman-Francis K, Desmarini D, Juillard PG, Li C, Stifter SA, et al. Pho4 Is essential for dissemination of *Cryptococcus neoformans* to the host brain by promoting phosphate uptake and growth at alkaline pH. mSphere. 2017;2(1). doi: 10.1128/mSphere.00381-16.

335. Aaron PA, Jamklang M, Uhrig JP, Gelli A. The blood–brain barrier internalises Cryptococcus neoformans via the EphA2-tyrosine kinase receptor. Cellular microbiology. 2018;20(3):e12811.

336. Jung K-W, Lee K-T, Averette AF, Hoy MJ, Everitt J, Heitman J, et al. Evolutionarily Conserved and Divergent Roles of Unfolded Protein Response (UPR) in the Pathogenic Cryptococcus Species Complex. Scientific reports. 2018;8(1):8132. doi: 10.1038/s41598-018-26405-5.

337. Paes HC, Derengowski LdS, Peconick LDF, Albuquerque P, Pappas GJ, Nicola AM, et al. A Wor1-Like Transcription Factor Is Essential for Virulence of Cryptococcus neoformans. Frontiers in Cellular and Infection Microbiology. 2018;8(369). doi: 10.3389/fcimb.2018.00369.

338. Bhakt P, Shivarathri R, Choudhary DK, Borah S, Kaur R. Fluconazole-induced actin cytoskeleton remodeling requires phosphatidylinositol 3-phosphate 5-kinase in the pathogenic yeast Candida glabrata. Molecular microbiology. 2018;110(3):425-43.

339. Flowers SA, Barker KS, Berkow EL, Toner G, Chadwick SG, Gygax SE, et al. Gain-of-function mutations in UPC2 are a frequent cause of ERG11 upregulation in azole-resistant clinical isolates of Candida albicans. Eukaryotic cell. 2012;11(10):1289-99.

340. Camps SM, Dutilh BE, Arendrup MC, Rijs AJ, Snelders E, Huynen MA, et al. Discovery of a HapE mutation that causes azole resistance in Aspergillus fumigatus through whole genome sequencing and sexual crossing. PloS one. 2012;7(11):e50034.

341. Gallo-Ebert C, Donigan M, Stroke IL, Swanson RN, Manners MT, Francisco J, et al. Novel antifungal drug discovery based on targeting pathways regulating the fungus-conserved Upc2 transcription factor. Antimicrobial agents and chemotherapy. 2014;58(1):258-66. doi: 10.1128/aac.01677-13.

342. Song M-H, Lee J-W, Kim MS, Yoon J-K, White TC, Floyd A, et al. A flucytosine-responsive Mbp1/Swi4-like protein, Mbs1, plays pleiotropic roles in antifungal drug resistance, stress response, and virulence of Cryptococcus neoformans. Eukaryotic cell. 2012;11(1):53-67.

343. Baxter BK, DiDone L, Ogu D, Schor S, Krysan DJ. Identification, in Vitro Activity and Mode of Action of Phosphoinositide-Dependent-1 Kinase Inhibitors as Antifungal Molecules. ACS Chemical Biology. 2011;6(5):502-10. doi: 10.1021/cb100399x.

344. Sussman A, Huss K, Chio L-C, Heidler S, Shaw M, Ma D, et al. Discovery of cercosporamide, a known antifungal natural product, as a selective Pkc1 kinase inhibitor through high-throughput screening. Eukaryotic cell. 2004;3(4):932-43.

345. Kozubowski L, Heitman J. Septins enforce morphogenetic events during sexual reproduction and contribute to virulence of Cryptococcus neoformans. Molecular Microbiology. 2010;75(3):658-75. doi: doi:10.1111/j.1365-2958.2009.06983.x.

346. Legland D, Arganda-Carreras I, Andrey P. MorphoLibJ: integrated library and plugins for mathematical morphology with ImageJ. Bioinformatics. 2016;32(22):3532-4.

347. Steger C. An unbiased detector of curvilinear structures. IEEE Transactions on pattern analysis and machine intelligence. 1998;20(2):113-25.

348. Schindelin J, Arganda-Carreras I, Frise E, Kaynig V, Longair M, Pietzsch T, et al. Fiji: an open-source platform for biological-image analysis. Nature methods. 2012;9(7):676.

349. Salvatier J, Wiecki TV, Fonnesbeck C. Probabilistic programming in Python using PyMC3. PeerJ Computer Science. 2016;2:e55.

350. Bi Z, Faloutsos C, Korn F, editors. The DGX distribution for mining massive, skewed data. Proceedings of the seventh ACM SIGKDD international conference on Knowledge discovery and data mining; 2001: ACM.

351. Pramila T, Miles S, GuhaThakurta D, Jemiolo D, Breeden LL. Conserved homeodomain proteins interact with MADS box protein Mcm1 to restrict ECB-dependent transcription to the M/G1 phase of the cell cycle. Genes & development. 2002;16(23):3034-45.

352. Darieva Z, Clancy A, Bulmer R, Williams E, Pic-Taylor A, Morgan BA, et al. A competitive transcription factor binding mechanism determines the timing of late cell cycle-dependent gene expression. Molecular cell. 2010;38(1):29-40.

353. Kelliher CM, Foster MW, Motta FC, Deckard A, Soderblom EJ, Moseley MA, et al. Layers of regulation of cell-cycle gene expression in the budding yeast Saccharomyces cerevisiae. Molecular biology of the cell. 2018;29(22):2644-55.

354. Kanehisa M, Furumichi M, Tanabe M, Sato Y, Morishima K. KEGG: new perspectives on genomes, pathways, diseases and drugs. Nucleic acids research. 2016;45(D1):D353-D61.

355. Cokus S, Rose S, Haynor D, Grønbech-Jensen N, Pellegrini M. Modelling the network of cell cycle transcription factors in the yeast Saccharomyces cerevisiae. BMC bioinformatics. 2006;7:381-. doi: 10.1186/1471-2105-7-381. PubMed PMID: 16914048.

356. Horak CE, Luscombe NM, Qian J, Bertone P, Piccirrillo S, Gerstein M, et al. Complex transcriptional circuitry at the G1/S transition in Saccharomyces cerevisiae. Genes & development. 2002;16(23):3017-33. doi: 10.1101/gad.1039602.

357. Kuge S, Jones N. YAP1 dependent activation of TRX2 is essential for the response of Saccharomyces cerevisiae to oxidative stress by hydroperoxides. The EMBO journal. 1994;13(3):655-64.

358. Stephen DW, Rivers SL, Jamieson DJ. The role of the YAP1 and YAP2 genes in the regulation of the adaptive oxidative stress responses of Saccharomyces cerevisiae. Molecular microbiology. 1995;16(3):415-23.

359. Kralova V, Hanusova V, Rudolf E, Canova K, Skalova L. Flubendazole induces mitotic catastrophe and senescence in colon cancer cells in vitro. J Pharm Pharmacol. 2016;68(2):208-18. Epub 2016/01/06. doi: 10.1111/jphp.12503. PubMed PMID: 26730435.

360. Rathinasamy K, Panda D. Suppression of microtubule dynamics by benomyl decreases tension across kinetochore pairs and induces apoptosis in cancer cells. The FEBS journal. 2006;273(17):4114-28.

361. Čáňová K, Rozkydalová L, Vokurková D, Rudolf E. Flubendazole induces mitotic catastrophe and apoptosis in melanoma cells. Toxicology in Vitro. 2018;46:313-22. doi: https://doi.org/10.1016/j.tiv.2017.10.025.

362. Kopecká M. Effects of microtubule and actin inhibitors on Cryptococcus neoformans examined by scanning and transmission electron microscopy. Chemotherapy. 2014;60(2):99-106.

363. Bürglin TR, Affolter M. Homeodomain proteins: an update. Chromosoma. 2016;125(3):497-521. Epub 2015/10/13. doi: 10.1007/s00412-015-0543-8. PubMed PMID: 26464018.

364. Abate-Shen C. Deregulated homeobox gene expression in cancer: cause or consequence? Nature Reviews Cancer. 2002;2(10):777.

365. Gómez-Escoda B, Ivanova T, Calvo IA, Alves-Rodrigues I, Hidalgo E, Ayté J. Yox1 links MBF-dependent transcription to completion of DNA synthesis. EMBO reports. 2011;12(1):84-9.

366. Hendler A, Medina EM, Kishkevich A, Abu-Qarn M, Klier S, Buchler NE, et al. Gene duplication and co-evolution of G1/S transcription factor specificity in fungi are essential for optimizing cell fitness. PLoS genetics. 2017;13(5):e1006778.

367. Koch C, Moll T, Neuberg M, Ahorn H, Nasmyth K. A role for the transcription factors Mbp1 and Swi4 in progression from G1 to S phase. Science. 1993;261(5128):1551-7.

368. Iyer VR, Horak CE, Scafe CS, Botstein D, Snyder M, Brown PO. Genomic binding sites of the yeast cell-cycle transcription factors SBF and MBF. Nature. 2001;409(6819):533.

369. Bähler J. Cell-cycle control of gene expression in budding and fission yeast. Annu Rev Genet. 2005;39:69-94.

370. Lacey E. Mode of action of benzimidazoles. Parasitology Today. 1990;6(4):112-5. doi: http://dx.doi.org/10.1016/0169-4758(90)90227-U.

371. Geary TG, Mackenzie CD, Silber SA. Flubendazole as a macrofilaricide: History and background. PLOS Neglected Tropical Diseases. 2019;13(1):e0006436. doi: 10.1371/journal.pntd.0006436.

372. Ceballos L, Mackenzie C, Geary T, Alvarez L, Lanusse C. Exploring the Potential of Flubendazole in Filariasis Control: Evaluation of the Systemic Exposure for Different Pharmaceutical Preparations. PLOS Neglected Tropical Diseases. 2014;8(5):e2838. doi: 10.1371/journal.pntd.0002838.

373. Ceballos L, Alvarez L, Mackenzie C, Geary T, Lanusse C. Pharmacokinetic comparison of different flubendazole formulations in pigs: A further contribution to its development as a macrofilaricide molecule. International Journal for Parasitology: Drugs and Drug Resistance. 2015;5(3):178-84. doi: https://doi.org/10.1016/j.ijpddr.2015.09.001.

374. Mackenzie CD, Geary TG. Flubendazole: a candidate macrofilaricide for lymphatic filariasis and onchocerciasis field programs. Expert review of anti-infective therapy. 2011;9(5):497-501.

375. Nobilis M, Jira T, Lísa M, Holčapek M, Szotáková B, Lamka J, et al. Achiral and chiral high-performance liquid chromatographic determination of flubendazole and its metabolites in biomatrices using UV photodiode-array and mass spectrometric detection. Journal of Chromatography A. 2007;1149(1):112-20. doi: https://doi.org/10.1016/j.chroma.2007.01.013.

376. Van den Mooter G. The use of amorphous solid dispersions: A formulation strategy to overcome poor solubility and dissolution rate. Drug Discovery Today: Technologies. 2012;9(2):e79-e85.

377. Tweats DJ, Johnson GE, Scandale I, Whitwell J, Evans DB. Genotoxicity of flubendazole and its metabolites in vitro and the impact of a new formulation on in vivo aneugenicity. Mutagenesis. 2016;31(3):309-21. Epub 2015/10/08. doi: 10.1093/mutage/gev070. PubMed PMID: 26443851; PubMed Central PMCID: PMCPMC4840262.

378. Lachau-Durand S, Lammens L, van der Leede B-j, Van Gompel J, Bailey G, Engelen M, et al. Preclinical toxicity and pharmacokinetics of a new orally bioavailable flubendazole formulation and the impact for clinical trials and risk/benefit to patients. PLOS Neglected Tropical Diseases. 2019;13(1):e0007026. doi: 10.1371/journal.pntd.0007026.

379. Truong M, Monahan LG, Carter DA, Charles IG. Repurposing drugs to fast-track therapeutic agents for the treatment of cryptococcosis. PeerJ. 2018;6:e4761.

380. Chandrika NT, Shrestha SK, Ngo HX, Garneau-Tsodikova S. Synthesis and investigation of novel benzimidazole derivatives as antifungal agents. Bioorganic & Medicinal Chemistry. 2016;24(16):3680-6. doi: https://doi.org/10.1016/j.bmc.2016.06.010.

381. Keller P, Müller C, Engelhardt I, Hiller E, Lemuth K, Eickhoff H, et al. An Antifungal Benzimidazole Derivative Inhibits Ergosterol Biosynthesis and Reveals Novel Sterols. Antimicrobial agents and chemotherapy. 2015;59(10):6296-307. doi: 10.1128/aac.00640-15.

382. Thamban Chandrika N, Shrestha SK, Ranjan N, Sharma A, Arya DP, Garneau-Tsodikova S. New Application of Neomycin B–Bisbenzimidazole Hybrids as Antifungal Agents. ACS Infectious Diseases. 2018;4(2):196-207. doi: 10.1021/acsinfecdis.7b00254.

383. Howes SC, Geyer EA, LaFrance B, Zhang R, Kellogg EH, Westermann S, et al. Structural and functional differences between porcine brain and budding yeast microtubules. Cell Cycle. 2018;17(3):278-87.

384. Loftus BJ, Fung E, Roncaglia P, Rowley D, Amedeo P, Bruno D, et al. The genome of the basidiomycetous yeast and human pathogen Cryptococcus neoformans. Science (New York, NY). 2005;307(5713):1321-4. Epub 2005/01/13. doi: 10.1126/science.1103773. PubMed PMID: 15653466.

385. Gonzalez-Hilarion S, Paulet D, Lee K-T, Hon C-C, Lechat P, Mogensen E, et al. Intron retention-dependent gene regulation in Cryptococcus neoformans. Scientific reports. 2016;6:32252. doi: 10.1038/srep32252.